REGULATION OF ENDOCYTIC RECYCLING IN *Caenorhabditis elegans*

by

ANBING SHI

A dissertation submitted to the

Graduate School-New Brunswick

Rutgers, The State University of New Jersey

and

The Graduate School of Biomedical Sciences

University of Medicine and Dentistry of New Jersey

In partial fulfillment of the requirements

For the degree of

Doctor of Philosophy

Graduate Program in Microbiology and Molecular Genetics

Written under the direction of

Dr. Barth D. Grant

And approved by

_____

_____

_____

_____

New Brunswick, New Jersey

May, 2010

ABSTRACT OF THE DISSERTATION

REGULATION OF ENDOCYTIC RECYCLING IN

Caenorhabditis elegans

By ANBING SHI

Dissertation Director:

Dr. Barth D. Grant

Eukaryotic endocytic pathway is important for the uptake, sorting, and the subsequential recycling or degradation processes of various cargos. It has been shown that the RME-1/EHD1 is a critical regulator of endocytic recycling. In *C. elegans* and MDCK cells, small GTPase RAB-10 has been specifically implicated in clathrin-independent cargo recycling. Alternatively, some cargos will be recycled from sorting endosomes to Golgi, and retromer complex was shown to be crucial for this transport in yeast and mammalian cells.

In our studies, we analyzed RME-1 and RAB-10 regulated recycling pathway, exploring additional players in the process. First, we demonstrated that ALX-1 is required for endocytic recycling of specific basolateral cargo. The interaction of ALX-1 with RME-1 is required for this recycling process. In our yeast two-hybrid screen for RAB-10-

interacting proteins, EHBP-1 and Arf6 GAP/CNT-1 were recovered and revealed to function together with RAB-10 regulating clathrin-independent cargo recycling. Loss of either EHBP-1 or CNT-1 produced *rab-10*-like cargo transport defects. Furthermore, we showed that EHBP-1 functions, as an unconventional effector, upstream of RAB-10. Nevertheless, similar to canonical Rab effectors, CNT-1 requires RAB-10 for the proper endosome localization. Collectively, our results demonstrate the functional connections of ALX-1/RME-1 and RAB-10/EHBP-1/CNT-1, provided insights into the detail mechanisms of RME-1 and RAB-10 recycling regulation.

We also studied the retromer regulated retrograde transport in *C. elegans*. We demonstrated the physical interaction of RME-8 with retromer component ALX-1. Additionally, we showed that loss-of-function in *rme-8* or *snx-1,* or depletion of *C. elegans* Hsc70 (HSP-1) by RNAi, disrupts endosome to Golgi transport of the retromer-dependent cargo protein MIG-14. Furthermore, we identified a previously unsuspected mechanism for the regulation of endosomal clathrin that is required for retrograde transport. We showed that loss of either RME-8, SNX-1 or HSP-1 leads to endosomal clathrin dynamics defect. Our work indicates that, through RME-8 and Hsc70, the retromer acts to limit clathrin accumulation, a prerequisite for the recycling of retrograde cargo.

ACKNOWLEDGEMENTS

As a former graduate from Rutgers, I decided to come back to Rutgers with a simple goal, namely, to be a well-trained scientific researcher. I made a final decision to join the Grant Lab, and I am glad it was a good one.

I am heartily thankful to my thesis supervisor, Dr. Barth D. Grant, whose encouragement, guidance, and support from the beginning to the end enabled me to develop an understanding of the dynamic trafficking world. Barth trained me with great patience and provided an outstanding and encouraging research environment. I have truly benefited a lot from his scientific mentorship and exploring spirit, which set up a paradigm for my future career.

I would like to thank members of my thesis committee Dr. Chris Rongo, Dr. Peter Lobel and Dr. Richard Padgett for their scientific supports and communication.

I would like to thank all the members of the Grant Lab, past and present, for providing a cooperative and friendly working environment, especially former graduate students Dr. Carlos Chen and Dr. Saumya Pant, as well as Laboratory Technician Peter Schweinsberg for their constant input and help on my thesis work.

Without the support from my wife, Xin Zhang, I would not be able to come back to Rutgers and finish my research. In particular, I thank her for the great efforts taking care of family while I am away. I would also like to thank my parents, my brothers and sister, for their support and encouragement in pursuing my graduate study.

Lastly, I offer my regards and blessings to all of those who supported me in any respect during the completion of the thesis.

DEDICATION

To my wife, Xin.

TABLE OF CONTENTS

ABSTRACT OF THE DISSERTATION ..... **ii**
ACKNOWLEDGEMENTS ..... **iv**
DEDICATION ..... **v**
TABLE OF CONTENTS ..... **vi**
CHAPTER 1: INTRODUCTION **1**
An Overview of Endocytosis 2
The Nematode *C. elegans* as a Model System 3
Endocytic Recycling Regulated by RABs and RME-1 4
Multi-function Protein ALX-1 8
Ehbp1 Functions in the GLUT4 Recycling Regulation 10
ARF-6 and its GTPase-Activating Protein (GAP) CNT-1 in Endocytic Recycling 11
Endosome to Golgi Retrograde Transport and RME-8 15
CHAPTER 2: A NOVEL REQUIREMENT FOR *C. elegans* Alix/ALX-1 IN RME-1 MEDIATED MEMBRANE TRANSPORT **17**
AUTHOR CONTRIBUTIONS 18
SUMMARY 19
INTRODUCTION 20
RESULTS 24
Physical association of ALX-1 and RME-1 24
ALX-1 is broadly expressed in *C. elegans* 25
ALX-1 is associated with recycling endosomes and MVEs in the intestine 25
ALX-1 positive structure number increases in *rme-1* mutants 27
Loss of ALX-1 results in intracellular accumulation of recycling cargo 28
alx-1 mutants accumulate abnormally high numbers of RME-1 positive endosomes. 30
SDPN-1 recruitment to basolateral endosomes fails in *alx-1* mutants. 31
alx-1 mutants are delayed in the degradation of membrane proteins 32
MVE and late endosome morphology is aberrant in *alx-1* mutants 33
Basolateral recycling endosomes require the interaction of RME-1 with ALX-1 34
DISCUSSION 36
MATERIALS AND METHODS 40
General Methods and Strains 40
Antibodies 40
Yeast two-hybrid analyses 40
Protein expression and Coprecipitation assays 41
Plasmids and Transgenic Strains 42
Microscopy and Image Analysis 44
Cell culture, transfections and pulse-chase analysis 45
ACKNOWLEDGEMENTS 48
Table 1. Transgenic and Mutant Strains Used in This Study 49
Figure 1. RME-1 Interacts with ALX-1 50
Figure 2. ALX-1 is Broadly Expressed in *C.elegans* 51
Figure 3. ALX-1 Associates with Two Types of Endosomes in the Intestine 52

Figure 4. *rme-1* Mutants Accumulate Abnormally Numerous GFP-ALX-1 Labeled Endosomes 53
Figure 5. Abnormal Trafficking of Recycling Cargo in *alx-1* Mutant *C. elegans* and in HeLa Cells Expressing Truncated Alix 54
Figure 6. Altered Endosome Populations in *alx-1* Mutants 57
Figure 7. Functional requirement for the ALX-1/RME-1 Interaction *in vivo* 58
Figure S1. *In vitro* Binding of RME-1 to ALX-1 61
Figure S2. ALX-1 Associates with Two Types of Endosomes in the Intestine. 63
Figure S3. mCherry-ALX-1 Partially Colocalizes with Early Endosome Marker (GFP-RAB-5) and Late Endosome Marker (GFP-RAB-7) in the intestine 64
Figure S4. No change in GFP-HGRS-1 Labeled Puncta Number in *rme-1* Mutants 65
Figure S5. Additional Analysis of GFP-tagged Endosome Markers and Endocytic Cargo Markers in *alx-1* Mutants. 66
Figure S6. *alx-1* Mutants are Delayed in the Degradation of Membrane Proteins... 67
Figure S7. mCherry-RME-1(ΔYPSL) Cannot Rescue Certain *rme-1(b1045)* Associated Phenotypes 69
Figure S8. mCherry-ALX-1(ΔNPF) Can Rescue MVE/late Endosome Associated *alx-1(gk275)* Defects, but not Recycling Endosome Associated Defects 71
CHAPTER 3: REGULATION OF ENDOSOMAL CLATHRIN AND RETROMER MEDIATED ENDOSOME TO GOLGI RETROGRADE TRANSPORT BY THE J-DOMAIN PROTEIN RME-8 73
AUTHOR CONTRIBUTIONS 74
SUMMARY 75
INTRODUCTION 76
RESULTS 80
RME-8 physically interacts with SNX-1 80
RME-8 colocalizes with SNX-1 81
RME-8 and SNX-1 localize to early endosomes but not Golgi 81
MIG-14/Wntless is missorted to the late endosome and lysosome in rme-8 and snx-1 mutants 82
MIG-14/Wntless trafficking defects occur after endocytosis in *rme-8* and *snx-1* mutants 85
Neuronal cell polarity is impaired in *rme-8* and *snx-1* mutants 86
Depletion of C. elegans Hsc70 (HSP-1) causes MIG-14/Wntless missorting to the late endosome and lysosome 86
Loss of SNX-1, RME-8, or HSP-1 leads to clathrin accumulation on endosomes .. 88
Loss of SNX-1, RME-8, or HSP-1/Hsc70 impairs clathrin dynamics 89
Intramolecular Interactions within RME-8 90
DISCUSSION 91
MATERIALS AND METHODS 95
General Methods and Strains 95
Antibodies 95
Yeast two-hybrid analyses 95
Protein expression and Coprecipitation assays 96
Plasmids and Transgenic Strains 97
Microscopy and Image Analysis 99

FRAP Analysis 100
Neuronal Polarity Assay 101
Western Analysis 101
ACKNOWLEDGEMENTS 102
Table 1. Transgenic and Mutant Strains Used in This Study 103
Figure 1. RME-8 physically interacts with SNX-1 104
Figure 2. RME-8 colocalizes with SNX-1 and RAB-5 on early endosomes 107
Figure 3. MIG-14 recycling requires RME-8 and SNX-1 108
Figure 4. Clathrin accumulates on endosomes in animals lacking RME-8, SNX-1, or HSP-1/Hsc70 111
Figure 5. Clathrin dynamics are impaired in *rme-8(b1023)*, *snx-1(tm847)* and *hsp-1(RNAi)* knock-down animals 113
Figure S1. RME-8 binding specificity 114
Figure S2. RME-8 colocalizes with SNX-1 in the hypodermis and coelomocyte .. 115
Figure S3. SNX-1 colocalizes with RAB-5 and EEA-1 on early endosomes 116
Figure S4. RME-8 colocalizes with RAB-5 and EEA-1 on early endosomes in the coelomocyte 117
Figure S5. Mislocalization of MIG-14 in animals lacking RME-8, SNX-1, and HSP-1/Hsc70. 118
Figure S6. *rme-8(b1023)* and *snx-1(tm847)* mutants display defective ALM and PLM posterior processes 120
Figure S7. Protein levels of retromer components, GFP-SNX-1 and GFP-VPS-35, are not affected by loss of RME-8 or HSP-1/Hsc70. 121
Figure S8. Degradation of membrane protein CAV-1-GFP is not delayed in *rme-8(b1023)* and *snx-1(tm847)* mutants 122
Figure S9. Aberrant accumulation of clathrin and altered early endosome morphology in *rme-8* mutants 123
Figure S10. The RME-8 J-domain can physically interact with other domains of RME-8 126
Figure S11. 127
CHAPTER 4: EHBP-1 FUNCTIONS WITH RAB-10 DURING ENDOCYTIC RECYCLING IN *C. elegans* **129**
AUTHOR CONTRIBUTIONS 130
SUMMARY 131
INTRODUCTION 132
RESULTS 135
EHBP-1 associates with active GTP-bound RAB-10 135
EHBP-1 is widely expressed in *C. elegans* 136
EHBP-1 is associated with endosomes but not Golgi in the intestine 137
Loss of EHBP-1 causes endocytic recycling defects 138
Cargo-specific requirements for EHBP-1 139
EHBP-1 is important for endosome morphology 140
EHBP-1 controls the localization of RAB-10 141
EHBP-1 regulates GLR-1 glutamate receptor trafficking 142
EHBP-1 is required in the germline 144
DISCUSSION 148

MATERIALS AND METHODS 152
General Methods and Strains 152
Antibodies 152
Yeast Two-hybrid Analyses 152
Tissue-specific steady-state endocytosis assays 153
Protein Expression and Coprecipitation Assays 154
Plasmids and Transgenic Strains 155
Microscopy and Image Analysis 156
Behavioral Assays 158
Protein secretion assay in the *C. elegans* germline 158
ACKNOWLEDGEMENTS 160
Table 1. Transgenic and Mutant Strains Used in This Study 161
Figure 1. EHBP-1 physically interacts with RAB-10(Q68L) and RAB-8(Q67L) .. 162
Figure 2. EHBP-1 is broadly expressed in *C. elegans*. 164
Figure 3. EHBP-1 colocalizes with RAB-10 and RAB-8 on endosomes. 166
Figure 4. Loss of EHBP-1 induces endocytic recycling defects in the *C. elegans* intestine. 168
Figure 5. Accumulation of RAB-5-positive early endosomes and disrupted RME-1-positive tubular recycling structures in *ehbp-1(tm2523)* and *rab-10(q373)* mutants. 169
Figure 6. RAB-10-positive endosomal labeling decreases in *ehbp-1(tm2523)* mutants, but accumulate in *rme-1(b1045)* mutants 170
Figure 7. EHBP-1 regulates GLR-1 glutamate receptor trafficking. 172
Figure 8. Depletion of EHBP-1 result in germline developmental defect. 174
Figure S1. 175
Figure S2. Over-expression of mutant form of EHBP-1(aa1-711) lacking RAB-10 interacting coiled-coil region induced dominant negative phenotypes 178
Figure S3. *ehbp-1* RNAi knockdown does not affect RAB-11-positive endosomal subcellular distribution 179
CHAPTER 5: ARF-6 GTPase-ACTIVATING PROTEIN CNT-1 INTERACTS WITH RAB-10 AND REGULATES ENDOCYTIC RECYCLING OF CLATHRIN-INDEPENDENT CARGO 180
AUTHOR CONTRIBUTIONS 181
SUMMARY 182
INTRODUCTION 184
RESULTS 188
RAB-10 binds to the C-terminal ANK repeats of CNT-1 188
CNT-1 colocalizes with RAB-10 189
CNT-1 functions with ARF-6 190
Loss of CNT-1 affects cargo localization 191
RAB-10 is required for CNT-1 endosomal recruitment 192
Loss of CNT-1 or RAB-10 leads to increased accumulation of PI(4,5)P2 193
Endosome morphology defects in CNT-1 and ARF-6 mutants 195
Clathrin accumulates on CNT-1 positive endosomes in *arf-6* mutants 197
DISCUSSION 198
MATERIALS AND METHODS 201

General Methods and Strains 201
Yeast Two-hybrid Analyses 201
Plasmids and Transgenic Strains 202
Microscopy and Image Analysis 202
ACKNOWLEDGEMENTS 204
Table 1. Transgenic and Mutant Strains Used in This Study 205
Figure 1. EHBP-1 physically interacts with RAB-10(Q68L) and RAB-8(Q67L) 207
Figure 2. CNT-1 colocalizes with RAB-10 on endosomes and regulates hTAC recycling 208
Figure 3. CNT-1 lost its endosomal association in *rab-10(q373)* mutants and ARF-6 associates with vacuoles in recycling mutants. 210
Figure 4. Up-regulation of subcellular PH-GFP (PI(4,5)P2) in *cnt-1(tm2313)* mutants. 211
Figure 5. PH-GFP labels recycling endosomes and accumulates on enlarged endosomes in recycling defective mutants. 212
Figure 6. Loss of CNT-1 induces RAB-10-labeled endosomes accumulation and recycling membrane structures mislocalization. 214
Figure 7. Clathrin accumulates and overlaps with CNT-1 on enlarged endosomes in *arf-6* mutants 215
Figure S1. RAB-8 colocalizes with CNT-1 on endosomes and accumulates in *cnt-1* mutants. 217
Figure S2. RAB-10 and CNT-1 co-accumulate on endosomes in *arf-6* mutants. 218
Figure S3. ARF-6 colocalizes with PH-GFP on basolateral tubular and puncta. 219
CHAPTER 6: CONCLUSIONS 220
REFERENCES 225
CURRICULUM VITA 239

CHAPTER 1: INTRODUCTION

An Overview of Endocytosis

Endocytosis and endocytic trafficking of eukaryotes is essential for the internalization and trafficking of macromolecules, fluid, membranes, and membrane proteins. This process is responsible for the uptake and sorting of extracellular macromolecules as well as the components of the cell membrane itself, allowing a complex interplay between cells and their environment. On the other hand, endocytosis process is maintaining cellular homeostasis by recovering protein and lipid components inserted into the plasma membrane by secretory activity in cells. Lots of activities involve endocytosis, such as the transmission of neuronal, metabolic, and proliferative signals, the uptake of essential nutrients, the regulated interaction with the external world, and the immuno-defense against invading microorganisms (Mellman, 1996).

The basic endocytosis cascade involved in the internalization and trafficking within the endosomal system has been well described, but many of the components mediating these steps at the molecular level remain to be identified (Mellman, 1996; Maxfield and McGraw, 2004). There are two basic pathways for endocytic internalization. Some receptors and their associated ligands cluster into clathrin-coated pits. The other type of endocytosis is clathrin-independent (Nichols, 2003; Gesbert *et al.*, 2004). In receptor mediated endocytosis through the clathrin dependent pathway, AP2 or other adaptors recognize cytoplasmic domains, containing aromatic residues usually tyrosine based motif or di-leucine-based motif, of transmembrane proteins. Clathrin is recruited to the plasma membrane (PM) by adaptors and form cage-like structure around pits. After internalization, clathrin uncoats, vesicles fuse with each other and with early endosomes. With reduced pH in early endosomes, some ligand-receptor complexes dissociate due to

slightly lower pH (6.0~6.8) of the endosomal lumen (Forgac, 1992). After dissociation, some receptors recycle to the plasma membrane either directly or indirectly via recycling endosomes (Maxfield and McGraw, 2004). While some specific cargos will utilize retrograde pathway to return to Golgi apparatus, this transport process is critical for the retrieval of the Golgi sorting receptors from endosomes to the TGN in yeast and mammalian cells (Bonifacino and Hurley, 2008). Ligands that are destined for degradation are transported from early to late endosomes and eventually to lysosomes (pH 5.5~6.0). In polarized epithelial cells such as cultured Madin-Darby canine kidney (MDCK) cells, a more complex system exists. There are different specialized apical and basolateral domains (Hoekstra *et al.*, 2004). Apical and basolateral membranes deliver cargo to common endosomes, which can sort cargo from either source to the basolateral PM or to apical recycling endosomes (ARE) which can then ultimately send cargo to the apical PM.

The Nematode *C. elegans* as a Model System

C. elegans is a small soil nematode chosen as a model organism to study development and behavior (Brenner, 1973). It has great potential for genetic analysis for many reasons: Its simplicity, both in anatomy and genomic organization; Short life cycle of 3 days; Small as adult and transparent throughout the life cycle; Large population can be grown on agar plates using E. coli as the food source; Strain can be kept as frozen stocks; Furthermore, it is easy to make and identify mutants using chemical mutagenesis.

C. elegans is used for endocytosis studies for several reasons. The molecular mechanisms of endocytosis are conserved in *C. elegans*. Virtually all of the genes that have been

implicated in endocytosis from previous biochemical and genetic studies can be found in worm genome. The excellent genetic system of worm allows epistasis analysis of complex biochemical pathways. Furthermore, it is common to see *C. elegans* genome contains only single copy of genes that are found in multiple copies in mammalian cells. This benefit reduces the difficulties in functional studies due to functional redundancy. Finally, it is relatively easy to generate mutations with gene disruptions, which offer great benefit to analyze endocytic pathways (Harris *et al.*, 2001). Based on previous studies in our lab, transparent worm intestine presents a good model to study polarized cell membrane trafficking (Chen *et al.*, 2006).

Endocytic Recycling Regulated by RABs and RME-1

Recycling pathways are essential for maintaining the proper composition of various organelles and for returning essential molecules to the appropriate membrane. Endocytic recycling is also essential for maintaining the distinction between apical and basolateral membranes in polarized cells. In all epithelia, the correct return of many proteins to the membrane from which they were removed is essential for maintaining the membrane-protein composition of the apical and basolateral plasma membranes (Maxfield and McGraw, 2004).

There are two main routes back to the cell surface from sorting endosomes. Some fraction of internalized molecules are delivered directly back to the PM whereas others are delivered to a long-lived endocytic recycling compartment (ERC) (Hao and Maxfield, 2000). The direct return of proteins or lipids to the cell surface has been reported to have a t1/2 of about 6 minutes (Sheff *et al.*, 1999). The molecular differences that determine

whether components are sorted back to the plasma membrane occurs using the direct or indirect recycling pathway are not known. The ERC is mainly a collection of tubular organelles that are associated with microtubules (Hopkins, 1983). The distribution of the ERC varies among different cell types. For example, tubules are distributed widely throughout the cytoplasm or can be clustered near the centriole (Lin *et al.*, 2002). The ERC can sort molecules to several different destinations, but most molecules in the ERC return to the plasma membrane. Transport from the ERC requires the formation of vesicular and tubular transport intermediates.

Among functional players involved in the regulation of intracellular trafficking pathways, Rab family GTPase, members of the Ras superfamily of small GTPases, has been extensively studied and demonstrated to function diversely in the intracellular trafficking, including, but not limited, membrane compartments biogenesis, endosomal identity maintenance and cargo sorting through different Rab effectors (Stenmark, 2009). Like other GTPases, Rabs cycle between active GTP-bound state and inactive GDP-bound state. Through direct or indirect interaction with effectors or binding proteins, Rabs functions as coordinator in intracellular trafficking events, such as cargo recruitment, vesicle budding, motor-based delivery of vesicles, vesicle tethering, and fusion of vesicle membrane with target compartment membranes (Grosshans *et al.*, 2006; Stenmark, 2009). Rabs have been shown to regulate endocytic recycling, both fast recycling route directly from early endosome and slow recycling route from ERC (Grant and Donaldson, 2009). Rab4 was identified as an important regulator for recycling of TfR (van der Sluijs *et al.*, 1992), although the precise function of Rab4 in recycling is still open. Rab5 is involved in the formation and function of the early sorting endosome. Rab5 coordinates

with early endosome antigen 1 (EEA1), a phosphoinositide-binding protein, to regulate fusion between primary endocytic vesicles and sorting endosomes (Lawe *et al.*, 2002). Rab5 is not limited to regulating fusion, but also has a role in controlling endosome dynamics by recruiting microtubule motor proteins to endosomes to establish membrane domains (Murray *et al.*, 2002). Rab11, which is localized to the ERC and trans-Golgi-network (TGN) membranes, has a role in recycling to the plasma membrane (Ren *et al.*, 1998). When Rab11 function is altered, transferrin receptors remain concentrated in the ERC. Efflux from the ERC is blocked. In addition, Rab11 was shown to mediate recycling transport of clathrin-independent recycling cargos (Powelka *et al.*, 2004; Weigert *et al.*, 2004). Studies by Kouranti et al. demonstrated Rab35 as an important regulator of TfR rapid recycling (Kouranti *et al.*, 2006). Whereas, in HeLa-CIITA cells, Rab35 was also found on Arf6 and EHD1 positive tubular endosomes of slow recycling pathway (Walseng *et al.*, 2008).

RAB-10 was demonstrated to be crucial for basolateral endocytic recycling in the *C. elegans* intestine (Chen *et al.*, 2006). In *C. elegans* intestine and polarized MDCK cells, RAB-10/Rab10 has been implicated in clathrin-independent recycling cargo transport between early endosomes and recycling endosomes (Babbey *et al.*, 2006; Chen *et al.*, 2006). Recent work in *C. elegans* suggests that interneuron postsynaptic glutamate receptor recycling also requires RAB-10 (Glodowski *et al.*, 2007). RAB-8 and RAB-10 are the closest relatives of yeast Sec4p in metazoans. Rab8 has been suggested to function in the secretary pathway in mammalian cells (Hattula *et al.*, 2002; Ang *et al.*, 2003), and this delivery process may use the recycling endosomes as an intermediate (Ang *et al.*, 2004). In polarized MDCK cells, simultaneous Rab8 and Rab10 siRNA

treatment produced more severe exocytosis defects than individual knockdown (Schuck *et al.*, 2007), implying that Rab8 and Rab10 may function redundantly in exocytic membrane trafficking.

Some recycling specific regulators have been characterized recently, such as Eps15-homology-domain protein Ehd1/RME-1 (Grant *et al.*, 2001; Lin *et al.*, 2001). *rme-1* mutants display endocytic recycling defects in several tissues (Grant *et al.*, 2001). *rme-1* related defects include strongly reduced uptake of yolk proteins by oocytes, because of poor recycling of yolk receptors, reduced uptake of fluid-phase markers by coelomocytes, and the accumulation of gigantic fluid-filled recycling endosomes in the intestinal cells, due to defective recycling of pseudocoelomic fluid. The accumulation of large fluid-filled endosomes in the worm intestine is a hallmark phenotype that can be used to identify mutants with basolateral recycling defects. When recycling is blocked by pharmacological means in either MDCK cells (Apodaca *et al.*, 1994) or HepG2 cells (van Weert *et al.*, 2000) gigantic endosomal structures similar to those described in *C. elegans rme-1* mutant intestinal cells are formed. Evidence from studies of mammalian Ehd1 also suggests a function for RME-1 in recycling, specifically in the exit of membrane proteins from recycling endosomes. All members of the RME-1 family contain a predicted P-loop nucleotide-binding site near the amino terminus, followed by a central predicted coiled-coil domain, and a predicted C-terminal EH domain (Grant *et al.*, 2001). The EH domain is associated with endocytic transport in mammalian cells and yeast (Santolini *et al.*, 1999). Previous studies indicated that the EH domain of RME-1 homologs and other EH domain proteins interact with target proteins through specific

binding to sequences containing *Asparagine-Proline-Phenylalanine* (NPF) motifs. These studies show a conserved function in the endocytic recycling for the RME-1 family.

Multi-function Protein ALX-1

In a yeast 2-hybrid screen using the RME-1 C-terminus, including EH domain, as bait, we identified a novel interacting protein called ALX-1. ALX-1 is the *C. elegans* homolog of mammalian Alix and yeast Bro1p. Alix and Bro1p have been reported to function in the MVB pathway (Katoh *et al.*, 2003; Odorizzi *et al.*, 2003).

Multi-vesicular bodies (MVBs) are endosomes containing lumenal vesicles formed by inward invagination of the limiting membrane. MVBs are believed to be intermediates in the maturation of early endosomes into late endosomes. Membrane proteins sorted into the lumenal vesicles of MVBs are degraded upon fusion of the MVBs with lysosomes in metazoans and with vacuoles in yeast (Gruenberg and Stenmark, 2004). MVBs are critical loci for sorting and the down-regulation of receptors such as growth factor receptors (Hicke, 2001). Mono-ubiquitination is a major signal for cargo entry into lumenal MVB vesicles. The sorting of cargo and budding of vesicles into the lumen of the MVB depends on a network of approximately 18 proteins in yeast (Bowers *et al.*, 2004). The sorting network is about 26 proteins in human (Strack *et al.*, 2003; von Schwedler *et al.*, 2003). The MVB sorting network proteins are organized into four major hetero-oligomeric complexes and several monomeric or homo-oligomeric proteins: Vps27/Hse1 complex (Hrs/STAM in humans), ESCRT-I, II, and III, and the AAA ATPase Vps4, the deubiquitinating enzyme Doa4, and Alix/Bro1p. According to the current model, the sorting of cargo into MVBs is initiated by Hrs, which is recruited to

phosphatidylinositol 3-phosphate (PI3P) containing endosomes by its FYVE domain (Raiborg *et al.*, 2001b). The Hrs and ESCRT-I and II complexes are assembled in the cytosol and translocate to endosomes. Mono-ubiquitinated cargo is recruited by Hrs and handed off to ESCRT-I, which binds mono-ubiquitin via the UEV domain of the Tsg101/Vps23 subunit (Katzmann *et al.*, 2001). There is a second hand-off to ESCRT-II. The ESCRT-III complex assembles on membranes and is intimately associated with the nascent invaginating vesicle. ESCRT-III is involved in recruiting Bro1 (Odorizzi *et al.*, 2003; von Schwedler *et al.*, 2003) as well as Vps4, which catalyzes the disassembly of ESCRT complexes from endosomal membranes.

Alix was first discovered as ALG-2-interacting protein 1 (AIP1) (Vito *et al.*, 1999) and referred as Alix (Missotten *et al.*, 1999). Alix contains a C-terminal Proline-Rich-Domain (PRD) that interacts with the endocytic proteins SETA (Schmidt *et al.*, 2004), endophilins (Chatellard-Causse *et al.*, 2002), and the ESCRT-I subunit Tsg101 (Strack *et al.*, 2003; von Schwedler *et al.*, 2003). Alix interacts with HIV-1 and other retroviral proteins containing the motif YPXL (Martin-Serrano *et al.*, 2003; Strack *et al.*, 2003; von Schwedler *et al.*, 2003), and the Aspergillus Alix homolog PalA interacts with the YPXL -containing host protein, PacC (Vincent *et al.*, 2003). Alix also interacts with the ESCRT-III subunit, CHMP4b (Katoh *et al.*, 2003; Katoh *et al.*, 2004). MVBs have been reported to be rich in the unusual phospholipid 2,2′ lysobisphosphatidic acid (2,2′ LBPA). Cytosolic Alix was found to be preferentially recruited by liposomes containing LBPA by comparasion with liposomes lacking LBPA. LBPA possesses the capacity to drive the formation of membrane invaginations within acidic liposomes. Alix could be a possible target for this lipid and potentially regulates invagination process (Matsuo *et al.*, 2004).

The yeast homolog of Alix, Bro1p recruits Doa4, which deubiquitinates MVB cargo proteins (Luhtala and Odorizzi, 2004). Yeast Bro1 lacks a PTAP sequence and does not interact strongly with Vps23, but Bro1 does bind to the yeast CHMP4 homolog Snf7 (Odorizzi *et al.*, 2003).

ALX-1, Alix and Bro1p have in common a conserved ~380 amino acid motif (Kim *et al.*, 2005) near their N terminus that is annotated as a "Bro1 domain" in the Pfam database (Bateman *et al.*, 2002). Bro1 domain is necessary and sufficient for the endosomal localization of Bro1 and mediates membrane binding. The C-terminal PRD of ALX-1/Alix/Bro1p is responsible for interacting with the most proteins that connect ALX-1 to different cellular processes. Studies in yeast have shown that Bro1p functions in concert with components of the ESCRT machinery to regulate MVB formation. Alix also associates with structural proteins of the cytoskeleton, including actin and tubulin, and is important for the actin-dependent intracellular positioning of endosomes in tissue culture cells (Cabezas *et al.*, 2005).

Although Alix/Bro1p has been suggested to function in multiple cellular processes, its precise function still remains poorly defined.

Ehbp1 Functions in the GLUT4 Recycling Regulation

Our yeast two-hybrid screen, using active RAB-10 mutant form as bait, recovered worm EHBP-1. Like its human homolog Ehbp1 (EH-domain binding protein 1), worm EHBP-1 contains an N-terminal type 1 like CH (Calponin Homology) domain. CH domain belongs to a superfamily of actin-binding domains found in cytoskeletal bundling proteins such as actinin, spectrin, and plectin (Gimona *et al.*, 2002; Borrego-Diaz *et al.*,

2006). Studies on CH domain interaction indicated that multiple CH domains are required to bind F-actin (tandem CH domains) (Gimona *et al.*, 2002). Recent works demonstrated novel microtubule binding capacity of CH domain, like actin binding, association with microtubule also needs two CH domains from two individual subunits within the same complex (Slep and Vale, 2007). Nevertheless, F-actin associating protein IQGAP1 N-terminal CH domain of IQGAP1 alone showed binding with actin filament and colocalization with cortical actin filaments in vivo (Mateer *et al.*, 2004). The presence of CH domain suggests that EHBP-1 may associate with actin and function in the processes of bundling actin fibers.

Additionally, studies in mammal indicated that Ehbp1 binds to Ehd1 (mammalian homologues of *C. elegans* RME-1) through its five NPF (Asn-Pro-Phe) motifs, regulating the endocytotic recycling of GLUT4 (Glucose transporter 4) (Guilherme *et al.*, 2004b).

ARF-6 and its GTPase-Activating Protein (GAP) CNT-1 in Endocytic Recycling

In addition to EHBP-1, our yeast two-hybrid screen of potential interaction partners of RAB-10 also yields full length CNT-1. CNT-1 is the *C. elegans* homolog of mammalian Arf6 GTPase-activating proteins ACAP1/2 (Arf GAP, with Coil, ANK repeat, PH domain). Arf6 (ADP-ribosylation factor 6) belongs to Arf family of small GTPase. There are six mammalian Arfs and many more Arf-like proteins. The ADP-ribosylation factor (Arf) family of proteins belongs to the Ras superfamily of small GTPases with low molecular mass (~20 kDa) expressed in all eukaryotes. Arf proteins have been shown to regulate membrane trafficking. Like other GTPases, Arf proteins cycle between inactive

GDP-bound and active GTP-bound states. In the active state, Arfs interact with proteins and other molecules to carry out their functions. Arf1 and Arf6 are the most well studied members of this family. Arf1 and its activities at the Golgi complex have been extensively reported. Unlike Arf1, Arf6 is involved in membrane trafficking and actin cytoskeleton regulation at the plasma membrane and endosomes.

Mammalian Arf6 and its *C. elegans* homolog share 89% identity. All Arfs are N-terminally myristoylated, which helps target them to membranes. A characteristic di-peptide sequence (Gln-Ser) (Al-Awar *et al.*, 2000) adjacent to the effector domain interaction site (Switch I) allows orthologues of Arf6 to be identified. During the GTPase cycle, Arf6-GDP, unlike Arf1-GDP, is retained on membranes to a large extent (Cavenagh *et al.*, 1996; Song *et al.*, 1998).

There are many cellular functions of Arf6 reported; especially the activities of Arf6 at the plasma membrane. Published data suggest Arf6 is activated and inactivated at many locations and are thought to recruit cytosolic coat proteins onto membranes *in vitro* to facilitate sorting and vesicle formation, activate lipid-modifying enzymes, and modulate of actin structures.

There have no identified coat proteins that are recruited to membranes by active Arf6 *in vivo*. But Arf6 can recruit AP2 to liposomes *in vitro* (Paleotti *et al.*, 2005). Arf6 has been shown to be closely associated with membrane lipid modifications and modulation of the actin cytoskeleton (D'Souza-Schorey and Chavrier, 2006). In tissue culture cells, Arf6 localizes with and activates PIP5KI (Honda *et al.*, 1999). PIP5KI is responsible for generating phosphatidylinositol 4,5-bisphosphate (PIP2), a major PM phosphoinositide involved in membrane traffic and actin rearrangements (Honda *et al.*, 1999; Yin and

Janmey, 2003). These results provide us with an important clue to understanding Arf6 function. Arf6 also activates phospholipase D (PLD), an enzyme that hydrolyzes phosphatidylcholine to produce phosphatidic acid (PA). PA can also activate PIP5KI. Thus by activating PIP5KI directly and indirectly, Arf6 stimulates production of PIP2.

Arf6-GTP has also been reported to be implicated in clathrin dependent endocytosis at the apical membrane in polarized epithelial MDCK cells. Arf6(Q67L) was shown to enhance endocytosis at the apical membrane only (Altschuler *et al.*, 1999). In HeLa cells, Arf6(Q67L) induces PIP2 and actin coated endosome accumulation, sequestering clathrin independent cargos but not affecting clathrin dependent cargo. These results suggest a different Arf6 function in clathrin independent endosomal transport (Brown *et al.*, 2001).

In addition to its PM localization, Arf6 is associated with endosomal membranes in many cells (Peters *et al.*, 1995). A requirement for Arf6 in endosome recycling was first documented in CHO cells, in which the expression of a dominant negative Arf6(T27N) mutant blocked the recycling of endosomal ligands (D'Souza-Schorey *et al.*, 1998). In TRVb-1 cells, EFA6 (Arf6 specific GEF) regulates constitutive endosomal recycling to the cell surface (Franco *et al.*, 1999). In HeLa cells, Arf6 activity affects the recycling of integral plasma-membrane proteins that lack cytoplasmic AP2 and clathrin sorting sequences, including the IL2 receptor α-subunit (TAC), MHCI, and glycosylphosphatidylinositol (GPI) anchored proteins (Radhakrishna and Donaldson, 1997; Naslavsky *et al.*, 2003). Arf6 labeled recycling tubules in these cells exhibit little overlap with early endosomes and radiate from the juxtanuclear cell region to the cell periphery. Recycling through this tubular system also involves the Ehd1/RME-1 (Caplan *et al.*, 2002) and PLD (Jovanovic *et al.*, 2006). MHCI and Arf6 are present on

Ehd1/RME-1 positive tubular compartments (Caplan *et al.*, 2002). Arf6(N48R/I) mutants expressed in HeLa cells blocked PLD activation by Arf6, inducing accumulation of tubular endosomes and blocking recycling. These results suggested functional involvement of PLD in the recycling pathway (Jovanovic *et al.*, 2006). The traffic of membrane proteins that enter cells either through clathrin independent pathways or through the classic clathrin mediated pathway may converge in early endosomes (Naslavsky *et al.*, 2003).

Arf6 activation and inactivation are catalyzed by guanine nucleotide exchange factors (GEFs) that facilitate GTP binding and GTPase-activating proteins (GAPs) that catalyze GTP hydrolysis. Generally Arf6 GEFs are fungal metabolite brefeldin A insensitive, in contrast with other Arf GEFs (Jackson and Casanova, 2000). The ARNO/cytohesin and EFA6 families of Arf6 GEFs contain a catalytic Sec7 homology domain and a pleckstrin homology domain (PH) thought to be involved in membrane targeting (Jackson and Casanova, 2000). Another Arf6-specific GEF, ARF-GEP100, also contains an IQ motif and localizes to endosomal membranes (Someya *et al.*, 2001).

There are even more candidate Arf6 GAPs. These multidomain GAPs proteins contain the Arf GAP domain, pleckstrin homology, Src homology 2/3, and proline rich domains capable of interacting with a multitude of signaling molecules that impact the actin cytoskeleton. There are two major types of Arf GAPs, ArfGAP1 and AZAP. ACAP1/2 (Centaurin beta 1/2) belongs to AZAP-type, characterized by a PH, Arf GAP and C-terminal ANK repeat (Inoue and Randazzo, 2007). Biochemical studies suggest that ACAP1/2 have preference for Arf6 over Arf1 and could be activated by PI(4,5)P2 (Jackson *et al.*, 2000). Previous studies on ACAP1 in mammalian cells showed that

ACAP1 is part of a clathrin complex and functions in the TfR and integrin recycling (Dai *et al.*, 2004; Li *et al.*, 2005; Li *et al.*, 2007). In addition, it has been reported that PI5-kinase, which produces PIP2 and positively regulated by Arf6, could function together with ACAP1 to enhance endosomal tubulation (Shinozaki-Narikawa *et al.*, 2006). These observations suggest that ACAP1 could function as adaptor in the recycling process. Although ACAPs/CNT-1 is identified as Arf6 GAP and thought to function in membrane recycling of some cargos in mammal, its precise role and its functional connection with other recycling regulators remain poorly defined in polarized epithelia.

Endosome to Golgi Retrograde Transport and RME-8

The early endosome is the major place where membrane proteins sorting happen. Some specific cargos will be recycled from endosomes to the trans-Golgi network (TGN) via retrograde transport. The retrograde pathway has been shown to be vital for the retrieval of the Golgi sorting receptors from endosomes to the TGN in yeast and mammalian cells (Bonifacino and Hurley, 2008), including receptors that transport degradative enzymes to the vacuole/lysosome such as Vps10 and CI-MPR (cation-independent mannose 6-phosphate receptor) (Marcusson *et al.*, 1994; Arighi *et al.*, 2004; Carlton *et al.*, 2004; Seaman, 2004). Interestingly, retromer-dependent retrieval of the Wnt-ligand chaperone MIG-14/Wntless has been demonstrated recently (Belenkaya et al., 2008; Franch-Marro et al., 2008; Pan et al., 2008; Port et al., 2008; Yang et al., 2008). Retromer is the major regulation complex in the retrograde transport, consisted of a core complex Vps5-Vps17 (SNX1/2-SNX5/6 in mammals) and a cargo recognition complex Vps26-Vps29-Vps35 (Bonifacino and Hurley, 2008; Collins, 2008). Additionally, clathrin and clathrin related proteins (such as epsinR and AP-1) have also been reported to function as components of

the retrograde transport machinery. Clathrin and clathrin adaptor epsinR are required for retrograde transport of the Shiga toxin B subunit (Lauvrak et al., 2004; Saint-Pol et al., 2004) and clathrin adaptor AP-1 is required for retrograde transport of CI-MPR (Meyer et al., 2000).

RME-8 was originally identified in *C. elegans* as a temperature sensitive lethal mutant defective in endocytosis (Grant and Hirsh, 1999; Zhang et al., 2001). RME-8 is normally abundant on endosomes but not the plasma membrane (Zhang et al., 2001). Studies in Drosophila also showed endocytic defects in several tissues of *rme-8* mutant (Chang et al., 2004). In our effort of looking for binding partner of RME-8, yeast two-hybrid screening yielded SNX-1, worm homolog of mammalian SNX1/2.

RME-8 contains a central DNA-J domain and four repeated motifs (IWN repeats) of unknown function (Zhang *et al.*, 2001; Chang *et al.*, 2004; Silady *et al.*, 2004; Girard *et al.*, 2005). DNA-J domains in general are a characteristic feature of Hsc70 co-chaperones, stimulating Hsc70 ATPase activity (Walsh et al., 2004). RME-8 is the only DNA-J domain protein reported to localize to endosomes. Drosophila and human RME-8 J-domains have been shown to physically interact with Hsc70 (Chang et al., 2004; Girard et al., 2005). Drosophila Hsc70 mutants interact with *rme-8* mutants genetically, and dominant negative Hsc70 expressed in mammalian cells impairs endosome function (Newmyer and Schmid, 2001; Chang *et al.*, 2002). These results suggested that RME-8 could mediate its effects on endosomes as an endosomal Hsc70 co-chaperone. However, precise membrane trafficking function of RME-8 and its functional connection with retromer remain unknown.

CHAPTER 2: A NOVEL REQUIREMENT FOR *C. elegans* Alix/ALX-1 IN RME-1 MEDIATED MEMBRANE TRANSPORT

AUTHOR CONTRIBUTIONS

This chapter was published as presented here in *Current Biology (Shi et al., 2007)*.

I participated in the experimental design, performed all the *C. elegans* related experiments, biochemical experiments (Figures 2-4, 6-7 and Supplemental figures 1-8) and wrote the paper. Dr. Saumya Pant performed the Beta Gal assay (Figure 1). Dr. Zita Balklava performed the mammalian cell experiments. Dr. Carlos Chen and Vanesa Figueroa participated in *C. elegans* strains buildup. Dr. Barth D. Grant designed the experiments, trained me for all *C. elegans* experiments and wrote the paper.

SUMMARY

Alix/Bro1p family proteins have recently been identified as important components of multivesicular endosomes (MVEs) involved in the sorting of endocytosed integral membrane proteins, interacting with components of the ESCRT complex, the unconventional phospholipid LBPA, and other known endocytosis regulators. During infection Alix can be co-opted by enveloped retroviruses, including HIV, providing an important function during virus budding from the plasma membrane. In addition Alix is associated with the actin cytoskeleton and may regulate cytoskeletal dynamics.

Here we demonstrate a novel physical interaction between the only apparent Alix/Bro1p family protein in *C. elegans*, ALX-1, and a key regulator of receptor recycling from endosomes to the plasma membrane called RME-1. Analysis of *alx-1* mutants indicates that ALX-1 is required for endocytic recycling of specific basolateral cargo in the *C. elegans* intestine, a pathway previously defined by analysis of *rme-1* mutants. Expression of truncated human Alix in HeLa cells disrupts recycling of MHCI, a known Ehd1/RME-1 dependent transport step, suggesting phylogenetic conservation of this function. We show that the interaction of ALX-1 with RME-1 in *C. elegans*, mediated by RME-1/YPSL and ALX-1/NPF motifs, is required for this recycling process. In the *C. elegans* intestine ALX-1 localizes to both recycling endosomes and MVEs, but the ALX-1/RME-1 interaction appears dispensable for ALX-1 function in MVEs/late endosomes.

This work provides the first demonstration of a requirement for an Alix/Bro1p family member in the endocytic recycling pathway in association with the recycling regulator RME-1.

INTRODUCTION

The endocytic pathway of eukaryotes is essential for the internalization and trafficking of macromolecules, fluid, membranes, and membrane proteins. Membrane associated receptors and ligands are endocytosed either through clathrin-dependent or clathrin-independent uptake mechanisms (Nichols, 2003; Gesbert *et al.*, 2004). After sorting in early endosomes, some cargo is transported from early to late endosomes and eventually to lysosomes for degradation (Mukherjee *et al.*, 1997). Other cargo types recycle to the plasma membrane either directly, or indirectly via recycling endosomes (Mukherjee *et al.*, 1997; Maxfield and McGraw, 2004). Studies in HeLa cells indicate that receptors internalized via clathrin-dependent and clathrin-independent mechanisms meet in the endosomal system, but then recycle to the cell surface in distinct carriers (Naslavsky *et al.*, 2004b).

In recent years it has become clear that Alix/Bro1p family proteins are conserved components of endosomal transport pathways. Alix and Bro1p are thought to function in the multivesicular endosome (MVE) pathway, promoting degradation of integral membrane proteins (Katoh *et al.*, 2003; Odorizzi *et al.*, 2003). Multi-vesicular endosomes contain lumenal vesicles formed by inward invagination of the limiting membrane, and likely represent intermediates in the maturation of the pleiomorphic early/sorting endosomes into late endosomes (Katzmann *et al.*, 2002). Membrane proteins sorted into the lumenal vesicles of MVEs are degraded upon fusion of the MVEs with lysosomes in metazoans and with the vacuole in yeast (Gruenberg and Stenmark, 2004). The sorting of cargo, and budding of vesicles into the lumen of the MVE, depends on a network of proteins organized into four major hetero-oligomeric complexes and several monomeric

or homo-oligomeric proteins: the Vps27/Hse1 complex (Hrs/STAM in humans), ESCRT-I, II, and III, the AAA ATPase Vps4, the ubiquitin hydrolase Doa4p, and Alix/Bro1p.

Alix and Bro1p contain a conserved ~380 amino acid "Bro1 domain" near their N termini (Bateman *et al.*, 2002; Kim *et al.*, 2005). Alix/Bro1p also contains a central V domain (aa 362-702 in Alix) consisting of two extended three-helix bundles and a conserved C-terminal Proline-Rich-Domain (PRD) (Fisher *et al.*, 2007). The Bro1 domain is necessary for the endosomal localization of Alix/Bro1p and mediates membrane association through binding to the ESCRT-III complex subunit Snf7p/CHMP4b (Gavin *et al.*, 2002; Katoh *et al.*, 2003; Katoh *et al.*, 2004; Odorizzi, 2006). The PRD of Alix interacts with a number of endocytic regulatory proteins including SETA (Schmidt *et al.*, 2004), endophilins (Chatellard-Causse *et al.*, 2002), and the ESCRT-I complex subunit Tsg101 (Strack *et al.*, 2003; von Schwedler *et al.*, 2003).

Through the second arm of its V domain, Alix also interacts with HIV-1 Gag and other retroviral proteins containing the motif YPXL, promoting the budding of viral particles from the plasma membrane (Martin-Serrano *et al.*, 2003; Strack *et al.*, 2003; von Schwedler *et al.*, 2003; Fisher *et al.*, 2007). Likewise the Aspergillus Alix homolog PalA interacts with the PacC protein through YPXL motifs (Vincent *et al.*, 2003). *In vitro* Alix is preferentially recruited by liposomes containing the phospholipid 2,2′ lysobisphosphatidic acid (LBPA) (Matsuo *et al.*, 2004). LBPA is enriched in the internal membranes of MVEs and possesses the capacity to drive the formation of membrane invaginations within acidic liposomes (Matsuo *et al.*, 2004). It has been suggested that Alix is a target for this important lipid, potentially regulating the invagination process or back fusion of internal vesicles with the limiting membrane (Matsuo *et al.*, 2004). Alix

also associates with structural proteins of the cytoskeleton, especially actin (Schmidt *et al.*, 2003; Pan *et al.*, 2006), and is important for the actin-dependent intracellular positioning of endosomes, and the formation of stress fibers, in tissue culture cells (Cabezas *et al.*, 2005; Pan *et al.*, 2006).

We and others have previously established *in vivo* endocytic assay systems for genetic analysis of trafficking in *C. elegans* tissues (Sato and Grant, ; Grant and Hirsh, 1999; Fares and Greenwald, 2001; Fares and Grant, 2002). Among the endocytic regulators found in our screens we identified RME-1 (Grant *et al.*, 2001). *rme-1* mutants display endocytic recycling defects in several tissues (Grant *et al.*, 2001), including strongly reduced uptake of yolk proteins by oocytes, due to poor recycling of yolk receptors, reduced uptake of fluid-phase markers by coelomocytes, and the accumulation of gigantic fluid-filled recycling endosomes in the intestinal cells, due to defective recycling of basolaterally endocytosed pseudocoelomic fluid. Evidence from studies of mammalian Ehd1/mRme-1 also indicates a function in recycling, specifically in the exit of membrane proteins from recycling endosomes (Lin *et al.*, 2001). All members of the RME-1 family contain a C-terminal EH domain (Grant *et al.*, 2001; Naslavsky and Caplan, 2005). The EH domain is associated with endocytic transport in mammalian cells and yeast (Page *et al.*, 1999; Santolini *et al.*, 1999). Previous studies showed that the EH domain of RME-1 homologs, and other EH domain proteins, interact with target proteins through specific binding to sequences containing *Asparagine-Proline-Phenylalanine* (NPF) motifs (Santolini *et al.*, 1999; de Beer *et al.*, 2000; Naslavsky and Caplan, 2005). In mammals, RME-1/Ehd1 forms protein complexes with Syndapin through EH-NPF interactions, which is important for recycling endosome function (Braun *et al.*, 2005).

Here we show that *C. elegans* ALX-1 is physically associated with both recycling endosomes and MVEs, and provide evidence that ALX-1 functions with RME-1 in the *C. elegans* intestine, promoting the recycling of basolateral cargo internalized independently of clathrin. This endocytic recycling regulation requires the RME-1/ALX-1 interaction, and is specifically mediated by RME-1-YPSL and ALX-1-NPF motifs.

.

RESULTS

Physical association of ALX-1 and RME-1

In order to identify new regulators of endocytic recycling we performed a yeast two-hybrid screen for binding partners of RME-1, using the C-terminal region of RME-1 including the EH-domain (isoform D, amino acids 442-576) as bait. This screen identified several interacting clones encoding ALX-1, the *C. elegans* ortholog of human Alix/AIP1 and yeast Bro1p (Figure 1 and Materials and Methods). We confirmed the binding interaction using an *in vitro* GST-pulldown assay (Supplementary Figure S1, as indicated). The novel interaction that we detected between ALX-1 and the recycling endosome protein RME-1 suggested that ALX-1 might function on recycling endosomes, in addition to MVE's, or that RME-1 has a previously undetected function in the MVE.

To clarify interaction domains within RME-1 and ALX-1, we tested a series of truncated versions of the proteins in the two-hybrid assay. This analysis identified two modes of binding between the two proteins. First we noted that the extreme C-terminus of RME-1, just after the EH-domain, contains a tyrosine-proline-X-leucine (YPSL) motif, similar to that used by mammalian Alix to bind to retroviral Gag proteins (Puffer *et al.*, 1997), and that used by Aspergillus PalA to bind to PacC (Vincent *et al.*, 2003). The central region of ALX-1 from amino acids 365-752 was sufficient to mediate the interaction, and deletion of the final nine amino acids of RME-1 including the YPSL sequence completely abrogated the interaction. In addition, we noted that the extreme C-terminus of ALX-1 contains an asparagine-proline-phenylalanine tri-peptide (NPF) motif. The EH-domain of RME-1 homologs, and other EH-domain proteins, are known to bind to NPF

containing sequences (de Beer *et al.*, 2000; Naslavsky and Caplan, 2005). Deletion of the NPF sequence in the context of the yeast two-hybrid prey construct reduced the RME-1/ALX-1 interaction by almost 3-fold, but did not completely block association (Figure 1). The Bro1 domain of ALX-1 was dispensable for the two-hybrid interaction. Taken together these results suggest that the central domain of ALX-1 contributes the main binding surface, interacting with the C-terminus of RME-1 through the YPSL containing tail, while the NPF sequence of ALX-1 interacts with the RME-1 EH-domain, perhaps modulating the interactions.

ALX-1 is broadly expressed in *C. elegans*

To determine what tissues express ALX-1, and are thus cell types where ALX-1 might interact with RME-1 *in vivo*, we created transgenic animals expressing a GFP-ALX-1 translational fusion gene driven by the *alx-1* promoter (see Materials and Methods). We observed ubiquitous expression of GFP-ALX-1 with notably high levels of expression in the intestine, hypodermis, body-wall muscles, nervous system, spermatheca, coelomocytes, and pharynx (Figure 2, A–F). The GFP-ALX-1 fusion protein appeared punctate in most tissues. In the intestine, GFP-ALX-1 was enriched near the apical PM and was also clearly enriched on distinct cytoplasmic puncta in the cytoplasm (Figure 2A, arrowheads). Intestine specific expression of equivalent fusions of ALX-1 to GFP or mCherry produced indistinguishable subcellular localization patterns and rescued *alx-1* mutant phenotypes (see below and Materials and Methods), indicating that the expression pattern and subcellular localization of the reporters very likely reflect those of the endogenous protein.

ALX-1 is associated with recycling endosomes and MVEs in the intestine

Since RME-1 and its mammalian homologs have not been found localized to MVEs, and are not required for membrane protein degradation, but rather are greatly enriched on recycling endosomes and function in recycling, we sought to determine if ALX-1 protein is present on recycling endosomes. First we compared the subcellular localization of intestinally expressed mCherry-ALX-1 with GFP-RME-1, which is found on basolateral recycling endosomes (Grant *et al.*, 2001; Chen *et al.*, 2006). mCherry-ALX-1 colocalized extensively with GFP-RME-1 (Figure 3, A–C). Puncta positive for mCherry-ALX-1 and GFP-RME-1 were more frequent close to the basolateral PM and are best observed in the "Top" focal plane (Figure 3, A–C; Supplementary Figure S2, A-D). Fewer ALX-1 and RME-1 double-positive structures were found in the "Middle" focal planes that offer better views of the medial and apical membranes. These results indicated that ALX-1 is present on basolateral recycling endosomes where it could interact with RME-1 to regulate recycling. Our results also indicated that ALX-1 is present on other unidentified structures in the intestine. We obtained identical results with the fluorescent tags reversed, comparing GFP-ALX-1 with mCherry-RME-1.

Since mammalian Alix and yeast Bro1p are thought to be associated with MVEs, we also compared the localization of mCherry-ALX-1 with GFP-tagged HGRS-1 (Roudier *et al.*, 2005; Yu *et al.*, 2006), the worm ortholog of the MVE protein Hrs/Vps27p. GFP-HGRS-1 mainly colocalized with mCherry-ALX-1 on puncta of the medial and apical cytoplasm (Figure 3, D–F, arrowheads; Supplementary Figure S2, E-H). These results suggest that ALX-1 is present on MVEs in addition to recycling endosomes. We confirmed that the RME-1-labeled recycling endosomes and the HGRS-1-labeled MVEs are independent vesicle populations by directly comparing the subcellular localization of GFP-HGRS-1

and mCherry-RME-1. We did not observe any colocalization between GFP-HGRS-1 and mCherry-RME-1 labeled puncta, substantiating this inference (Figure 3, G–I).

We also compared mCherry-ALX-1 with markers for early endosomes (GFP-RAB-5), late endosomes (GFP-RAB-7), and TGN/apical recycling endosomes (GFP-RAB-11) (Supplementary Figure S3). We observed occasional colocalization of mCherry-ALX-1 with the early endosome markers GFP-RAB-5 and did not observe colocalization with the TGN/ARE marker. mCherry-ALX-1 did not clearly label the large ring-like GFP-RAB-7 positive late endosomes, but some mCherry-ALX-1 puncta appeared on or near the rings. The weak colocalization with early and late endosome markers is consistent with the presence of ALX-1 on MVEs, since MVEs represent an intermediate in the maturation of early endosomes to late endosomes.

Taken together our results indicate that ALX-1 resides on two independent classes of endosomes in the worm intestine where it could potentially contribute to membrane traffic.

ALX-1 positive structure number increases in *rme-1* mutants

As an additional test of the association of ALX-1 with recycling endosomes, we quantified the number of GFP-ALX-1 positive puncta in an *rme-1*(*b1045*) null mutant background. For comparison we also assayed GFP-HGRS-1, which is expected to label MVEs but not recycling endosomes. We previously established that *rme-1* mutant intestines specifically accumulate abnormally high numbers of basolateral recycling endosomes, but do not accumulate increased numbers of early, late, or apical recycling endosomes (Chen *et al.*, 2006). Thus if ALX-1 is associated with basolateral recycling endosomes we would expect to observe an increase in GFP-ALX-1 puncta number. *rme-*

1 null mutant intestines showed a nearly three-fold increase in GFP-ALX-1 puncta number, but no change in GFP-HGRS-1 puncta number (Figure 4, B and C; Supplementary Figure S4). These results are entirely consistent with residence of ALX-1 on basolateral recycling endosomes. These results also indicate that ALX-1 association with such endosomes does not require RME-1.

Loss of ALX-1 results in intracellular accumulation of recycling cargo

Given the physical association and colocalization of ALX-1 and RME-1, we sought to determine if loss of ALX-1 affects basolateral recycling. Toward this end we obtained a deletion allele of *alx-1*, *gk275*, created by the *C. elegans* Gene Knockout Consortium. This mutation deletes the first exon and part of the second exon, and is not predicted to produce any functional ALX-1 protein. *alx-1(gk275)* mutants are viable and at the gross organismal level appeared fairly normal, similar to *rme-1* mutants and several other endocytic trafficking mutants we have previously examined.

As a first step to determine if *alx-1* is required for basolateral recycling, we assayed the localization of basolaterally recycling transmembrane cargo proteins at steady-state, comparing wild-type animals with *alx-1*(*gk275*) mutant animals. Equivalent GFP-fusions for these cargo proteins have previously been shown to be functional and traffic normally in mammalian cells, and we have previously characterized them in the *C. elegans* intestine (Chen *et al.*, 2006). First we assayed for effects on the localization of the α-chain of the human IL-2 receptor TAC (hTAC-GFP), which is a marker for clathrin-independent uptake and *rme-1*-dependent recycling in mammalian cells (Caplan *et al.*, 2002; Naslavsky *et al.*, 2004b), and which we have previously shown accumulates extensively in aberrant endosomes in *C. elegans rme-1* mutants (Chen *et al.*, 2006). We

observed significant aberrant accumulation of hTAC-GFP in cytoplasmic puncta in *alx-1* mutant intestines. hTAC-GFP puncta number was increased by threefold in *alx-1* mutants compared with wild-type controls (Figure 5, C, D and E). These results suggest that the recycling of clathrin-independent cargo requires ALX-1.

We then assayed the human transferrin receptor (hTfR-GFP), which is a marker for clathrin-dependent uptake and *rme-1*-dependent recycling in mammalian cells (Yamashiro and Maxfield, 1984; Burack *et al.*, 2000; Lin *et al.*, 2001). We have previously shown that hTfR-GFP accumulates in aberrant endosomes in *C. elegans rme-1* mutants, but not as extensively as hTAC-GFP (Chen *et al.*, 2006). We could not detect any changes in localization for hTfR-GFP (Figure 5, A and B), suggesting that clathrin dependent cargo recycles normally in the absence of ALX-1.

In order to determine if human Alix is also required for recycling of clathrin-independent cargo, we analyzed major histocompatibility complex class I (MHCI) recycling in HeLa cells using a previously established pulse-chase assay that follows a non-perturbing anti-MHCI monoclonal antibody (Weigert *et al.*, 2004). MHCI is a well documented marker for clathrin-independent uptake and Ehd1/mRme-1-dependent recycling in mammalian cells (Caplan *et al.*, 2002; Naslavsky *et al.*, 2003). Cells transfected with an mRFP1 control vector were compared to cells co-transfected with mRFP1, and a FLAG-tagged dominant negative form of Alix (Alix-CT, amino acids 467-869) (Sadoul, 2006).

MHCI uptake was similar between mRFP1 transfected cells and mRFP1/FLAG-Alix(467-869) co-transfected cells (Figure 5, F, G and J). MHCI recycling in mRFP1/FLAG-Alix(467-869) co-transfected cells was reduced by 12-fold compared to

control mRFP1 transfected cells (Figure 5, H, I and K), suggesting that the requirement for Alix/ALX-1 in this recycling pathway is conserved from worms to mammals.

We also analyzed clathrin-dependent cargo Tf uptake and recycling in HeLa cells using a previously described assay (Weigert and Donaldson, 2005). eGFP/FLAG-Alix(467-869) co-transfected cells showed slightly reduced, but not statistically different, Alexa568-Tf uptake (84.4%±9.8% of control, p=0.055), when compared to control cells transfected with EGFP control plasmid only. There was also no significant difference in the amount of recycled Alexa568-Tf between control eGFP transfected cells (62.2%±15.6%) and eGFP/FLAG-Alix(467-869) co-transfected cells (71.9%±13.9%), which is in agreement with previously published data using Alix siRNA (Cabezas *et al.*, 2005).

***alx-1* mutants accumulate abnormally high numbers of RME-1 positive endosomes.**

The increased number and size of hTAC-GFP labeled puncta in *alx-1* mutants suggested a block in hTAC recycling and a concomitant increase in basolateral recycling endosome number and size, similar to the phenotype of *rme-1* mutants (Grant *et al.*, 2001; Chen *et al.*, 2006). To further analyze the effect of the *alx-1* knockout on recycling endosome number and size we quantified the number of GFP-RME-1 labeled endosomes in *alx-1* mutants. In wild-type animals, GFP-RME-1 strongly labels endosomes very near the basolateral PM (Figure 6A). GFP-RME-1 also weakly labels structures very near the apical PM that could be apical recycling endosomes (Chen *et al.*, 2006). In *alx-1* mutants an abnormally large number of GFP-RME-1 labeled endosomes accumulated, most notably appearing in large numbers throughout the cytoplasm in addition to the normally localized cortical structures (Fig 6B). Image quantitation revealed an approximately three-fold increase in GFP-RME-1 puncta number and size (Figure 6, I and J). No defects

were found in the localization of an apical recycling endosome/TGN associated marker, GFP-RAB-11, in the intestine of *alx-1* mutants (Supplementary Figure S5). These results suggest that ALX-1 is important for the normal function of RME-1-positive basolateral recycling endosomes, and taken together with the effects on hTAC-GFP accumulation in worms, and MHCI recycling in HeLa cells, suggest that ALX-1/Alix is important for efficient export of certain cargo proteins from recycling endosomes. These results also indicate that ALX-1 is not required for the association of RME-1 with endosomes, suggesting that ALX-1 affects RME-1 function rather than its recruitment.

SDPN-1 recruitment to basolateral endosomes fails in *alx-1* mutants.

The F-Bar and SH3 domain protein Syndapin is a regulator of endocytic transport and actin dynamics. Previous work in HeLa cells showed that Syndapin is a binding partner of mammalian Ehd1/mRme-1 on recycling endosomes, and functions with Ehd1/mRme-1 in recycling (Braun *et al.*, 2005). This lead us to test if Syndapin is also involved in the basolateral recycling pathway described here. *C. elegans* has a single ortholog of syndapin, called SDPN-1, and we found that SDPN-1-GFP expressed from its own promoter is highly expressed in the intestine and colocalizes with RME-1 on basolateral recycling endosomes (data not shown). Further analysis showed that *alx-1* mutants lack SDPN-1 on basolateral structures, implying an inability to recruit SDPN-1 to basolateral endosomes (Figure 7, B and H). In *rme-1* mutants basolateral SDPN-1-GFP labeled structures were also significantly altered, characterized by loss of most basolateral SDPN-1-GFP labeled structures, and with many of the remaining structures appearing greatly enlarged (Figure 7, C and F). *alx-1* mutant animals depleted of RME-1 by RNAi displayed a mixed phenotype, with weaker SDPN-1-GFP labeling of endosomes that

appeared enlarged, but less enlarged than in animals lacking RME-1 only (Figure 7, C and D). Apical SDPN-1 appeared normally localized in *alx-1* and *rme-1* mutants. Since Syndapin regulates membrane-associated actin dynamics and promotes membrane tubulation, failure to recruit SDPN-1 to basolateral recycling endosomes may be the primary defect resulting in intracellular accumulation of recycling cargo in *alx-1* mutants.

alx-1 mutants are delayed in the degradation of membrane proteins

Yeast Bro1p functions at the MVE with the ESCRT complex to downregulate membrane associated receptors (Hicke, 2001). Mammalian Alix has also been implicated in the multivesicular body pathway, interacting with ESCRT-I and III (Katoh *et al.*, 2004), and in vitro regulates the dynamics and function of the internal membranes of MVEs through interaction with the LBPA lipid (Matsuo *et al.*, 2004). However, degradation of EGF-Rs, a classic MVE mediated transport event, was unaffected by siRNA mediated knockdown of Alix in HeLa cells (Cabezas *et al.*, 2005). To test for defects in MVE pathway-mediated degradation in *alx-1* mutant worms we analyzed the degradation of CAV-1 protein in early *C. elegans* embryos. This analysis was facilitated by the use of transgenic animals expressing a well characterized CAV-1-GFP fusion protein (Sato *et al.*, 2006). In normal zygotes CAV-1-GFP is exocytosed in a nearly simultaneous wave during Anaphase I of meiosis. CAV-1-GFP is then rapidly internalized and degraded through the standard clathrin pathway (Sato *et al.*, 2006). In normal embryos most CAV-1-GFP disappears by the two-cell stage, and none is visible by the four cell stage (Supplemental Figure S6 A). In *alx-1* mutants, CAV-1-GFP degradation was significantly delayed, with abnormally high levels of internalized CAV-1-GFP remaining in 2-cell and 4-cell embryos (Supplemental Figure S6 C). Quantitative fluorescence measurements of CAV-

1-GFP in 2-cell embryos showed a 12-fold average increase in puncta number compared to wild type (Supplemental Figure S6 I). We observed a similar delay in degradation of RME-2-GFP yolk receptors in *alx-1* mutant embryos (data not shown). These results indicate that ALX-1 is required for efficient degradation of integral membrane proteins, consistent with a conserved role for this protein in MVE function.

We also examined the degradation of a lumenal cargo protein in embryos, YP170-GFP (Grant and Hirsh, 1999). YP170 is a major yolk protein responsible for transporting lipids from the intestine to the oocyte (Matyash *et al.*, 2001). YP170 is secreted by the intestine and endocytosed by oocytes in wild type (Sharrock, 1983; Grant and Hirsh, 1999). During embryogenesis yolk stores are gradually depleted by lysosomal degradation, with some remaining in newly hatched embryos (Sharrock, 1983; Grant and Hirsh, 1999). We did not find any change in the pattern or timing of YP170-GFP degradation in *alx-1* mutants (Supplemental Figure S6, E and G). These results suggest that ALX-1 is not required for transport of lumenal endosome content to lysosomes for degradation.

MVE and late endosome morphology is aberrant in *alx-1* mutants

Analysis in early embryos indicated that ALX-1 is required for degradation of integral membrane proteins (see Supplemental results and Supplementary Figure S6, A-D), a process that does not require RME-1 but does require ESCRT proteins (Audhya *et al.*, 2007b). To assay for changes in the MVE/late endosome pathway in the intestine, we performed endosome morphometric analysis of *alx-1* mutant animals. We did not observe any effect of the loss of ALX-1 on RAB-5 positive early endosome number or size (Supplementary Figure S5). Consistent with a role for ALX-1 in intestinal MVE function we found a two-fold increase in MVE number and size in *alx-1* mutants in GFP-HGRS-1-

expressing strains (Figure 6, D, I and J). We also observed a dramatic effect on GFP-RAB-7 and LMP-1-GFP positive late endosomes, which accumulated in normal numbers but which displayed grossly abnormal morphology (Figure 6, F and H), with an average five-fold increase in late endosome size (Figure 6J). Consistent with our cargo analysis in *alx-1* mutant embryos, these results indicate that MVE and late endosome morphology, and likely their functions, require ALX-1 *in vivo*.

Basolateral recycling endosomes require the interaction of RME-1 with ALX-1

Finally, we sought to specifically test the role of the RME-1/ALX-1 interaction in transport, as opposed to the roles of the individual proteins. This was accomplished by reintroducing interaction defective forms of RME-1 or ALX-1 into their cognate null mutants and assaying for rescue of the loss-of-function phenotypes.

Our yeast two-hybrid studies indicated that RME-1 C-terminal tail containing the YPSL motif is required for RME-1 to bind to ALX-1. To determine the importance of the YPSL tail *in vivo*, and the contribution of ALX-1 binding to RME-1 function, we tested the ability of mCherry-RME-1 lacking the YPSL tail (mCherry-RME-1ΔYPSL) to rescue *rme-1(b1045)* mutants. Expression of mCherry-RME-1(+) or mCherry-RME-1(ΔYPSL) in *rme-1* null mutants fully rescued the formation of abnormal RE vacuoles containing accumulated basolaterally recycling fluid (Figure 7E), indicating that the interaction of RME-1 with ALX-1 is not required for fluid recycling. In stark contrast we found that expression of mCherry-RME-1(+), but not mCherry-RME-1(ΔYPSL), rescued the abnormal intracellular accumulation of hTAC-GFP and the abnormal localization/morphology of GFP-SDPN-1 (Figure 7F; Supplementary Figure S7). The

failure of mCherry-RME-1(ΔYPSL) to rescue these phenotypes suggests that RME-1's function in SDPN-1 recruitment and hTAC recycling requires interaction with ALX-1.

In a similar set of experiments we compared the ability of mCherry-ALX-1 or mCherry-ALX-1 lacking the C-terminal NPF tri-peptide (mCherry-ALX-1ΔNPF) to rescue *alx-1* mutant phenotypes. Interestingly, we found that mCherry-ALX-1(ΔNPF) fully rescued *alx-1(gk275)* phenotypes associated with MVEs and late endosomes, including the abnormal increase in the number of GFP-HGRS-1-labeled endosomes and the size/morphology defects in LMP-1-GFP labeled late endosomes (Figure 7, G and H; Supplementary Figure S8). These results further confirm that RME-1 is not required for these functions of ALX-1. By contrast mCherry-ALX-1(ΔNPF) could not rescue the recycling associated phenotypes of *alx-1* mutants, including hTAC-GFP accumulation or basolateral recruitment of GFP-SDPN-1 (Figure 7H; Supplementary Figure S8). As expected mCherry-ALX-1(+) rescued both the MVE/late endosome and RE associated phenotypes of *alx-1* mutants (Figure 7, G and H; Supplementary Figure S8). These results genetically separate the functions of ALX-1, indicating that the effects of *alx-1* mutants on hTAC and SDPN-1 are through RME-1 on recycling endosomes, and are not indirect effects produced by defective MVEs or late endosomes.

DISCUSSION

In this study we show for the first time that an Alix/Bro1p family member functions in the endocytic recycling pathway, in association with the recycling endosome regulator RME-1. We also show that ALX-1 is required for the degradation of membrane proteins in *C. elegans*, likely functioning with the ESCRT machinery in the multivesicular endosome, as is thought to be the case for other members of the Alix/Bro1p family (Odorizzi *et al.*, 2003). Consistent with our previous studies showing that RME-1 does not function in early or late endosomes, we found that RME-1 does not colocalize with HGRS-1-positive MVE's in the intestine and *rme-1* null mutants display normal degradation of membrane proteins in early embryos. In addition *rme-1* mutants display normal HGRS-1 labeled MVE morphology and number in the intestine. Thus our studies indicate a dual requirement for ALX-1 in both the recycling and degradative pathways, while RME-1 is specific for recycling.

Previous studies indicated that mammalian Alix facilitates virus budding from the plasma membrane of infected cells through direct binding to the sequence motif YPXL within viral Gag protein late-budding domains (Martin-Serrano *et al.*, 2003; Strack *et al.*, 2003; von Schwedler *et al.*, 2003). Similarly the Aspergillus Alix/Bro1p homologue PalA interacts with its partner protein PacC through YPXL motifs (Vincent *et al.*, 2003). Our studies indicate an important interaction between the central region of ALX-1 and a C-terminal YPSL sequence in RME-1. In addition, the C-terminal NPF sequence in ALX-1 contributes to the interaction between ALX-1 and RME-1, presumably through the NPF-binding pocket present in the EH-domain. The NPF-mediated interaction between ALX-1 and RME-1 is required for the function of ALX-1 in recycling, but appears to be

dispensable for ALX-1 function in MVE's/late endosomes. This genetic separation of the two functions of ALX-1 indicates mechanistic differences between ALX-1's roles in these two aspects of endocytic transport.

Consistent with a dual function for ALX-1 *in vivo*, we found evidence for ALX-1 localization to both types of endocytic organelles, the HGRS-1-positive MVE and the RME-1-positive recycling endosomes. Interestingly, recent studies in human T cells and macrophages using quantitative EM methods revealed an enrichment of endogenous human Alix on tubular-vesicular endosomal membranes containing transferrin, consistent with residence of human Alix on recycling endosomes (Welsch *et al.*, 2006). Alix siRNA in HeLa cells was reported not to affect transferrin recycling but did affect endosome morphology (Cabezas *et al.*, 2005). In this study we found that expression of dominant negative Alix in HeLa cells dramatically interfered with MHCI recycling, but did not significantly affect transferrin recycling, suggesting that the role of Alix in recycling cargo endocytosed independently of clathrin is a conserved function. We note however that the interaction sites that we identified between *C. elegans* RME-1 and ALX-1 do not seem to be conserved in their human homologues. Similarly, although human Syndapin binds to Ehd1/mRme-1 directly, and worm SDPN-1 appears to function with RME-1 in recycling, the NPF containing sequences in Syndapin I and II recognized by Ehd1 are lacking in Ce-SDPN-1. Thus while our results suggest that these proteins function together in worms and mammals, the binding modes among those proteins may have been shuffled during metazoan evolution.

In yeast, the ALX-1 homolog Bro1p is required at the limiting membrane of specialized MVEs (Odorizzi *et al.*, 2003) for the sorting of mono-ubiquitinated membrane proteins

into lumenal vesicles and productive transport to the vacuole (Katzmann *et al.*, 2002). However some controversy remains over the requirement for Alix in MVE-mediated degradation of membrane proteins, since Alix depleted HeLa cells were not delayed in the degradation of EGF receptors (Cabezas *et al.*, 2005). Alix is clearly required for the budding of retroviruses in mammals, another transport process that utilizes the MVE/ESCRT machinery (Martin-Serrano *et al.*, 2003; Strack *et al.*, 2003; von Schwedler *et al.*, 2003; Fisher *et al.*, 2007). In *C. elegans alx-1* mutants we observed defects in intestinal MVE/late endosome morphology and a very significant delay in the degradation of endocytosed membrane proteins CAV-1-GFP and RME-2-GFP in embryos, indicating conservation of this function in nematodes. Consistent with our results, Shaye and Greenwald (Shaye and Greenwald, 2005) reported that degradation of LIN-12/Notch receptors in vulval precursor cells is delayed in animals depleted of ALX-1 by RNAi methods. Although there are no previously known mechanistic links between the degradative and recycling branches of the endocytic pathway, it may be advantageous for the cell to coordinate transport through multiple branches in the pathway, perhaps allowing a coordinated response to changes in cargo-type, overall cargo-load, and/or the local cellular environment.

While RME-1/mRme-1/Ehd1 is required for the efficient recycling of cargo internalized by clathrin-dependent and clathrin-independent mechanisms (Grant *et al.*, 2001; Lin *et al.*, 2001; Caplan *et al.*, 2002; Chen *et al.*, 2006), our results suggest that ALX-1 is specifically required to recycle cargo of the clathrin-independent class. Consistent with this functional difference, not all basolateral RME-1 positive structures appear positive

for ALX-1. Also, basolateral fluid recycling, that can likely utilize either RME-1 dependent recycling pathway, does not appear to require the RME-1/ALX-1 interaction.

While the mechanisms controlling the recycling of clathrin-independent cargo remain poorly defined, it is clear that local actin dynamics on endosomal membranes are important for productive transport of such cargo from recycling endosomes to the plasma membrane. For instance inhibition of actin polymerization using drugs such as latrunculin A or cytochalasin D, specifically disrupts recycling of clathrin-independent cargo in HeLa cells such as MHCI and Tac, while under the same conditions the clathrin-dependent cargo transferrin recycles normally (Radhakrishna and Donaldson, 1997; Brown *et al.*, 2001; Weigert *et al.*, 2004). Likewise the membrane associated actin regulator Arf6 is required to recycle clathrin-independent, but not clathrin-dependent cargos (Naslavsky *et al.*, 2004b). Interestingly knockdown of Alix in HeLa cells is known to perturb intracellular actin distribution, and Alix has been reported to copurify with cytoskeleton components, suggesting a possible functional link between Alix family proteins and membrane associated actin dynamics (Schmidt *et al.*, 2003; Cabezas *et al.*, 2005; Pan *et al.*, 2006). Syndapin is known to facilitate recruitment of N-WASP to membranes, thus activating Arp2/3-directed actin branching and polymerization (Qualmann and Kelly, 2000; Kessels and Qualmann, 2004). We found that *alx-1* mutants showed greatly reduced recruitment of SDPN-1/Syndapin to basolateral endosomes, suggesting that ALX-1 promotes recycling through SDPN-1/Syndapin, and possibly N-WASP and the Arp2/3 machinery. As actin dynamics are thought to promote vesicle scission at the plasma membrane of yeast and mammalian cells, RME-1, ALX-1, and SDPN-1 may act in a similar way to promote endosomal carrier scission.

MATERIALS AND METHODS

General Methods and Strains

All *C. elegans* strains were derived originally from the wild-type Bristol strain N2. Worm cultures, genetic crosses, and other *C. elegans* husbandry were performed according to standard protocols (Brenner, 1974). Strains expressing transgenes in the germline were grown at 25°C. Other strains were grown at 20°C. A complete list of strains used in this study can be found in Supplementary Table.

RNAi was performed by the feeding method (Timmons and Fire, 1998). Feeding constructs were prepared by PCR from EST clones provided by Dr. Yuji Kohara (National Institute of Genetic, Japan) followed by subcloning into the RNAi vector L4440 (Timmons and Fire, 1998). RNAi-treated F1 animals were used for the assay. Phenotypes were scored in adults.

Antibodies

The following antibodies were used in this study: mouse anti-HA monoclonal antibody (16B12) Covance Research Products (Berkeley, CA), rabbit anti-GST polyclonal antibody (Z-5) Santa Cruz Biotechnologies (Santa Cruz, CA), mouse anti-human HLA-A,B,C monoclonal antibody (w6/32) BioLegend (San Diego, CA). Fluorescent dye conjugated secondary antibodies, and Alexa568-Tf, were purchased from Molecular Probes (Invitrogen, Carlsbad, CA).

Yeast two-hybrid analyses

The yeast two-hybrid screen was performed using the Gal4-based Proquest System (Invitrogen, Carlsbad, CA) according to manufacturer's instructions. The pDBLeu-RME-

1(442-576) bait plasmid was transformed into yeast strain MaV203. MaV203 bearing the bait plasmid was amplified and transformed with the Vidal *C. elegans* library in prey vector PC86, essentially as described (Walhout *et al.*, 2000; Walhout and Vidal, 2001). 2.25 million clones were screened on histidine dropout plates containing 20 mM 3-AT. 21 positives were recovered that re-tested as positive in the His and β-Gal assays, after isolation and re-transformation with fresh bait plasmid. Six of these 21 positive clones contained portions of *alx-1* cDNA.

The LexA-based DupLEX-A yeast two-hybrid system (OriGene Technologies Inc., Rockville, MD) was used for all subsequent analysis, according to the manufacturer's instructions. pSH18-34 was used as reporter in all the yeast two-hybrid experiments. Constructs were introduced into the yeast strain EGY48 included in the system. To assess the expression of the *LEU2* reporter, transformants were selected on plates lacking leucine, histidine, tryptophan and uracil, containing 2% galactose/1% raffinose at 30^{o}C for 3 days. β-galactosidase activity was measured using the standard ONPG (o-nitrophenyl β-D-galactopyranoside) test (Choi *et al.*, 1996). β–Galactosidase activity in Miller units were plotted as an average from assays performed in duplicate.

Protein expression and Coprecipitation assays

N-terminally HA-tagged ALX-1 protein was synthesized *in vitro* using the TNT coupled transcription-translation system (Promega) using DNA template pcDNA3.1-2xHA-ALX-1 (1.6 μg/each 50 μl reaction). The reaction cocktail was incubated at 30°C for 90 minutes. Control Glutathione S-transferase (GST), or GST-RME-1d (aa 442-576) fusion protein, was expressed in *Escherichia coli* BL21 cells. Bacterial pellets were lysed in 3 ml B-PER Bacterial Protein Extraction Reagent (Pierce) with Complete Protease

Inhibitor Cocktail Tablets (Roche). Extracts were cleared by centrifugation and supernatants were incubated with glutathione-Sepharose 4B beads (Amersham Pharmacia) at 4°C overnight. Beads were then washed six times with cold STET buffer (10mM Tris-HCl pH8.0, 150mM NaCl, 1mM EDTA, 0.1% Tween-20). *In vitro* synthesized HA-tagged ALX-1 (10 µl TNT mix diluted in 500 µl STET) was added to the beads and allowed to bind at 4°C for 2 hours. After six additional washes in STET the proteins were eluted by boiling in 30 µl 2xSDS-PAGE sample buffer. Eluted proteins were separated on SDS-PAGE (10% polyacrylamide), blotted to nitrocellulose, and probed with anti-HA (16B12). Subsequently the blots were stripped and re-probed with anti-GST (Z-5) antibodies.

Plasmids and Transgenic Strains

The Proquest system two-hybrid bait plasmid pDBLeu-RME-1 contained a region of cDNA yk271a1, encoding RME-1 isoform D amino acids 442-576, cloned into the unique SalI-NotI sites. An equivalent *rme-1*(442-576) PCR product was introduced in frame into the BamHI and EcoRI sites of the pGEX-2T vector (GE Healthcare Life Sciences) for GST pulldown experiments. All Origene system two-hybrid plasmids were generated as PCR products with Gateway attB.1 and attB.2 sequence extensions, and were introduced into the Gateway entry vector pDONR221 by BP reaction. They were then transferred into the final destination vector using Gateway recombination cloning (Invitrogen) LR reaction. The bait vector pEG202 and target vector pJG4-5 (OriGene) were modified in-house with the Gateway cassette (Invitrogen, Carlsbad, CA). RME-1 sequences were cloned into the bait vector pEG202-Gtwy. Target constructs were introduced into vector pJG4-5-Gtwy. Origene system two-hybrid bait plasmids contained

the complete RME-1 isoform F C-terminal region (aa 447-555) or a slightly smaller region lacking the extreme C-terminal 9 amino acids including the YPSL motif (aa 447-546, ΔYPSL). Prey plasmids encoded full length ALX-1 isoform B (aa 1-882), ALX-1b lacking the C-terminal NPF tripeptide (precise deletion of aa 879-881), ALX-1b N-terminal fragment (aa 1-752), ALX-1b BRO1 domain (aa 1-365), the central fragment of ALX-1b (aa 365-752), or the C-terminal fragment (aa 753-882) amplified from *alx-1* cDNA clone yk2c8. All amplified regions were confirmed by DNA sequencing. The same pDONR221-ALX-1(aa 1-882) cDNA clone was transferred into an in-house modified pcDNA3.1 (+) (Invitrogen, Carlsbad, CA) with 2xHA epitope tag and Gateway cassette (Invitrogen, Carlsbad, CA) for *in vitro* transcription/translation experiments.

To create the GFP-ALX-1 plasmid driven by the *alx-1* promoter, 1.145 kb of *alx-1* promoter sequence was PCR amplified from *C. elegans* genomic DNA with primers containing XbaI and NotI restriction sites and cloned into the same sites in the *C. elegans* GFP vector pPD117.01 (gift of Andrew Fire). The entire *alx-1* gene body and 3' UTR (5.595 kb) was then PCR amplified with primers including NaeI and BspEI restriction sites and cloned into the same sites downstream of GFP. The GFP-ALX-1 plasmid (10µg/ml) was co-injected with plasmid pRF4 encoding *rol-6(su1006)*, to establish transgenic lines. Integrated transgenic lines were generated by standard gamma irradiation methods (Wilkinson *et al.*, 1994).

To construct GFP or mCherry fusion transgenes for expression in the worm intestine, two previously described Gateway destination vectors (Chen *et al.*, 2006) were used that contain the promoter region of the intestine-specific gene *vha-6* cloned into the *C. elegans* pPD117.01 vector, followed by GFP or mCherry coding sequences, a Gateway

cassette (Invitrogen, Carlsbad, CA), and let-858 3' UTR sequences, followed by the unc-119 gene of *C. briggsae*. The sequences of *C. elegans hgrs-1(genomic), alx-1b (cDNA)* and *rme-1d (cDNA)* were cloned individually into entry vector pDONR221 by PCR and BP reaction, and then transferred into intestinal expression vectors by Gateway recombination cloning LR reaction to generate N-terminal fusions. The *sdpn-1* expression plasmid was created by PCR amplification and Gateway cloning of the complete *sdpn-1a* genomic region (7.870 kb), lacking a stop codon and including the predicted *sdpn-1* promoter region (4.259 kb), into vector pPD117.01 modified with a Gateway cassette inserted at the Asp718I site just upstream of the GFP coding region. Complete plasmid sequences are available on request. Low copy integrated transgenic lines were obtained by the microparticle bombardment method (Praitis *et al.*, 2001).

Microscopy and Image Analysis

Live worms were mounted on 2% agarose pads with 10 mM levamisol as described previously (Sato *et al.*, 2005). Fluorescence images were obtained using an Axiovert 200M (Carl Zeiss MicroImaging, Oberkochen, Germany) microscope equipped with a digital CCD camera (C4742–12ER, Hamamatsu Photonics, Hamamatsu, Japan), captured using Metamorph software (Universal Imaging, West Chester, PA), and then deconvolved using AutoDeblur software (AutoQuant Imaging, Watervliet, NY). Images taken in the DAPI channel were used to identify broad-spectrum intestinal autofluorescence caused by lipofuscin-positive lysosomes (Clokey and Jacobson, 1986). To obtain images of GFP fluorescence without interference from autofluorescence, we used a Zeiss LSM510 Meta confocal microscope system (Carl Zeiss MicroImaging) with argon 488 excitation (Chen *et al.*, 2006). Quantification of images was performed with

Metamorph software (Universal Imaging). Most GFP/mCherry colocalization analysis was performed on L3 larvae generated as F1 cross-progeny of GFP-marker males crossed to mCherry-marker hermaphrodites (Chen *et al.*, 2006).

Cell culture, transfections and pulse-chase analysis

All tissue culture supplies were from Gibco (Invitrogen, Carlsbad, CA). HeLa cells were a kind gift from Dr. J. Donaldson and were grown in DMEM medium containing 5% FBS and 100 U/ml penicillin–streptomycin.

MHCI uptake and recycling in HeLa cells was done essentially as previously described (Weigert and Donaldson, 2005). HeLa cells were seeded onto glass coverslips at a density of 10,000 cells per well, in 24-well plates, and grown for 24 hours before they were transfected with 0.5µg of plasmid DNA (EGFP, FLAG-Alix(467-869), mRFP1 or mRFP1 co-transfected with FLAG-Alix(467-869) using jetPEI reagent (Polyplus-transfection, San Marcos, CA). All experiments were done 24 hours after transfection. Co-transfection efficiency in control experiments was determined after the cells were fixed for 15 minutes in 3.7 % (v/v) paraformaldehyde in PBS at room temperature, followed by permeabilization of the cells with 0.1 %(v/v) Triton X-100 for 15 minutes at room temperature. After blocking cells for 30 minutes in 3 % BSA, the cells were labeled with anti-FLAG primary antibody for 1 hour at room temperature, followed by incubation with secondary antibody for 1 hour at room temperature. Cells expressing mRFP and FLAG-Alix (467-869) were counted in three random fields. 98.6% of cells expressing mRFP also expressed FLAG-Alix (467-869), and 68% of cells expressing FLAG-Alix (467-869) also expressed mRFP1. MHCI and transferrin uptake and recycling assays were done as previously described (Weigert and Donaldson, 2005).

To analyze MHCI uptake and recycling, cells were incubated on ice for 30 minutes with 50 µg/ml of W6/32 antibody to allow antibody binding to endogenous MHCI. Cells were then washed with ice cold PBS to remove unbound antibody, and incubated for 30 minutes at 37ºC in the presence of 1 mM LatrunculinA, to allow uptake and accumulation of MHCI in recycling endosomes. Remaining surface bound antibody was removed by incubating the cells for 40 seconds in 'stripping buffer' (0.5 % acetic acid, 0.5 M NaCl, pH3.0), followed by 2 washes with PBS and 2 washes with DMEM. A set of cells were fixed for 15 minutes at room temperature in 3.7% paraformaldehyde in PBS (representing MHCI uptake), while another set of cells were transferred to full supplemented DMEM, for 30 minutes at 37ºC, to allow MHCI recycling, and then fixed as above. The internalized or recycled MHCI antibody was revealed by incubation of cells with Alexa-488 conjugated anti-mouse secondary antibody in the presence (total pool) or absence (surface pool) of 0.2 % saponin, respectively.

To analyze Alexa568-Transferrin (Alexa568-Tf) uptake and recycling, cells were serum starved for 30 min at 37°C in DMEM containing 0.5 % bovine serum albumin. Then 5 µg/ml Alexa 568-Tf was internalized for 30 minutes at 37°C. At the end of the internalization, cells were stripped of surface-bound Tf as described above, and one set of cells were fixed (representing Tf uptake), while other set of cells was incubated in complete medium for 30 minutes followed by fixation (representing Tf recycling).

Images of at least 100 cells per trial from random fields on each coverslip were captured using a Zeiss F-fluor 40x/1.3 oil objective. Fluorescence intensities in HeLa cells were measured by thresholding and outlining whole individual cells, followed by determination of integrated fluorescence intensities, which were then normalized to cell

area. Average recycled MHCI surface values (30min-0min) and average MHCI total values (0min) were expressed as a ratio relative to control cells. Each bar in Figure 5 J and K represents average values from 4 experiments ± (s.d.). Average internalized Alexa568-Tf was expressed as a ratio relative to control (control set to 100%) ± standard deviation (s.d.) from three experiments. Average recycled Alexa568-Tf was expressed as a percentage of internalized Alexa568-Tf ± s.d. from three experiments

ACKNOWLEDGEMENTS

We thank J. Donaldson, R. Sadoul and C. Chatellard-Causse for important reagents. We also thank J. Donaldson, R. Weigert, C. Martin, P. Schweinsberg and Z. Pan for their generous advice and technical assistance. This work was supported by NIH Grant GM67237 to B.D.G.

Table 1. Transgenic and Mutant Strains Used in This Study

Transgenic and Mutant Strains Used in This Study
*pwIs1(*p*alx-1::GFP::ALX-1)*
*pwIs112(*p*vha6::hTAC::GFP)(Chen et al., 2006)*
*pwIs170(*p*vha6::GFP::RAB-7)(Chen et al., 2006)*
*pwIs206(*p*vha6::GFP::RAB-10)(Chen et al., 2006)*
*pwIs281(*p*pie1::CAV-1::GFP)(Sato et al., 2006)*
*pwIs116(*p*rme-2::RME-2::GFP)(Sato et al., 2006)*
*pwIs50(*p*lmp-1::LMP-1::GFP)(Treusch et al., 2004)*
*pwIs518(*p*vha6::GFP::HGRS-1)*
*pwIs521(*p*vha6::mCherry::ALX-1)*
*pwIs522(*p*vha6::mCherry::ALX-1)*
*pwIs524(*p*vha6::GFP::ALX-1)*
*pwIs590(*p*vha6::mCherry::ALX-1ΔNPF)*
*pwIs621(*p*vha6::mCherry::RME-1)*
*pwIs626(*p*vha6::mCherry::RME-1ΔYPSL)*
*pwIs69(*p*vha6::GFP::RAB-11)(Chen et al., 2006)*
*pwIs72(*p*vha6::GFP::RAB-5)(Chen et al., 2006)*
*pwIs76(*p*sdpn-1::SDPN-1::GFP)*
*pwIs87(*p*vha6::GFP::rme-1)(Chen et al., 2006)*
*pwIs90(*p*vha6::hTfR::GFP)(Chen et al., 2006)*
rme-1(b1045)(Grant et al., 2001)
alx-1(gk275)(From C. elegans Gene Knockout Consortium)

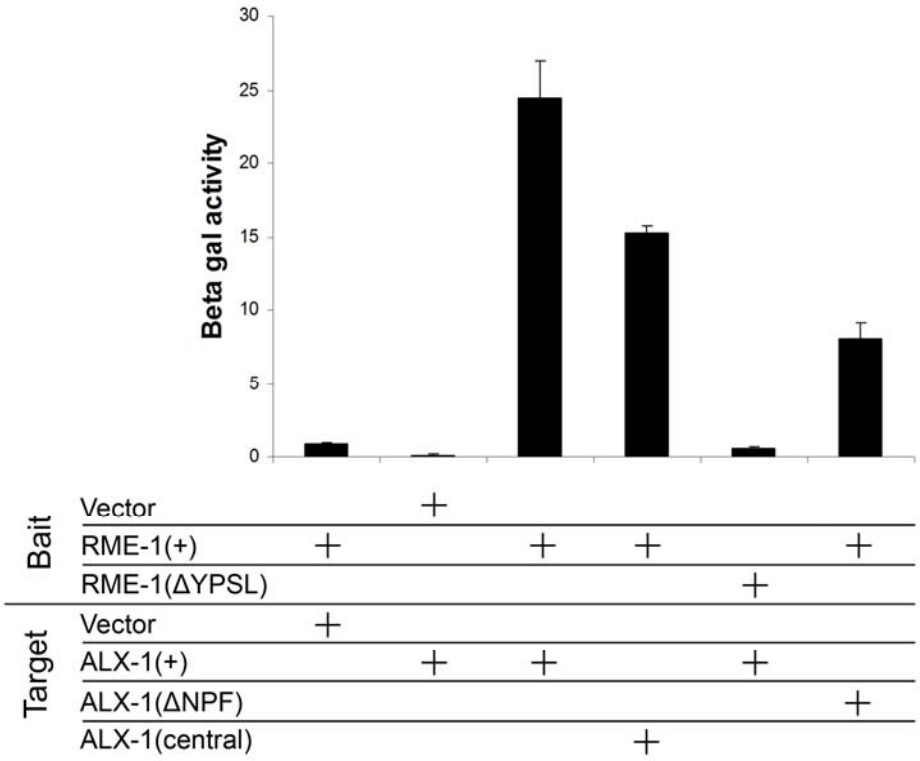

Figure 1. RME-1 Interacts with ALX-1

Quantitative yeast two-hybrid beta-galactosidase assays show that the ALX-1 C-terminal NPF motif contributes to the interaction with RME-1, while the central domain (aa 365-752) of ALX-1 contributes the main binding surface, interacting with RME-1 through its C-terminal YPSL sequence. Y-axis is labeled in Miller Units.

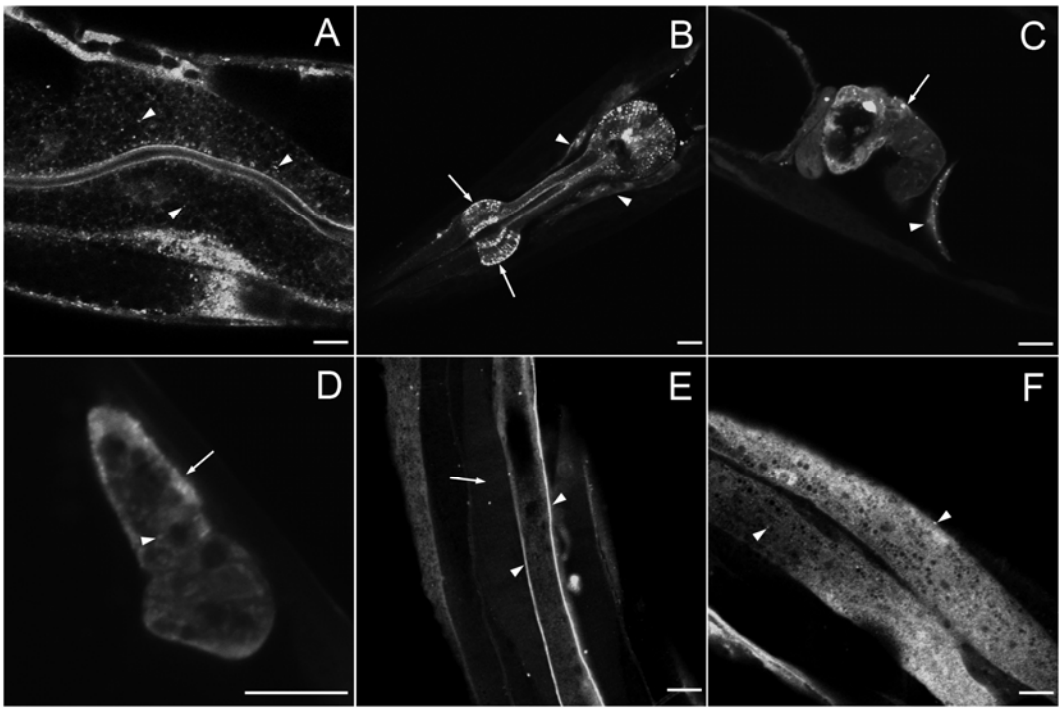

Figure 2. ALX-1 is Broadly Expressed in *C.elegans*

Expression of a GFP-ALX-1 transgene driven by the *alx-1* promoter is indicated in (A-F). (A) Intestine, arrowheads indicate cytoplasmic puncta. (B) Pharynx is indicated by arrows and nerve ring indicated by arrowheads. (C) Arrow indicates spermatheca and arrowhead indicates cytoplasmic puncta. (D) Coelomocyte, cytoplasmic puncta (arrowheads). (E) Nerve cord (arrowheads) and body-wall muscle (arrow). (F) Hypodermis, cytoplasmic puncta (arrowheads). Scale bars represent 10 μm.

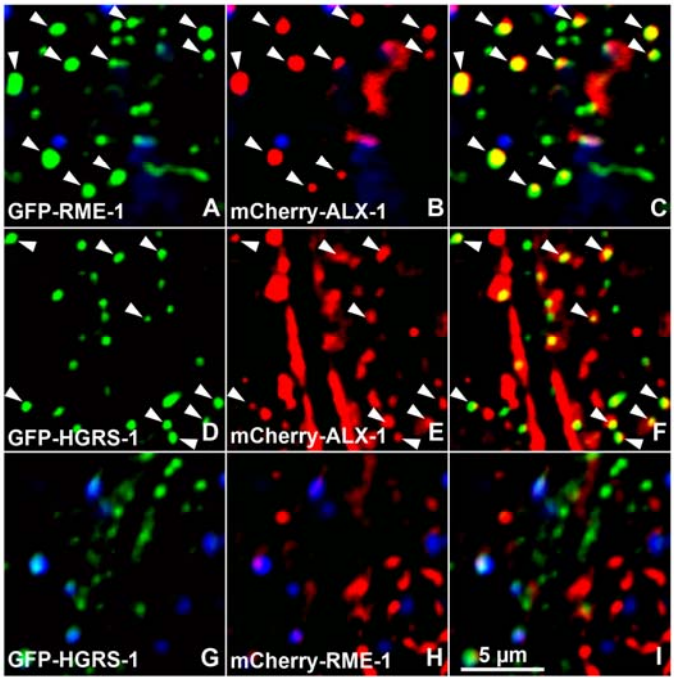

Figure 3. ALX-1 Associates with Two Types of Endosomes in the Intestine

(A-C) mCherry-ALX-1 colocalizes with GFP-RME-1 on basolateral recycling endosomes. Arrowheads indicate endosomes labeled by both GFP-RME-1 and mCherry-ALX-1. (D-F) Some mCherry-ALX-1 also colocalizes with MVE marker GFP-HGRS-1, mostly in the medial and apical cytoplasm. Arrowheads indicate puncta labeled by both mCherry-ALX-1 and GFP-HGRS-1. (G-I) mCherry-RME-1 and GFP-HGRS-1 label different endosome types. Virtually no overlap was observed between mCherry-RME-1 and GFP-HGRS-1. In each image autofluorescent lysosomes can be seen in all three channels with the strongest signal in blue, whereas GFP appears only in the green channel and mCherry only in the red channel. Signals observed in the green or red channels that do not overlap with signals in the blue channel are considered bone fide GFP or mCherry signals, respectively. Scale bar represents 5 µm.

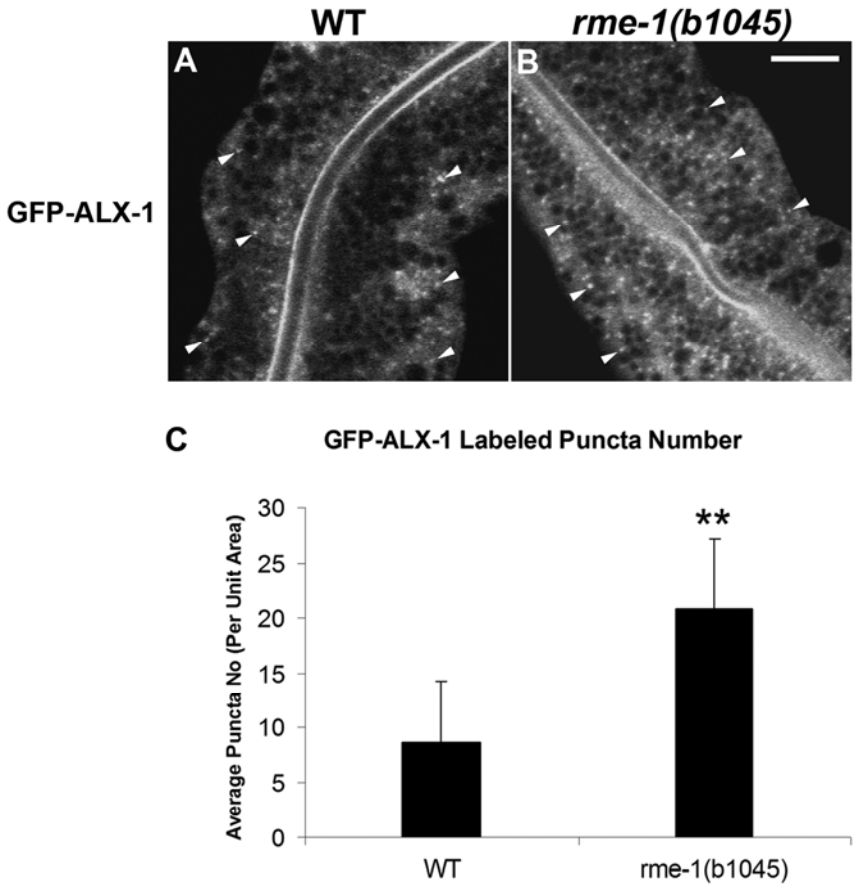

Figure 4. *rme-1* Mutants Accumulate Abnormally Numerous GFP-ALX-1 Labeled Endosomes

Confocal images of wild-type animals (A) and *rme-1(b1045)* mutant animals (B) showing GFP-ALX-1 labeled endosomes in the intestine. Arrowheads indicate GFP-ALX-1 puncta. (C) Quantification of endosome number in wild type animals and mutants as visualized by GFP-ALX-1. Error bars represent standard deviations from the mean (n=18 each, 6 animals of each genotype sampled in three different regions of each intestine). Asterisks indicate a significant difference in the one-tailed Student's t-test ($p<0.01$). Scale bar represents 10 μm.

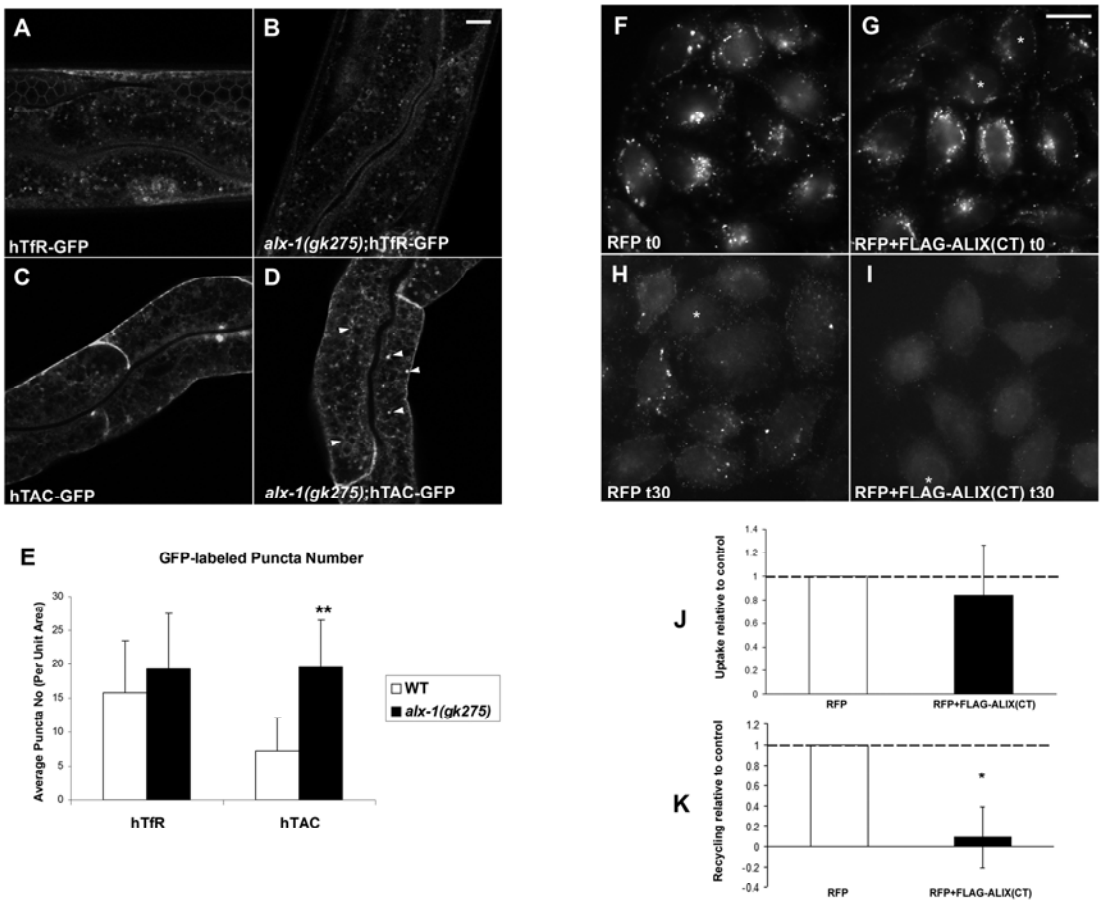

Figure 5. Abnormal Trafficking of Recycling Cargo in *alx-1* Mutant *C. elegans* and in HeLa Cells Expressing Truncated Alix

(A-B) Localization and morphology of hTfR-GFP, a clathrin-dependent cargo protein, appears unchanged in *alx-1(gk275)* mutants compared to wild-type animals. (C-D) hTAC-GFP, a cargo protein internalized independently of clathrin, becomes trapped in endosomal structures of *alx-1* mutants. Arrowheads indicate punctate and tubular endosomes labeled by hTAC-GFP in the intestine. (E) Quantification of cargo-labeled puncta number. Error bars represent standard deviations from the mean (n=18 each, 6 animals of each genotype sampled in three different regions of each intestine). (F-I)

Representative images showing anti-MHCI labeling in control HeLa cells transfected with RFP expression plasmid only (F, H) or for cells co-transfected with RFP and truncated Alix expression plasmids (G, I). The first pair of images (F, G) show anti-MHCI uptake after 30 min incubation. The second pair of images (H, I) show surface MHCI after 30 minutes of recycling (H, I). Cells that were negative for the RFP signal are marked with asterisks. In co-transfection experiments these RFP-negative cells may or may not express Alix(467-869) (see Methods) and were therefore not included in the quantification. Conversely nearly all RFP expressing cells were found to also express FLAG-Alix(467-869) in control experiments. Therefore only RFP expressing cells were quantified for anti-MHCI uptake or recycling. (J-K) The amount of MHCI antibody internalized after a 30 min pulse, or recycled after a 30 min chase, is shown as a ratio relative to control cells (see Methods). MHCI antibody recycling (K), but not MHCI antibody uptake (J), was impaired by expression of truncated FLAG-Alix(467-869). The asterisk in panel K indicates a significant difference in the one-tailed Student's t-test ($p=0.004$). Scale bars represent 10 μm in (A-D) and 20 μm in (F-I).

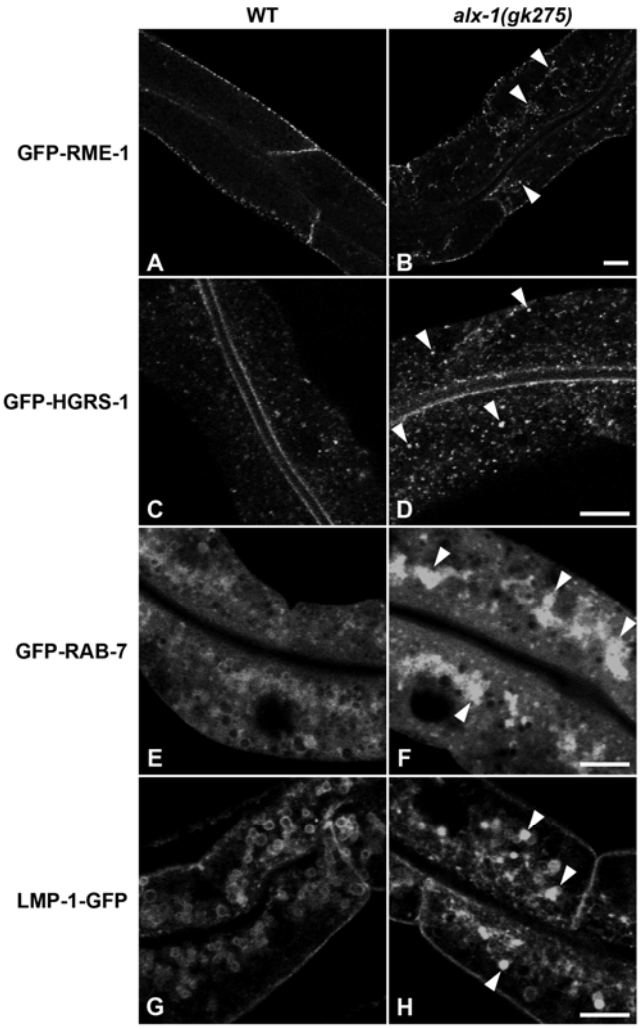
WT
alx-1(gk275)
GFP-RME-1
GFP-HGRS-1
GFP-RAB-7
LMP-1-GFP
A
B
C
D
E
F
G
H

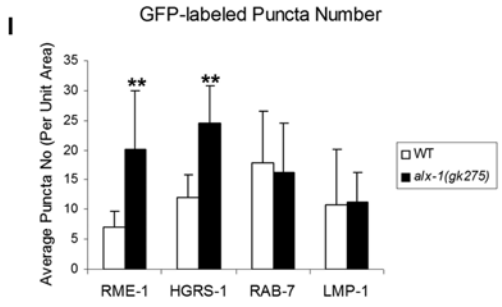
I
GFP-labeled Puncta Number
Average Puncta No (Per Unit Area)
35
30
25
20
15
10
5
0
**
**
RME-1
HGRS-1
RAB-7
LMP-1
WT
alx-1(gk275)

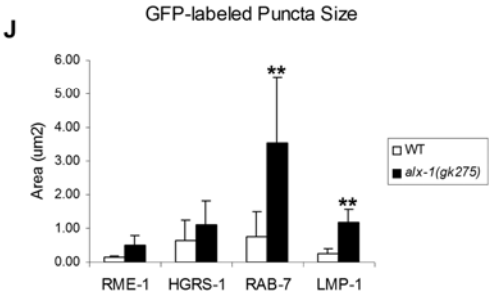
J
GFP-labeled Puncta Size
Area (um2)
6.00
5.00
4.00
3.00
2.00
1.00
0.00
**
**
RME-1
HGRS-1
RAB-7
LMP-1
WT
alx-1(gk275)

Figure 6. Altered Endosome Populations in *alx-1* Mutants

(A-B) GFP-RME-1 labeled recycling endosomes increase in number in *alx-1* mutant intestinal cells. Arrowheads indicate punctate and tubular endosomes labeled by GFP-RME-1. (C-D) GFP-HGRS-1 positive endosomes increase in number in *alx-1* mutant intestinal cells. Arrowheads indicate punctate endosomes labeled by GFP-HGRS-1. (E-H) GFP-RAB-7 and LMP-1-GFP labeled late endosomes appear enlarged and aggregated in *alx-1(gk275)* mutant intestinal cells. (J-K) Quantification of GFP-labeled puncta number and puncta size. Error bars represent standard deviations from the mean (n=18 each, 6 animals of each genotype sampled in three different regions of each intestine). The asterisks indicate a significant difference in the one-tailed Student's t-test ($p<0.01$). Scale bars represent 10 μm.

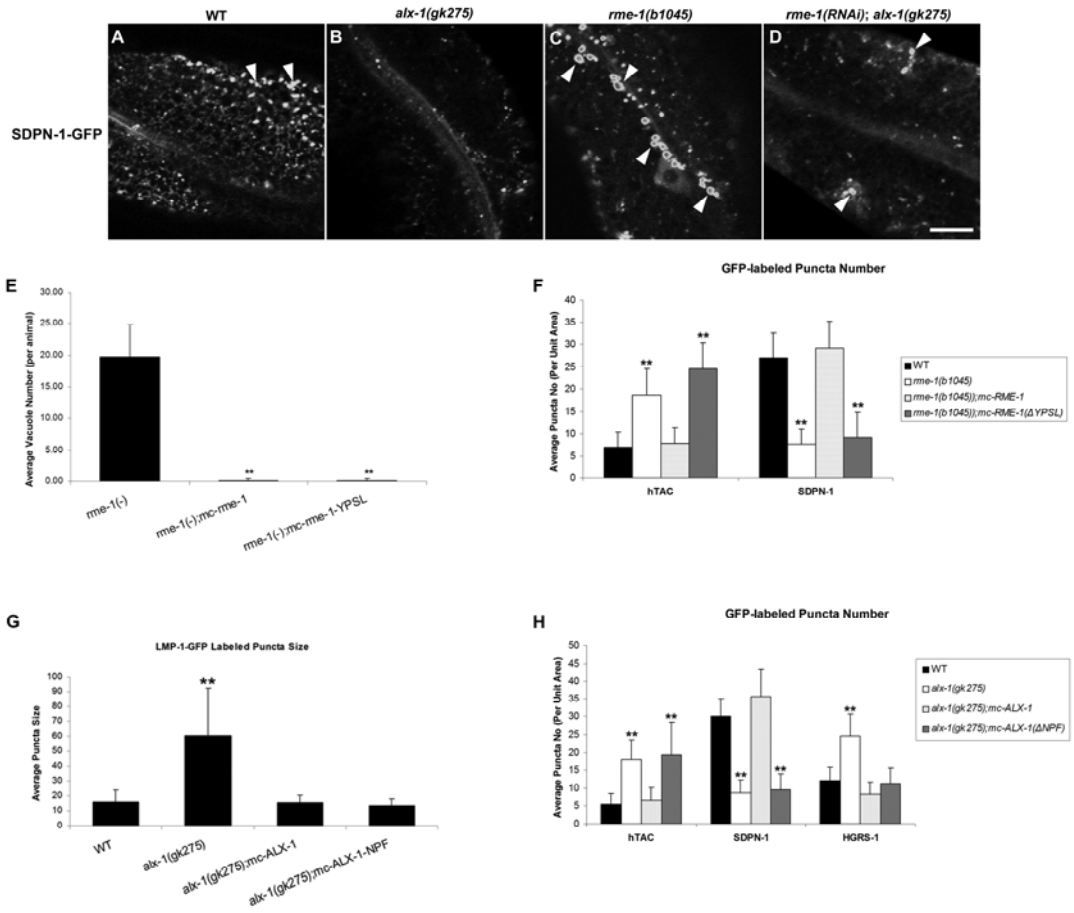

Figure 7. Functional requirement for the ALX-1/RME-1 Interaction *in vivo*

(A-D) Syndapin/SDPN-1-GFP Localization is Abnormal in *alx-1* Mutant and *rme-1* Mutant Intestinal Cells.

(A) Confocal images of wild-type animals show abundant SDPN-1-GFP labeled basolateral punctate and tubular endosomes. (B) In *alx-1* mutant animals most basolateral SDPN-1-GFP positive structures are missing, and most of the remaining SDPN-1-GFP signal appears diffuse. (C) In *rme-1* mutant animals basolateral SDPN-1-GFP labeled structures are fewer, and many of those that remain are enlarged. (D) *alx-1(gk275);rme-1(RNAi)* animals lack most basolateral SDPN-1-GFP labeled structures like *alx-1* mutant

animals, but the remaining structures appear enlarged. Arrowheads indicate endosomes labeled by SDPN-1-GFP. Scale bar represents 10 μm.

(E-H) Rescue Experiments Genetically Separate ALX-1 Functions and Indicate a Requirement for the ALX-1/RME-1 Interaction *in vivo*.

Interaction defective mutant forms of RME-1 (ΔYPSL) or ALX-1 (ΔNPF), expressed as mCherry (MC) fusions, were compared to wild-type forms in their ability to rescue specific *rme-1(b1045)* or *alx-1(gk275)* mutant phenotypes in the intestine. One set of phenotypes that were assayed focused on recycling endosomes: abnormal accumulation of basolaterally recycling pseudocoelomic fluid in enlarged vacuoles/REs, intracellular recycling cargo hTAC-GFP accumulation, and basolateral SDPN-1-GFP recruitment/morphology. In addition, ALX-1(ΔNPF) was compared to intact ALX-1 in its ability to rescue *alx-1* mutant associated defects in the degradative pathway: multi-vesicular endosome number, as assayed by GFP-HGRS-1, and late endosome size, as assayed by LMP-1-GFP. (E) Expression of either MC-tagged RME-1 or MC-tagged RME-1(ΔYPSL) rescues basolateral fluid accumulation in *rme-1(b1045)* mutants. (F) The last two bars in each group show the relative degree of rescue of *rme-1(b1045)* mutant defects achieved by expression of MC-tagged RME-1, or MC-tagged RME-1(ΔYPSL). Note that wild-type MC-RME-1 rescues both defects, while MC-RME-1(ΔYPSL) cannot rescue the *rme-1(b1045)* associated defects. (G-H) The last two bars in each graph show the relative degree of rescue of *alx-1(gk275)* mutant defects achieved by expression of MC-tagged ALX-1, or MC-tagged ALX-1(ΔNPF). Note that wild-type MC-ALX-1 rescues all defects, while MC-ALX-1(ΔNPF) can only rescue *alx-1* associated phenotypes of the degradative pathway, LMP-1-GFP endosome size (G) and

GFP-HGRS-1 puncta number (H), but cannot rescue phenotypes associated with the recycling pathway, hTAC-GFP and SDPN-1-GFP puncta number (H). Asterisks indicate a significant difference in the one-tailed Student's t-test ($p<0.01$).

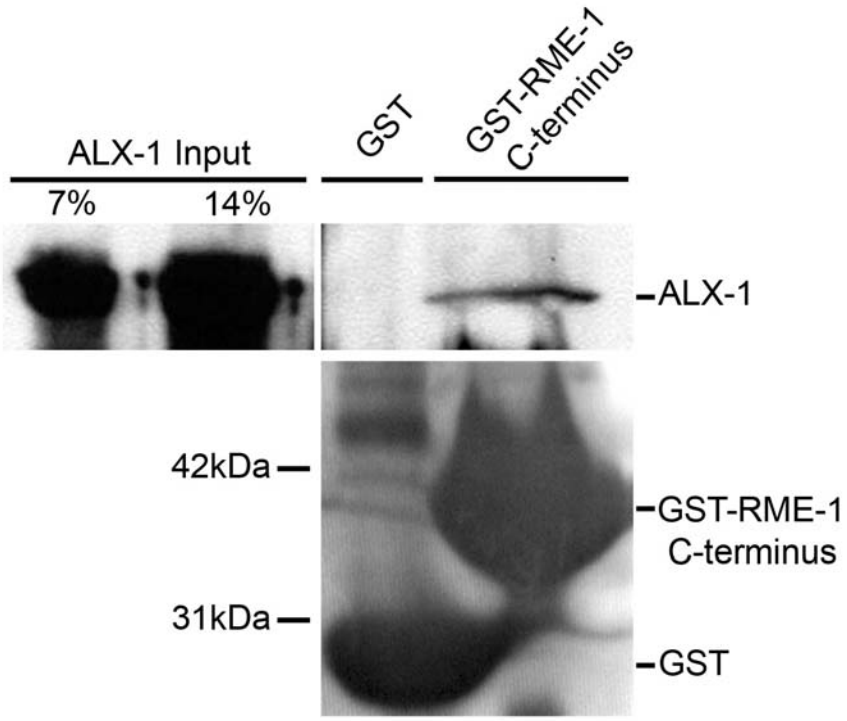

Figure S1. *In vitro* Binding of RME-1 to ALX-1

Glutathione beads loaded with recombinant GST or GST-RME-1(442-576) were incubated with *in vitro* expressed HA-ALX-1, then washed to remove unbound proteins. Bound proteins were eluted by laemmli sample buffer, separated by SDS-PAGE, analyzed by western blotting assays using anti-HA (top) and anti-GST (bottom) antibodies. Input lanes contain *in vitro* expressed HA-ALX-1 used for binding assays (7% and 14%).

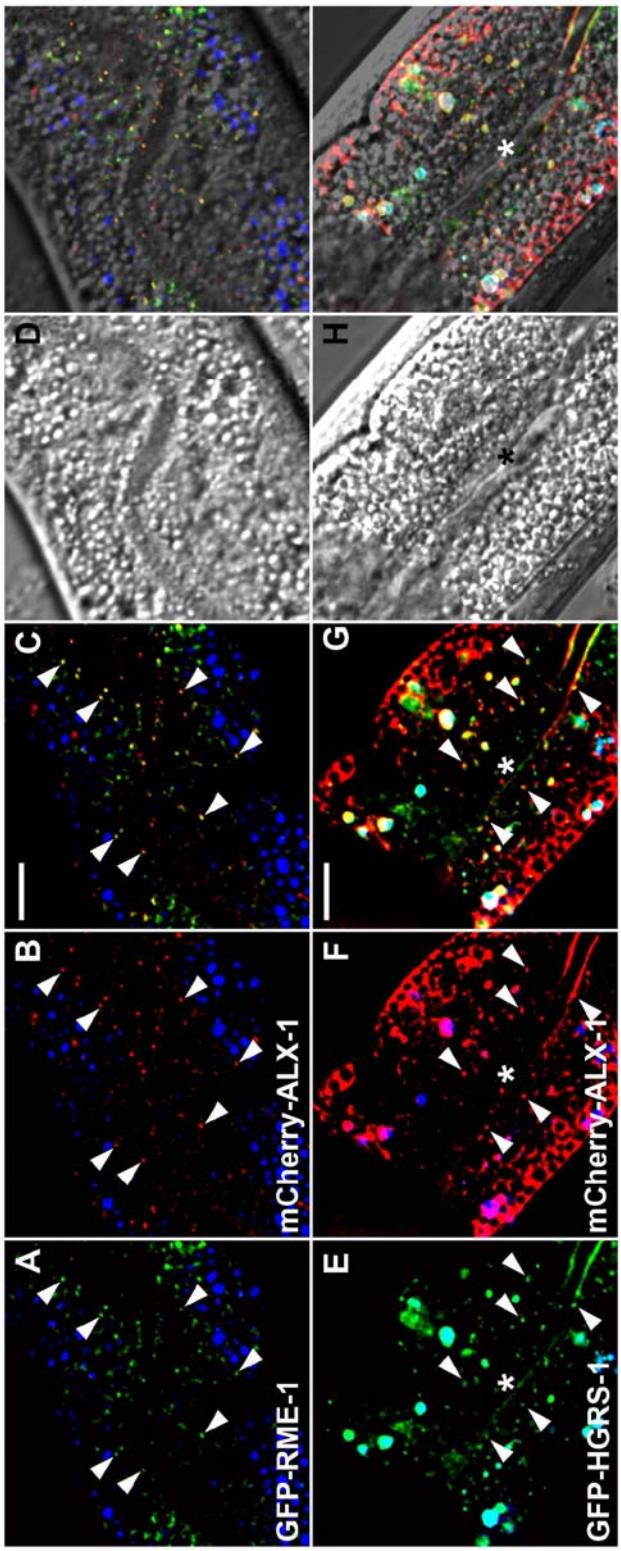
A
B
C
D
E
F
G
H
GFP-RME-1
mCherry-ALX-1
GFP-HGRS-1
mCherry-ALX-1

Figure S2. ALX-1 Associates with Two Types of Endosomes in the Intestine.

(A-C) mCherry-ALX-1 colocalizes with GFP-RME-1 on basolateral recycling endosomes, (D) DIC image shows basolateral focal plane of the intestine. Note that the depth of field is much greater for the DIC image than for the deconvolved epifluorescence. Arrowheads indicate endosomes labeled by both GFP-RME-1 and mCherry-ALX-1. (E-F) mCherry-ALX-1 colocalizes with MVE marker GFP-HGRS-1 in the medial and apical cytoplasm, (H) DIC image showing medial focal plane of the intestine. Arrowheads indicate puncta labeled by both mCherry-ALX-1 and GFP-HGRS-1. Scale bars represent 10 μm.

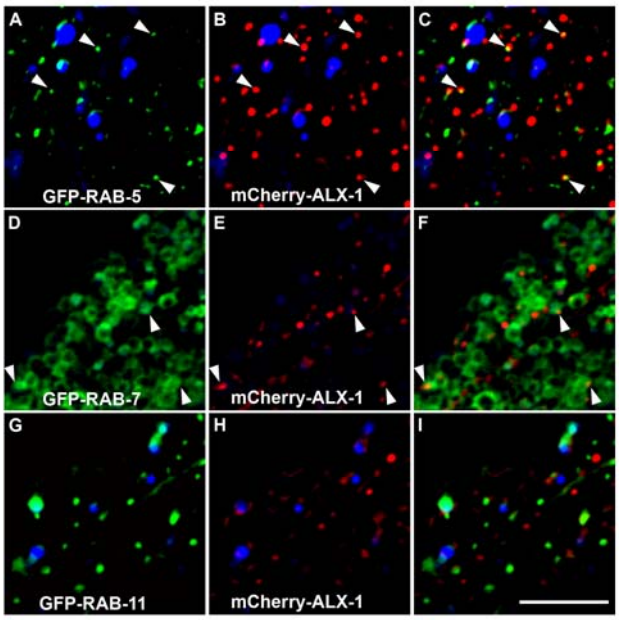

Figure S3. mCherry-ALX-1 Partially Colocalizes with Early Endosome Marker (GFP-RAB-5) and Late Endosome Marker (GFP-RAB-7) in the intestine

(A-C) mCherry-ALX-1 partially colocalizes with GFP-RAB-5 on early endosomes. Arrowheads indicate basolateral puncta labeled by both GFP-RAB-5 and mCherry-ALX-1. (D-F) mCherry-ALX-1 occasionally appears as puncta on or near the rim of GFP-RAB-7 labeled late endosomal rings. Arrowheads indicate puncta labeled by mCherry-ALX-1 on or near GFP-RAB-7 rings. (G-I) ALX-1 and RAB-11 label different endosome types. In each image autofluorescent lysosomes can be seen in all three channels with the strongest signal in blue, whereas GFP appears only in the green channel and mCherry only in the red channel. Signals observed in the green or red channels that do not overlap with signals in the blue channel are considered bone fide GFP or mCherry signals, respectively. Scale bar represents 10 μm.

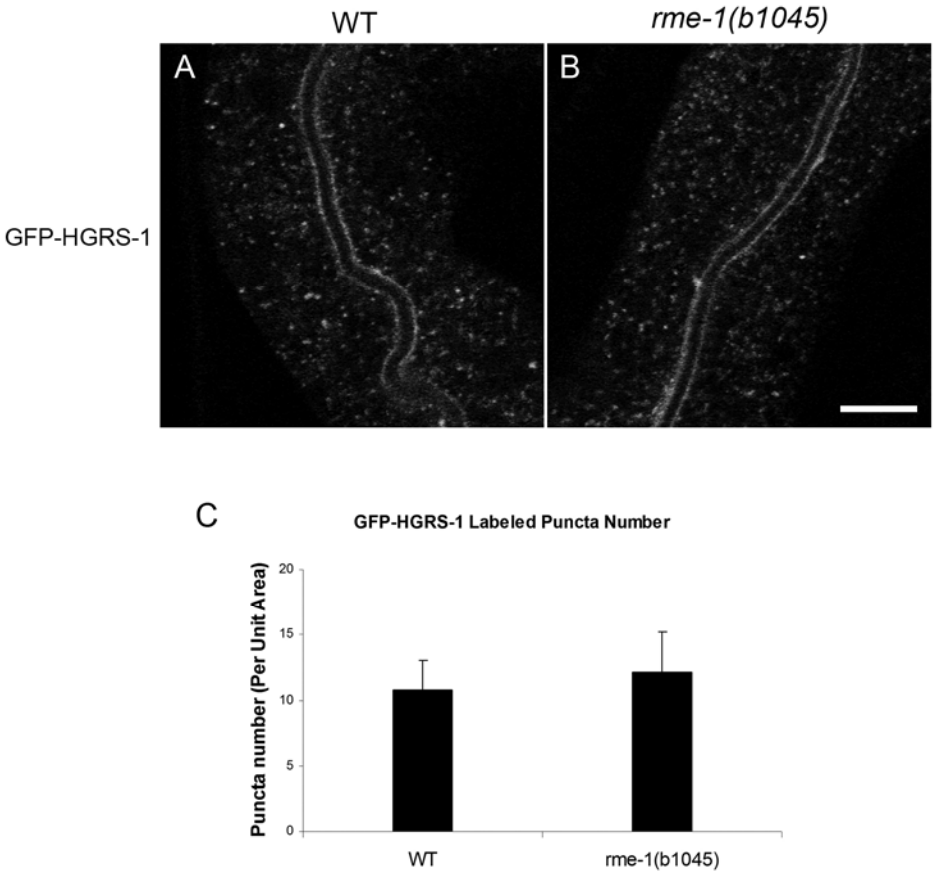

Figure S4. No change in GFP-HGRS-1 Labeled Puncta Number in *rme-1* Mutants

(A-B) Confocal images in wild-type (A) and *rme-1(b1045)* mutant (B) intestinal cells expressing MVE marker GFP-HGRS-1. (C) Quantification of endosome number in wild type animals and *rme-1* mutants as visualized by GFP-HGRS-1. Error bars represent standard deviations from the mean (n=18 each, 6 animals of each genotype sampled in three different regions of each intestine). Scale bar represents 10 μm.

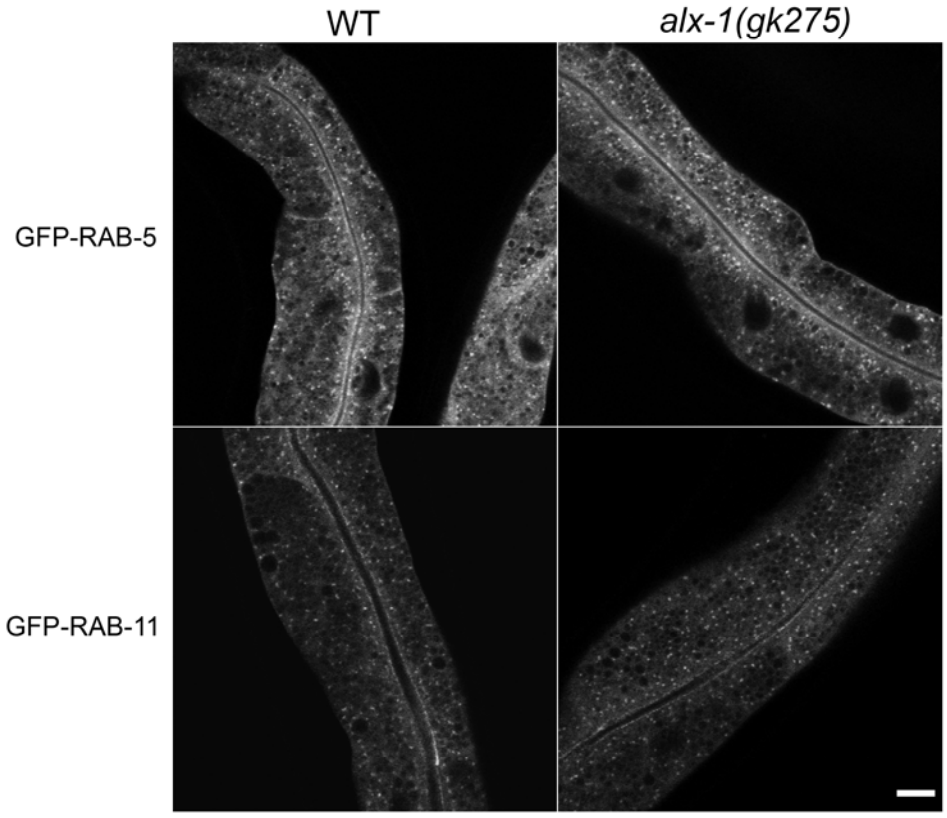

Figure S5. Additional Analysis of GFP-tagged Endosome Markers and Endocytic Cargo Markers in *alx-1* Mutants.

Confocal images of wild-type and mutant animals showing GFP-labeled structures (as indicated). GFP-RAB-5 labels early endosomes in the intestine; GFP-RAB-11 is a marker for apical recycling endosomes and TGN; Scale bar represents 10 μm.

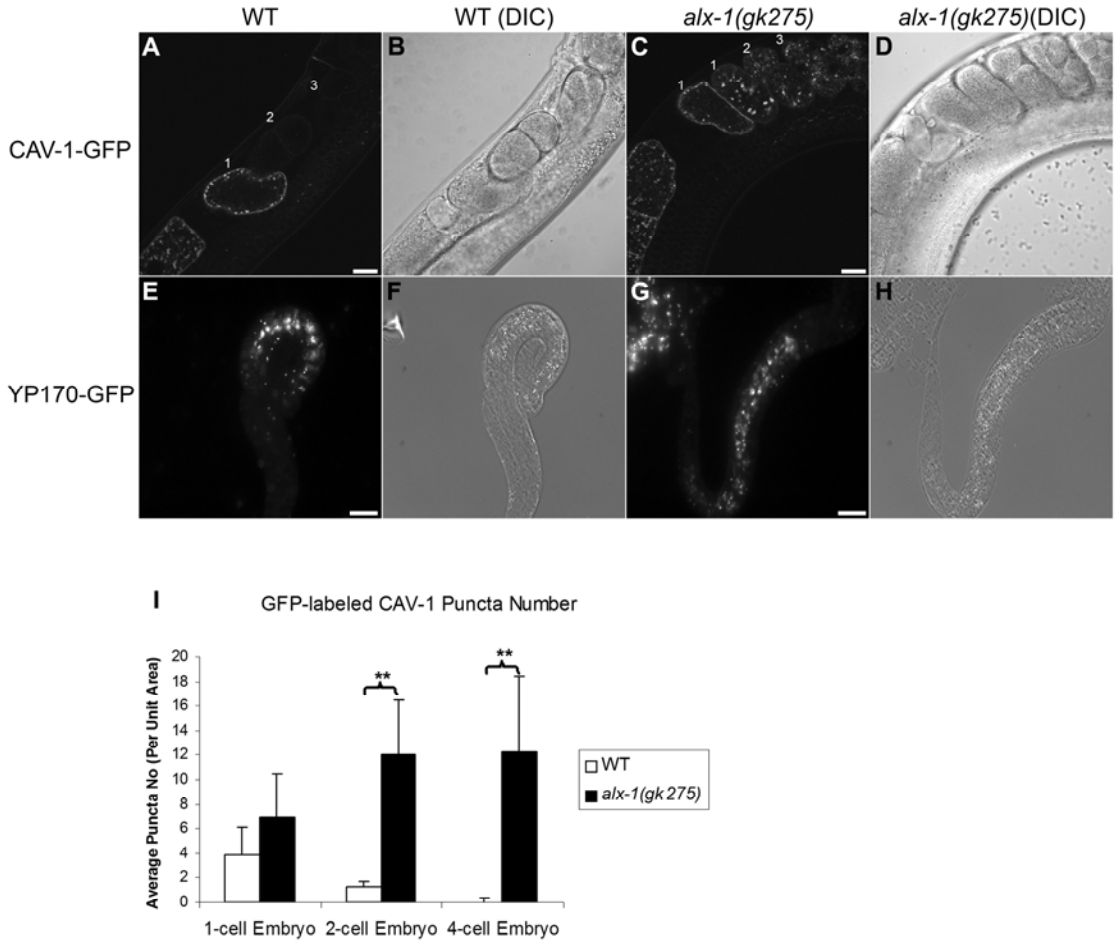

Figure S6. *alx-1* Mutants are Delayed in the Degradation of Membrane Proteins.

CAV-1-GFP is normally exocytosed in a nearly simultaneous wave during anaphase of the first embryonic meiosis. CAV-1-GFP is then rapidly endocytosed and degraded through the standard clathrin pathway. (A-B) In wild-type embryos CAV-1-GFP is degraded by the 2-cell stage with virtually no visible CAV-1-GFP labeled structures remaining by the 4-cell stage. (C-D) Degradation of internalized CAV-1-GFP is severely delayed *alx-1* mutants. CAV-1-GFP punctae remain in *alx-1* mutant 2-cell and 4-cell embryos. 1-cell, 2-cell, and 4-cell embryos are indicated by numbers 1, 2 and 3

respectively. (I) Quantification of CAV-1-GFP punctae. Asterisks indicate a significant difference in the one-tailed Student's t-test ($p<0.01$). (E-H) No change in the pattern or timing of lumenal cargo protein YP170-GFP degradation was found in *alx-1* mutant embryos. Remaining levels of undegraded YP170-GFP in 3-fold stage embryos (G-H) was similar to that of wild-type embryos (E-F) at the same stage. Scale bars represent 10 μm.

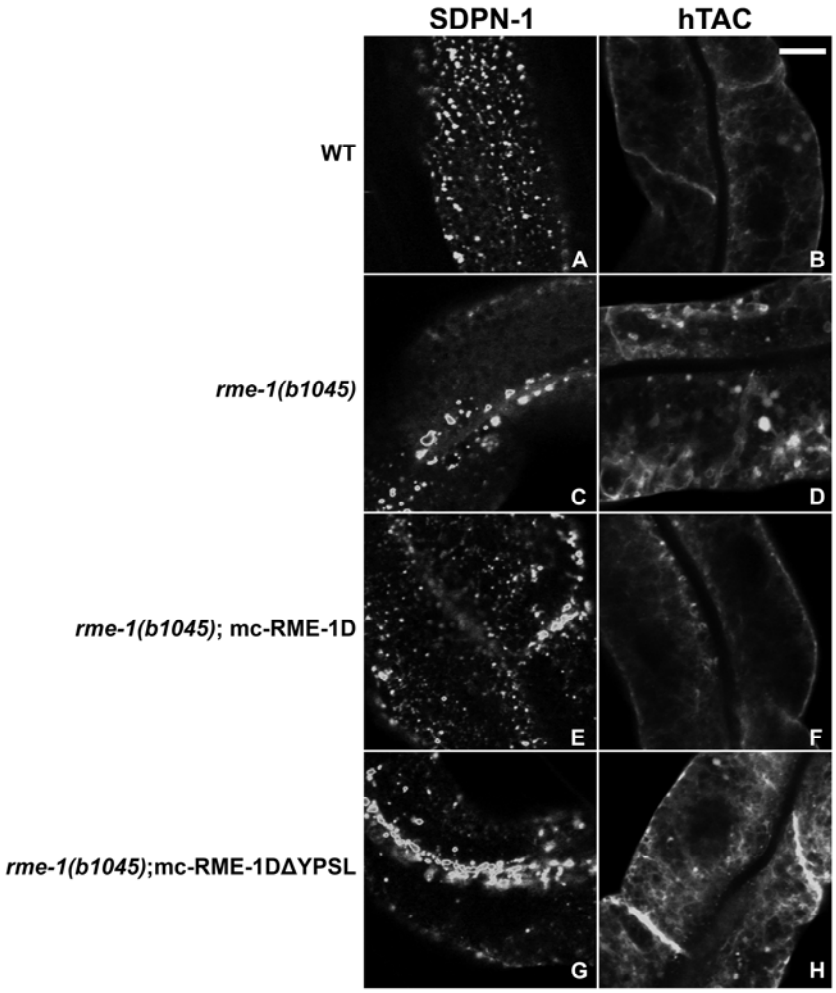

Figure S7. mCherry-RME-1(ΔYPSL) Cannot Rescue Certain *rme-1(b1045)* Associated Phenotypes.

(A, C, E, G) Confocal images of SDPN-1-GFP labeled endosomes (top focal plane near the intestinal basal membrane) in wild-type, *rme-1(b1045)* mutant, *rme-1(b1045)*; mCherry-RME-1 and *rme-1(b1045)*;mCherry-RME-1ΔYPSL. Note the rescue of SDPN-1-GFP localization by expression of full-length mCherry-RME-1, and the lack of rescue by mCherry-RME-1ΔYPSL. (B, D, F, H) Confocal images of hTAC-GFP labeled structures (middle focal plane showing the intestine in cross-section) in wild-type, *rme-*

1(b1045) mutant, *rme-1(b1045)*; mCherry-RME-1 and *rme-1(b1045)*;mCherry-RME-1ΔYPSL. Note the rescue of hTac-GFP localization by expression of full-length mCherry-RME-1, and the lack of rescue by mCherry-RME-1ΔYPSL. Scale bar represents 10 μm.

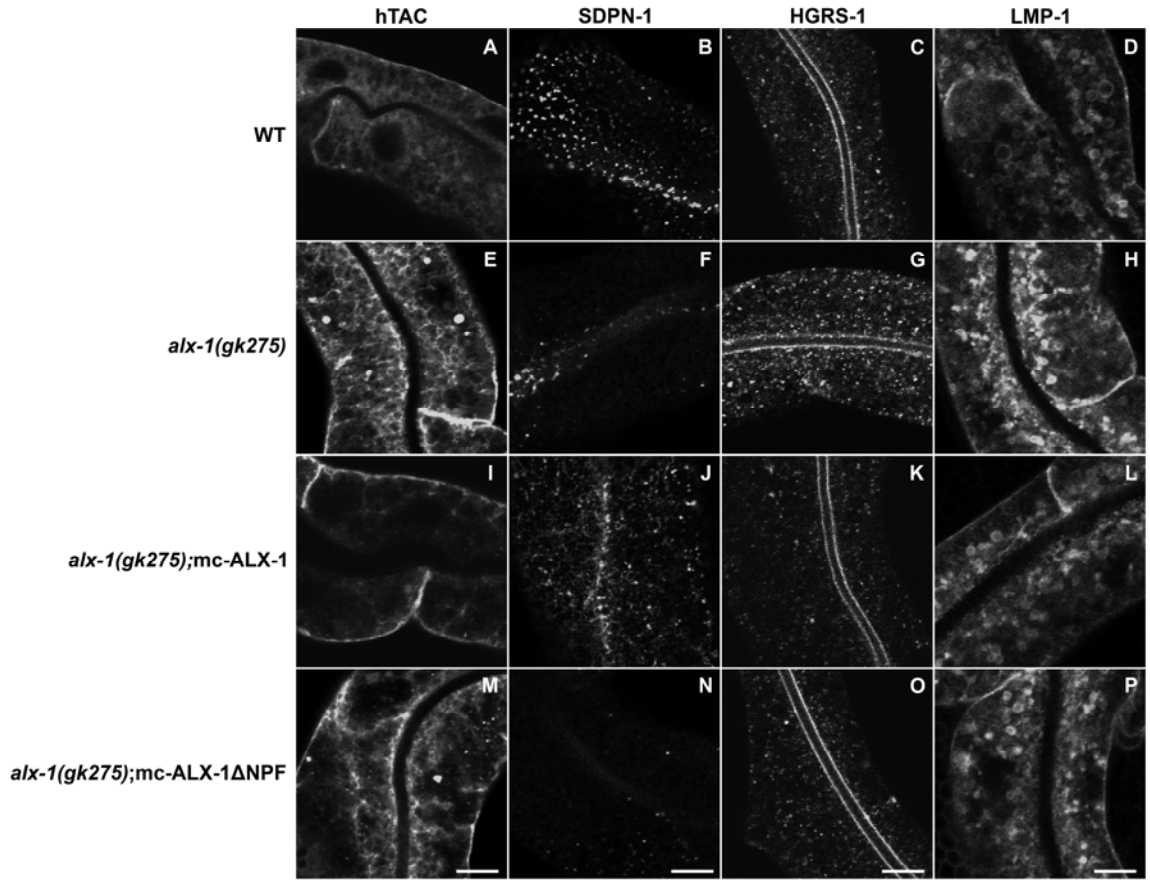

Figure S8. mCherry-ALX-1(ΔNPF) Can Rescue MVE/late Endosome Associated *alx-1(gk275)* Defects, but not Recycling Endosome Associated Defects.

(A, E, I, M) Confocal images of hTAC-GFP labeled structures (middle focal plane showing the intestine in cross-section) in wild-type, *alx-1(gk275)* mutant, *alx-1(gk275)*;mCherry-ALX-1 and *alx-1(gk275)*;mCherry-ALX-1ΔNPF. (B, F, J, N) Confocal images of SDPN-1-GFP labeled structures (top focal plane near the intestinal basal membrane) in wild-type, *alx-1(gk275)* mutant, *alx-1(gk275)*;mCherry-ALX-1 and *alx-1(gk275)*;mCherry-ALX-1ΔNPF. (C, G, K, O) Confocal images of GFP-HGRS-1

labeled structures (middle focal plane showing the intestine in cross-section) in wild-type, *alx-1(gk275)* mutant, *alx-1(gk275)*;mCherry-ALX-1 and *alx-1(gk275)*;mCherry-ALX-1ΔNPF. (D, H, L, P) Confocal images of LMP-1-GFP labeled structures (middle focal plane showing the intestine in cross-section) in wild-type, *alx-1(gk275)* mutant, *alx-1(gk275)*;mCherry-ALX-1 and *alx-1(gk275)*;mCherry-ALX-1ΔNPF. Scale bars represent 10 μm.

CHAPTER 3: REGULATION OF ENDOSOMAL CLATHRIN AND RETROMER MEDIATED ENDOSOME TO GOLGI RETROGRADE TRANSPORT BY THE J-DOMAIN PROTEIN RME-8

AUTHOR CONTRIBUTIONS

This chapter was published as presented here in *The EMBO Journal (Shi et al., 2009)*.

I participated in the experimental design, performed all the *C. elegans* related experiments, biochemical experiments (Figures 1-5 and Supplemental figures 1, 3-11) and wrote the paper. Dr. Lin Sun performed the *hsp-1(RNAi)* assays (Figure 3-4 and Supplemental figures 5 and 9). Riju Banerjee performed the yeast two hybrid assays (Figure 1 and Supplemental figures 10). Dr. Yinhua Zhang performed the yeast two hybrid screening for RME-8 binding proteins. Michael Tobin participated in yeast two hybrid vectors construction. Dr. Barth D. Grant designed the experiments, trained me for all experiments and wrote the paper.

SUMMARY

After endocytosis most cargo enters the pleiomorphic early endosomes where sorting occurs. As endosomes mature transmembrane cargo can be sequestered into inwardly budding vesicles for degradation, or can exit the endosome in membrane tubules for recycling to the plasma membrane, the recycling endosome, or the Golgi apparatus. Endosome to Golgi transport requires the retromer complex. Without retromer, recycling cargo such as the MIG-14/Wntless protein aberrantly enters the degradative pathway and is depleted from the Golgi. Endosome associated clathrin is also affects the recycling of retrograde cargo and has been shown to function in the formation of endosomal subdomains. Here we find that the *C. elegans* endosomal J-domain protein RME-8 associates with the retromer component SNX-1. Loss of SNX-1, RME-8, or the clathrin chaperone Hsc70/HSP-1 leads to over-accumulation of endosomal clathrin, reduced clathrin dynamics, and missorting of MIG-14 to the lysosome. Our results indicate a mechanism whereby retromer can regulate endosomal clathrin dynamics through RME-8 and Hsc70, promoting the sorting of recycling cargo into the retrograde pathway.

INTRODUCTION

RME-8 was originally identified in *C. elegans* in our previous genetic screens, isolated as a temperature sensitive lethal mutant defective in endocytosis (Grant and Hirsh, 1999; Zhang *et al.*, 2001). Further analysis showed that RME-8 is normally abundant on endosomes but not the plasma membrane, suggesting a role for RME-8 in endosome function rather than plasma membrane uptake processes (Zhang *et al.*, 2001). Subsequently *rme-8* mutants were also identified in genetic screens in Drosophila, showing endocytic defects in several tissues (Chang *et al.*, 2004). Further analysis also showed that as in *C. elegans*, Drosophila RME-8 protein was associated with endosomes and not the plasma membrane (Chang *et al.*, 2004). Likewise the RME-8 ortholog in mammals is tightly associated with the membranes of endosomes but is not enriched on the plasma membrane (Girard *et al.*, 2005; Fujibayashi *et al.*, 2008). In plants RME-8 is also endosome associated and is required for gravitropism, probably due to abnormalities in the vacuole of rme-8 mutant cells that alters amyloplast sedimentation (Silady *et al.*, 2008). Despite all of these observations, an understanding of the precise membrane trafficking defect in *rme-8* mutants has remained elusive.

RME-8 in all of these species is a large protein (>200 kDa) with highly conserved features including a central DNA-J domain and four repeated motifs (IWN repeats) of unknown function (Zhang *et al.*, 2001; Chang *et al.*, 2004; Silady *et al.*, 2004; Girard *et al.*, 2005). DNA-J domains are known to bind to the ubiquitous Hsc70 chaperone, and J-domains in general are a characteristic feature of Hsc70 co-chaperones, proteins that recruit Hsc70 to specific cellular compartments and stimulate Hsc70 ATPase activity

(Walsh *et al.*, 2004). For example the auxillin DNA-J domain protein recruits and activates Hsc70 on clathrin-coated vesicles to facilitate uncoating, a prerequisite for downstream fusion steps (Ungewickell *et al.*, 1995). While auxillin and its paralog GAK mediate this function for CCVs derived from the plasma membrane and Golgi (Greener *et al.*, 2001; Eisenberg and Greene, 2007), RME-8 is the only DNA-J domain protein reported to localize to endosomes. Drosophila and human RME-8 J-domains have been shown to physically interact with Hsc70 (Chang *et al.*, 2004; Girard *et al.*, 2005). Drosophila Hsc70 mutants interact with *rme-8* mutants genetically, and dominant negative Hsc70 expressed in mammalian cells impairs endosome function (Newmyer and Schmid, 2001; Chang *et al.*, 2002). These results suggested that RME-8 could mediate its affects on endosomes via a role as an endosomal Hsc70 co-chaperone.

The early endosome is known to be a hub for the sorting of membrane proteins after endocytosis. In the endosome cargo proteins can either be delivered to lysosomes through multivesicular bodies (MVBs) for degradation, recycled to the plasma membrane directly or indirectly through the recycling endosome, or can be recycled via retrograde transport from endosomes to the trans-Golgi network (TGN). The retrograde pathway and retromer, the major regulatory complex associated with this pathway, are vital for the retrieval of the Golgi sorting receptors from endosomes to the TGN in yeast and mammalian cells (Bonifacino and Hurley, 2008). This includes receptors that transport degradative enzymes to the vacuole/lysosome such as Vps10 and CI-MPR (cation-independent mannose 6-phosphate receptor) (Marcusson *et al.*, 1994; Arighi *et al.*, 2004; Carlton *et al.*, 2004; Seaman, 2004). Recently, retromer-dependent retrieval of the Wnt-

ligand chaperone MIG-14/Wntless has also been demonstrated (Belenkaya *et al.*, 2008; Franch-Marro *et al.*, 2008; Pan *et al.*, 2008; Port *et al.*, 2008; Yang *et al.*, 2008).

Retromer consists of a core complex Vps5-Vps17 (SNX1/2-SNX5/6 in mammals) and a cargo recognition complex Vps26-Vps29-Vps35 (Bonifacino and Hurley, 2008; Collins, 2008). In addition to retromer, clathrin and clathrin related proteins (such as epsinR and AP-1) have also been reported to function as components of the retrograde transport machinery. Clathrin and clathrin adaptor epsinR have been shown to be required for retrograde transport of the Shiga toxin B subunit (Lauvrak *et al.*, 2004; Saint-Pol *et al.*, 2004). Clathrin adaptor AP-1 is also required for retrograde transport of mannose 6-phosphate receptor MPR46 (Meyer *et al.*, 2000). Vps27/Hrs together with the ESCRT-I,II,III (Endosomal Sorting Complex Required for Transport) complexes also functions on early endosomes and MVBs, but rather than promoting retrograde recycling, these proteins are best known for promoting degradation of integral membrane proteins (Katoh *et al.*, 2003; Odorizzi *et al.*, 2003). Importantly Hrs has been linked to the accumulation of endosomal clathrin, promoting the formation of degradative ESCRT-enriched endosomal subdomains (Raiborg *et al.*, 2001a; Raiborg *et al.*, 2002).

In this study, we analyze retrograde transport in C. elegans and identify a previously unsuspected mechanism for the regulation of endosomal clathrin that is required for retrograde transport from endosomes to the Golgi. We show that the J-domain protein RME-8 binds to SNX-1, and that loss-of-function in *rme-8* or *snx-1,* or depletion of *C. elegans* Hsc70 (HSP-1) by RNAi, disrupts endosome to Golgi transport of the retromer-dependent cargo protein MIG-14/Wntless. In the absence of any of RME-8, SNX-1, or HSP-1/Hsc70, MIG-14 is missorted to the late endosome and lysosome and is depleted

from the Golgi. Furthermore we show that loss of any of these three proteins leads to accumulation of clathrin on endosomes and loss of endosomal clathrin dynamics. Our work shows that retromer, through RME-8 and Hsc70, acts to limit clathrin accumulation, a prerequisite for the recycling of retrograde cargo. In the absence of this regulation, the retrograde transport route is lost and cargo that should be retrieved from the endosome is instead degraded.

.

RESULTS

RME-8 physically interacts with SNX-1

In order to better understand the function of RME-8 as an endosomal regulator we screened for interacting proteins using the yeast two-hybrid system. The bait construct included the DNA-J domain and the entire C-terminal half of the RME-8 protein (amino acids 1337-2279; Figure 1C) including IWN repeats 3 and 4 and the intervening ANK-like region. One clone encoding a portion of the retromer component SNX-1 was recovered from this interaction screen (see Methods). Further analysis showed that full-length SNX-1 also interacts with RME-8 in this assay (data not shown). Successively smaller regions of RME-8 were used as bait, narrowing the interacting region to amino acids 1388-1950 (Figure 1B and C). Deletion of amino acids 1388-1619 or 1732-1950 of RME-8 abrogated the interaction, indicating a requirement for RME-8 sequences corresponding to C-terminal region beyond the DNA-J domain, including the adjacent linker between the J-domain and IWN3, IWN3 itself, and the ARM-Like domain (Figure 1B and C). Sequences C-terminal to the ARM-like domain, including IWN4, were dispensable for the interaction.

Residues 423-466 of SNX-1, corresponding to a portion of helix 3 of the SNX-1 VPS5/BAR domain, were necessary and sufficient for the interaction in the yeast 2-hybrid system (Figure 1A and C). This region of the SNX-1 BAR domain is phylogenetically highly conserved, and molecular modeling of the SNX-1 BAR domain suggests that it would be exposed to the cytoplasm, away from the membrane binding surface, where it could interact with other proteins (data not shown).

We also confirmed the binding and the specificity of the RME-8/SNX-1 interaction using an independent GST-pulldown assay. Recombinant GST-SNX-1 (aa 271-472), GST-Y59A8B.22/Snx5, GST-LST-4/Snx9, or GST only, was immobilized on glutathione sepharose beads and incubated with *in vitro* transcribed and translated HA-tagged RME-8 (aa 1337-2279). Only GST-SNX-1, but not other SNX proteins, pulled down RME-8 (Figure 1D; Supplementary Figure 1).

RME-8 colocalizes with SNX-1

SNX-1 is the only *C. elegans* homolog of mammalian Sorting Nexin 1 and Sorting Nexin 2, PX and BAR domain proteins that function in endosome to Golgi retrograde transport with VPS-26, VPS-29, and VPS-35 as part of the retromer complex (Bonifacino and Hurley, 2008). The physical association of RME-8 with SNX-1 suggested that RME-8 might function with the retromer complex on endosomes to mediate retrograde transport. If the RME-8/SNX-1 physical interaction is functionally relevant *in vivo*, then the two proteins would be expected to colocalize on endosomes. Indeed we found that mCherry-RME-8 colocalized extensively with GFP-SNX-1 in several different tissues, including the intestine, the hypodermis, and coelomocytes (Figure 2A-A"; Supplementary Figure 2A-B").

RME-8 and SNX-1 localize to early endosomes but not Golgi

In other organisms the retromer complex, including Snx1 and Snx2, is found primarily on early endosomes, and to a lesser extent on or near the Golgi apparatus (Bonifacino and Hurley, 2008). As expected we found that in *C. elegans* mCherry-SNX-1 colocalized well with early endosomal markers GFP-EEA-1 and GFP-RAB-5 in several tissues of

living animals (Figure 2B-B"; Supplementary Figure 3). GFP-RME-8 also colocalized well with early endosome markers (Figure 2D-D"; Supplementary Figure 4). Like all invertebrate Golgi, *C. elegans* Golgi appears as dispersed ministacks throughout the cell rather than in one large juxtanuclear stack (Sato and Grant). In the intestine the Golgi ministacks are similar in size to early endosomes (Chen *et al.*, 2006). We found very little direct overlap of mCherry-SNX-1 or mCherry-RME-8 with Golgi marker Mannosidase(MANS)-GFP (Figure 2C-C" and E-E"). Rather, we noted that RME-8 and SNX-1 labeled endosomes were very often directly juxtaposed to MANS-labeled Golgi, a localization that could potentially facilitate retrograde transport (Figure 2C" and E", note insets). GFP-RAB-5 also shows a similar high incidence of juxtaposition to MANS-labeled Golgi, further suggesting a close association of a population of endosomes with Golgi ministacks (data not shown).

MIG-14/Wntless is missorted to the late endosome and lysosome in rme-8 and snx-1 mutants

Previous analysis of Golgi-resident retromer-dependent cargo proteins, including the mammalian CI-MPR (cation independent mannose-6-phosphate receptor) and the *C. elegans*, Drosophila, and human MIG-14/Wntless proteins, showed that in the absence of retromer function such cargo is depleted from the Golgi and is missorted to the late endosome and lysosome (Belenkaya *et al.*, 2008; Franch-Marro *et al.*, 2008; Pan *et al.*, 2008; Port *et al.*, 2008; Yang *et al.*, 2008). The resulting increase in CI-MPR and MIG-14/Wntless lysosomal degradation leads to reduced steady-state levels of these cargo proteins in the cell (Rojas *et al.*, 2007). Thus we reasoned that if RME-8 functions with SNX-1 in retrograde transport, rather than in endocytic uptake at the plasma membrane,

then *rme-8* mutants should missort cargo in the same manner as *snx-1* mutants. Conversely, defective endocytosis of such cargo would be expected to lead to cargo accumulation at the plasma membrane, as was previously observed for MIG-14-GFP in *dpy-23/mu2-adaptin* mutants (Pan *et al.*, 2008). To date the only retromer-dependent cargo protein known in *C. elegans* is MIG-14 (Pan *et al.*, 2008; Yang *et al.*, 2008). Thus to determine if RME-8 is required for retrograde transport we assayed for changes in MIG-14-GFP endocytic sorting, comparing wild-type animals with *rme-8* mutants. We also assayed for changes in MIG-14-GFP localization in *snx-1* deletion mutants.

As expected in wild-type animals, MIG-14-GFP colocalized well with the early endosome marker mCherry-RAB-5 and the Golgi marker MANS-mCherry, but not with mCherry-RAB-7, a marker for late endosomes and lysosomes (Supplementary Figure 5A-A", E-E"; Figure 3O-O"). Consistent with the proposition that RME-8 functions with SNX-1 in retrograde transport, both *rme-8* and *snx-1* mutants displayed a greater than 10-fold reduction in average intestinally expressed MIG-14-GFP fluorescence intensity compared to wild-type controls (Figure 3A-C', quantified in Figure 3H). Furthermore, overexpression of RFP fused to SNX-1(423-466), the 43 amino acid fragment of SNX-1 identified above that interacts with RME-8, resulted in a three-fold reduction in MIG-14-GFP fluorescence, presumably by interfering with the association of the endogenous SNX-1 and RME-8 proteins (Supplementary Figure 11A-C). The reduction in MIG-14-GFP signal all of these backgrounds is equivalent to the phenotype previously reported for MIG-14-GFP in *vps-35* mutants (Pan *et al.*, 2008; Yang *et al.*, 2008). In the case of the *rme-8* mutant, which is temperature sensitive, the dramatic redistribution of MIG-14-GFP only occurred at the restrictive temperature (data not shown). We observed similar

reductions in MIG-14-GFP levels in *rme-8* mutant early embryos, indicating that the requirement for RME-8 in sorting of retrograde cargo is not cell-type specific (Supplementary Figure 5I-J).

As controls we assayed the distribution of previously characterized model transmembrane cargos that recycle via the recycling endosome and not the Golgi: the human transferrin receptor (hTfR-GFP) and the IL-2 receptor alpha chain (hTac-GFP) (Chen *et al.*, 2006; Shi *et al.*, 2007). The localization and steady-state levels of these receptors in the intestine were unaffected by mutation of *rme-8* or *snx-1* (Figure 3I-N). Consistent with our results, transferrin endocytosis in mammalian cells is normal after depletion of RME-8 by RNAi (Girard *et al.*, 2005).

In subsequent experiments we boosted the remaining signal for intestinal MIG-14-GFP in mutant animals, in order to determine the fate of MIG-14 under these conditions (Figure 3P-R"; Supplementary Figure 5B-D" and F-H"). Most of the remaining MIG-14-GFP protein in *rme-8* and *snx-1* mutants was found in ring-like late endosomes and lysosomes positive for mCherry-RAB-7, a localization not found in wild-type animals (Figure 3P-Q"). In *rme-8* and *snx-1* mutant cells MIG-14-GFP colocalized with mCherry-RAB-7 on the apparent limiting membrane of these large endosomes, and on mCherry-RAB-7 negative puncta apparently contained within the endosome, possibly intralumenal vesicles (Figure 3P-Q"). MIG-14-GFP could also still be observed in enlarged mCherry-RAB-5 labeled early endosomes in *rme-8* and *snx-1* mutants (Supplementary Figure 5B-C"). However even with the boosted MIG-14-GFP signal, most MANS-labeled Golgi displayed only weak or adjacent MIG-14-GFP labeling in *rme-8* and *snx-1* mutants (Supplementary Figure 5F-G").

MIG-14/Wntless trafficking defects occur after endocytosis in *rme-8* and *snx-1* mutants

To further establish that the altered trafficking itinerary of MIG-14-GFP in *rme-8* and *snx-1* mutants, we blocked endocytic uptake of MIG-14-GFP in the *rme-8* and *snx-1* mutant backgrounds by RNAi-mediated depletion of the mu2 subunit of the clathrin adaptor complex AP-2 (DPY-23) (Pan *et al.*, 2008). This blockade at the cell surface restored MIG-14-GFP fluorescence to levels equal to or above wild-type and enhanced cell surface localization of MIG-14-GFP in both *rme-8* and *snx-1* mutants (Figure 3D-E' and H), indicating that the trafficking defects associated with MIG-14 in *rme-8* and *snx-1* mutants occur after endocytosis, consistent with a role for both proteins in endosomal sorting events. We also inhibited lysosome-mediated degradation by depletion of CUP-5/mucolipin1, a transmembrane protein required for normal lysosome biogenesis and normal levels of hydrolytic activity (Treusch *et al.*, 2004). Such depletion of CUP-5 by RNAi blocked much of the abnormal degradation of MIG-14-GFP in *rme-8* and *snx-1* mutants (Figure 3F-G' and H), indicating that loss of *rme-8* or *snx-1* leads to degradation of MIG-14 via missorting into the lysosomal pathway. Similarly, the loss of MIG-14-GFP in *rme-8* and *snx-1* mutants was also ameliorated by RNAi-mediated depletion of VPS-37, a component of the ESCRT-I complex (data not shown).

The increased degradation of MIG-14-GFP suggested that MVB-mediated transport of membrane proteins to the lysosome does not require RME-8 or SNX-1. To examine this point further we also assayed degradation of CAV-1-GFP in early embryos (Sato *et al.*, 2006; Shi *et al.*, 2007). CAV-1 is a known transmembrane cargo protein that is degraded in the one cell embryo after the metaphase to anaphase transition (Sato *et al.*, 2006;

Bembenek *et al.*, 2007; Sato *et al.*, 2008a). Degradation of CAV-1-GFP requires endocytosis and ESCRT-mediated endosomal sorting (Sato *et al.*, 2006; Audhya *et al.*, 2007b). CAV-1-GFP degradation was unaffected in *rme-8(b1023)* and *snx-1(tm847)* mutants, further suggesting that RME-8 and SNX-1 are not required for ESCRT-mediated degradation of integral membrane proteins (Supplementary Figure 8A-C′).

Neuronal cell polarity is impaired in *rme-8* and *snx-1* mutants

The observed abnormal degradation of MIG-14 in *rme-8* and *snx-1* mutants would be expected to impair Wnt signaling, as shown previously for *vps-35* mutants. To test for an effect of loss of RME-8 and SNX-1 on Wnt signaling, we examined the control of mechanosensory neuron polarity, a process that requires MIG-14 and retromer regulated Wnt signaling (Prasad and Clark, 2006; Pan *et al.*, 2008). Since *rme-8(b1023)* is lethal at 20ºC or higher we examined the *rme-8* effect on this phenotype at the permissive temperature (15ºC), where *rme-8* mutants display partially penetrant phenotypes. We found that *rme-8(b1023)* and *snx-1(tm847)* display defective ALM posterior processes at a penetrance similar to that previously shown for *vps-35* mutants (Supplementary Figure 6A-C and G) (Pan *et al.*, 2008). Defective PLM posterior processes were also observed in both mutants, although in this case the *snx-1* null mutant showed a higher penetrance than the partial loss of RME-8 (Supplementary Figure 6D-F and H). These results are consistent with the requirements we identified for RME-8 and SNX-1 in the control of MIG-14 trafficking.

Depletion of C. elegans Hsc70 (HSP-1) causes MIG-14/Wntless missorting to the late endosome and lysosome

We next sought to better understand the mechanism by which RME-8 influences endosome function and regulates retrograde transport. Recent work has shown that retrograde transport of the glycosphingolipid binding bacterial Shiga toxin (STxB), and another retrograde cargo protein TGN46, from the early endosome to the Golgi, requires endosomal clathrin and the clathrin adaptor epsinR (Saint-Pol *et al.*, 2004; Popoff *et al.*, 2007). Depletion of RME-8 from the cells of several organisms has been shown to produce abnormal clathrin distribution *in vivo* (Chang *et al.*, 2004; Girard *et al.*, 2005), and like human and Drosophila RME-8, we found that the *C. elegans* RME-8 J-domain binds to HSP-1/Hsc70 *in vitro* (Supplementary Figure 11D). Thus to better understand how RME-8 functions, we examined the relationship between endosomal clathrin, RME-8, and SNX-1. One simple model that could explain these observations would be that SNX-1 cooperates with RME-8 to activate endosomal Hsc70, and in turn Hsc70 chaperone activity on the endosome controls endosomal clathrin dynamics to promote retrograde sorting.

Consistent with this model we found that depletion of *C. elegans* Hsc70 (HSP-1) by RNAi resulted in aberrant sorting of MIG-14-GFP, very similar to the phenotype observed for *rme-8* and *snx-1* mutants (Figure 3R-R"; Supplementary Figure 5D-D", H-H"). After HSP-1 RNAi, MIG-14-GFP levels were reduced and most of the remaining MIG-14-GFP signal was found within large mCherry-RAB-7 labeled endosomes/lysosomes (Figure 3R-R"). Similar to the effects observed in *rme-8* and *snx-1* mutants, *hsp-1(RNAi)* led to MIG-14-GFP labeling of the mCherry-RAB-7 labeled limiting membrane, and smaller mCherry-RAB-7 negative puncta that appeared to be within the RAB-7-labeled ring (Figure 3R-R"). GFP-SNX-1 and GFP-VPS-35 protein

levels were not reduced in *rme-8(b1023)* or *hsp-1(RNAi)* animals, suggesting that the defects in retrograde transport were not via effects on retromer protein stability (Supplementary Figure 7A and B). The congruence of *snx-1*, *rme-8*, and *hsp-1* phenotypes indicates that all three proteins function in a common process.

Loss of SNX-1, RME-8, or HSP-1 leads to clathrin accumulation on endosomes

Next we examined the localization of a fully functional GFP-tagged clathrin heavy chain (GFP-CHC-1) (Greener *et al.*, 2001; Sato, 2008). In *rme-8* and *snx-1* mutants GFP-CHC-1 accumulated in abnormally bright puncta throughout the cell, suggesting an accumulation of membrane bound clathrin (Figure 4A-C, quantified in Figure 4E; Supplementary Figure 9E-F). A similar effect was observed in GFP-CHC-1 expressing animals after RNAi-mediated depletion of HSP-1/Hsc70 (Figure 4D-E). Further analysis showed that many of the intracellular GFP-CHC-1 puncta were positive for mCherry-RAB-5, indicating that much of the accumulated clathrin was on early endosomes (Figure 4F-I; Supplementary Figure 9A-D"). The observed enlargement of early endosomes did not require overexpression of clathrin, as enlargement was also found in GFP-RAB-5 and GFP-RAB-10 positive early endosomes in *rme-8* mutants not expressing GFP-CHC-1 (Supplementary Figure 9G-J). Further analysis showed that in *rme-8* mutants mCherry-SNX-1 and GFP-CHC-1 accumulated together in these structures (Figure 4L-M"). Single labeled GFP-SNX-1 or GFP-CHC-1 puncta also appeared morphologically abnormal in other tissues of *rme-8* mutants (Supplementary Figure 9E-F and K-N). Likewise in *snx-1* mutants, mCherry-RME-8 and GFP-CHC-1 co-accumulated on the same structures (Figure 4J-K"). These results indicate that RME-8, SNX-1, and HSP-1/Hsc70 are all

important for the regulation of endosomal clathrin, and that the presence of only RME-8 or SNX-1 on the endosome is not sufficient for proper clathrin regulation.

Loss of SNX-1, RME-8, or HSP-1/Hsc70 impairs clathrin dynamics

Expression of ATPase-defective forms of Hsc70 in mammalian cells is known to result in the loss of the unassembled cytosolic pool of clathrin (Newmyer and Schmid, 2001). Likewise, in Drosophila Hsc70 partial loss-of-function mutants, GFP-tagged clathrin was previously shown to aggregate within the cell, although the labeled compartment was not identified (Chang *et al.*, 2002). These results are consistent with the phenotype we show above for *hsp-1/Hsc70* RNAi in *C. elegans*. *In vivo* membrane-bound clathrin is highly dynamic as evidenced by its rapid exchange with free cytosolic clathrin (Newmyer and Schmid, 2001; Lee *et al.*, 2005). This dynamic exchange of cytosolic and membrane bound clathrin is generally measured using Fluorescence Recovery After Photobleaching (FRAP) in cells expressing GFP-tagged clathrin (Greener *et al.*, 2001; Wu *et al.*, 2001). In the absence of Hsc70 co-chaperone activity, or in the absence of Hsc70 itself, the levels of membrane associated GFP-clathrin would be expected to increase, and exchange of such GFP-clathrin with cytosolic pools would be expected to decrease, interfering with fluorescence recovery. We compared the recovery after photobleaching of GFP-CHC-1 puncta in wild-type animals with those lacking RME-8, SNX-1, or HSP-1/Hsc70 due to mutation or RNAi. Consistent with a role for these three proteins functioning together to regulate clathrin dynamics/disassembly on endosomes, GFP-CHC-1 fluorescence recovery in cytoplasmic puncta was greatly impaired in animals deficient in RME-8, SNX-1, or HSP-1/Hsc70 (Figure 5A-E). HSP-1 RNAi produced a weaker effect than

mutation of RME-8 or SNX-1, likely due to residual HSP-1 after RNAi treatment, and/or the expression of additional Hsc70 homologs in the animal.

Intramolecular Interactions within RME-8

The above data suggests that SNX-1 is required for RME-8 function, but not for RME-8 stability or localization. Many proteins are not constitutively active, but rather are autoinhibited and can only achieve full activity when autoinhibitory interactions are disrupted via intermolecular binding to a partner protein. As first step toward understanding the mechanism of RME-8 regulation, we sought to determine if the RME-8 DNA-J domain has the potential to form intramolecular interactions with other domains within RME-8. To test this idea we separated the J-domain (aa1322-1388) from regions of RME-8 c-terminal to the J-domain (aa1388-2279), and assayed for interaction between the two pieces of RME-8. Yeast 2-hybrid and GST-pulldown assays both indicated that the J-domain of RME-8 can bind to the C-terminal half of RME-8 (Supplementary Figure10A-B), indicating that *in vivo* the J-domain of RME-8 may be occupied in an intramolecular interaction.

DISCUSSION

In this work we have shown that RME-8 and SNX-1 are required to rescue MIG-14 from degradation after its endocytosis. Our results showing the aberrant sorting and degradation of MIG-14 in *snx-1* and *rme-8* mutants are quite similar to those previously shown for CI-M6PR after co-depletion of Snx1 and Snx2, or single depletion of other retromer components, in mammalian cells (Rojas *et al.*, 2007). Our results are also reminiscent of the aberrant sorting and degradation of the EGF-R after siRNA-mediated depletion of RME-8 in mammalian cells (Girard and McPherson, 2008). In fact this similarity in phenotype may indicate that a fraction of EGF-Rs recycle via the retrograde endosome to Golgi pathway.

However CI-M6PR steady state levels were not reported to be reduced after siRNA-mediated depletion of RME-8 (Girard *et al.*, 2005). Rather CI-M6PR was reported to aberrantly accumulate in or near the Golgi (Girard *et al.*, 2005). We do not yet understand this apparent difference in RME-8 and Snx1/2 phenotype with respect to M6PR, but suspect that they may reflect differences in the requirements for RME-8 and retromer in sorting of specific cargo, and/or their requirements in alternative retrograde pathways. For instance, in addition to the early endosome to Golgi route, the CI-M6PR is known to recycle to the Golgi via the late endosome, using a Rab9-dependent pathway (Lombardi *et al.*, 1993). In addition, after endocytosis CI-M6PR retrieval to the Golgi has been shown to be mediated by the recycling endosome (Lin *et al.*, 2001; Lin *et al.*, 2004). RME-8 may be specific to the early endosome, while retromer may be more generally required. In the worm MIG-14-GFP trafficking was identically affected by loss of RME-8 or SNX-1. It is not known if worm and mammalian MIG-14 have access to alternative

retrograde routes. It is also worth noting that in the case of the worm, the Rab9 pathway may not even exist, since the *C. elegans* genome lacks a Rab9 homolog.

With regard to the early endosome, our data indicates that RME-8 and SNX-1 are important clathrin regulators, and strongly suggests that SNX-1 and RME-8 regulate endosomal clathrin disassembly through HSP-1/Hsc70. Previous analysis has indicated that clathrin functions on endosomes, at least in part, to create endosomal subdomains (Raiborg *et al.*, 2001b; Raiborg *et al.*, 2002; Raiborg *et al.*, 2006). Such subdomains have been implicated in the sorting of cargo into the degradative compartment through their association with the ubiquitin and clathrin scaffolding protein Hrs. Hrs, along with its partner STAM, is often referred to as ESCRT-0 to denote its physical connection to the TSG101 component of the ESCRT-I complex and its role in cargo recognition. The ESCRT machinery functions to sort mono-ubiquitinated integral membrane cargo into intralumenal vesicles of the endosome, leading to their degradation in the lysosome. Hrs binds to ubiquitinated cargo and to endosomal clathrin, and when Hrs is depleted endosomal clathrin is lost (Raiborg *et al.*, 2001b; Raiborg *et al.*, 2002; Raiborg *et al.*, 2006). In the absence of Hrs or endosomal clathrin, the normal subdomain organization of the early endosome is disrupted (Raiborg *et al.*, 2001b; Raiborg *et al.*, 2002; Raiborg *et al.*, 2006).

Within these same endosomes, clathrin has been recently shown to regulate endosomal sorting into the retrograde recycling pathway, somehow cooperating with the retromer complex to recycle cargo from endosomes to the Golgi (Saint-Pol *et al.*, 2004). Related work suggests that clathrin functions early in the sorting process (Popoff *et al.*, 2007). In the absence of clathrin, retrograde sorting is altered (Saint-Pol *et al.*, 2004; Popoff *et al.*,

2007; Skanland *et al.*, 2009). In the case of ricin toxin, clathrin depletion increases transport from endosomes to the Golgi (Skanland *et al.*, 2009). Our work indicates that the SNX-1 component of retromer, previously known to provide membrane binding and curvature inducing abilities to the complex, also physically interacts with RME-8 to negatively regulate endosomal clathrin accumulation and promote clathrin dynamics, such that sorting into the retrograde pathway can proceed. In the absence of the SNX-1/RME-8/Hsc70-mediated regulation, degradative sorting appears to continue, but is deregulated, depleting the cell of cargo that would normally be recycling to the Golgi. Thus, with respect to clathrin, SNX-1, RME-8, and HSP-1/Hsc70 appear to act oppositely to Hrs in the endosome (Supplementary Figure 10C). The opposing activities of Hrs and RME-8 on clathrin accumulation could maintain an equilibrium between endosomal subdomains, such that degradative and recycling functions can coexist in the same endosome.

Unlike the well studied clathrin co-chaperones auxilin and GAK, RME-8 does not appear to bind directly to clathrin (Girard *et al.*, 2005). Interestingly, recent studies showed that the N-terminal PX domains of several sorting nexins, including human SNX-1 orthologs Snx1 and Snx2, bind to clathrin via an inverted clathrin box motif (Skanland *et al.*, 2009). This inverted clathrin-binding motif is identical in *C. elegans* and human SNX-1/Snx1, suggesting that SNX-1 family protein could act to bridge RME-8 and clathrin, thus completing the Hsc70 to clathrin connection.

An additional, and not mutually exclusive, model for the role of RME-8/SNX-1 binding is that the RME-8 J-domain might normally be autoinhibited by interaction with other domains within RME-8. If so then SNX-1 binding to RME-8 might relieve this

autoinhibition, allowing the J-domain to bind and stimulate Hsc70. This idea is supported by our observation that the isolated RME-8 J-domain can bind to the C-terminal half of RME-8 *in vitro*. Significant future work will be required to better understand the relationship between RME-8 and SNX-1, testing such models to obtain greater insight into the formation and maintenance of endosomal subdomains and retrograde transport.

MATERIALS AND METHODS

General Methods and Strains

All *C. elegans* strains were derived originally from the wild-type Bristol strain N2. Worm cultures, genetic crosses, and other *C. elegans* husbandry were performed according to standard protocols (Brenner, 1974). Strains expressing transgenes were grown at 20°C. A complete list of strains used in this study can be found in Supplementary Table 1.

RNAi was performed using the feeding method (Timmons and Fire, 1998). Feeding constructs were either from the Ahringer library (Kamath and Ahringer, 2003) or prepared by PCR from EST clones provided by Dr. Yuji Kohara (National Institute of Genetic, Japan) followed by subcloning into the RNAi vector L4440 (Timmons and Fire, 1998). For most experiments synchronized L1 or L3 stage animals were treated for 48-72 hours and were scored as adults.

Antibodies

The following antibodies were used in this study: mouse anti-HA monoclonal antibody (16B12) Covance Research Products (Berkeley, CA), rabbit anti-GST polyclonal antibody (Z-5) Santa Cruz Biotechnologies (Santa Cruz, CA).

Yeast two-hybrid analyses

The yeast two-hybrid screen was performed using the Gal4-based Proquest System (Invitrogen, Carlsbad, CA) according to manufacturer's instructions. The pDBLeu-RME-8 bait plasmid, containing the C-terminal 951 amino acids of RME-8 (aa 1337-2279), was transformed into yeast strain MaV203. MaV203 bearing the bait plasmid was amplified and transformed with the Vidal *C. elegans* library in prey vector PC86,

essentially as described (Walhout *et al.*, 2000). Approximately four million clones were screened on histidine dropout plates. A single positive clone was recovered and re-tested as positive in the His and β-Gal assays after isolation and re-transformation with fresh bait plasmid. This positive clone contained a portion of a *snx-1* cDNA encoding the C-terminal 251 amino acids (aa 221-472). The LexA-based DupLEX-A yeast two-hybrid system (OriGene Technologies Inc., Rockville, MD) was used for all subsequent analysis, according to the manufacturer's instructions. pSH18-34 was used as reporter in all the yeast two-hybrid experiments. Constructs were introduced into the yeast strain EGY48 included in the system. To assess the expression of the *LEU2* reporter, transformants were selected on plates lacking leucine, histidine, tryptophan and uracil, containing 2% galactose/1% raffinose at 30^{o}C for 3 days. Blue/white B-galactosidase assays, performed according to manufacturer's instructions, confirmed results shown for growth assays.

Protein expression and Coprecipitation assays

N-terminally HA-tagged proteins: RME-8 (aa 1337-2279), RME-8 (aa1388-2279); HSP-1 were synthesized *in vitro* using the TNT coupled transcription-translation system (Promega) using DNA templates pcDNA3.1-2xHA-RME-8(1337-2279), pcDNA3.1-2xHA-RME-8(1388-2279), pcDNA3.1-2xHA-HSP-1 respectively (1.6 µg/each 50 µl reaction). The reaction cocktail was incubated at 30°C for 90 minutes. Control Glutathione S-transferase (GST), GST-SNX-1(aa271-472), GST-Y59A8B.22, GST-LST-4, GST-RME-8(aa1322-1388) fusion proteins were expressed in the *ArcticExpress*™ strain of *E. coli* (Stratagene). Bacterial pellets were lysed in 10 ml B-PER Bacterial Protein Extraction Reagent (Pierce) with Complete Protease Inhibitor Cocktail Tablets

(Roche). Extracts were cleared by centrifugation and supernatants were incubated with glutathione-Sepharose 4B beads (Amersham Pharmacia) at 4°C overnight. Beads were then washed six times with cold STET buffer (10mM Tris-HCl pH8.0, 150mM NaCl, 1mM EDTA, 0.1% Tween-20). *In vitro* synthesized HA-tagged protein (10 µl TNT mix diluted in 500 µl STET) was added to the beads and allowed to bind at 4°C for 2 hours. After six additional washes in STET the proteins were eluted by boiling in 30 µl 2xSDS-PAGE sample buffer. Eluted proteins were separated on SDS-PAGE (10% polyacrylamide), blotted to nitrocellulose, and probed with anti-HA (16B12). Subsequently the blots were stripped and re-probed with anti-GST (Z-5) antibodies.

Plasmids and Transgenic Strains

The Proquest system two-hybrid bait plasmid pDBLeu-RME-8(1337-2279) was generated as a PCR product from template cDNA clone yk398h12, cloned into the unique SalI-NotI sites of the vector. All Origene system two-hybrid plasmids were generated as PCR products with Gateway attB.1 and attB.2 sequence extensions, and were introduced into the Gateway entry vector pDONR221 by BP reaction. They were then transferred into the final destination vector using Gateway recombination cloning (Invitrogen) LR reaction. The bait vector pEG202-Gtwy and target vector pJG4-5-Gtwy have been described previously (Sato *et al.*, 2008b). Prey plasmids encoded full length SNX-1 (aa1-472) and SNX-1 truncations (aa 221-472, aa 271-472, aa 221-422, aa271-466, and aa423-466) were amplified from *snx-1* cDNA clone yk290f7. All amplified regions were confirmed by DNA sequencing. RME-8(1337-2279), RME-8(1388-2279) and HSP-1 (gift of Jon Audhya) cDNA clones were transferred into an in-house modified vector pcDNA3.1 (+) (Invitrogen, Carlsbad, CA) with 2xHA epitope tag and Gateway cassette

(Invitrogen, Carlsbad, CA) for *in vitro* transcription/translation experiments. For GST pulldown experiments an equivalent *snx-1*(271-472) PCR product, *Y59A8B.22/SNX5* PCR product (from cDNA clone yk1476h03), *lst-4/Snx4p* PCR product (from cDNA clone yk1061f06) and *rme-8(1322-1388)* PCR product were introduced in frame into vector pGEX-2T (GE Healthcare Life Sciences) modified with a Gateway cassette.

To create the GFP-SNX-1 plasmid driven by the *snx-1* promoter, 738 bp of *snx-1* promoter sequence was PCR amplified from *C. elegans* genomic DNA with primers containing Sal I and Kpn I restriction sites and cloned into the same sites in the *C. elegans* GFP vector pPD117.01 (gift of Andrew Fire). The entire *snx-1* gene body and 3' UTR (3848 bp) was then PCR amplified with primers including Ngo MI and Apa I restriction sites and cloned into the same sites downstream of GFP. The equivalent RFP-SNX-1 plasmid was created by cloning mRFP1 (gift of Roger Tsien) into the unique Kpn I and EcoR I sites, replacing GFP. The GFP-RME-8 and mRFP1-RME-8 fusion plasmids and strains driven by the *rme-8* promoter was previously described (Zhang *et al.*, 2001; Treusch *et al.*, 2004). To construct GFP or mCherry/RFP fusion transgenes for expression specifically in the worm intestine, two previously described Gateway destination vectors (Chen *et al.*, 2006) were used that contain the promoter region of the intestine-specific gene *vha-6* cloned into the *C. elegans* pPD117.01 vector, followed by GFP or mCherry/RFP coding sequences, a Gateway cassette (Invitrogen, Carlsbad, CA), and *let-858* 3' UTR sequences, followed by the *unc-119* gene of *C. briggsae*. The sequences of *C. elegans rme-8(minigene)*, *snx-1(cDNA), snx-1(423-466)* and *vps-35(genomic DNA)* were cloned individually into entry vector pDONR221 by PCR and BP reaction, and then transferred into intestinal expression vectors by Gateway

recombination cloning LR reaction to generate N-terminal fusions. The *mig-14* expression plasmid was created by PCR amplification and Gateway cloning of the *mig-14* cDNA (gift of Iva Greenwald), lacking a stop codon, into a previously described *vha-6* promoter driven vector modified with a Gateway cassette inserted at the Asp718I site just upstream of the GFP coding region (Chen *et al.*, 2006). Germline MIG-14 expression was driven by the *pie-1* promoter using Gateway vector pJK7 (gift of Jayne Squirrel). Complete plasmid sequences are available on request. Low copy integrated transgenic lines for all of these plasmids were obtained by the microparticle bombardment method (Praitis *et al.*, 2001).

Microscopy and Image Analysis

Live worms were mounted on 2% agarose pads with 10 mM levamisol as described previously (Sato *et al.*, 2005). Multi-wavelength fluorescence images were obtained using an Axiovert 200M (Carl Zeiss MicroImaging, Oberkochen, Germany) microscope equipped with a digital CCD camera (C4742–12ER, Hamamatsu Photonics, Hamamatsu, Japan), captured using Metamorph software ver 6.3r2 (Universal Imaging, West Chester, PA), and then deconvolved using AutoDeblur Gold software ver 9.3 (AutoQuant Imaging, Watervliet, NY). Images taken in the DAPI channel were used to identify broad-spectrum intestinal autofluorescence caused by lipofuscin-positive lysosome-like organelles (Clokey and Jacobson, 1986; Hermann *et al.*, 2005). To obtain images of GFP fluorescence without interference from autofluorescence, we used argon 488nm excitation and the spectral fingerprinting function of the Zeiss LSM510 Meta confocal microscope system (Carl Zeiss MicroImaging) as described previously (Chen *et al.*,

2006). Quantification of images was performed with Metamorph software ver 6.3r2 (Universal Imaging).

Most GFP/mCherry colocalization experiments were performed on L3 and L4 larvae expressing GFP and mCherry-markers as previously described. In colocalization assays of MIG-14-GFP with mCherry-RAB-7, mCherry-RAB-5 and MANS-mCherry (Figure 3O-R"; Supplementary Figure 5A-H") in *rme-8(b1023)* and *snx-1(tm847)* mutants, or *hsp-1(RNAi)* knock-down animals, we boosted MIG-14-GFP intensity by doubling the exposure time (200ms) compared to wild-type controls (100ms). We further altered the scaling factor in the Metamorph software to reveal the low intensity GFP signal in the mutant backgrounds. Without these changes to the imaging protocol the MIG-14-GFP intensity was too weak to localize in these mutants.

FRAP Analysis

Worms were grown at 25°C overnight, then mounted live on 2% agarose pads with 10 mM levamisol and imaged at room temperature (approximately 22°C) on the stage of a Zeiss LSM 510 laser scanning confocal microscope using the argon 488nm 25mW laser and water-immersion objective (× 63). GFP-CHC-1 fluorescence was photobleached in a small defined region with 30 iterations at 25% laser power/100% excitation. After bleaching, fluorescence intensity in the bleached area was monitored over time by scanning at 5% excitation every 10 s. Data sets where the focal planes shifted due to animal movement were discarded.

To assess differences in GFP-CHC-1 recovery in different mutants or RNAi knock-down animals, we determined recovery curves of fluorescence intensities at the same

photobleaching setting and corrected for background versus time. Error bars represent standard deviations from the mean (n=8 each time point, 8 animals of each genotype were sampled). All data points shown were collected on the same day. Similar experiments done on two other occasions gave equivalent results.

Neuronal Polarity Assay

Transgenic line zdIs5[Pmec-4::gfp] was used to assay neuronal polarity of mechanosensory ALM and PLM neurons as described previously (Prasad and Clark, 2006; Pan *et al.*, 2008). An ALM posterior process that was longer than five ALM cell body diameters in length was scored as defective (numbers of axons scored: wild-type: 100; *rme-8(b1023)*: 120; *snx-1(tm847)*: 100). A PLM posterior process that extends to the tip of the tail was scored as defective (numbers of axons scored: wild-type: 60; *rme-8(b1023)*: 90; *snx-1(tm847)*: 80).

Western Analysis

Total protein extracts were made from synchronized *C.elegans* adult animals (n=40 each). 40µl worm boil buffer (100 mM Tris pH 6.8, 8% SDS, 20 mM b-mercaptoethanol) was added to the pellet. The worm mixture was boiled for 60 minutes at 100ºC, then checked for complete solublization of protein under a dissecting microscope. Proteins were size separated by SDS-PAGE and transferred to nitrocellulose. Probing and visualization of GFP-SNX-1 and GFP-VPS-35 were performed using HRP-conjugated GFP Abs (1:10000 dilution) incubated with the blot overnight at 4°C.

ACKNOWLEDGEMENTS

We thank Iva Greenwald, Andrew Fire, Roger Tsien, Jon Audhya, Monica Driscoll and Jayne Squirrel for important reagents. We also thank P. Schweinsberg and Z. Pan for their generous advice and technical assistance. R.B. was supported by Aresty Research Center grant. This work was supported by March of Dimes grant #5-FY02-252 and NIH Grant GM067237 to B.D.G.

Table 1. Transgenic and Mutant Strains Used in This Study

Transgenic and Mutant Strains Used in This Study
pwIs82[snx-1::mRFP1::snx-1](Sakisaka et al., 1997)
pwIs94[psnx-1::GFP::snx-1](Sakisaka et al., 1997)
*bIs34[*p*rme-8::GFP::RME-8](Zhang et al., 2001)*
*cdIs73[*p*rme-8::mRFP1::RME-8](Treusch et al., 2004)*
*pwIs784[*p*vha6::GFP::SNX-1](Sakisaka et al., 1997)*
*pwIs782[*p*vha6::mCherry::SNX-1](Sakisaka et al., 1997)*
*pwIs780 [*p*vha6::mCherry::RME-8](Sakisaka et al., 1997)*
*pwIs439[*p*rab-5::GFP::RAB-5](Sakisaka et al., 1997)*
*pwIs72[*p*vha6::GFP::RAB-5](Chen et al., 2006)*
pwIs493[vha6::mCherry::RAB-5](Sakisaka et al., 1997)
*pwIs481[*p*vha6::MANS::GFP](Chen et al., 2006)*
pwEx102[vha6::MANS::mCherry](Sakisaka et al., 1997)
*pwIs765[*p*vha6::MIG-14::GFP](Sakisaka et al., 1997)*
*pwIs792[*p*pie1::MIG-14::GFP](Sakisaka et al., 1997)*
*pwIs170[*p*vha6::GFP::RAB-7](Chen et al., 2006)*
pwIs429[vha6::mCherry::RAB-7](Sakisaka et al., 1997)
*pwIs112[*p*vha6::hTAC::GFP](Chen et al., 2006)*
*pwIs90[*p*vha6::hTfR::GFP](Chen et al., 2006)*
*dkIs8 [*p*vha6::GFP::CHC-1](Sato, 2008)*
*pwIs126[*p*eea-1::GFP::EEA-1](Sakisaka et al., 1997)*
*pwIs206[*p*vha6::GFP::RAB-10](Chen et al., 2006)*
*pwIs823[*p*vha6::GFP::VPS-35]*
pwIs856[vha6::RFP::SNX-1 aa423-466]
*zdIs5[*p*mec-4::GFP, lin-15(+)](Pan et al., 2008)*
rme-8(b1023)(Zhang et al., 2001)
snx-1(tm847) (kindly provided by Dr. Shohei Mitani, Japanese National Bioresource Project for the Experimental Animal "Nematode *C. elegans*"*)*

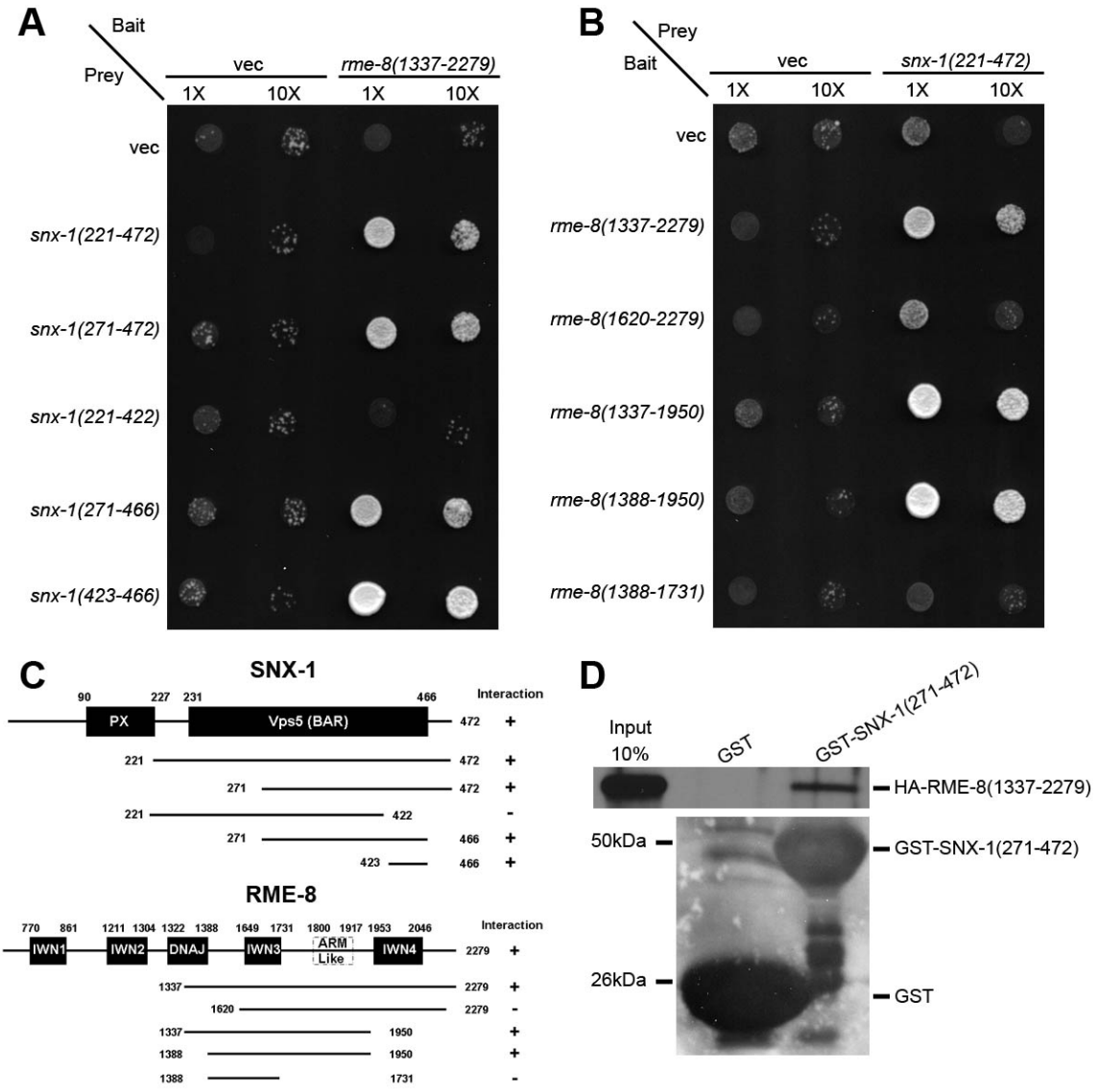

Figure 1. RME-8 physically interacts with SNX-1

(A) The interaction between RME-8 and SNX-1 requires C-terminal SNX-1 residues span 423-466. RME-8 (residues 1337–2279) was expressed in a yeast reporter strain as a fusion with the DNA-binding domain of LexA (bait). SNX-1 and its truncated forms were expressed in the same yeast cells as fusions with the B42 transcriptional activation domain (prey). Interaction between bait and prey was assayed by complementation of leucine auxotrophy (LEU2 growth assay). Colonies were diluted in liquid and spotted on

solid growth medium directly or after further 10X dilution. **(B)** The interaction of RME-8 with SNX-1 requires RME-8 C-terminal sequences to the DNA-J domain. SNX-1 (residues 221–472) was expressed in a yeast reporter strain a fusion with the B42 transcriptional activation domain (prey). Mutant forms of RME-8 were expressed in the same yeast cells as a fusion with the DNA-binding domain of LexA (bait). Interaction between bait and prey was assayed by complementation of leucine auxotrophy (LEU2 growth assay) as above. **(C)** Schematic representations of SNX-1 and RME-8 and the regions of each used in the Y2H analysis. Protein domains are displayed as boxes (white for the ARM-Like domain, dark for others) above protein sequences used in the study (shown as dark lines). Amino acid numbers are indicated. **(D)** Glutathione beads loaded with recombinant GST or GST-SNX-1(271-472) were incubated with *in vitro* expressed HA-RME-8(1337-2279), and then washed to remove unbound proteins. Bound proteins were eluted and analyzed by western blot using anti-HA (top) or anti-GST (bottom) antibodies. Input lane contain *in vitro* expressed HA-RME-8(1337-2279) used in the binding assays (10%).

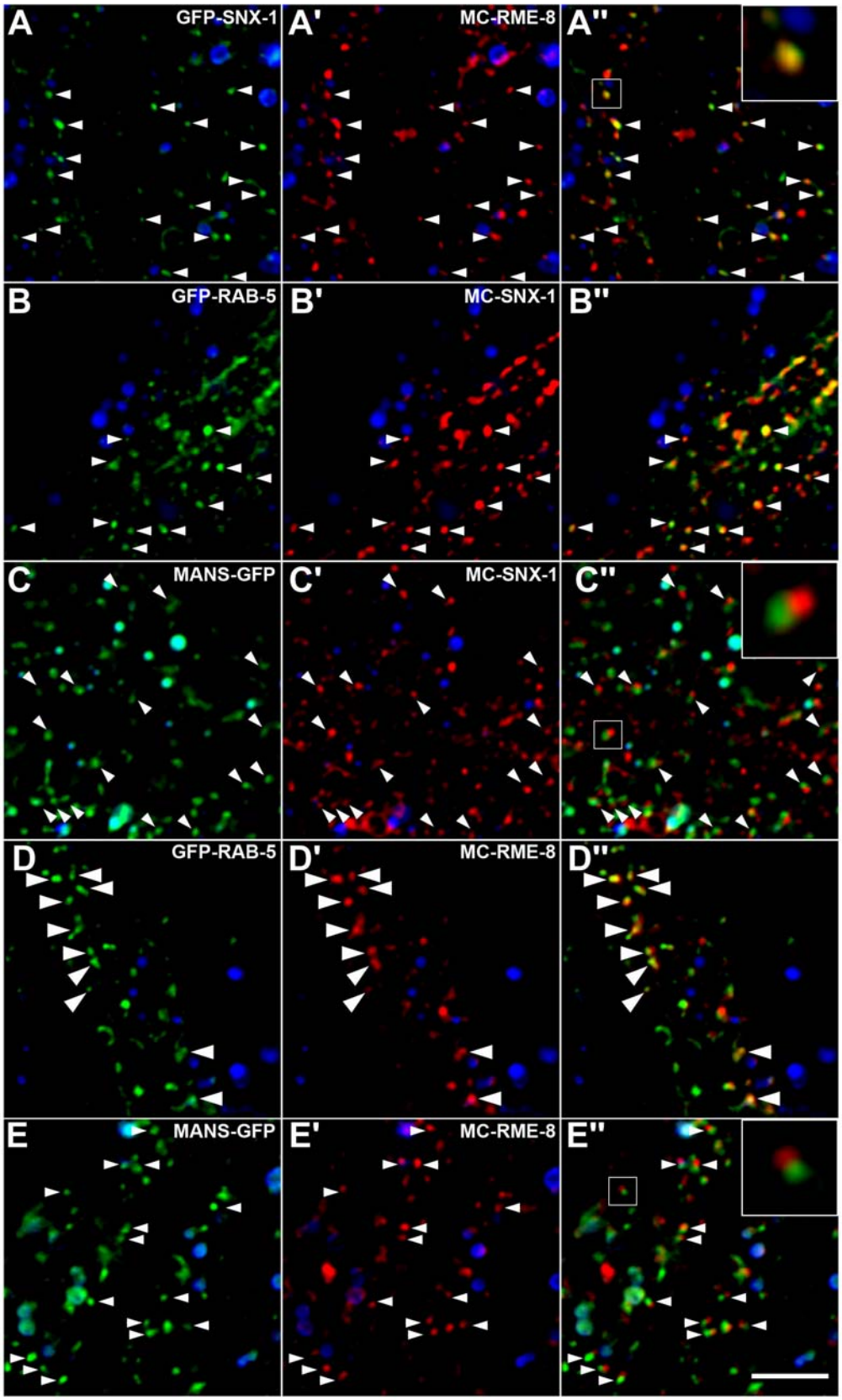
A
GFP-SNX-1
A'
MC-RME-8
A''
B
GFP-RAB-5
B'
MC-SNX-1
B''
C
MANS-GFP
C'
MC-SNX-1
C''
D
GFP-RAB-5
D'
MC-RME-8
D''
E
MANS-GFP
E'
MC-RME-8
E''

Figure 2. RME-8 colocalizes with SNX-1 and RAB-5 on early endosomes

Representative images from deconvolved 3-D image stacks are shown. All images were acquired in intact living animals expressing GFP and mCherry tagged proteins specifically in intestinal epithelial cells. **(A-A")** mCherry-RME-8 colocalizes with GFP-SNX-1. Arrowheads indicate endosomes labeled by both GFP-SNX-1 and mCherry-RME-8. **(B-B")** mCherry-SNX-1 colocalizes with early endosome marker GFP-RAB-5. Arrowheads indicate endosomes labeled by both GFP-RAB-5 and mCherry-SNX-1. **(C-C")** mCherry-SNX-1 does not colocalize well with Golgi marker Mannosidase-GFP. Arrowheads and the inset indicate mCherry-SNX-1 positive endosomes juxtaposed to Mannosidase-GFP labeled Golgi ministacks. **(D-D")** mCherry-RME-8 colocalizes with early endosome marker GFP-RAB-5. Arrowheads indicate endosomes labeled by both GFP-RAB-5 and mCherry-RME-8. (**E-E")** mCherry-RME-8 does not colocalize well with Golgi marker Mannosidase-GFP. Arrowheads and the inset indicate mCherry-RME-8 positive endosomes juxtaposed to Mannosidase-GFP labeled Golgi ministacks. Enlarged images (4x) of boxed regions are shown in the insets. In each image autofluorescent lysosome-like organelles can be seen in all three channels with the strongest signal in blue, whereas GFP appears only in the green channel and mCherry only in the red channel. Signals observed in the green or red channels that do not overlap with signals in the blue channel are considered bone fide GFP or mCherry signals, respectively. Scale bar represents 10 μm.

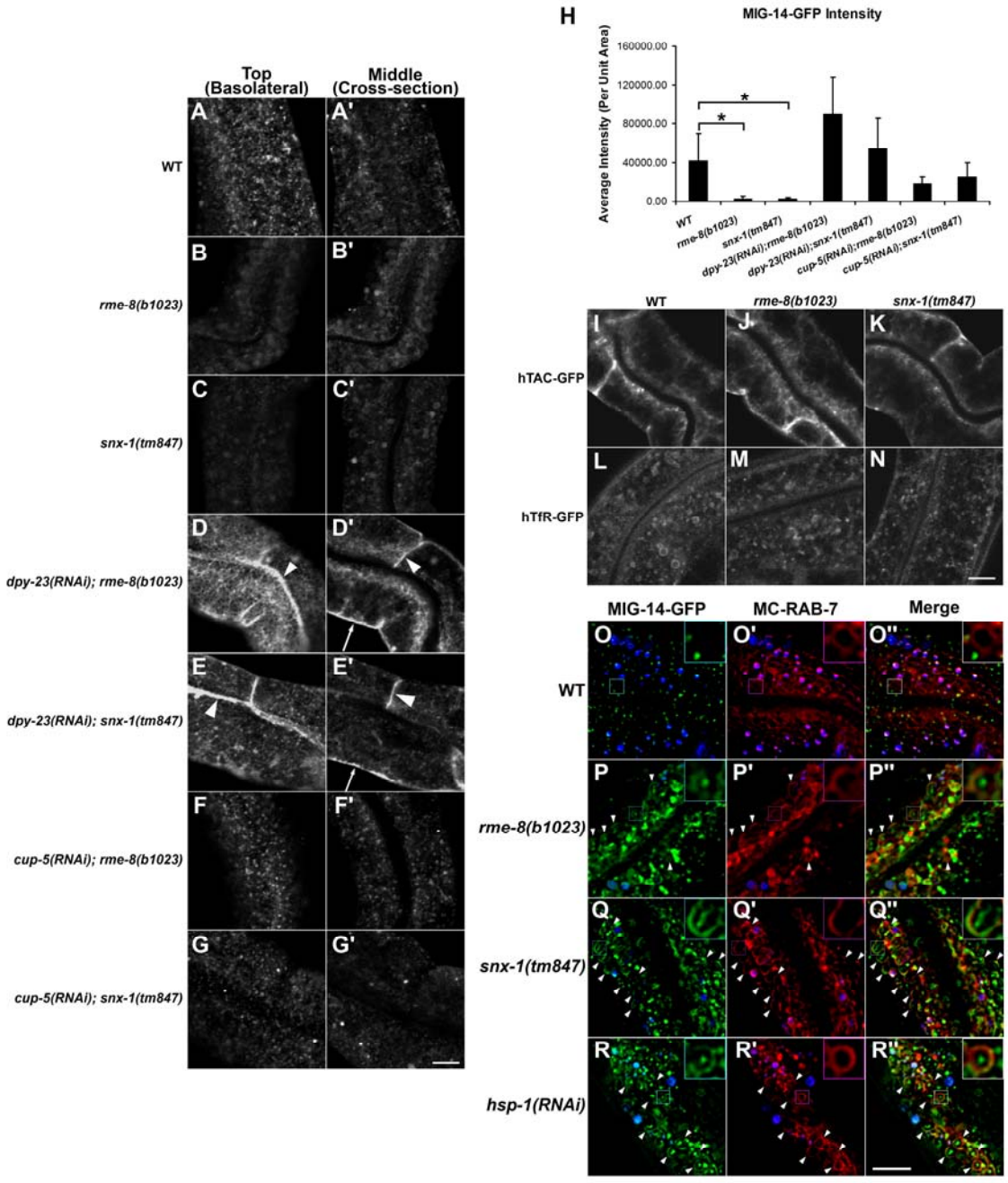

Figure 3. MIG-14 recycling requires RME-8 and SNX-1

Panels A-G' show confocal micrographs of intestinally expressed MIG-14-GFP in top and middle focal planes in intact living animals. Note the reduced MIG-14-GFP intensity, and altered subcellular localization, in *rme-8* and *snx-1* mutants **(A-C")**. RNAi-mediated

depletion of the mu2 subunit of AP-2 (DPY-23) restored MIG-14-GFP fluorescence, and enhanced cell surface localization, in both *rme-8* and *snx-1* mutants **(D-E" and H)**, arrowheads indicate lateral membrane, arrows indicate basal membrane. RNAi-mediated depletion of lysosome biogenesis protein CUP-5/mucolipin1 inhibited loss of MIG-14-GFP signal in *rme-8* and *snx-1* mutants **(F-G")**. Bar graph indicating average MIG-14-GFP fluorescence intensity calculated described in Methods **(H)**. Asterisks indicate a significant difference in the one-tailed Student's t-test (P <0.01). P values for MIG-14-GFP were 6.58×10^{-7} for wild type (WT) vs. *rme-8(b1023*) and 5.43×10^{-7} for WT vs. *snx-1(tm847)*. Cargo proteins that recycle via the recycling endosome, the human transferrin receptor (hTfR-GFP) and the IL-2 receptor alpha chain (hTAC-GFP), were not affected in *rme-8* and *snx-1* mutants **(I-N).** For panels O-R" images from deconvolved 3-D image stacks are shown. All images were acquired in intact living animals expressing GFP and mCherry tagged proteins specifically in intestinal epithelial cells. Autofluorescent lysosome-like organelles are shown in blue. In *rme-8(b1023)*, *snx-1(tm847)* and *hsp-1/hsc70(RNAi)* animals, but not wild-type animals **(O-O")**, MIG-14-GFP colocalizes with late endosome and lysosome marker mCherry-RAB-7 **(P-R").** MIG-14-GFP localizes to the apparent limiting membrane of the late endosomes/lysosomes as well as apparent intralumenal structures. Note that the signal intensity for MIG-14-GFP in mutant and RNAi animals was boosted to allow visualization and colocalization. Arrowheads indicate late endosomes/lysosomes labeled by both mCherry-RAB-7 and MIG-14-GFP. Insets show enlargements (x3) of the boxed area. Scale bar represents 10 μm.

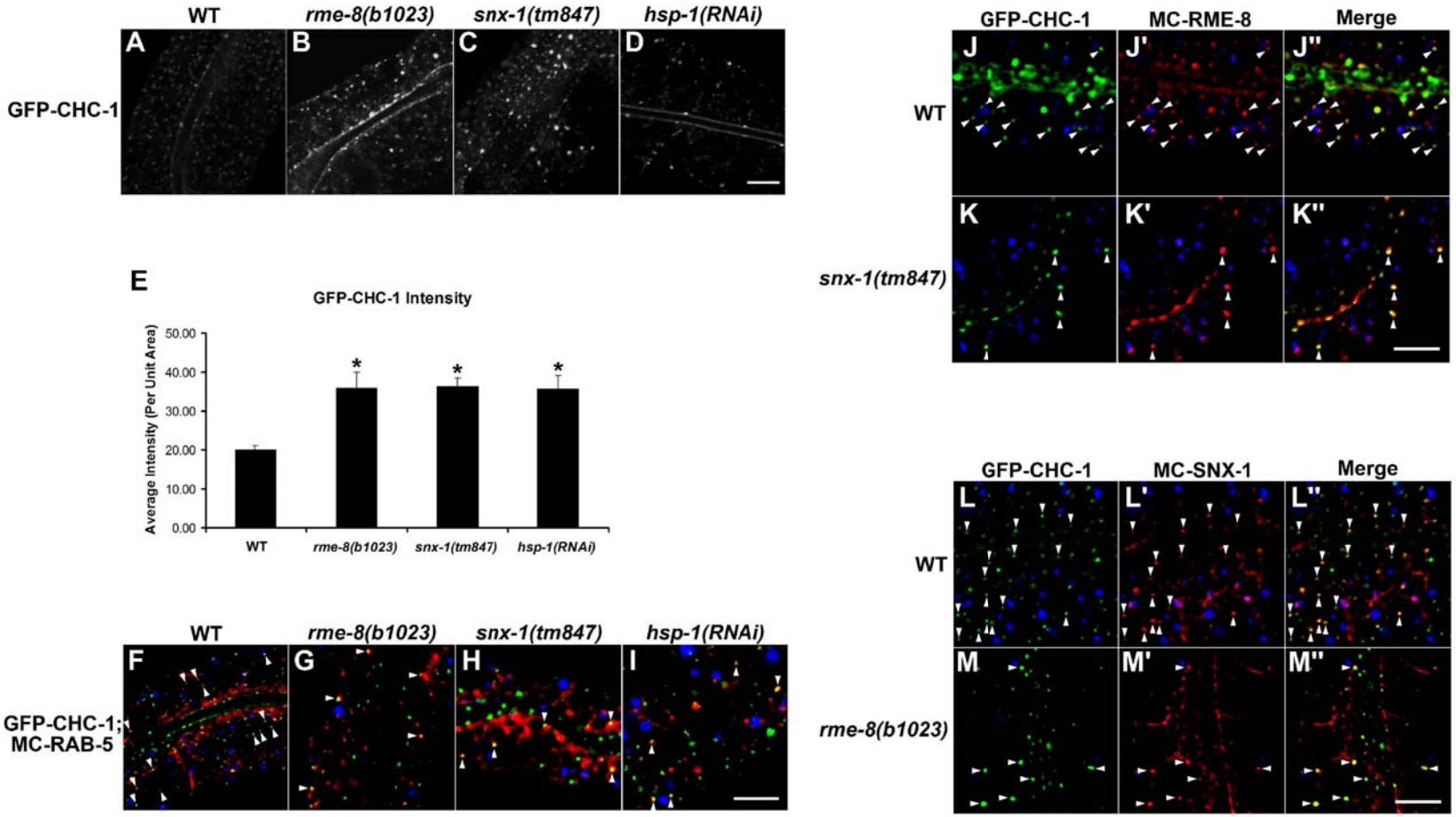
WT
rme-8(b1023)
snx-1(tm847)
hsp-1(RNAi)
GFP-CHC-1
A
B
C
D
E
GFP-CHC-1 Intensity
Average Intensity (Per Unit Area)
50.00
40.00
30.00
20.00
10.00
0.00
WT
rme-8(b1023)
snx-1(tm847)
hsp-1(RNAi)
GFP-CHC-1;
MC-RAB-5
F
G
H
I
GFP-CHC-1
MC-RME-8
Merge
J
J'
J''
K
K'
K''
MC-SNX-1
L
L'
L''
M
M'
M''

Figure 4. Clathrin accumulates on endosomes in animals lacking RME-8, SNX-1, or HSP-1/Hsc70

Panels show confocal micrographs of intestinally expressed GFP-tagged clathrin heavy chain (GFP-CHC-1) in intact living animals **(A-D)**. Note the increased GFP-CHC-1 intensity in *rme-8(b1023)*, *snx-1(tm847) and hsp-1(RNAi)* animals. **(E)** Bar graph indicates average GFP-CHC-1 fluorescence intensity in the indicated genetic backgrounds. Asterisks indicate a significant difference in the one-tailed Student's t-test (P <0.01). P values for GFP-CHC-1 were 4.27×10^{-17} for wild type (WT) vs. *rme-8(b1023*), 5.92×10^{-26} for WT vs. *snx-1(tm847)* and 3.05×10^{-19} for WT vs. *hsp-1(RNAi)*. For panels F-M" images from deconvolved 3-D image stacks are shown. All images were acquired in intact living animals expressing GFP and mCherry tagged proteins specifically in intestinal epithelial cells. Autofluorescent lysosome-like organelles are shown in blue. GFP-CHC-1 could be visualized on wild-type and mutant mCherry-RAB-5 labeled endosomes in wild-type and mutants. Arrowheads indicated colocalization of the GFP-CHC-1 and mCherry-RAB-5 signals **(F-I)**. GFP-CHC-1 could be visualized on wild-type and *snx-1* mutant mCherry-RME-8 labeled endosomes. Arrowheads indicated colocalization of the GFP-CHC-1 and mCherry-RME-8 signals **(J-K")**. GFP-CHC-1 could be visualized on wild-type and *rme-8* mutant mCherry-SNX-1 labeled endosomes. Arrowheads indicated colocalization of the GFP-CHC-1 and mCherry-SNX-1 signals **(L-M")**. Scale bars represent 10 μm.

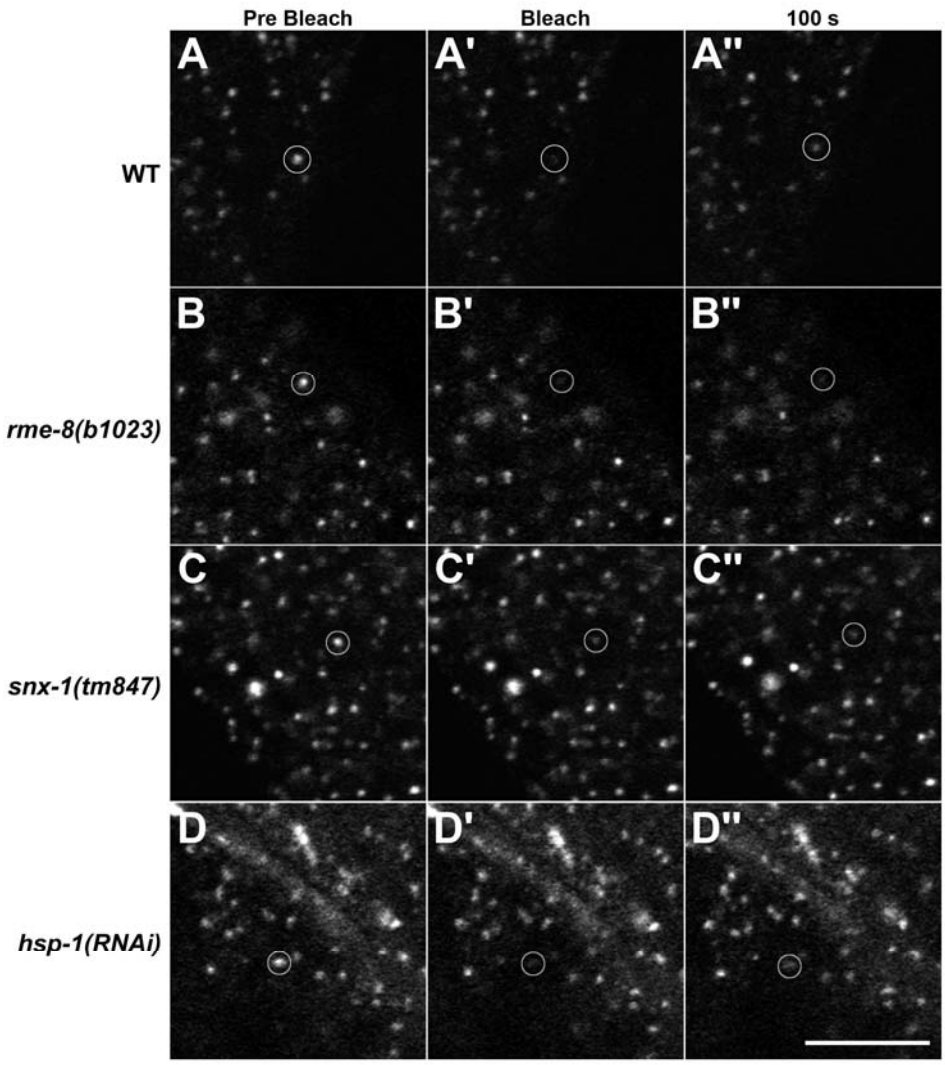
Pre Bleach
Bleach
100 s
A
A'
A''
WT
B
B'
B''
rme-8(b1023)
C
C'
C''
snx-1(tm847)
D
D'
D''
hsp-1(RNAi)

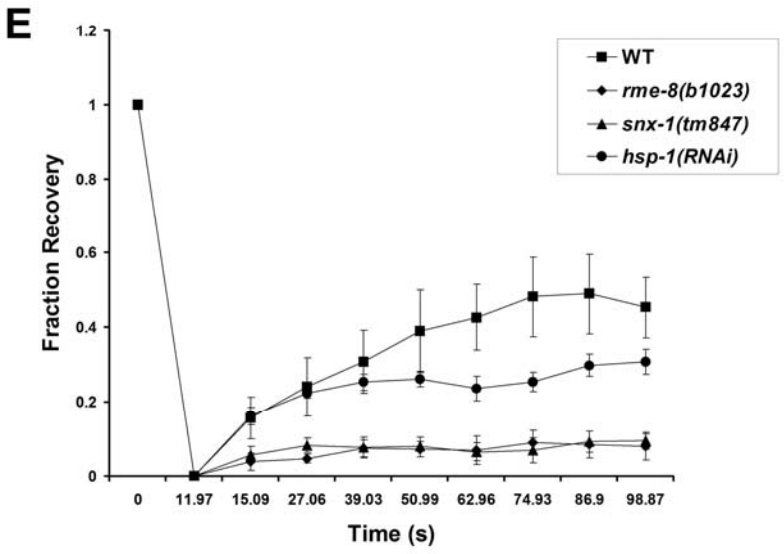
E
Fraction Recovery
1.2
1
0.8
0.6
0.4
0.2
0
0
11.97
15.09
27.06
39.03
50.99
62.96
74.93
86.9
98.87
Time (s)
WT
rme-8(b1023)
snx-1(tm847)
hsp-1(RNAi)

Figure 5. Clathrin dynamics are impaired in *rme-8(b1023)*, *snx-1(tm847)* and *hsp-1(RNAi)* knock-down animals

(A-D") Representative images of GFP-CHC-1 in wild type control, *rme-8(b1023)*, *snx-1(tm847)* and *hsp-1(RNAi)* animals before bleaching (prebleach), immediately after bleaching (bleach) and 100 s after bleaching (100 s). Bleached areas are shown by white-bordered circles. Fluorescence intensities in bleached areas were recorded every 10 s. **(E)** Mean time courses of FRAP (±s.d.) from 8 animals of each genotype as indicated with WT (wild type control), *rme-8(b1023)*, *snx-1(tm847)* and *hsp-1(RNAi)*. Error bars represent standard deviations from the mean (n=8 each time point, 8 animals of each genotype were sampled in the intestine). Scale bar represents 10 μm.

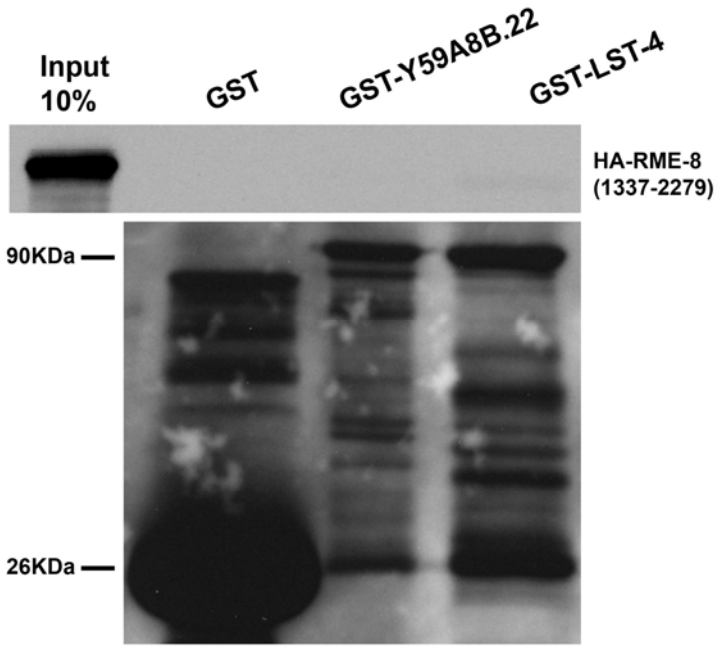

Figure S1. RME-8 binding specificity

Glutathione beads loaded with recombinant GST, GST-Y59A8B.22/SNX5 and GST-LST-4/snx4p were incubated with *in vitro* expressed HA-RME-8(1337-2279), and then washed to remove unbound proteins. Bound proteins were eluted and analyzed by western blot using anti-HA (top) or anti-GST (bottom) antibodies. The input lane contains *in vitro* expressed HA-RME-8(1337-2279) used in the binding assays (10%).

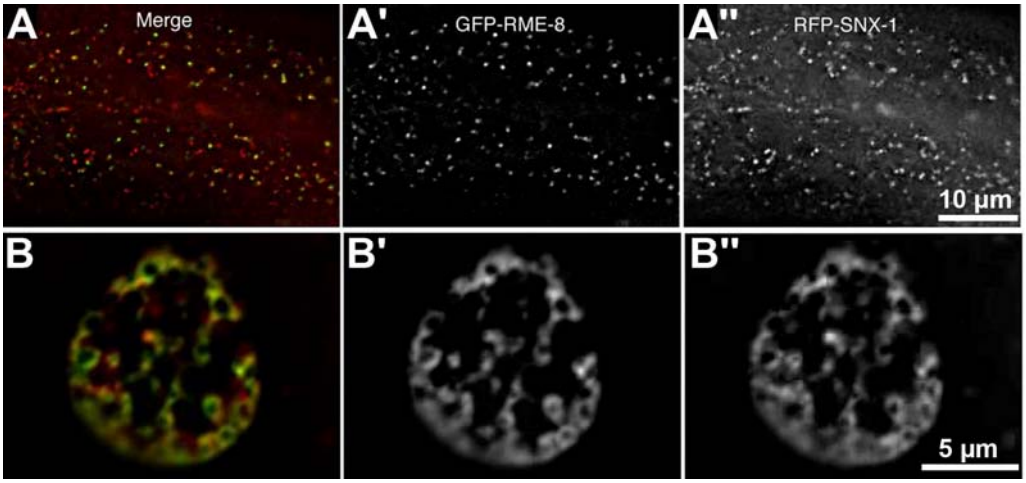

Figure S2. RME-8 colocalizes with SNX-1 in the hypodermis and coelomocyte

(A-A") GFP-RME-8 colocalizes with RFP-SNX-1 on endosomal structures in the hypodermis. **(B-B")** GFP-RME-8 colocalizes with RFP-SNX-1 on endosomal structures in the coelomocyte.

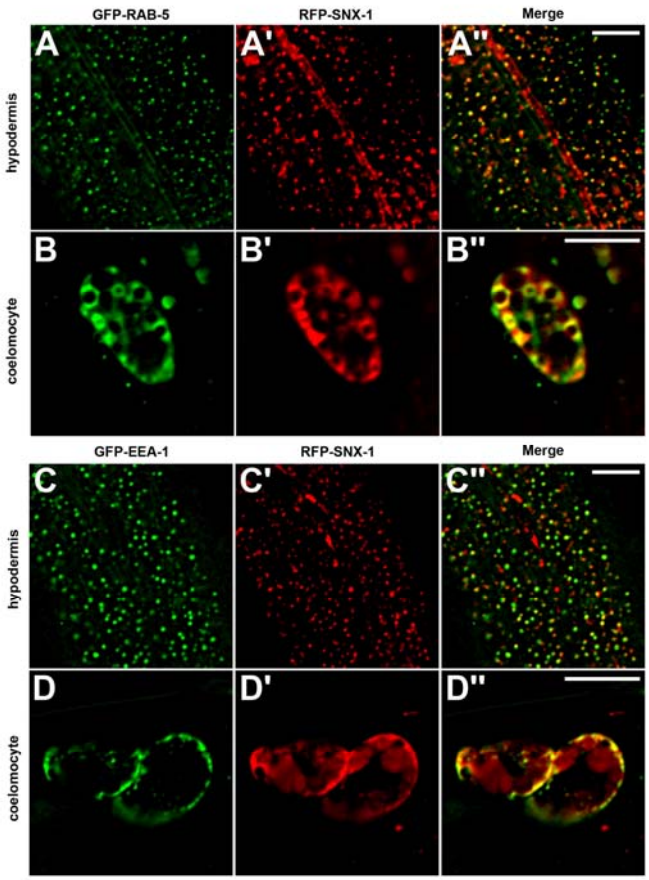

Figure S3. SNX-1 colocalizes with RAB-5 and EEA-1 on early endosomes

Representative images from deconvolved 3-D image stacks are shown. All images were acquired in intact living animals expressing GFP and RFP tagged proteins in the hypodermis and coelomocyte. **(A-A")** RFP-SNX-1 colocalizes with early endosome marker GFP-RAB-5 on endosomal structures in the hypodermis, and in the coelomocyte **(B-B")**. RFP-SNX-1 also colocalizes with early endosome marker GFP-EEA-1 on endosomal structures in the hypodermis **(C-C"),** and in the coelomocyte **(D-D")**. Scale bar represents 10 μm.

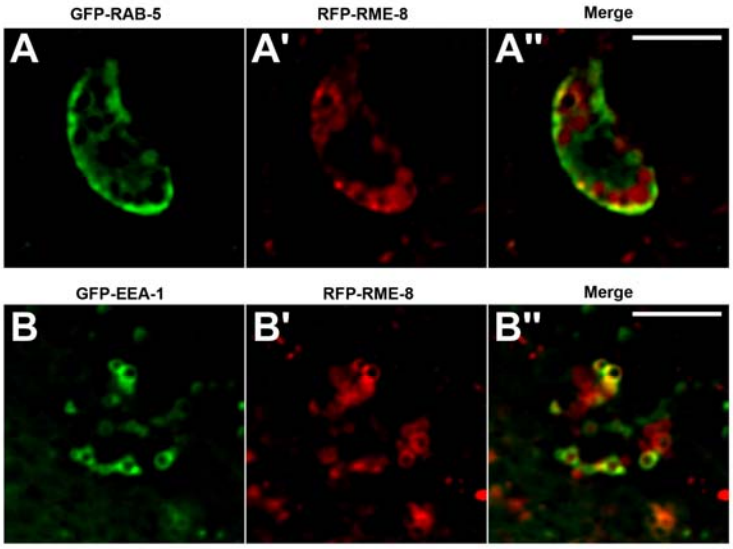

Figure S4. RME-8 colocalizes with RAB-5 and EEA-1 on early endosomes in the coelomocyte

(A-A") RFP-RME-8 colocalizes with GFP-RAB-5 on endosomal structures in the coelomocyte. **(B-B")** RFP-RME-8 colocalizes with GFP-EEA-1 on early endosomal structures in the coelomocyte. Scale bar represents 10 μm.

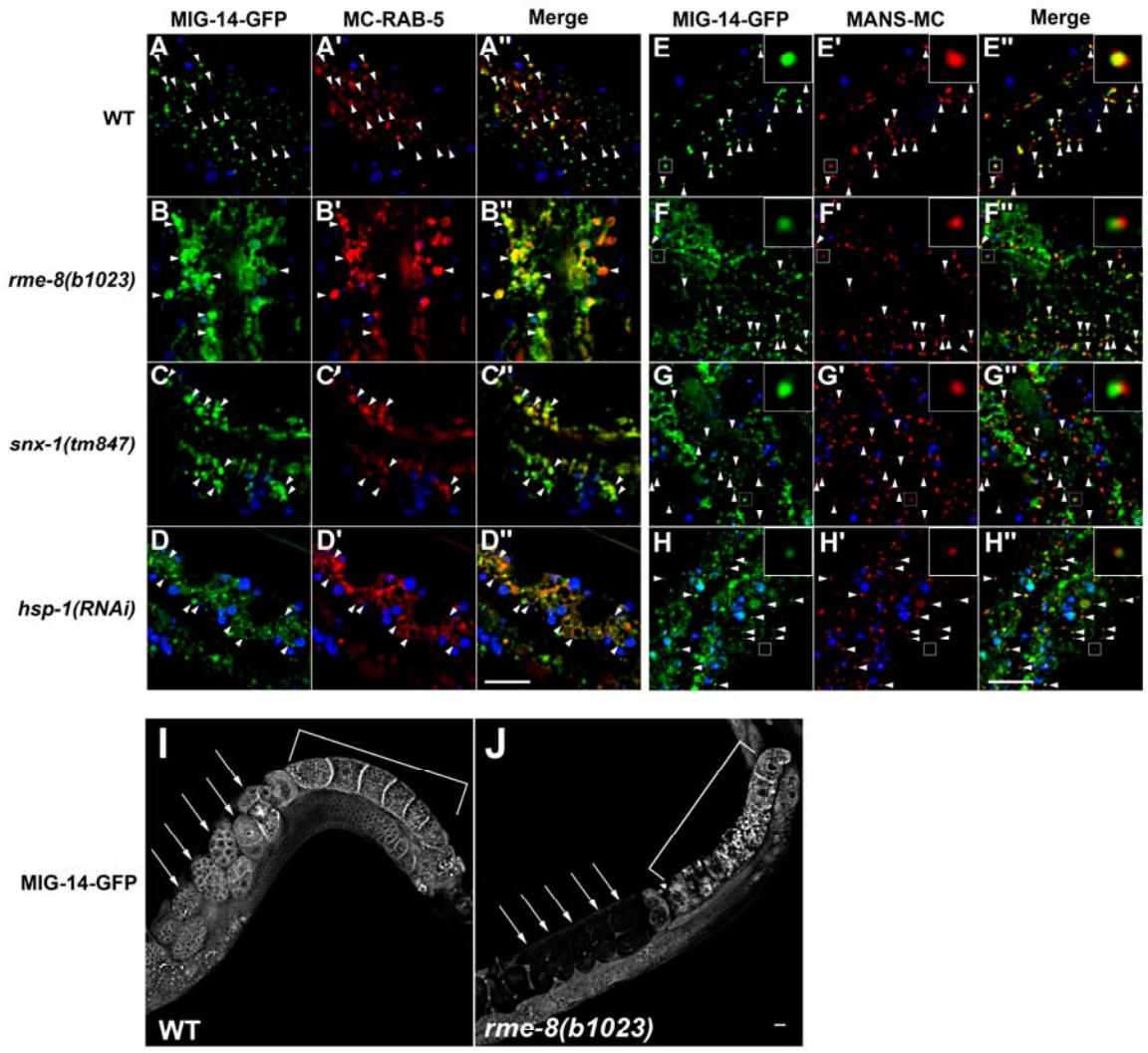

Figure S5. Mislocalization of MIG-14 in animals lacking RME-8, SNX-1, and HSP-1/Hsc70.

For panels A-H", images from deconvolved 3-D image stacks are shown. All images were acquired in intact living animals expressing GFP and RFP (mCherry) tagged proteins specifically in intestinal epithelial cells. Autofluorescent lysosome-like organelles are shown in blue. In wild-type animals (WT), MIG-14-GFP colocalized well with the early endosome marker mCherry-RAB-5 **(A-A")** and the Golgi marker MANS-

mCherry **(E-E")**. Arrowheads indicate early endosomes labeled by both mCherry-RAB-5 and MIG-14-GFP or Golgi ministacks labeled by both MANS-mCherry and MIG-14-GFP. In *rme-8* and *snx-1* mutants, or *hsp-1(RNAi)* animals, MIG-14-GFP could be observed in enlarged mCherry-RAB-5 labeled early endosomes **(B-D")** (arrowheads). However, most MANS-mCherry labeled Golgi either displayed weak colocalization or were adjacent to MIG-14-GFP labeling in *rme-8* and *snx-1* mutants or *hsp-1(RNAi*) knock-down animals **(F-H")**. Arrowheads and insets indicate MANS-mCherry labeled Golgi apparatus juxtaposed to MIG-14-GFP positive endosomes. Note that the signal intensity for MIG-14-GFP in mutant and RNAi animals was boosted to allow visualization and colocalization. Enlarged image (4x) of boxed regions are shown in the insets. Scale bar represents 10 μm.

(I-J) Images from deconvolved 3-D image stacks are shown. All images were acquired in intact living animals expressing GFP tagged proteins specifically in germline cells. Compared with wild type control **(I)**, MIG-14-GFP intensity were significantly reduced in early embryos in *rme-8(b1023)* mutant animals **(J)**. Arrows indicate embryos, brackets indicate oocytes. Scale bar represents 10 μm.

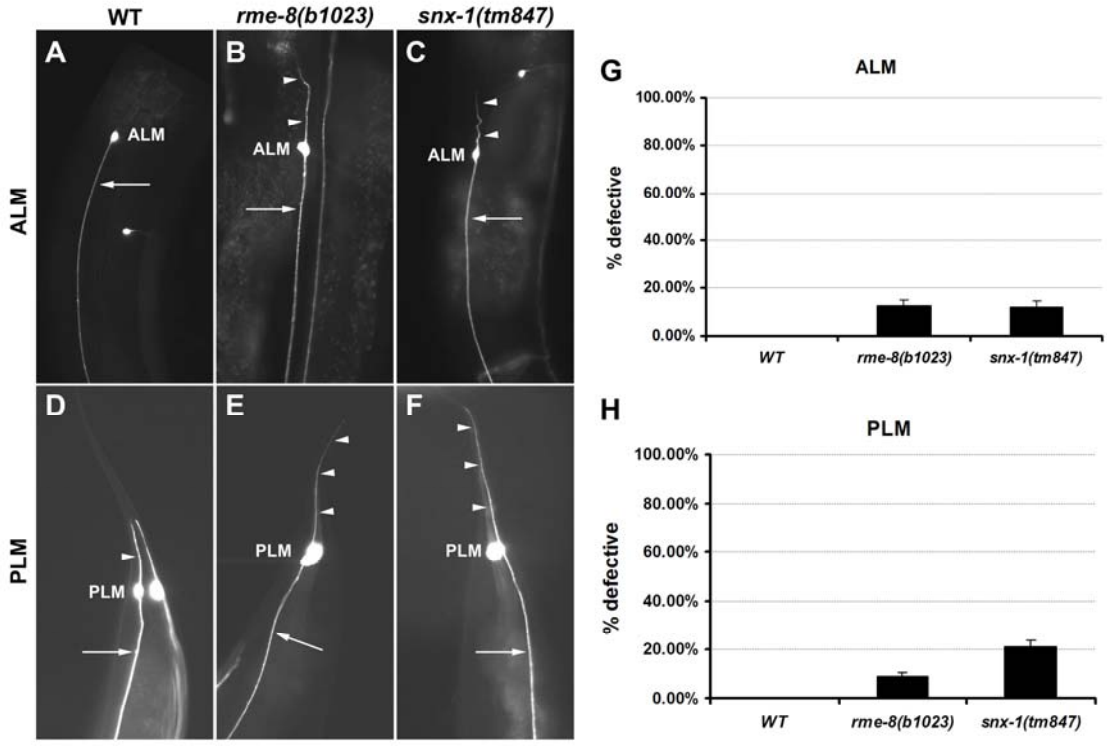

Figure S6. *rme-8(b1023)* and *snx-1(tm847)* mutants display defective ALM and PLM posterior processes

(A–C) ALM neuronal morphology. *rme-8(b1023)* and *snx-1(tm847)* mutants show longer posterior processes than wild type animals. **(D–F)** PLM neuronal morphology. *rme-8(b1023)* and *snx-1(tm847)* mutants show long posterior process, extending to the tip of the tails. Anterior processes are indicated by arrows and posterior processes by arrowheads. **(G and H)** Bar graphs indicate the percentage of ALM or PLM neurons with defective posterior processes in the indicated genetic background.

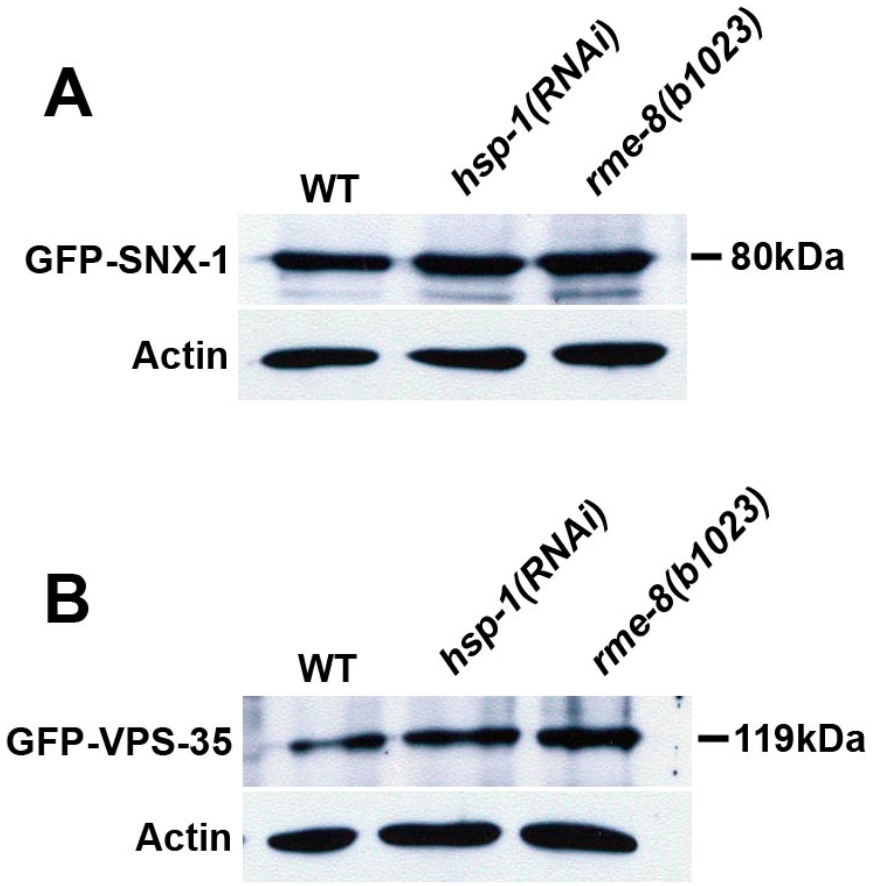

Figure S7. Protein levels of retromer components, GFP-SNX-1 and GFP-VPS-35, are not affected by loss of RME-8 or HSP-1/Hsc70.

(A) GFP-SNX-1 levels in wild-type, *rme-8(b1023)* and *hsp-1(RNAi)* animals. **(B)** GFP-VPS-35 levels in wild-type, *rme*-8(b1023) and *hsp-1(RNAi)* animals.

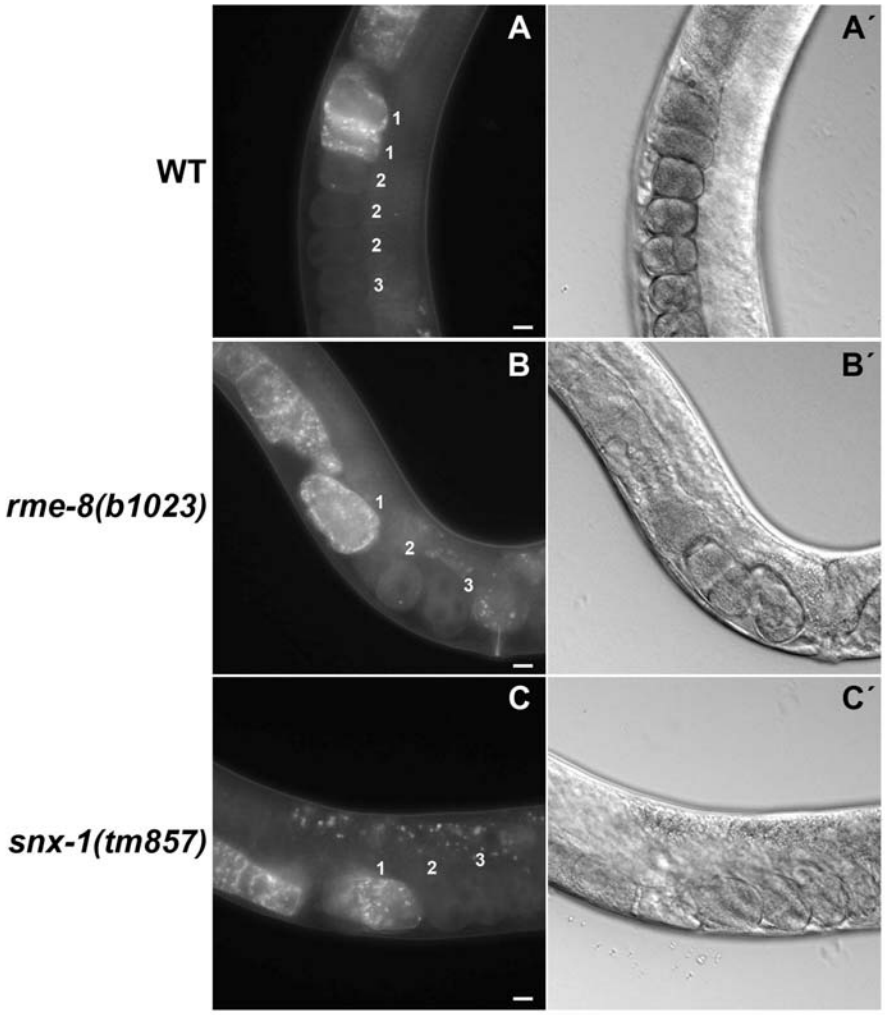

Figure S8. Degradation of membrane protein CAV-1-GFP is not delayed in *rme-8(b1023)* and *snx-1(tm847)* mutants

(A–A') CAV-1-GFP is degraded by the 2-cell stage with little visible CAV-1-GFP remaining by the 4-cell stage in wild-type embryos. **(B–C')** No changes of CAV-1-GFP degradation were observed in *rme-8(b1023)* or *snx-1(tm847)* mutant embryos. 1-cell, 2-cell, and 4-cell embryos are indicated by numbers 1, 2 and 3 respectively. Scale bars represent 10 μm.

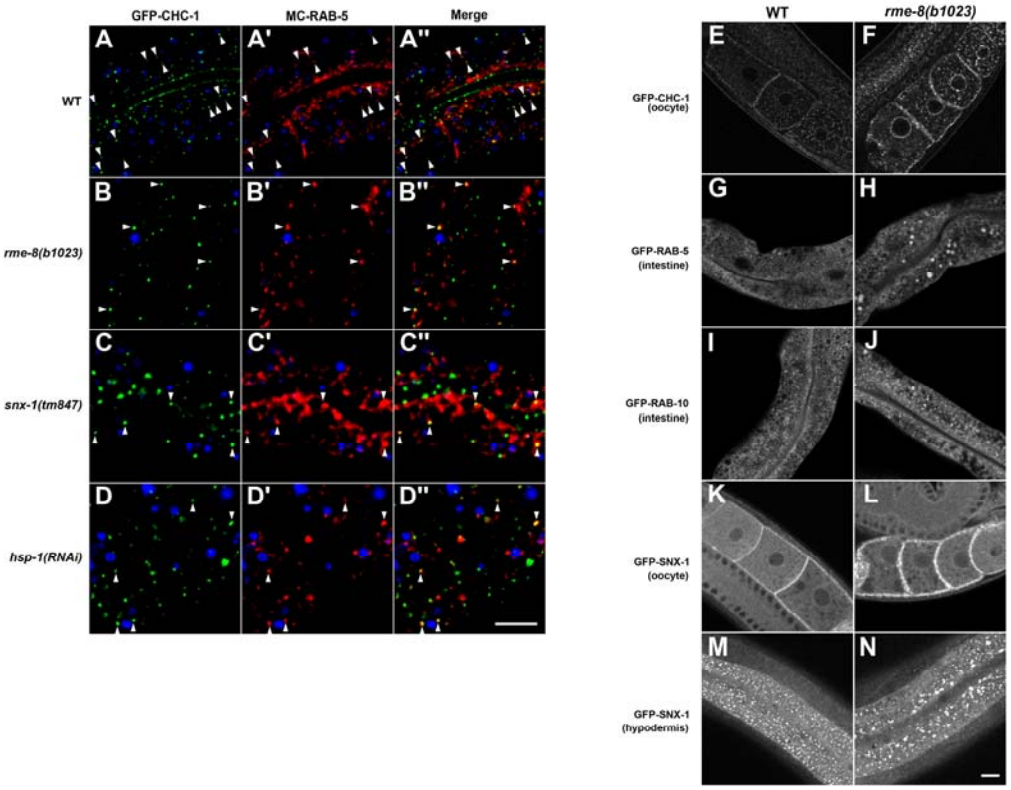

Figure S9. Aberrant accumulation of clathrin and altered early endosome morphology in *rme-8* mutants

For panels A-D", images from deconvolved 3-D image stacks are shown. All images were acquired in intact living animals expressing GFP and mCherry tagged proteins specifically in intestinal epithelial cells. Autofluorescent lysosome-like organelles are shown in blue. In *rme-8* and *snx-1* mutants, or *hsp-1(RNAi)* animals, GFP-CHC-1 accumulated on brighter puncta in the intestines. GFP-CHC-1 could be visualized on mCherry-RAB-5 labeled endosomes in wild-type and mutants. Arrowheads indicated colocalization of the GFP-CHC-1 and mCherry-RAB-5 signals **(A-D")**. **(E-F)** GFP-CHC-1 showed similar accumulation on abnormally bright puncta in oocytes. **(G-H)**

GFP-RAB-5 accumulated on enlarged early endosomes in the intestine. **(I-J)** GFP-RAB-10 labeled early endosomal structures were also enlarged in the intestine. Both germline expressed GFP-SNX-1 **(K-L)** and hyperdermis expressed GFP-SNX-1 **(M-N)** showed accumulation on enlarged puncta in *rme-8(b1023)* mutants. Scale bars represent 10 μm.

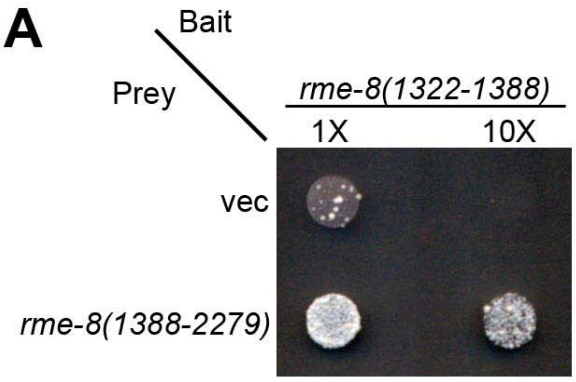
A
Bait
Prey
rme-8(1322-1388)
1X
10X
vec
rme-8(1388-2279)

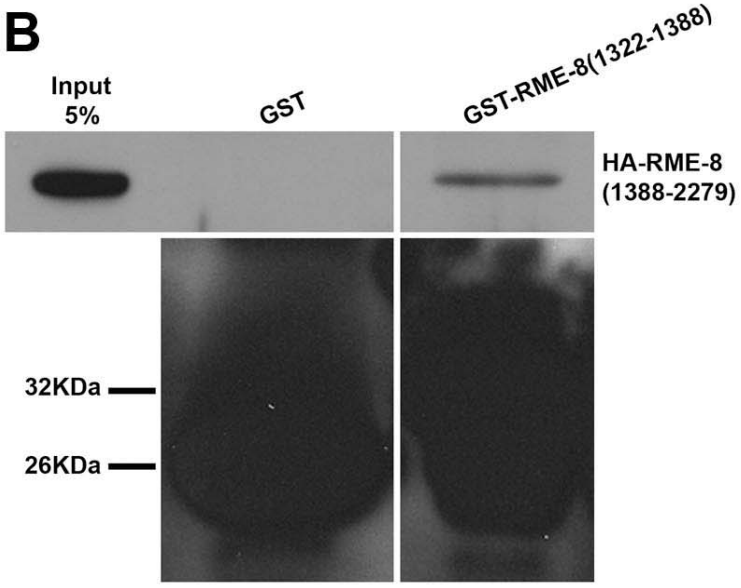
B
Input
5%
GST
GST-RME-8(1322-1388)
HA-RME-8
(1388-2279)
32KDa
26KDa

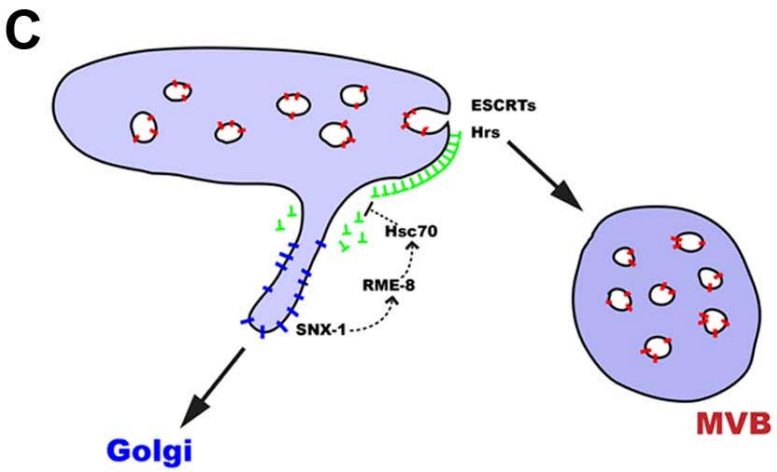
C
ESCRTs
Hrs
Hsc70
RME-8
SNX-1
Golgi
MVB

Figure S10. The RME-8 J-domain can physically interact with other domains of RME-8

(A) RME-8 J-domain (aa1322–1388) was expressed in a yeast reporter strain as a fusion with the DNA-binding domain of LexA (bait). RME-8 C-terminal residues (aa1388-2279) was expressed in the same yeast cells as fusions with the B42 transcriptional activation domain (prey). Interaction between bait and prey was assayed by complementation of leucine auxotrophy (LEU2 growth assay). Colonies were diluted in liquid, adjusted to the same concentration and spotted on solid growth medium directly or after further 10X dilution. **(B)** Glutathione beads loaded with recombinant GST or GST-RME-8 J-domain (1322–1388) were incubated with *in vitro* expressed HA-RME-8(1388-2279), and then washed to remove unbound proteins. Bound proteins were eluted and analyzed by western blot using anti-HA (top) or anti-GST (bottom) antibodies. Input lane contain *in vitro* expressed HA-RME-8(1388-2279) used in the binding assays (5%). **(C)** Model for retrograde sorting on MVBs/early endosomes. SNX-1 binds to RME-8, allowing RME-8 to activate endosomal Hsc70, and in turn Hsc70 chaperone activity on the endosome removes clathrin, maintaining a subdomain required for retrograde transport.

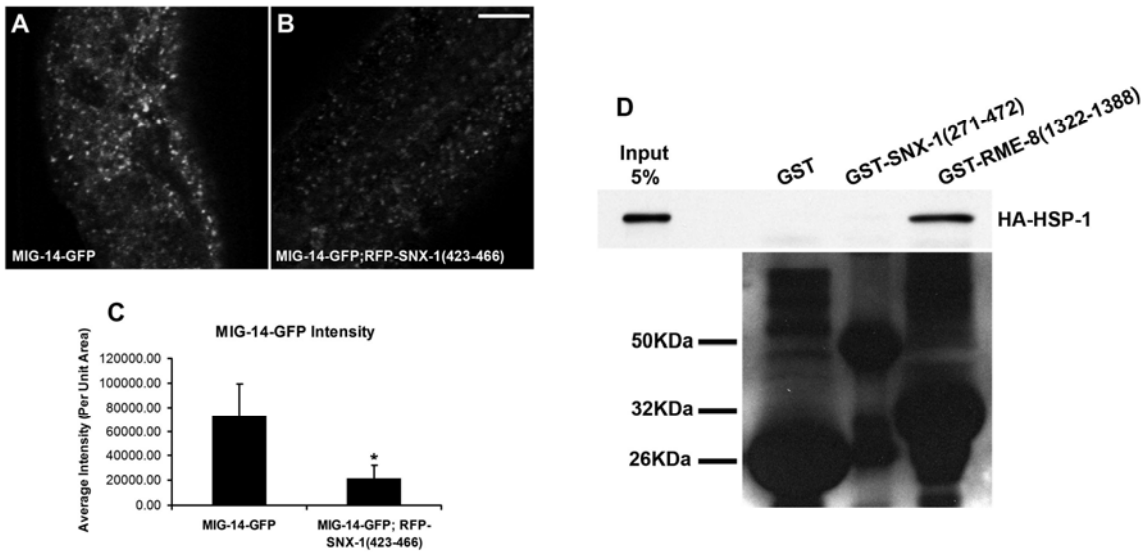

Figure S11.

(A-C) Over-expression of SNX-1(aa423-466) interferes MIG-14 trafficking. Confocal micrographs of intestinally expressed MIG-14-GFP in top focal planes in living animals. MIG-14-GFP intensity is reduced in animals with expressing RFP-SNX-1(aa423-466) **(A-B).** Bar graph indicating average MIG-14-GFP fluorescence intensity calculated described in Methods **(C)**. Asterisk indicates a significant difference in the one-tailed Student's t-test (P <0.05). P value was 2.373×10^{-9}. Scale bar represents 10 μm.

(D) Glutathione beads loaded with recombinant GST, or GST-SNX-1(271-472), GST-RME-8 J-domain (1322–1388) were incubated with *in vitro* expressed HA-HSP-1 (10 μl TNT mix diluted in 500 μl binding buffer: 10mM Tris-HCl pH7.5, 150mM NaCl, 125mM KCl, 2mM $MgCl_2$, 2mM ATP, 0.1% Tween-20) at 4°C for 2 hours, and then washed to remove unbound proteins with wash buffer (10mM Tris-HCl pH7.5, 150mM NaCl, 125mM KCl, 2mM $MgCl_2$, 0.1mM ATP, 0.1% Tween-20). Bound proteins were

eluted and analyzed by western blot using anti-HA (top) or anti-GST (bottom) antibodies. Input lane contains *in vitro* expressed HA-HSP-1 used in the binding assays (5%).

CHAPTER 4: EHBP-1 FUNCTIONS WITH RAB-10 DURING ENDOCYTIC RECYCLING IN *C. elegans*

AUTHOR CONTRIBUTIONS

This chapter was submitted as presented here to *Molecular Biology of the Cell*.

I participated in the experimental design, performed the *C. elegans* related experiments, biochemical experiments (Figures 1, 3-6, 8 and Supplemental figures 1-3) and wrote the paper. Dr. Carlos Chen performed the yeast two-hybrid screening for RAB-10 binding proteins, RABs binding specificity assay and the *C. elegans* related experiments (Figure 1-2, 4 and 7). Riju Banerjee performed the yeast two hybrid assays (Figure 1). Dr. Doreen Glodowski participated the glutamate receptor trafficking assay (Figure 7). Dr. Anjon Audya performed the germline secretory assay and wrote the related text (Figure 8). Dr. Christopher Rongo designed, performed the glutamate receptor trafficking assays and wrote the glutamate receptor trafficking related text (Figure 7). Dr. Barth D. Grant designed the experiments, trained me for all experiments and wrote the paper.

SUMMARY

C. elegans RAB-10 functions in endocytic recycling in polarized cells, regulating basolateral cargo transport in the intestinal epithelia and postsynaptic cargo transport in interneurons. A similar role was found for mammalian Rab10 in MDCK cells, suggesting that a conserved mechanism regulates these related pathways in metazoans. In a yeast two-hybrid screen for binding partners of RAB-10 we identified EHBP-1, a calponin homology domain (CH) protein, whose mammalian homolog Ehbp1 was previously shown to function during endocytic transport of GLUT4 in adipocytes. *In vivo* we find that EHBP-1-GFP colocalizes with RFP-RAB-10 on endosomal structures of the intestine and interneurons, and that *ehbp-1* loss-of-function mutants share with *rab-10* mutants specific endosome morphology and cargo localization defects. We also show that loss of EHBP-1 disrupts transport of membrane proteins to the plasma membrane of the non-polarized germline cells, a defect that can be phenocopied by co-depletion of RAB-10 and its closest paralog RAB-8. Taken together these results indicate that RAB-10 and EHBP-1 function together in many cell types, and suggests that there are differences in the level of redundancy among Rab family members in polarized versus non-polarized cells.

INTRODUCTION

The endocytic pathways of eukaryotes regulate the uptake, sorting and the subsequent recycling or degradation of macromolecules, fluid, membranes, and membrane proteins. After endocytosis through either clathrin-dependent or one of several clathrin-independent uptake mechanisms (Nichols, 2003; Gesbert *et al.*, 2004), cargo proteins are delivered to early endosomes, where sorting occurs. Some cargo will be sorted for delivery to lysosomes for degradation (Mukherjee *et al.*, 1997), whereas others will be directly or indirectly routed back to the plasma membrane or Golgi apparatus through various recycling pathways (Maxfield and McGraw, 2004; Rojas *et al.*, 2007; Grant and Donaldson, 2009).

The Rab family of GTPases function as master regulators, controlling diverse aspects of intracellular trafficking and organelle identity (Stenmark, 2009). Like other Ras superfamily GTPases, Rabs cycle between an active GTP-bound state and an inactive GDP-bound state. Through their direct or indirect interactions with effectors and binding proteins, Rabs function as coordinators of intracellular trafficking events, often controlling motor-based delivery of vesicles and vesicle tethering, and in some cases affecting cargo recruitment, vesicle budding, and vesicle fusion with target compartment membranes (Grosshans *et al.*, 2006; Stenmark, 2009).

Rabs have been shown to regulate both fast recycling directly from early endosomes and slow recycling from the endocytic recycling compartment (ERC) (Grant and Donaldson, 2009). Rab4 was identified as an important regulator of transferrin receptor (TfR) recycling (van der Sluijs *et al.*, 1992), although the precise function of Rab4 in recycling

remains unclear. Studies by Kouranti et al. indicated that Rab35 is also an important regulator of TfR rapid recycling (Kouranti *et al.*, 2006), whereas other studies indicate a role for Rab35 on the Arf6- and EHD1-containing tubular endosomes of the slow recycling pathway (Walseng *et al.*, 2008). Another well established Rab involved in recycling is Rab11, a resident of the ERC that mediates recycling from the ERC to the plasma membrane (Powelka *et al.*, 2004; Weigert *et al.*, 2004). In polarized cells, Rab11 activity appears restricted to the apical membrane, while other proteins must regulate recycling to the basolateral surface. Thus, polarized cells appear to use different mechanisms to regulate trafficking at their different, specialized membrane surfaces.

Regulated recycling has also been demonstrated in non-polarized cells. Interestingly, such cells still employ multiple mechanisms in the trafficking of different recycling cargo. For instance in HeLa cells Arf6 and Rab22a are important for the recycling of MHCI and TAC (IL2-receptor alpha chain), but have little or no effect on TfR (Weigert *et al.*, 2004). MHCI and TAC are internalized by clathrin-independent endocytosis (CIE), while TfR is internalized by clathrin-dependent endocytosis (CDE). The two cargo classes appear to converge in the endosomal system after uptake, but diverge again upon exit from the ERC. It remains unclear if their divergence in recycling is related to the difference in their uptake routes. Rab11 and EHD1 proteins are important for the recycling of both cargo types, although there are likely to be differences in the mechanisms used to recycle these two cargo types.

RAB-10 has been implicated in the recycling of clathrin-independent cargo in the *C. elegans* intestine, probably at the level of transport between early endosomes and recycling endosomes (Babbey *et al.*, 2006; Chen *et al.*, 2006). Recent work in *C. elegans*

suggests that interneuron postsynaptic glutamate receptor recycling also requires RAB-10 (Glodowski *et al.*, 2007). In mammalian systems, Rab10 has been implicated in basolateral recycling in MDCK cells, and in Glut4 recycling in adipocytes (Babbey *et al.*, 2006; Sano *et al.*, 2007). RAB-10, and another similar GTPase, RAB-8, are the closest metazoan relatives of yeast Sec4p, the final Rab in the yeast secretory pathway. Rab8 has been suggested to function in the secretory pathway in mammalian cells (Hattula *et al.*, 2002; Ang *et al.*, 2003), and this delivery process may use the recycling endosomes as an intermediate (Ang *et al.*, 2004). In polarized MDCK cells, simultaneous Rab8 and Rab10 siRNA treatment produced more severe exocytosis defects than individual knockdown (Schuck *et al.*, 2007), implying that Rab8 and Rab10 may function redundantly in exocytic membrane trafficking, perhaps by sharing some effectors. Whether the different Rabs that regulate different recycling pathways use different effector molecules remains an open question.

Here we report the physical association of RAB-10 with the effector molecule EHBP-1. We show that *ehbp-1* mutants share several of the specific recycling defects observed in *rab-10* mutants, including preferential effects on the CIE cargo protein TAC in the intestine. We also provide evidence that EHBP-1 functions with RAB-10 in neurons, and might regulate secretion in germ cells in a pathway that is redundantly regulated by RAB-10 and RAB-8. Surprisingly, unlike conventional Rab effectors, our results suggest that EHBP-1 functions upstream of RAB-10, and is important for the endosomal association of RAB-10.

.

RESULTS

EHBP-1 associates with active GTP-bound RAB-10

To identify other proteins that function with RAB-10 in endocytic recycling, we performed a yeast two-hybrid screen for binding partners of the active GTP-bound form of RAB-10, using a predicted constitutively active mutant, RAB-10(Q68L), as bait. We identified 27 positive interacting clones encoding C-terminal portions of EHBP-1, the only *C. elegans* homolog of mammalian Ehbp1, a protein previously implicated in Glut4 trafficking in mammalian adipocytes (Guilherme *et al.*, 2004b). Previous reports on mammalian Ehbp1 had not linked it to a Rab GTPase, but rather to EHD1 and EHD2, two membrane associated proteins of the RME-1 family of ATPases, which function in membrane tubulation and potentially membrane fission (Pant *et al.*, 2009). The smallest recovered interacting clone encompassed EHBP-1 amino acids 662-901 (Figure 1A-B and Materials and Methods). We further delimited the RAB-10 interacting domain of EHBP-1 to amino acids 712-851, a predicted coiled-coil region of the protein (Figure 1C-D). No interaction could be detected between EHBP-1(662-901) and a predicted constitutively inactive GDP-bound mutant form RAB-10(T23N) (Figure 1B). These data suggest that EHBP-1 specifically binds to the active GTP-bound form of RAB-10.

We next screened other Rab GTPases for their ability to bind EHBP-1 using the yeast two-hybrid system. We found that GTP-bound RAB-8(Q67L), but not GDP-bound RAB-8(Q23N), also bound to EHBP-1 (Figure 1B). RAB-8 is the closest paralog of RAB-10 in *C. elegans*, and together RAB-8 and RAB-10 represent the branch of the metazoan Rabs closest to Sec4p, the final Rab in the yeast secretory pathway (Salminen and Novick,

1987). We did not detect interactions between EHBP-1 and the active forms of several other Rabs, including RAB-5, RAB-7, RAB-11, or RAB-35 (Figure 1B). We further confirmed the binding interaction between RAB-8/10 with EHBP-1 using an *in vitro* GST-pulldown assay (Figure 1A and Materials and Methods). In addition, this assay also detected a weak interaction with RAB-5(Q78L). Together, these data indicate that EHBP-1 is a Rab-interacting protein, with a strong preference for the active forms of RAB-8 and RAB-10.

In previous studies, we showed that RME-1, a regulator of endocytic recycling, functions downstream of RAB-10 (Chen *et al.*, 2006). The mammalian homologs of RME-1, EHD1 and EHD2, have been shown to interact with Ehbp1 in a manner dependent on the NPF motifs within Ehbp1 (Guilherme *et al.*, 2004a; Guilherme *et al.*, 2004b). However, *C. elegans* EHBP-1 lacks NPF motifs and we were unable to detect any interaction between the *C. elegans* proteins RME-1 and EHBP-1 using the yeast two-hybrid system, suggesting that this interaction is not conserved (Figure 1B).

EHBP-1 is widely expressed in *C. elegans*

To determine the expression pattern and subcellular localization of EHBP-1, we established transgenic lines expressing an EHBP-1-GFP fusion protein, driven by *ehbp-1* upstream sequences (the predicted promoter region). EHBP-1-GFP fusion proteins were expressed in most *C. elegans* tissues, including the pharynx and nerve ring, body-wall muscles, seam cells, intestine, oviduct sheath cell and spermatheca (Figure 2, A-F). The EHBP-1-GFP fusion protein was localized in a punctate or tubular pattern in most tissues. In the intestine, EHBP-1-GFP was localized to both the apical and basolateral plasma membranes (Figure 2E). Near basolateral membranes, EHB-1-GFP labeled distinct

cytoplasmic puncta resembling endosomes ranging in size from 0.5 to 1.0 μm (Figure 2D). In addition to punctate structures, EHBP-1-GFP also labeled tubular structures close to the basolateral plasma membrane of the intestine (Figure 2D).

EHBP-1 is associated with endosomes but not Golgi in the intestine

To determine where EHBP-1 is normally localized, and to help test the hypothesis that EHBP-1 functions with RAB-10 in endocytic recycling, we performed a series of colocalization studies in the intestinal cells of living animals, comparing functional GFP-tagged EHBP-1 with a set of RFP-tagged endosomal markers described previously (Chen *et al.*, 2006). We observed the highest degree of colocalization of EHBP-1-GFP with RFP-RAB-10 and RFP-RAB-8 labeled endosomal puncta in the intestine (Figure 3B-C"). In polarized MDCK cells, Rab10 labels the common recycling endosome, and our previous work in *C. elegans* had indicated a function for RAB-10 in transport between basolateral early and recycling endosomes (Babbey *et al.*, 2006; Chen *et al.*, 2006). Rab8 has also been reported to localize to recycling endosomal structures (Roland *et al.*, 2007). In *C. elegans,* we find that RFP-RAB-10 and GFP-RAB-8 colocalize extensively (Supplemental Figure S1A-B"). Closer examination showed that EHBP-1 colocalized with RAB-10 and RAB-8 on punctate endosomal membranes. EHBP-1 also localized to tubular elements associated with the puncta and the plasma membrane (Figure 6D). These results are consistent with EHBP-1 functioning with RAB-10 and/or RAB-8 *in vivo*.

EHBP-1 occasionally colocalized with basolateral recycling endosome marker RME-1, as we had found previously for RAB-10 (Figure 3D-D") (Chen *et al.*, 2006). EHBP-1-GFP also occasionally overlapped with the early endosome marker RFP-RAB-5, but the

EHBP-1-GFP labeled structures more often localized near RFP-RAB-5 puncta rather than overlapping with them directly (Figure 3A-A"). EHBP-1-GFP was not found to colocalize with the apical recycling marker RFP-RAB-11 or the Golgi marker MANS-RFP (Figure 3E-F"). Taken together these results indicate that EHBP-1 is enriched on endosomes, where it could potentially interact with RAB-10 and RAB-8 to regulate endosome-to-plasma membrane transport of cargo.

Loss of EHBP-1 causes endocytic recycling defects

Loss of RAB-10 results in dramatic endocytic trafficking defects in the *C. elegans* intestine (Chen *et al.*, 2006). One of the most obvious phenotypes observed in RAB-10 loss-of-function animals is the formation of grossly enlarged intestinal endosomes that are filled with fluid-phase markers taken up from the basolateral surface (Fares and Greenwald, 2001; Chen *et al.*, 2006). To determine if EHBP-1 shares some functions with RAB-10 *in vivo*, we first analyzed the intestines of animals depleted of EHBP-1 by RNAi–mediated knockdown, or animals containing a deletion allele of *ehbp-1* obtained from the National Bioresource Project for the Experimental Animal "Nematode *C. elegans*" in Japan. This *ehbp-1* mutant allele, *tm2523*, deletes 503 bp of genomic DNA corresponding to portions of the fifth and sixth exons, and is predicted to place all coding regions downstream of the deletion out of frame, effectively truncating any remaining expressed protein after amino acid 302.

ehbp-1(RNAi) animals were slow growing and produced fewer progeny than control animals, while *ehbp-1(tm2523)* animals often arrested as larvae, and animals that reached adulthood were sterile (see below). *ehbp-1(RNAi)*-treated animals contained grossly enlarged intestinal endosomes that could be filled with a signal sequence-modified form

of GFP (ssGFP) that is secreted from body-wall muscle cells, a phenotype very similar to that produced by *rab-10* loss-of-function mutants or *rab-10(RNAi)* (Figure 4B and D)(Chen *et al.*, 2006). Such vacuolated structures were also visible in the intestine of homozygous *ehbp-1(tm2523)* mutant animals, and could be rescued by intestine specific expression of EHBP-1-GFP (Supplemental Figure S1 C-D'). *ehbp-1* RNAi knockdown was considered effective because it blocked expression of EHBP-1-GFP transgenes in control experiments, and produced a spectrum of phenotypes very similar to the *ehbp-1(tm2523)* deletion mutant. These results suggest that loss of EHBP-1, like loss of RAB-10, produces severe defects in basolateral endocytic recycling.

Cargo-specific requirements for EHBP-1

To test the importance and specificity of EHBP-1 in cargo recycling, we assayed the effect of *ehbp-1* mutation on well established recycling cargo proteins hTAC-GFP (CIE marker) and hTfR-GFP (CDE marker) in *ehbp-1* mutant animals (Chen *et al.*, 2006; Shi *et al.*, 2007). We previously found that loss of RAB-10 caused dramatic intracellular accumulation of hTAC-GFP, consistent with a defect in hTAC recycling (Chen *et al.*, 2006). Loss of RAB-10 had only minor effects on hTfR-GFP (Chen *et al.*, 2006). These results suggested a cargo-specific role for RAB-10 in the recycling pathway.

In *ehbp-1(tm2523)* mutant animals, hTAC-GFP accumulated dramatically within the intestinal cells in intracellular tubules and enlarged puncta (Figure 4F and K), very similar to the phenotype observed in *rab-10* mutants (Figure 4G and K). hTfR-GFP localization appeared normal in *ehbp-1(tm2523)* mutant animals, suggesting that like RAB-10, EHBP-1 affects recycling in a cargo-specific manner (Figure 4I-J and K). Consistent with the direct action of EHBP-1 on endosomes transporting hTAC, we found

a high degree of colocalization between EHBP-1-mCherry and hTAC-GFP on intracellular tubules (Supplemental Figure S2 A-A").

While overexpression of full length EHBP-1-mCherry did not overtly affect the localization of hTAC-GFP, we found that overexpression of a truncated form of EHBP-1(aa1-711), lacking the RAB-10 interacting coiled-coil domain, induced dominant negative phenotypes including over-accumulation of intracellular hTAC-GFP and the formation of grossly enlarged intestinal vacuoles similar to those observed in *ehbp-1* loss-of-function mutants (Supplemental Figure S2 C-F). Colocalization studies clearly showed that the truncated form of EHBP-1(aa1-711) colocalizes with hTAC-GFP on the accumulated intracellular structures (Supplemental Figure S2 B-B").

EHBP-1 is important for endosome morphology

Our previous work indicated that the grossly enlarged endosomes in *rab-10* mutants are labeled by the early endosome marker GFP-RAB-5, but not by the basolateral recycling endosome marker GFP-RME-1. In fact, *rab-10* mutants extensively over-accumulate GFP-RAB-5 labeled early endosomes of all sizes, and display abnormal localization of the recycling endosome marker GFP-RME-1. In *rab-10* mutants GFP-RME-1 is more diffusely distributed, with the remaining GFP-RME-1 labeled structures being larger, fewer in number, and displaying a pronounced loss of their normal tubular morphology (Chen *et al.*, 2006). *ehbp-1* mutants displayed very similar endosomal defects, including increased GFP-RAB-5 labeling and loss of GFP-RME-1-labeled recycling endosome tubular morphology (Figure 5A-F, quantified in G-H). In contrast, there was no effect on the subcellular localization or number of RAB-11-labeled apical recycling endosomes in *ehbp-1* mutants (Supplemental Figure S3).

These results suggest that EHBP-1 and RAB-10 function at a similar step in endocytic transport, upstream of RME-1. Consistent with the idea that RME-1 functions downstream of RAB-10, we found that in *rme-1(b1045)* mutants the average intensity of GFP-RAB-10-labeled endosomes increased by about 3-fold (Figure 6A, C and H). This result suggests a blockage of the recycling pathway downstream of RAB-10 in cells lacking RME-1. We also found that the morphology of EHBP-1-GFP labeled structures was perturbed in *rme-1* mutants. EHBP-1-GFP localization appeared less tubular, with abnormal accumulation in patches and enlarged puncta (Figure 6D, F and I). Lack of RME-1 did not appear to affect the association of EHBP-1-GFP with membranes however.

EHBP-1 controls the localization of RAB-10

In many cases proteins that interact with GTP-bound Rabs are effector proteins, and such effectors are often localized and/or activated by interaction with the Rab protein (Stenmark, 2009). To determine if RAB-10 and EHBP-1 display such a relationship we assayed for changes in the localization of EHBP-1-GFP in a *rab-10* mutant background. In the absence of RAB-10, the morphology of EHBP-1-GFP labeled structures was perturbed, but EHBP-1 localization to membranes was not significantly affected (Figure 6, D-E and quantified in I). EHBP-1-GFP localization appeared less tubular, with abnormal accumulation in patches and enlarged puncta (Figure 6D-E). These results suggested that while RAB-10 is important for the morphology of EHBP-1 associated endosomes, it is not required to recruit EHBP-1 to the endosomal membrane.

We also performed the converse experiment, testing for changes in GFP-RAB-10 localization in animals lacking EHBP-1. Surprisingly, we found that GFP-RAB-10 was

much more diffusive in the cytosol of *ehbp-1(tm2523)* mutants than in control animals (Figure 6A-B). The intensity of GFP-RAB-10-labeled puncta was reduced by approximately 20-fold in *ehbp-1* mutants (Figure 6H). The increased diffusion and reduced intensity of GFP-RAB-10 endosomal labeling suggests that EHBP-1 functions upstream of RAB-10, promoting the association of RAB-10 with endosomes.

EHBP-1 regulates GLR-1 glutamate receptor trafficking

In addition to its role in the intestinal epithelium, *C. elegans* RAB-10 has also been reported to regulate the endocytic recycling of the AMPA-type glutamate receptor GLR-1, which is localized to synapses and controls the command interneuron circuit that mediates reversal behavior while animals forage (Hart *et al.*, 1995; Maricq *et al.*, 1995; Glodowski *et al.*, 2007). To determine whether, like RAB-10, EHBP-1 has a similar role in GLR-1 trafficking, we introduced a transgene expressing a full-length GLR-1-GFP chimeric protein into *ehbp-1* mutants (Rongo *et al.*, 1998). In control animals, GLR-1-GFP is localized to small (~0.5 μm) punctate structures that colocalize with other postsynaptic proteins along ventral cord neurites (Figure 7A) (Rongo *et al.*, 1998; Burbea *et al.*, 2002). In both *rab-10* and *ehbp-1* mutant animals, we found an abnormal accumulation of GLR-1-GFP in elongated (~2-5 μm) accretions along the ventral cord neurites (Figure 7B-C). These accretions are thought to be receptors trapped in internal compartments, most likely endosomes (Glodowski *et al.*, 2007; Chun *et al.*, 2008; Park *et al.*, 2009). We quantified the magnitude of the effect of *rab-10* and *ehbp-1* mutations on GLR-1 localization by classifying localized GLR-1-GFP into either small puncta or long accretions based on their size and morphology. Both mutants had elevated numbers of GLR-1 accretions (Figure 7D), with a mean size greater than that found for the rare

accretion seen in wild type (Figure 7E). In contrast, *ehbp-1* and *rab-10* mutants contained fewer than wild-type numbers of small GLR-1-GFP puncta, which are thought to be receptors clustered at postsynaptic elements (Figure 7F) (Rongo *et al.*, 1998; Burbea *et al.*, 2002).

The change in GLR-1-GFP localization in *ehbp-1* mutants could be due to defects in synapse formation. To test this possibility, we introduced a transgene expressing synaptic vesicle marker SNB-1-GFP (synaptobrevin), which labels synaptic terminals in the interneurons, into *ehbp-1* mutants (Nonet *et al.*, 1998; Rongo *et al.*, 1998). The number and distribution of SNB-1-GFP-labeled structures were similar in both wild type and *ehbp-1* mutant animals (Figure 7 G-I), indicating that the observed defects in GLR-1 localization are unlikely to be due to gross defects in synapse formation.

If *ehbp-1* mutations prevent the recycling of GLR-1, and instead result in GLR-1 accumulating in internal accretions, then these mutations should result in corresponding GLR-1-mediated behavioral defects (Burbea *et al.*, 2002; Glodowski *et al.*, 2007). GLR-1 positively regulates spontaneous reversals in locomotion during foraging, and the frequency of these reversals provides a quantitative measure of GLR-1 activity (Zheng *et al.*, 1999; Mellem *et al.*, 2002). We measured the spontaneous reversal frequency of wild type, *glr-1* mutants, *rab-10* mutants, *ehbp-1* homozygous mutants, and *ehbp-1* heterozygotes (30 animals, 5 minute trials). As previously described, *rab-10* mutants change direction at half the rate of wild-type animals, similar to the rate observed in *glr-1* null mutants (Glodowski *et al.*, 2007) (Figure 7J). Like *rab-10* mutants, *ehbp-1* mutants reversed direction at a depressed rate. Taken together, these results indicate that EHBP-1

and RAB-10 regulate the trafficking of GLR-1 from endosomal compartments within the neurites to synaptic membranes.

As described above, RAB-10 and EHBP-1 can physically interact. To determine whether EHBP-1 and RAB-10 associate at similar compartments in the ventral cord neurites, we introduced transgenes that express EHBP-1-GFP and mRFP-RAB-10 in the interneurons via the *glr-1* promoter. We found extensive colocalization of EHBP-1-GFP and RFP-RAB-10 along the ventral cord neurites (Figure 7K-M). These findings indicate that EHBP-1 and RAB-10 are largely present at the same subcellular structures along the ventral cord.

In *C. elegans* intestinal cells, EHBP-1 regulates RAB-10 subcellular localization. To test for a similar role in neurons, we assayed *ehbp-1* mutants for changes in GFP-RAB-10 localization in internurons. Whereas GFP-RAB-10 is localized at both large accretions and small punctate structures along the ventral nerve cord in control animals (Figure 7N), it is only localized to small puncta in *ehbp-1* mutants (Figure 7O). In *ehbp-1* mutant animals, the average number of GFP-RAB-10-containing accretions was reduced dramatically (approximately six-fold lower than that in control animals) (Figure 7P), and the mean size of the accretions was also reduced (Figure 7Q). The number of small GFP-RAB-10 puncta remained the same (Figure 7R). Taken together, these results indicate that, similar to what was observed in the intestinal cells, EHBP-1 regulates the subcellular localization of RAB-10 in neurons.

EHBP-1 is required in the germline

As mentioned earlier, we found that adult *ehbp-1(tm2523)* mutant animals are sterile. The sterile adults have abnormally small gonads and completely lack the characteristic row of large squared-off oocyte cells in the proximal gonad region (Figure 8A and E, arrows). This suggests a defect in oocyte growth and/or differentiation in these animals. While such a phenotype might be explained by severe membrane trafficking defects in the germline cells, this phenotype cannot be completely explained simply by loss of RAB-10 function from endosomes of the germ cells, since *rab-10* null mutants are not sterile (Chen *et al.*, 2006). In fact no defects were found in yolk endocytosis in *rab-10* mutants, suggesting relatively normal endosomal transport in *rab-10* mutant oocytes (Chen *et al.*, 2006). Thus we sought to determine if the sterile phenotype might be explained by loss of RAB-8 function, in addition to RAB-10 function, in the *ehbp-1* mutant germ cells. This was suggested by the finding that EHBP-1 can physically interact with RAB-8 in addition to RAB-10, that RAB-8 and RAB-10 are very similar to each other at the sequence level, both being apparent homologs of yeast Sec4p, and previous RNAi evidence that RAB-8 and RAB-10 possess an essential overlapping function in the germline (Audhya *et al.*, 2007a). There have also been suggestions of redundancy in this Rab pair in mammalian MDCK cells (Schuck *et al.*, 2007). Thus we compared the germline phenotype of *ehbp-1* mutants with that of animals depleted of RAB-8, or animals depleted of both RAB-8 and RAB-10. We found that while RNAi-mediated depletion of RAB-8 did not affect wild-type animals, RNAi-mediated depletion of RAB-8 in a *rab-10* mutant background produced larval arrest and sterile adult phenotypes that strongly resembled those in the *ehbp-1* mutant animals (Figure 8D-E, arrows).

Given the poor growth of the germline, and the abnormal oocytes in particular, the typical assay used to measure endocytic transport in the germline – following uptake of GFP-tagged yolk proteins by oocytes – did not appear appropriate. In addition, our previous work indicated that oocytes of nearly normal size are produced in animals with severe defects in oocyte endocytosis, while defects in secretion frequently lead to small and abnormal oocytes (Grant and Hirsh, 1999; Balklava *et al.*, 2007). Thus we performed a functional assay for protein secretion in the germline focusing on a GFP fusion to the transmembrane SNARE protein, SNB-1. At steady state, GFP-SNB-1 localized mostly to the plasma membrane of developing compartments in the germline, although a subpopulation could also be found on punctate structures that correspond to secretory vesicles and endosomes (Figure 8F' and data not shown). The accumulation of GFP-SNB-1 on the plasma membrane was confirmed by co-localization studies with an mCherry fusion to the PH domain derived from rat PLC1δ, which binds specifically to the plasma membrane-localized lipid, phosphatidylinositol 4,5-bisphosphate (Figure 8F-F"). Linescan analysis showed that the fluorescence intensities of GFP-SNB-1 and mCherry-PH peaked at identical points, illustrating a high degree of colocalization (Figure 8F'"). Co-depletion of RAB-8 and RAB-10 caused a striking defect in the accumulation of GFP-SNB-1 at the plasma membrane. Instead, the SNARE protein accumulated almost exclusively on internal punctate structures, and failed to co-localize with the plasma membrane mCherry-PH marker (Figure 8G-G'"). Depletion of EHBP-1 caused a similar defect in GFP-SNB-1 transport to the plasma membrane (Figure 8H-H'"). Taken together, these results indicate that RAB-8 and RAB-10 function redundantly

in the secretory pathway of *C. elegans* germ cells, and further suggest that EHBP-1 functions with RAB-8 and RAB-10 in this process.

DISCUSSION

Here we present the first functional studies of *ehbp-1* mutant animals, and demonstrate an important relationship between EHBP-1 with RAB-10 during endocytic recycling. We show that a predicted coiled-coil domain in the C-terminus of EHBP-1 binds directly to active GTP-bound RAB-10, that a functional EHBP-1-GFP fusion protein colocalizes with RFP-RAB-10 in epithelial cells and neurons, and that animals lacking EHBP-1 or RAB-10 share a specific set of endosomal defects, miss-sort cargo proteins in a similar manner, and display similar defects in organismal behavior. The RAB-10-like phenotypes found in *ehbp-1* mutants appear to result from a failure to efficiently recruit RAB-10 to endosomal membranes. However, in some respects, loss of EHBP-1 more severely impacts *C. elegans* development as compared to the loss of RAB-10, more closely resembling the defects found in animals lacking both RAB-10 and RAB-8, to which EHBP-1 can also bind.

The finding that EHBP-1 is important for RAB-10 membrane recruitment is unexpected, because EHBP-1 appears to interact with the GTP-bound form of RAB-10. Membrane recruitment of Rabs is most commonly associated with Rab guanine nucleotide exchange factors (GEFs), but GEFs interact with the GDP-bound or nucleotide-free forms of the Rab and promote GDP/GTP exchange. Proteins that bind to GTP-bound Rabs are typically thought of as Rab effectors, and Rab effectors are typically recruited to the membrane by the Rab GTPase, and not *vice-versa* as was observed in this case. However, there is an interesting recent precedent for this type of interaction. While this manuscript was in preparation, a paper by Sharma *et al.* showed that mammalian MICAL-L1, identified as a Rab8(GTP) binding partner, functions as an upstream

regulator of Rab8 that is important for the association of Rab8 with endosomal membranes (Sharma *et al.*, 2009). This study is also particularly relevant because MICAL-L1 has a similar domain structure to EHBP-1, including a central CH-domain and a C-terminal Rab-binding domain predicted to adopt a coiled-coil structure. Mammalian cells express Ehbp1 in addition to several different MICAL proteins, and the MICAL proteins all engage various members of the Rab10/Rab8/Rab13 family to promote endocytic transport (Weide *et al.*, 2003; Yamamura *et al.*, 2008). EHBP-1 appears to be the only *C. elegans* protein bearing a similar domain structure to mammalian Ehbp1 and MICAL-L1 in the predicted worm proteome.

Mammalian Ehbp1 was originally identified in NIH3T3 cells as a binding partner of EHD1 and EHD2, members of the RME-1 family of ATPases (Guilherme *et al.*, 2004a; Guilherme *et al.*, 2004b). Likewise, MICAL-L1 was recently shown to bind to EHD1 (Sharma *et al.*, 2009). Mammalian Ehbp1 and MICAL-L1 contain N-terminal NPF sequences that bind to the C-terminal EH-domain of the EHD proteins. RME-1/EHD family proteins are ATPases that are thought to function as membrane tubulation and/or fission molecules on endosomes, possibly functioning in a manner analogous to the well-studied fission regulator Dynamin (Daumke *et al.*, 2007; Grant and Caplan, 2008; Pant *et al.*, 2009). The direct association of EHBP-1/MICAL-L1 type proteins with RME-1/EHDs does not appear to be evolutionarily conserved, however, since *C. elegans* EHBP-1 lacks NPF sequences, and we could not detect a physical interaction between RME-1 with EHBP-1. Rather, EHBP-1's effects on RME-1 localization appear to be indirect, mediated through regulation of RAB-10. EHBP-1 and RAB-10 function

upstream of RME-1 at the basolateral early and/or recycling endosome in intestinal cells, affecting RME-1 localization to tubular membranes of the recycling endosome.

It is also interesting to note that in the 3T3 adipocyte model, siRNA-mediated depletion of Ehbp1 abolished the insulin-regulated endosome to plasma membrane transport of the glucose transporter Glut4 (Guilherme *et al.*, 2004b). Since mammalian Rab10 (in adipocytes) and mammalian Rab8 (in muscle cells) are now known to be important for Glut4 recycling in response to an insulin signal (Sano *et al.*, 2007; Randhawa *et al.*, 2008), it is reasonable to suspect that mammalian Ehbp1 might mediate its effects on Glut4 via interaction with Rab10 and/or Rab8.

Rab family GTPases have been shown to function in the generation, maintenance and membrane trafficking processes of intracellular compartments (Stenmark, 2009). Different Rab GTPases can coexist on the same compartment in distinct subdomains, and in some cases Rab cascades have been proposed (Sonnichsen *et al.*, 2000; Ortiz *et al.*, 2002). For instance Rab5 is thought to recruit activators of Rab7 to the endosome during endosome maturation, promoting entry of cargo into the degradative compartment and recycling of retromer-dependent cargo to the Golgi (Rink *et al.*, 2005). However, Rab5 also interacts with the recycling machinery that promotes transport to recycling endosomes. For instance, Rab5 binds to Rabenosyn-5, a protein that also interacts with recycling associated proteins Rab4 and EHD1 (Naslavsky *et al.*, 2004a; Naslavsky *et al.*, 2006). *In vitro,* we observed a weak binding of EHBP-1 to RAB-5, albeit not as strong an interaction as was found with RAB-10 or RAB-8. Interestingly, we observed that RNAi-mediated knockdown of RAB-5 resulted in poor recruitment of EHBP-1 to endosomal membranes (Figure 6G and I). Conversely, loss of EHBP-1 caused the

abnormally high accumulation of GFP-RAB-5, in parallel with a defect in proper recruitment of RAB-10. Thus, one possibility is that EHBP-1 interacts with RAB-5 and RAB-10 sequentially, acting to promote the exchange of RAB-5 for RAB-10 on endosomes as they mature along the recycling pathway. Further analysis will be required to substantiate such a model.

The CH-domain of EHBP-1 is also interesting with regard to endosome function, as CH-domains are thought to interact with cytoskeletal elements. Classically CH-domains are thought to be actin-interaction modules, although recent work suggests that in some proteins CH-domains can interact with microtubules (Sjoblom *et al.*, 2008). Actin in particular is important for the recycling of CIE cargo such as TAC and MHCI, and EHBP-1 and RAB-10 are preferentially involved in the recycling of such cargo (Radhakrishna and Donaldson, 1997; Weigert *et al.*, 2004). Future analysis will be focused on determining if EHBP-1 helps to connect endosomes to cytoskeletal networks to promote endocytic recycling function.

MATERIALS AND METHODS

General Methods and Strains

All *C. elegans* strains were derived originally from the wild-type Bristol strain N2. Worm cultures, genetic crosses, and other *C. elegans* husbandry were performed according to standard protocols (Brenner, 1974). Strains expressing transgenes were grown at 20°C. A complete list of strains used in this study can be found in Supplementary Table 1.

RNAi was performed using the feeding method (Timmons and Fire, 1998). Feeding constructs were either from the Ahringer library (Kamath and Ahringer, 2003) or prepared by PCR from EST clones provided by Dr. Yuji Kohara (National Institute of Genetic, Japan) followed by subcloning into the RNAi vector L4440 (Timmons and Fire, 1998). For most experiments synchronized L1 or L4 stage animals were treated for 24-72 hours and were scored as adults.

Antibodies

The following antibodies were used in this study: mouse anti-HA monoclonal antibody (16B12) Covance Research Products (Berkeley, CA), rabbit anti-GST polyclonal antibody (Z-5) Santa Cruz Biotechnologies (Santa Cruz, CA).

Yeast Two-hybrid Analyses

Yeast two-hybrid screen for candidates of RAB-10 interacting proteins was performed according to the procedure of the DupLEX-A yeast two-hybrid system (OriGene Technologies, Rockville MD). The cDNA sequences of *C. elegans* rab-10(Q68L) in the entry vector pDONR221 were cloned into the pEG202-Gtwy bait vector by Gateway recombination cloning (Invitrogen, Carlsbad, CA) to generate N-terminal fusions with the

LexA DNA binding domain. The pEG202-rab-5(Q78L), rab-7(Q68L), rab-8(Q67L), rab-11(Q70L), rab-35(Q69L), rme-1 and inactive rab-10(QT23N), rab-8(QT23N) were constructed accordingly. The prenylation motifs for membrane attachment at the C-terminal ends of RAB were also deleted to improve entry of bait fusion proteins into the yeast nucleus. The *C. elegans* cDNA library was purchased from the DupLEX-A yeast two-hybrid system (OriGene Technologies, Rockville MD).

The LexA-based DupLEX-A yeast two-hybrid system (OriGene Technologies Inc., Rockville, MD) was used for all subsequent truncation analysis. All two-hybrid plasmids were generated as PCR products with Gateway attB.1 and attB.2 sequence extensions, and were introduced into the Gateway entry vector pDONR221 by BP reaction. The bait vector pEG202-Gtwy and target vector pJG4-5-Gtwy have been described previously (Sato *et al.*, 2008b). Prey plasmids encoded EHBP-1 truncations were amplified from *C. elegans* EST clone yk1543d03 (Dr. Yuji Kohara, National Institute of Genetic, Japan), all amplified regions were confirmed by DNA sequencing. Origene plasmid pSH18-34 [*URA3*, 8 ops.-LacZ] was used as reporter in all the yeast two-hybrid experiments. Constructs were introduced into the yeast strain EGY48 [MATα trp1 his3 ura3 leu2::6 LexAop-*LEU2*] included in the system. Transformants were selected on plates lacking leucine, histidine, tryptophan and uracil, containing 2% galactose/1% raffinose at 30^{o}C for 3 days and assayed for the expression of the *LEU2* reporter. Blue/white β-galactosidase assays confirmed results shown for growth assays, according to manufacturer's instructions.

Tissue-specific steady-state endocytosis assays

Intestinal basolateral endocytosis was visualized using muscle-secreted GFP (transgenic strain *arIs37[myo-3::ssGFP])* as a fluid-phase marker in a *cup-4* mutant background. The *cup-4* mutation was included to reduce uptake by coelomocytes and increase availability of the marker in the body cavity (Patton *et al.*, 2005).

Protein Expression and Coprecipitation Assays

N-terminally HA-tagged proteins, RAB-5(Q78L), RAB-7(Q68L), RAB-8(Q67L) and RAB-10(Q68L), were synthesized *in vitro* using the TNT coupled transcription-translation system (Promega) using DNA templates pcDNA3.1-2xHA-RAB-5(Q78L), pcDNA3.1-2xHA-RAB-7(Q68L), pcDNA3.1-2xHA-RAB-8(Q67L) and pcDNA3.1-2xHA- RAB-10(Q68L) respectively (1.6 µg/each 50 µl reaction). The reaction cocktail was incubated at 30°C for 90 minutes. Control Glutathione S-transferase (GST), GST-EHBP-1(aa662-901) fusion proteins were expressed in the *ArcticExpress*™ strain of *E. coli* (Stratagene). Bacterial pellets were lysed in 10 ml B-PER Bacterial Protein Extraction Reagent (Pierce) with Complete Protease Inhibitor Cocktail Tablets (Roche). Extracts were cleared by centrifugation and supernatants were incubated with glutathione-Sepharose 4B beads (Amersham Pharmacia) at 4°C overnight. Beads were then washed six times with cold STET buffer (10mM Tris-HCl pH8.0, 150mM NaCl, 1mM EDTA, 0.1% Tween-20). *In vitro* synthesized HA-tagged protein (10 µl TNT mix diluted in 500 µl STET) was added to the beads and allowed to bind at 4°C for 2 hours. After six additional washes in STET the proteins were eluted by boiling in 30 µl 2xSDS-PAGE sample buffer. Eluted proteins were separated on SDS-PAGE (10% polyacrylamide), blotted to nitrocellulose, and probed with anti-HA (16B12). Subsequently the blots were stripped and re-probed with anti-GST (Z-5) antibodies.

Plasmids and Transgenic Strains

rab-5(Q78L), *rab-7*(Q68L), *rab-8*(Q67L) and *rab-10*(Q68L) cDNA clones were transferred into an in-house modified vector pcDNA3.1 (+) (Invitrogen, Carlsbad, CA) with 2xHA epitope tag and Gateway cassette (Invitrogen, Carlsbad, CA) for *in vitro* transcription/translation experiments. For GST pulldown experiments an equivalent *ehbp-1*(aa662-901) PCR product was introduced in frame into vector pGEX-2T (GE Healthcare Life Sciences) modified with a Gateway cassette.

To construct the GFP-tagged *ehbp-1* transgene driven by its own promoter, *ehbp-1* genomic sequences and presumed promoter sequences were PCR amplified from *C. elegans* genomic DNA and cloned into the entry vector pDONR221, then transferred into the *C. elegans* pPD117.01 vector with Gateway cassettes (Invitrogen, Carlsbad, CA) followed by GFP coding sequences, *let-858* 3' UTR sequences, and the *unc-119* gene of *C. briggsae*. The GFP-tagged plasmids (10 μg each) were bombarded into *unc-119(ed3*) mutant animals to establish low copy integrated transgenic lines by micro-particle bombardment method (Praitis *et al.*, 2001). Integrated transgenic lines used in this study were listed in Supplementary Table 1.

To construct GFP or RFP/mCherry (a gift from R. Tsien, Stanford University School of Medicine) fusion transgenes for expression specifically in the worm intestine, a previously described *vha-6* promoter driven vector modified with a Gateway cassette inserted at the Asp718I site just upstream of the GFP or RFP coding region was used. The sequences of *C. elegans ehbp-1(cDNA)* and *ehbp-1(1-711)* lacking stop codon were cloned individually into entry vector pDONR221 by PCR and BP reaction, and then transferred into intestinal expression vectors by Gateway recombination cloning LR

reaction to generate C-terminal fusions (Chen *et al.*, 2006). Complete plasmid sequences are available on request. Low copy integrated transgenic lines for all of these plasmids were obtained by the microparticle bombardment method (Praitis *et al.*, 2001).

Transgenic strains used in the GLR-1 glutamate receptor trafficking study were isolated after microinjecting various plasmids (5–50 ng/µl) along with *rol-6dm* (a gift from C. Mello, University of Massachusetts Medical School) or ttx-3::rfp as a transgenic marker (monomeric RFP; a gift from R. Tsien, Stanford University School of Medicine). Plasmids containing the *glr-1* promoter, followed by a gene encoding either RFP::RAB-10 or EHBP-1::GFP, were introduced into the germline by microinjection or microparticle bombardment, and followed as extrachromosomal arrays. To generate these plasmids, LR reactions (Gateway Technology; Invitrogen, Carlsbad, CA) were performed using entry clones containing genomic DNA encoding EHBP-1 or cDNA encoding RAB-10. For these reactions, the destination vector, which contains the *glr-1* promoter upstream of a *ccdB* gene that is flanked by *attR* sites, was generated from the plasmid pV6 (a gift from V. Maricq, University of Utah), following manufacturer's protocols (Invitrogen). For RFP::RAB-10, stable transgenic lines, including *odIs42*, were obtained by γ-irradiation followed by four generations of backcrossing.

Microscopy and Image Analysis

Live worms were mounted on 2% agarose pads with 10 mM levamisol as described previously (Sato *et al.*, 2005). Multi-wavelength fluorescence images were obtained using an Axiovert 200M (Carl Zeiss MicroImaging, Oberkochen, Germany) microscope equipped with a digital CCD camera (C4742–12ER, Hamamatsu Photonics, Hamamatsu, Japan), captured using Metamorph software ver 6.3r2 (Universal Imaging, West Chester,

PA), and then deconvolved using AutoDeblur Gold software ver 9.3 (AutoQuant Imaging, Watervliet, NY). Images taken in the DAPI channel were used to identify broad-spectrum intestinal autofluorescence caused by lipofuscin-positive lysosome-like organelles (Clokey and Jacobson, 1986; Hermann *et al.*, 2005). To obtain images of GFP fluorescence without interference from autofluorescence, we used argon 488nm excitation and the spectral fingerprinting function of the Zeiss LSM510 Meta confocal microscope system (Carl Zeiss MicroImaging) as described previously (Chen *et al.*, 2006). Quantification of images was performed with Metamorph software ver 6.3r2 (Universal Imaging). Most GFP/RFP colocalization experiments were performed on L3 and L4 larvae expressing GFP and RFP-markers as previously described.

For fluorescence microscopy of *C. elegans* ventral cord neurites, details were as described previously, but with some modifications (Glodowski *et al.*, 2007). GFP and RFP-tagged fluorescent proteins were visualized in nematodes by mounting young adult (16-18 hour post L4 statge) on 2% agarose pads with 100 mM tetramisole in M9 buffer. Fluorescent images were observed using an Axioplan II (Carl Zeiss, Thornwood, NY). A 100X (numerical aperture 1.4) PlanApo objective was used to detect GFP and RFP signal. Imaging was done with an ORCA charge-coupled device camera (Hamamatsu, Bridgewater, NJ) by using iVision software (Scanalytics, Fairfax, VA). Exposure times were chosen to fill the 12-bit dynamic range without saturation. Maximum intensity projections of z-series stacks were obtained, and out-of-focus light was removed with a constrained iterative deconvolution algorithm. Puncta outlines were automatically calculated for fluorescent signals that were two standard deviations above the unlocalized baseline by using a macro written for ImageJ64 software. Puncta size was measured as

the maximum diameter for each outlined cluster. Puncta outline data included both small puncta (e.g., as observed GLR-1-GFP and GFP-RAB-10 in wild type, classified based on a diameter cutoff of less than 1 μm and circular morphology using a program written in ImageJ), as well as long accretions (e.g., as observed GFP-RAB-10 in wild-type and GLR-1-GFP in *rab-10* and *ehbp-1* mutants, classified based on a width cutoff of greater than 1 μm and elongated morphology). Numbers were calculated by counting the average number of small puncta or large accretions per 10 μm or 100 μm of neurite length, respectively.

Behavioral Assays

The reversal frequency of individual animals was assayed as described previously, but with some modifications (Zheng *et al.*, 1999). Single young adult hermaphrodites were placed on nematode growth medium plates in the absence of food. The animals were allowed to adjust to the plates for 5 min, and the number of spontaneous reversals for each animal was counted over a 5-min period. Thirty animals were tested for each genotype, and the reported scores reflect the mean number of reversals per minute.

Protein secretion assay in the *C. elegans* germline

The generation of a *C. elegans* strain expressing mCherry-PH $^{PLC1\ \ 1}$ has been described previously (Kachur *et al.*, 2008). A GFP fusion to SNB-1 (T10H9.4) was generated by cloning the unspliced genomic loci into the SpeI site of pIC26 (GFP) (Cheeseman *et al.*, 2004). The construct was integrated into DP38 (unc-119 (ed3)) as described previously (Praitis *et al.*, 2001) using a particle delivery system (Biolistic PDS-1000/He; Bio-Rad Laboratories, Inc).

Double stranded RNA (dsRNA) was prepared as described previously (Oegema *et al.*, 2001) from templates prepared by using the primers listed (below) to amplify N2 genomic DNA. For depletions, L4 hermaphrodites were injected with dsRNA and incubated at 20ºC for 45 hours before analysis.

RNA 210, D1037.4, RAB-8, 1.9 mg/mL:

Oligo 1: AATTAACCCTCACTAAAGGgcttttgcatgccaagatgtc

Oligo 2: TAATACGACTCACTATAGGCGGGACGAAAATGGTAAAAA

RNA 311, T23H2.5, RAB-10, 2.3 mg/mL:

Oligo 1: AATTAACCCTCACTAAAGGGTGCTGCTAATAGGCGACTCA

Oligo 2: TAATACGACTCACTATAGGTTGCTCGTCAGTGGAATCAG

RNA KOEHBP-1, F25B3.1, EHBP-1, 2.4 mg/mL:

Oligo 1: AATTAACCCTCACTAAAGGGATTTCAGTTCGTCCCCAATG

Oligo 2: TAATACGACTCACTATAGGACGAATTGCTCCAACTCCTG

For analysis of gonads, animals were anesthetized in 0.1% tricane (Sigma), mounted on agarose pads, and imaged at 20 ºC on a spinning disc confocal (Nikon Eclipse TE2000-E) microscope equipped with a Nikon 60X, 1.4NA Planapo oil objective lens and a Hamamatsu Orca-ER CCD camera. Linescan analysis was performed using Metamorph software.

ACKNOWLEDGEMENTS

We thank Yuji Kohara and Shohei Mitani for important reagents, and we thank Karen Oegema for generously providing unpublished marker strains for this study. We thank Saumya Pant, Peter Schweinsberg and Zui Pan for their generous advice and technical assistance. R.B. was supported by Aresty Research Center grant. This work was supported by NIH R01 NS42023 to C.R. This work was supported by NIH Grant GM067237 to B.D.G.

Table 1. Transgenic and Mutant Strains Used in This Study

Transgenic and Mutant Strains Used in This Study
pwIs451[ehbp-1p::EHBP-1::GFP]
*pwIs666[*p*vha6::EHBP-1::GFP]*
*pwIs846[*p*vha6::RFP::RAB-5]*
*pwIs414[*p*vha6::RFP::RAB-10](Chen et al., 2006)*
*pwIs500[*p*vha6:: RFP::RAB-8]*
*pwIs852[*p*vha6:: RFP::RME-1]*
*pwIs428[*p*vha6::RFP::RAB-11](Chen et al., 2006)*
*pwEx102[*p*vha6::MANS::RFP](Shi et al., 2007)*
bIs1[vit-2::GFP, rol-6(su1006)](Grant and Hirsh, 1999)
*arIs37[myo3*p*::ssGFP, dpy-20(+)](Fares and Greenwald, 2001)*
*pwIs112[*p*vha6::hTAC::GFP](Chen et al., 2006)*
*pwIs90[*p*vha6::hTfR::GFP](Chen et al., 2006)*
*pwIs87[*p*vha6::GFP::RME-1](Chen et al., 2006)*
*pwIs72[*p*vha6::GFP::RAB-5](Chen et al., 2006)*
*pwIs206[*p*vha6::GFP::RAB-10](Chen et al., 2006)*
*pwIs69[*p*vha6::GFP::RAB-11](Chen et al., 2006)*
*pwIs883[*p*vha6::EHBP-1::mCherry]*
*pwIs888[*p*vha6::EHBP-1(1-711)::mCherry]*
nuIs25[*GLR-1::GFP*](Glodowski *et al.*, 2007)
odIs42[p*glr-1::RFP::RAB-10*](Glodowski *et al.*, 2007)
odEx1 [p*glr-1::EHBP-1::GFP*]
*odIs1[*p*glr-1::SNB-1::GFP](Glodowski et al., 2007)*
p*pie-1::mCherry::PH*$^{PLC1\delta1}$ *(Kachur et al., 2008)*
p*pie-1::SNB-1::GFP*
glr-1(ky176) (From C. elegans Gene Knockout Consortium)
rme-1(b1045)(Grant et al., 2001)
rab-10(q373)(Chen et al., 2006)
ehbp-1(tm2523) (kindly provided by Dr. Shohei Mitani, Japanese National Bioresource Project for the Experimental Animal "Nematode *C. elegans*"*)*

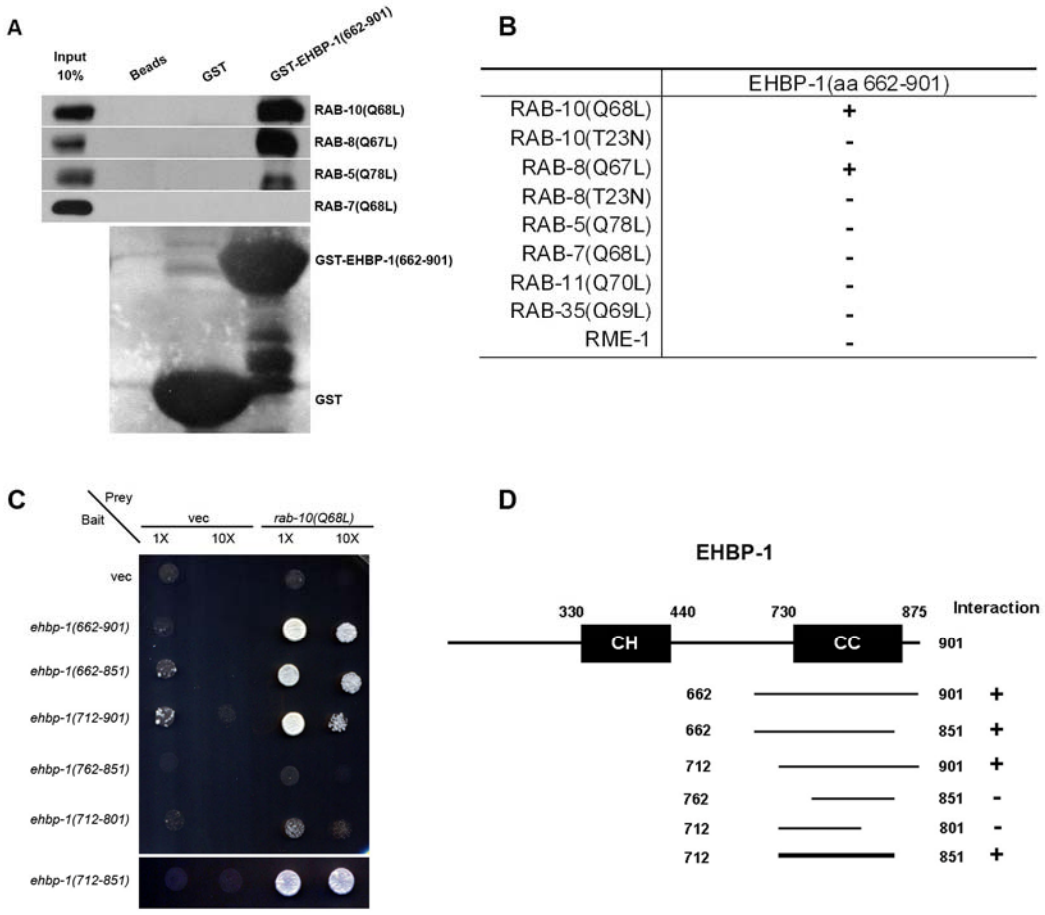

Figure 1. EHBP-1 physically interacts with RAB-10(Q68L) and RAB-8(Q67L)

(A) Glutathione beads loaded with recombinant GST or GST-EHBP-1(662-901) were incubated with *in vitro* expressed HA-RAB-5(Q78L), RAB-7(Q68L), RAB-8(Q67L), and RAB-10(Q68L), and then washed to remove unbound proteins. Bound proteins were eluted and analyzed by western blot using anti-HA (top) or anti-GST (bottom) antibodies. Input lanes contain *in vitro* expressed HA-conjugated RABs used in the binding assays (10%). (B) Using EHBP-1 (aa662-901) as bait, RME-1 and RABs with reported endosomal trafficking involvement were used as prey in yeast two-hybrid assays,

including active RAB-5(Q78L), RAB-7(Q68L), RAB-8(Q67L), RAB-10(Q68L), RAB-11(Q70L), RAB-35(Q69L) and inactive RAB-8(QT23N) and RAB-10(QT23N). (C) RAB-10(Q68L) was expressed in a yeast reporter strain as a fusion with the DNA-binding domain of LexA (bait). EHBP-1 truncated forms were expressed in the same yeast cells as fusions with the B42 transcriptional activation domain (prey). Interaction between bait and prey was assayed by complementation of leucine auxotrophy (LEU2 growth assay). Colonies were diluted in liquid and spotted on solid growth medium directly or after further 10X dilution. (D) Schematic representations of EHBP-1 domains and the truncated fragments used in yeast two-hybrid analysis. Protein domains are displayed as dark boxes above protein sequence used in the study (shown as dark lines). Amino acid numbers are indicated.

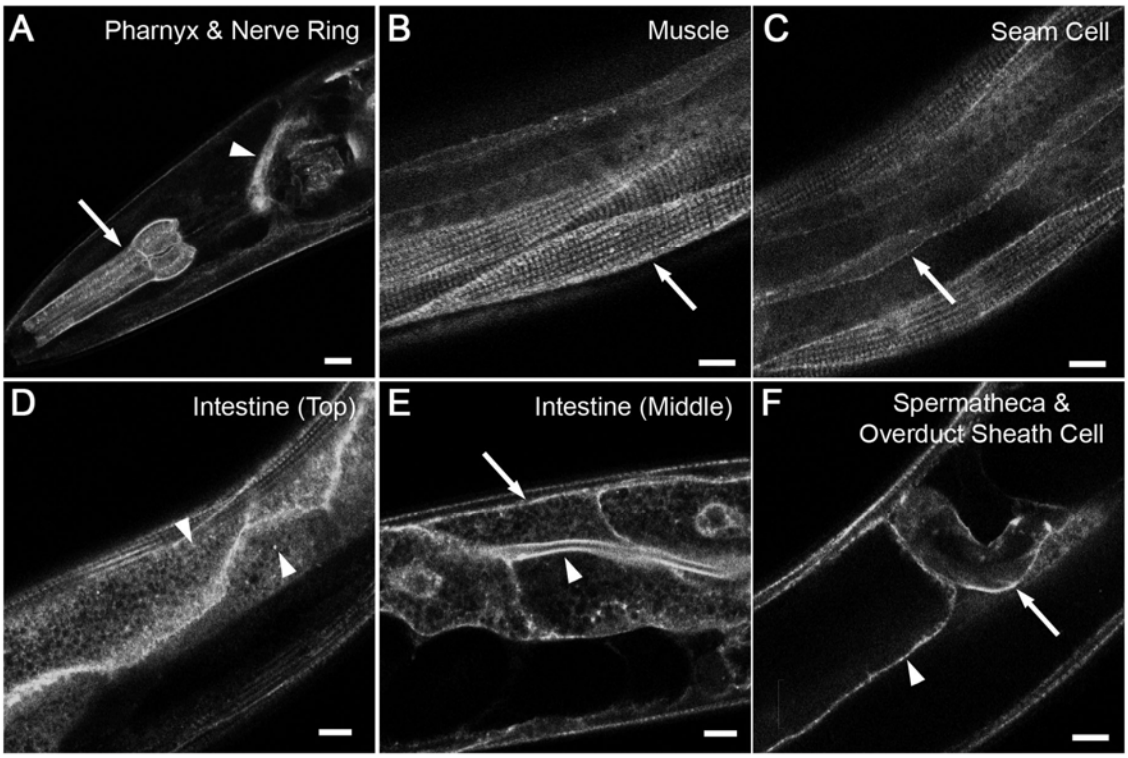

Figure 2. EHBP-1 is broadly expressed in *C. elegans.*

Confocal images of EHBP-1-GFP transgene expression driven by the *ehbp-1* promoter. Tissue-specific expression was observed in (A), pharynx (arrows), nerve ring (arrowhead); (B), myofilament of body-wall muscle (arrows); (C), seam cells (arrows); (D), intestine (Top); (E), intestine (Middle), arrows indicate the basolateral intestinal membranes and arrowheads indicate the apical intestinal membranes and basolateral cytoplasmic puncta; (F), spermatheca (arrowheads) and oviduct sheath cells (arrows). Scale bar represents 10 μm.

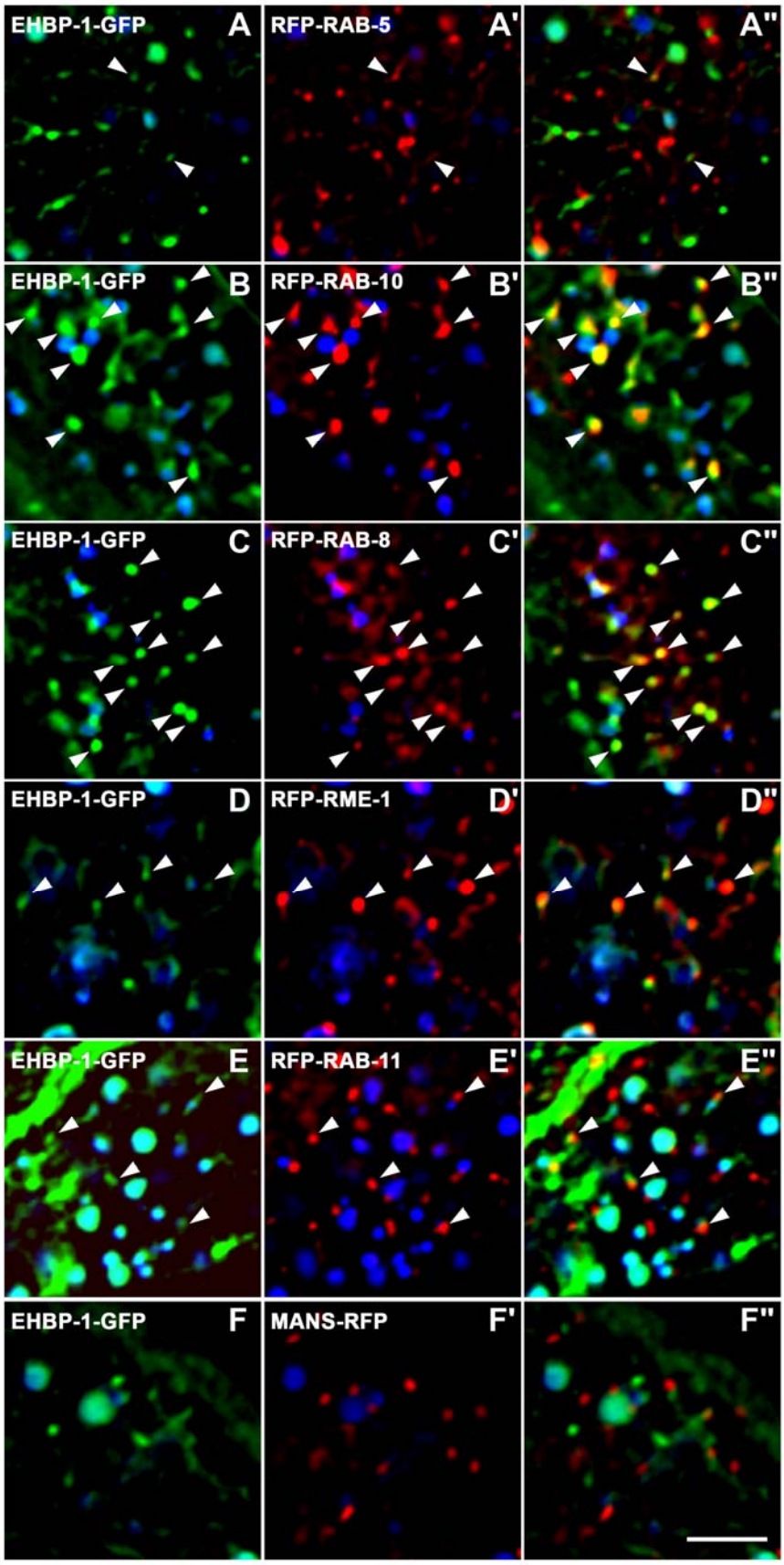
EHBP-1-GFP
A
RFP-RAB-5
A'
A"
EHBP-1-GFP
B
RFP-RAB-10
B'
B"
EHBP-1-GFP
C
RFP-RAB-8
C'
C"
EHBP-1-GFP
D
RFP-RME-1
D'
D"
EHBP-1-GFP
E
RFP-RAB-11
E'
E"
EHBP-1-GFP
F
MANS-RFP
F'
F"

Figure 3. EHBP-1 colocalizes with RAB-10 and RAB-8 on endosomes.

All images are from deconvolved 3-D image stacks acquired in intact living animals expressing GFP and RFP tagged proteins specifically in intestinal epithelial cells. (A-A") Arrowheads indicate endosomes labeled by both EHBP-1-GFP and RFP-RAB-5. (B-B") Arrowheads indicate endosomes labeled by both EHBP-1-GFP and RFP-RAB-10. (C-C") Arrowheads indicate endosomes labeled by both EHBP-1-GFP and RFP-RAB-8. (D-D") Arrowheads indicate endosomes labeled by both EHBP-1-GFP and RFP-RME-1. (E-E") Arrowheads indicate EHBP-1-GFP positive endosomes juxtaposed to RFP-RAB-11 labeled structures. (F-F") EHBP-1-GFP does not colocalize with Golgi marker Mannosidase-RFP. In each image autofluorescent lysosome-like organelles can be seen in all three channels with the strongest signal in blue, whereas GFP appears only in the green channel and RFP only in the red channel. Signals observed in the green or red channels that do not overlap with signals in the blue channel are considered bone fide GFP or RFP signals, respectively. Scale bar represents 10 μm.

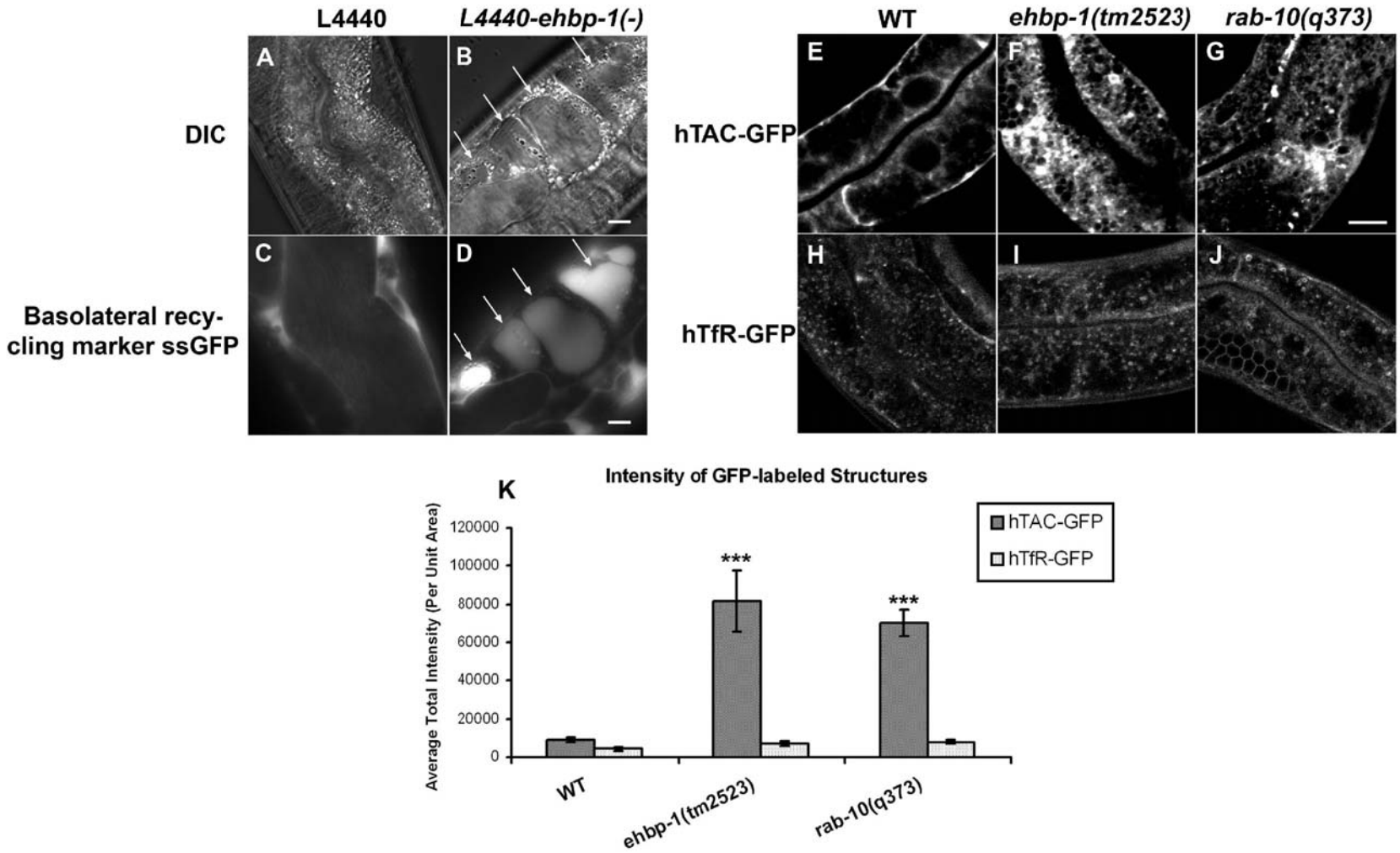
L4440
L4440-ehbp-1(-)
DIC
Basolateral recy-
cling marker ssGFP
A
B
C
D
WT
ehbp-1(tm2523)
rab-10(q373)
hTAC-GFP
hTfR-GFP
E
F
G
H
I
J
K
Intensity of GFP-labeled Structures
Average Total Intensity (Per Unit Area)
120000
100000
80000
60000
40000
20000
0
hTAC-GFP
hTfR-GFP
***
***
WT
ehbp-1(tm2523)
rab-10(q373)

Figure 4. Loss of EHBP-1 induces endocytic recycling defects in the *C. elegans* intestine.

(A-B) Nomarski images of the intestines in wild type (*L4440*) and *ehbp*-1(RNAi) animals. Large transparent vacuoles were found in the intestines of *ehbp*-1(RNAi) animals (B). Arrows indicate the positions of vacuoles. (C-D) Intestinal endocytosis of the basolateral recycling marker ssGFP in the wild-type and *ehbp*-1(RNAi) animals. Compared with wild type animals, little ssGFP accumulates because of efficient recycling back to the body cavity (C), *ehbp*-1(RNAi) animal specific vacuoles were filled with basolaterally endocytosed ssGFP (D, arrows). A *cup-4(ar494*) mutation was also included in the strain shown in (C-D) to impair coelomocyte function and increase steady-state levels of secreted ssGFP in the body cavity. (E-K) Confocal images of the worm intestine expressing GFP-tagged cargo proteins that recycle via the recycling endosome, the human transferrin receptor (hTfR-GFP) and the IL-2 receptor alpha chain (hTAC-GFP) in wild type, *ehbp-1(tm2523)*, and *rab-10(q373)* mutant animals. Compared with wild type animals (E), hTAC-GFP accumulates significantly on the intestinal cytosolic endosomal structures in *ehbp-1(tm2523)* and *rab-10(q373)*, approximately 8-fold and 7-fold increase of the average total GFP intensity respectively (F-G and K). hTfR-GFP was not affected in *ehbp-1(tm2523)* and *rab-10(q373)* mutants (H-J and K). Error bars are SEM (n=18 each, 6 animals of each genotype sampled in three different regions of each intestine defined by a 100 x 100 (pixel^2) box positioned at random). Asterisks indicate a significant difference in the one-tailed Student's t-test ($p<0.001$). Scale bar represents 10 μm.

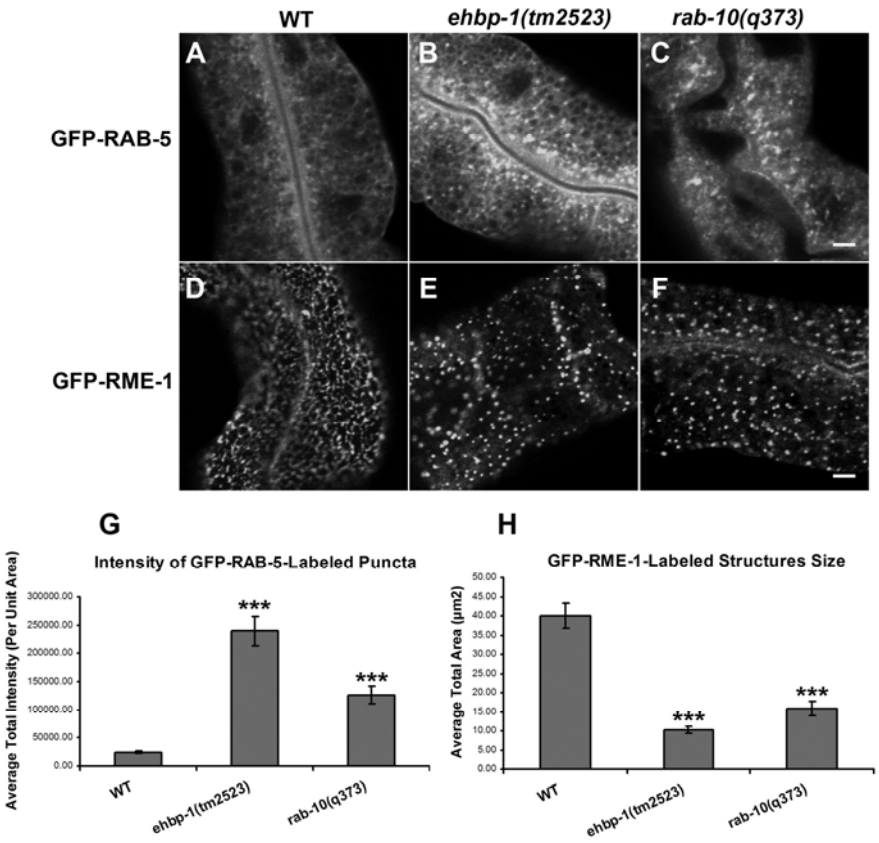

Figure 5. Accumulation of RAB-5-positive early endosomes and disrupted RME-1-positive tubular recycling structures in *ehbp-1(tm2523)* and *rab-10(q373)* mutants.

Representative confocal images are shown for GFP-RAB-5 (A-C) and GFP-RME-1 (D-F). Approximate 10-fold and 5-fold average total intensity increase of GFP-RAB-5 were observed in *ehbp-1(tm2523)* and *rab-10(q373)* mutants (A-C, G). To quantify the RME-1-labeled structures disruption, average total area of positive GFP labeling per unit area was measured (H). Error bars are SEM (n=18 each, 6 animals of each genotype sampled in three different regions of each intestine). Asterisks indicate a significant difference in the one-tailed Student's t-test ($p<0.001$). Scale bar represents 10 μm.

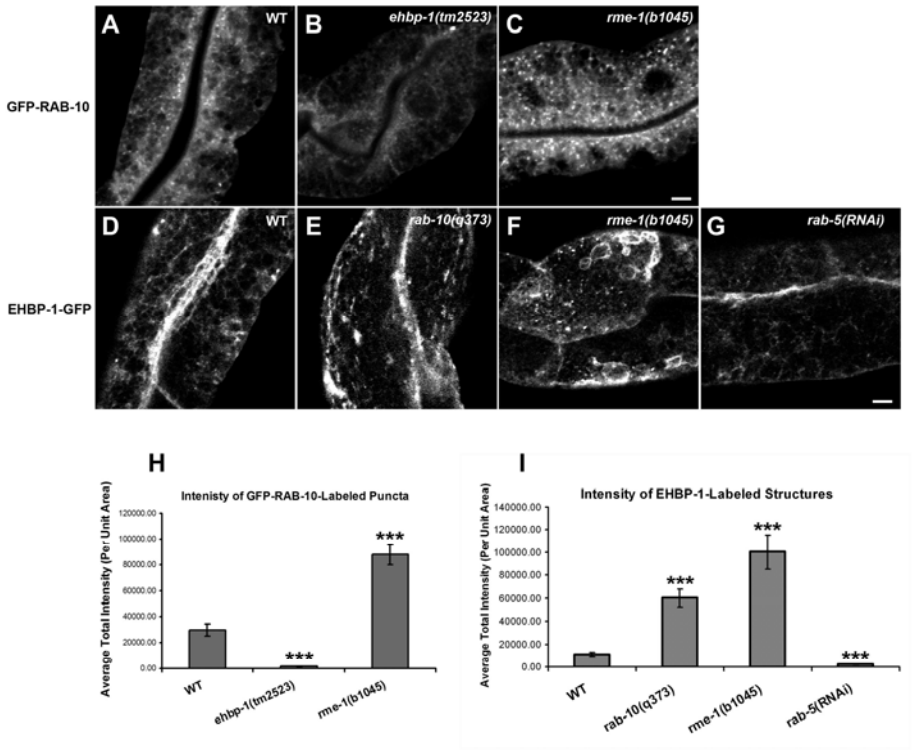

Figure 6. RAB-10-positive endosomal labeling decreases in *ehbp-1(tm2523)* mutants, but accumulate in *rme-1(b1045)* mutants.

(A-C, H). Representative confocal images of wild-type animals and mutants are shown for GFP-RAB-10 (A-C) and average total intensity of GFP-RAB-10 in unit area was quantified in (H). The number of EHBP-1-labeled endosomal structures were significantly increased in *rab-10(q373)* and *rme-1(b1045)* mutants (D-F, I), but *rab-5* RNAi knockdown significantly diminished labeling of EHBP-1 on tubular and punctuate structures (G and I). Representative confocal images of wild-type animals and mutants are shown for EHBP-1-GFP (D-G) and average total intensity of EHBP-1-GFP in unit area was quantified in (I). Error bars are SEM (n=18 each, 6 animals of each genotype sampled in three different regions of each intestine). Asterisks indicate a significant difference in the one-tailed Student's t-test ($p<0.001$). Scale bar represents 10 μm.

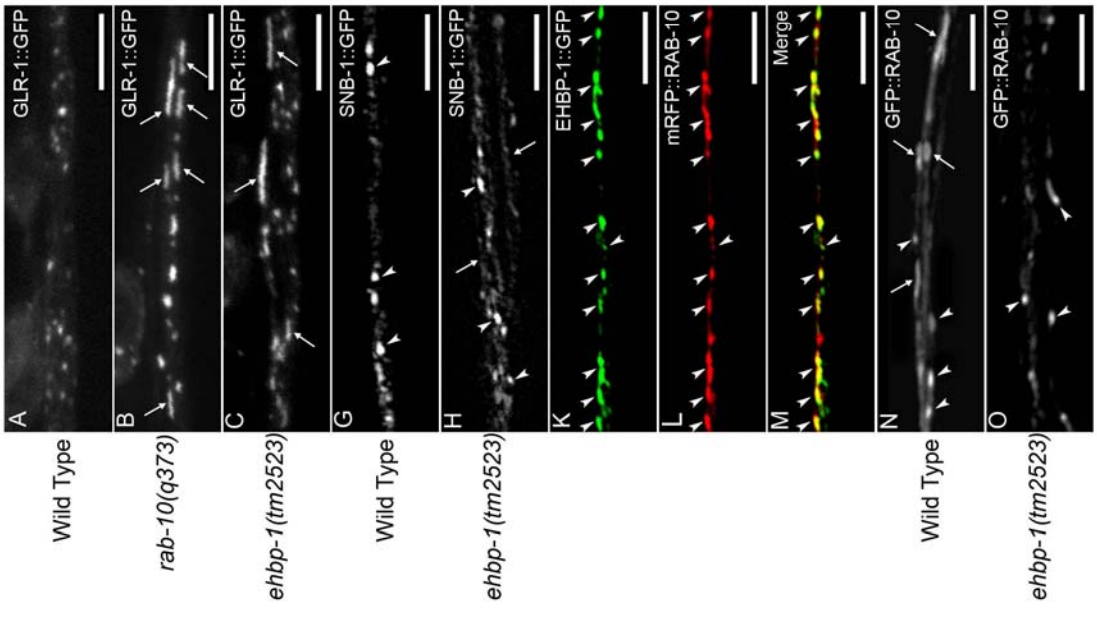
A
GLR-1::GFP
Wild Type
B
GLR-1::GFP
rab-10(q373)
C
GLR-1::GFP
ehbp-1(tm2523)
D
Number of GLR-1 Accretions
Accretions / 100 µm
Wild Type
rab-10
ehbp-1
E
Size of GLR-1 Accretions
Accretion Width (µm)
F
Number of GLR-1 Puncta
Puncta / 10 µm
G
SNB-1::GFP
Wild Type
H
SNB-1::GFP
ehbp-1(tm2523)
I
Number of SNB-1 Puncta
J
Spontaneous Reversals
Reversals / min.
glr-1
ehbp-1/+
K
EHBP-1::GFP
L
mRFP::RAB-10
M
Merge
N
GFP::RAB-10
Wild Type
O
GFP::RAB-10
ehbp-1(tm2523)
P
Number of RAB-10 Accretions
Q
Size of RAB-10 Accretions
R
RAB-10 Puncta Number

Figure 7. EHBP-1 regulates GLR-1 glutamate receptor trafficking.

GLR-1-GFP fluorescence was observed along ventral cord neurites of (A) wild-type animals, (B) *rab-10(q373)* mutants, and (C) *ehbp-1(tm2523)* mutants. In wild-type animals, GLR-1-GFP is localized to small (~0.5 μm) synaptic puncta. By contrast, *ehbp-1* mutants, like in *rab-10* mutants, accumulate GLR-1-GFP in elongated (~2-5 μm) accretions (arrows). The (D) mean number (per 100 μm of ventral cord) and (E) size (length in μm) of GLR-1-GFP accretions is plotted. The (F) mean number of GLR-1-GFP puncta (per 100 μm of ventral cord) is also plotted. Presynaptic marker SNB-1-GFP shows similar localization to puncta along the ventral cord of (G) wild-type and (H) *ehbp-1* mutant animals; the (I) mean number is indicated. Occasionally some neurites are found outside of the main ventral cord fascicle of *ehbp-1* mutants (arrow in H), although this does not appear to grossly affect synapse formation. (J) The mean spontaneous reversal frequency (number of reversals per minute over a 5-min period) is plotted for the given genotype. (K) EHBP-1-GFP and (L) mRFP-RAB-10 are co-localized to subcellular compartments (arrowheads) in the ventral nerve cords. (M) Merged image. (N) GFP-RAB-10 is localized to small puncta (arrowheads) and large accretions (arrows) along the ventral cord of wild-type animals, but is only found in puncta in (O) *ehbp-1* mutants, indicating that EHBP-1 regulates RAB-10 subcellular localization. The (P) number per ventral cord length and (Q) mean size of GFP-RAB-10 accretions, as well as the (R) number of GFP-RAB-10 puncta are plotted. Scale bar represents 5 μm. Error bars are SEM. N= 15–20 animals for each genotype. *$p < 0.05$, **$p < 0.01$, ***$p < 0.001$ by analysis of variance (ANOVA) followed by Dunnett's multiple comparison to wild type (D-F, J), or by t-test (P-Q).

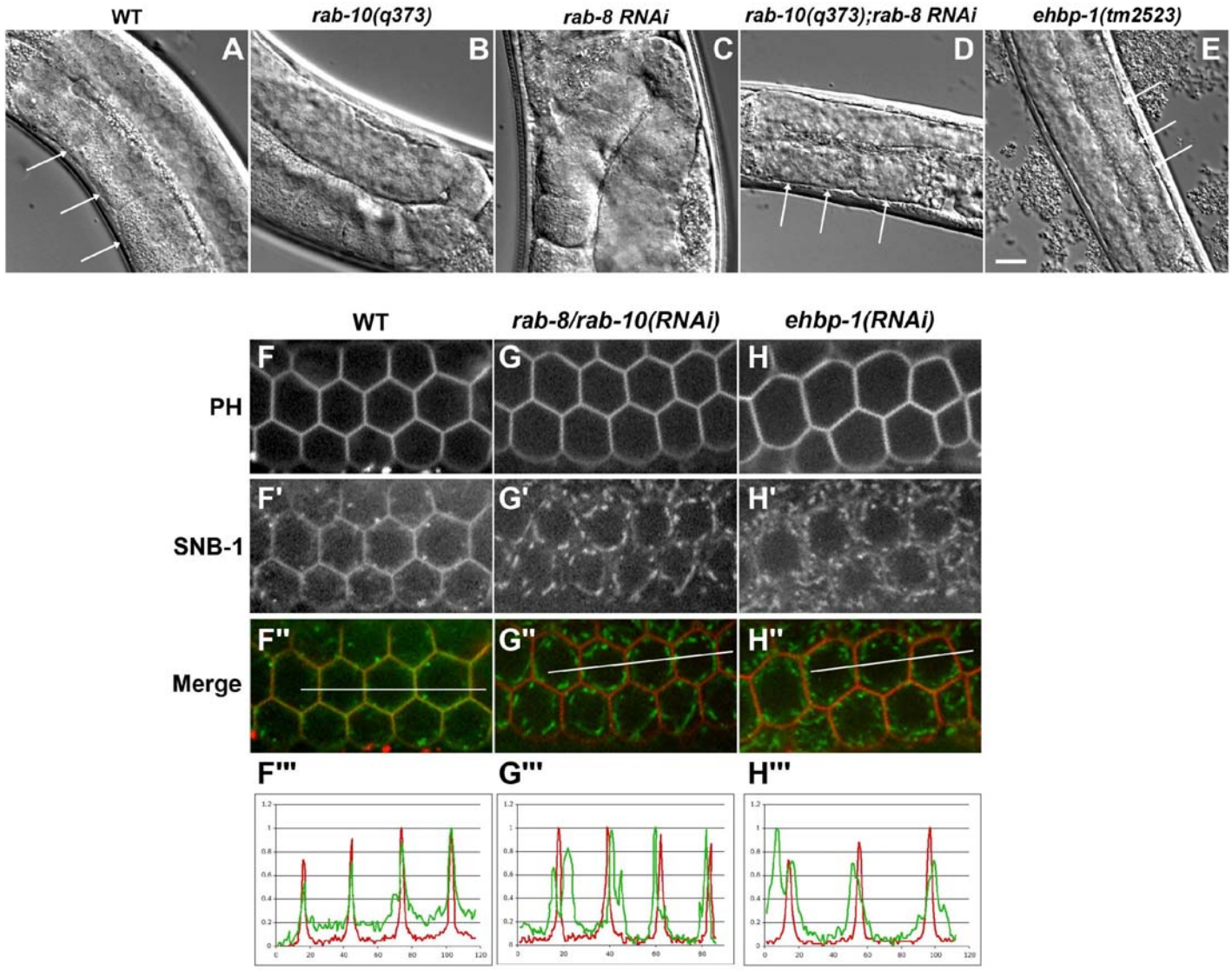
WT
rab-10(q373)
rab-8 RNAi
rab-10(q373);rab-8 RNAi
ehbp-1(tm2523)
A
B
C
D
E
WT
rab-8/rab-10(RNAi)
ehbp-1(RNAi)
PH
SNB-1
Merge
F
G
H
F'
G'
H'
F''
G''
H''
F'''
G'''
H'''

Figure 8. Depletion of EHBP-1 result in germline developmental defect.

(A-E) Nomarski images of the gonads in wild type, *rab-10(q373)*, *rab-8(RNAi)*, *rab-10(q373)*;*rab-8(RNAi)*, and *ehbp-1(tm2523)* animals. Developmental defects of gonads were found in *rab-10(q373)*;*rab-8(RNAi)* double knockdown animals and *ehbp-1(tm2523)* mutants (D-E). Arrows indicate the normal large squared-off oocyte cells in the proximal gonad region (A) and the lack of the characteristic row of oocyte cells in the proximal gonad regions (D-E). Scale bar represents 10 μm. (F-H''') Depletion of EHBP-1 or co-depletion of RAB-8 and RAB-10 result in a similar defect in germline secretion. GFP-SNB-1 localized mostly to the plasma membrane of developing compartments in the germline and colocalized with mCherry-PH at steady state (F-F''). Linescan analysis showed that fluorescence intensity of GFP-SNB-1 and mCherry-PH peaked at identical points (F'''). RNAi depletion of RAB-8 and RAB-10 caused a defect in the localization of GFP-SNB-1 at the plasma membrane (G-G'''). RNAi depletion of EHBP-1 caused a similar defect in GFP-SNB-1 delivery to the plasma membrane (H-H''').

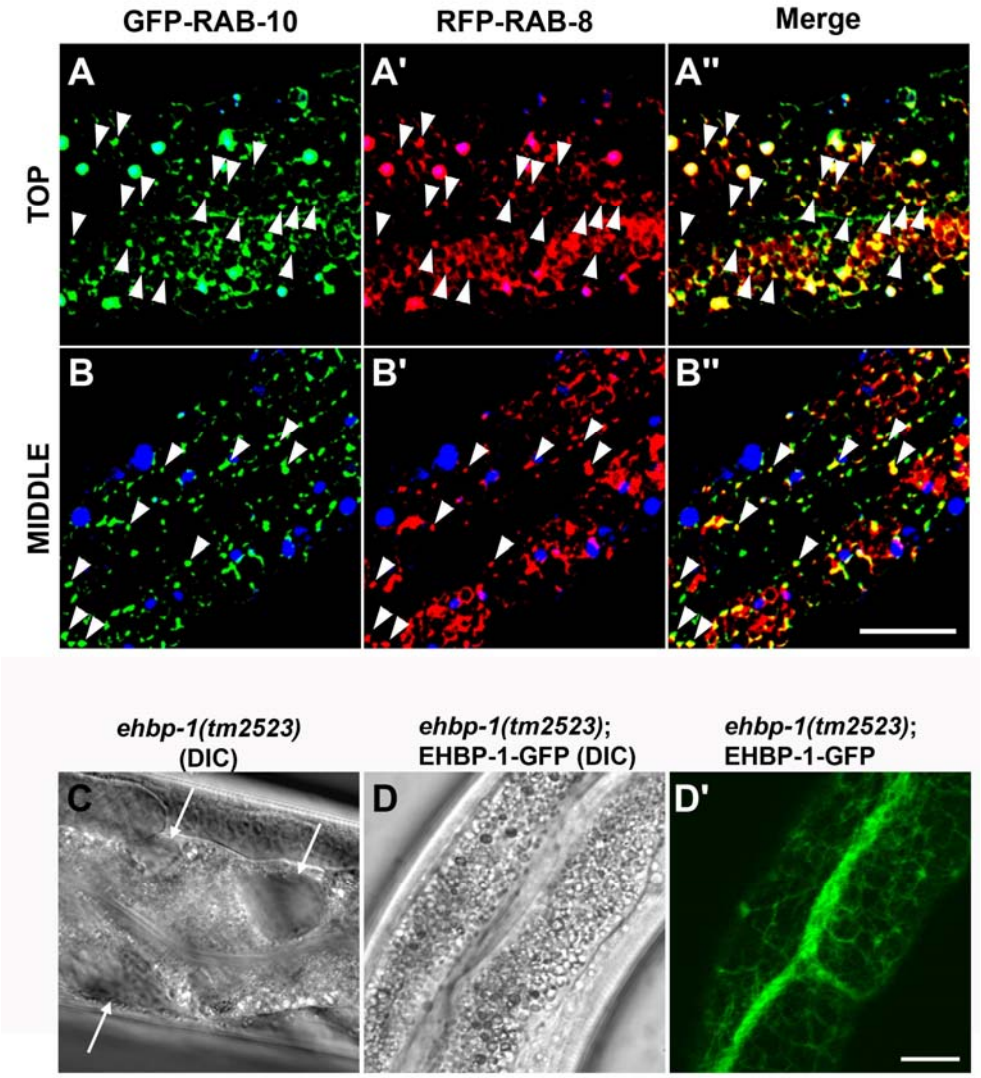

Figure S1.

RAB-10 colocalizes with RAB-8 on endosomes. All images are from deconvolved 3-D image stacks acquired in intact living animals expressing GFP and RFP- tagged proteins specifically in intestinal epithelial cells. (A-A") GFP-RAB-10 extensively overlaps with RFP-RAB-8 on endosomes near intestine basolateral membrane. Arrowheads indicate endosomes labeled by both GFP-RAB-10 and RFP-RAB-8. (B-B") GFP-RAB-10 partially colocalizes with RFP-RAB-8 on endosomal structures deep in intestinal cytosol.

Arrowheads indicate endosomes labeled by both GFP-RAB-10 and RFP-RAB-8. In each image autofluorescent lysosome-like organelles can be seen in all three channels with the strongest signal in blue, whereas GFP appears only in the green channel and RFP only in the red channel. Signals observed in the green or red channels that do not overlap with signals in the blue channel are considered bone fide GFP or RFP signals, respectively.

(C-D) Nomarski images of the intestines in *ehbp-1(tm2523)* mutants and *ehbp-1(tm2523)* animals with intestine specific transgenic expression of EHBP-1-GFP. Large transparent vacuoles were found in the intestines of *ehbp-1(tm2523)* animals (C). Vacuole phenotype could be rescued by intestine specific expression of EHBP-1-GFP (D-D'). Scale bar represents 10 μm.

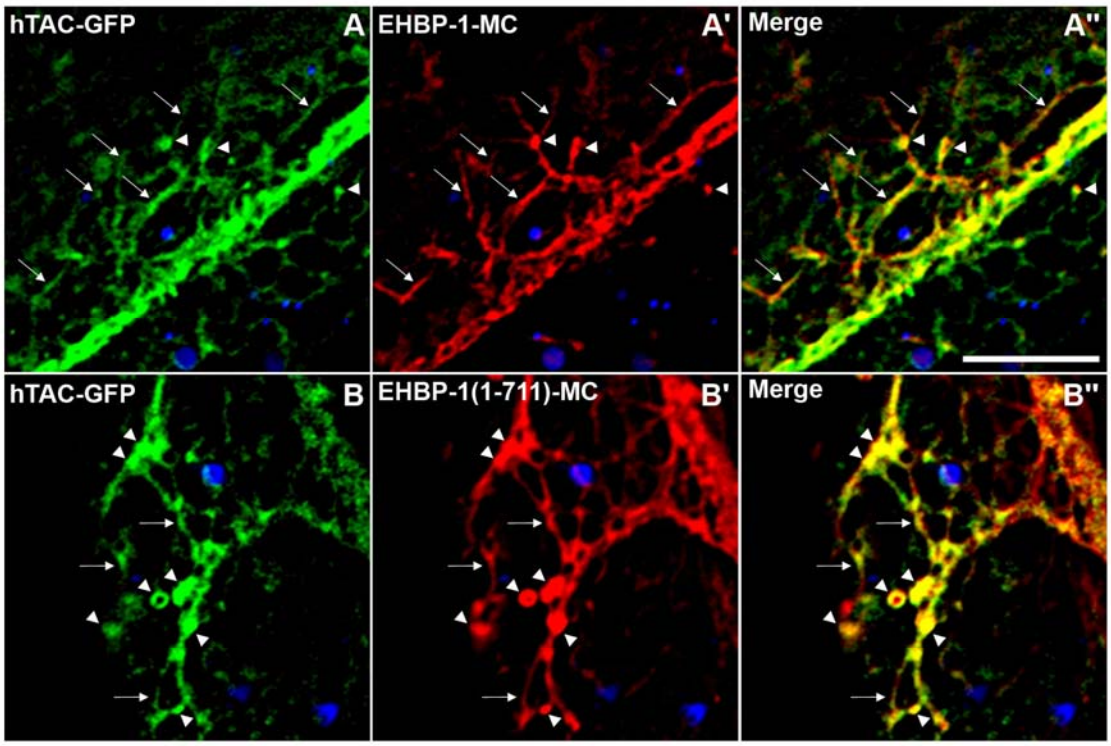
hTAC-GFP
A
EHBP-1-MC
A'
Merge
A''
hTAC-GFP
B
EHBP-1(1-711)-MC
B'
Merge
B''

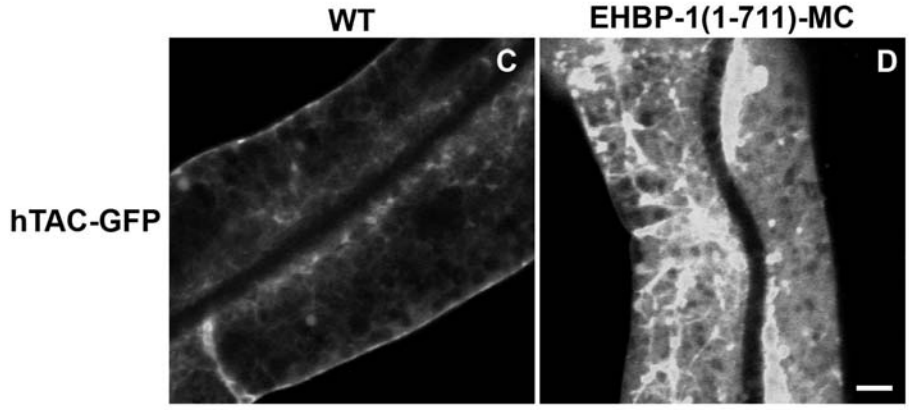
WT
EHBP-1(1-711)-MC
hTAC-GFP
C
D

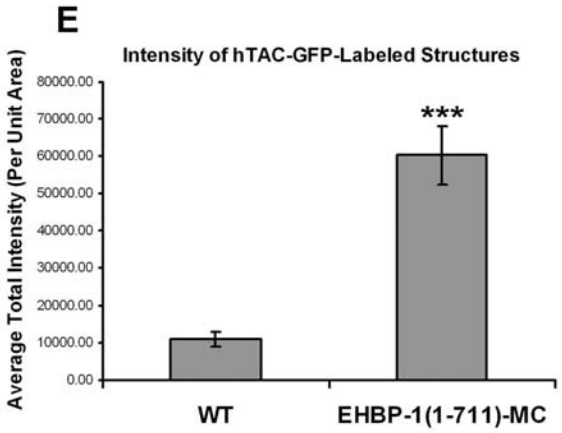
E
Intensity of hTAC-GFP-Labeled Structures
Average Total Intensity (Per Unit Area)
80000.00
70000.00
60000.00
50000.00
40000.00
30000.00
20000.00
10000.00
0.00
***
WT
EHBP-1(1-711)-MC

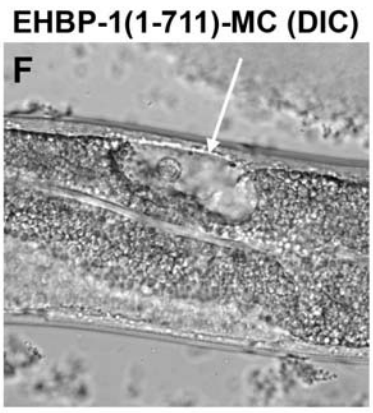
EHBP-1(1-711)-MC (DIC)
F

Figure S2. Over-expression of mutant form of EHBP-1(aa1-711) lacking RAB-10 interacting coiled-coil region induced dominant negative phenotypes.

In wild-type animals, GFP-TAC colocalized with full-length EHBP-1-mCherry on tubules and small puncta (A-A"). Over-expression of EHBP-1(aa1-711) induced accumulation of GFP-hTAC in the intestines, and accumulated GFP-hTAC colocalized with EHBP-1(aa1-711)-mCherry on tubular and those enlarged punctuate structures (B-B"). In each image autofluorescent lysosome-like organelles can be seen in all three channels with the strongest signal in blue, whereas GFP appears only in the green channel and mCherry only in the red channel. Signals observed in the green or red channels that do not overlap with signals in the blue channel are considered bone fide GFP or mCherry signals, respectively.

(C-F) Dominant negative phenotypes induced by expression of EHBP-1(aa1-711). Over-accumulation of intracellular hTAC-GFP in animals with transgenic over-expression of EHBP-1(aa1-711)-mCherry (C-E). (F) Nomarski image of the intestine in animal with transgenic over-expression of EHBP-1(aa1-711)-mCherry. Arrow indicates the enlarged intestinal vacuole. Error bars are SEM (n=18 each, 6 animals of each genotype sampled in three different regions of each intestine). Asterisks indicate a significant difference in the one-tailed Student's t-test ($p<0.001$). Scale bar represents 10 μm.

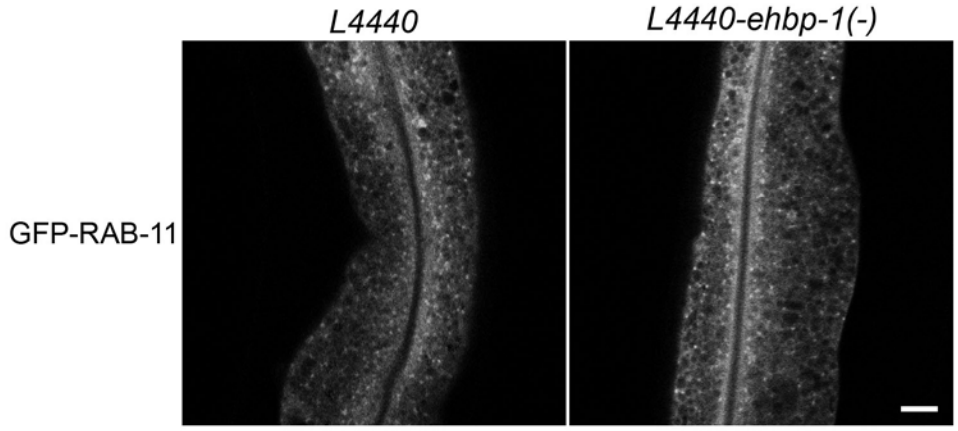

Figure S3. *ehbp-1* RNAi knockdown does not affect RAB-11-positive endosomal subcellular distribution.

Confocal images in a wild-type and *ehbp-1(RNAi)* animals are shown for GFP-RAB-11 in the intestines. Scale bar represents 10 μm.

CHAPTER 5: ARF-6 GTPase-ACTIVATING PROTEIN CNT-1 INTERACTS WITH RAB-10 AND REGULATES ENDOCYTIC RECYCLING OF CLATHRIN-INDEPENDENT CARGO

AUTHOR CONTRIBUTIONS

I participated in the experimental design, performed all the *C. elegans* related experiments, yeast two-hybrid experiments (Figures 1-7 and Supplemental figures 1-4) and wrote the paper. Dr. Carlos Chen performed the yeast two-hybrid screening for RAB-10 binding proteins, RABs binding specificity assay (Figure 1). Riju Banerjee performed the yeast two hybrid assays (Figure 1). Dr. Barth D. Grant designed the experiments, trained me for all experiments and wrote the paper.

SUMMARY

The endocytic pathway of eukaryotes is essential for the internalization and trafficking of macromolecules, fluid, membranes, and membrane proteins. In a yeast 2-hybrid screen using a predicted constitutively active mutant of RAB-10 as bait, we identified a novel binding partner called CNT-1. CNT-1 is the *C. elegans* homolog of mammalian ACAP1 and ACAP2, Arf6 GTPase-activating proteins. Previous studies indicated that ACAP1 is associated with endosomal clathrin and functions in the endocytic recycling pathway. Mammalian Arf6 has been implicated in the regulation of clathrin mediated uptake of apical cargo in polarized epithelia (MDCK) and has been shown to regulate the recycling of clathrin independent cargo in non-polarized (HeLa) cells. Both aspects of Arf6 function have been primarily investigated using dominant mutants of Arf6. Arf6(GTP) activates PIP5KI (phophatidylinositol 4-phosphate 5 kinase type I), which generates PIP2 (phosphatidylinositol 4,5-biphosphate). Arf6(GTP) also activates phospholipase D (PLD), an enzyme that hydrolyses phosphatidylcholine to produce phosphatidic acid (PA) and diacylglycerol (DAG). PIP5KI activity and PIP2 turnover are thought to be important for trafficking through the recycling pathway. Although Arf6 is known to function in membrane trafficking, its precise role in the process and its functional connection with other recycling regulators remains poorly defined. Here we find that CNT-1 binds to RAB-10 through its C-terminal ANK repeats, and colocalizes with RAB-10 on endosomes *in vivo*. Furthermore, the interaction with RAB-10 is required for the recruitment of CNT-1 to endosomal membranes. We also showed that *cnt-1* and *rab-10* mutants overaccumulate endosomal PIP2, consistent with a function for these proteins in negative regulation of ARF-6. Moreover, like RAB-10 and ARF-6, we find that loss of

CNT-1 causes intracellular accumulation of recycling cargo marker hTAC-GFP in the *C. elegans* intestine. For the first time, our data provide evidence of a key interaction between small GTPases RAB-10 and ARF-6 through CNT-1, and show genetic evidence that ARF-6 and its GAP CNT-1 function with RAB-10 in basolateral endocytic recycling pathway.

INTRODUCTION

Endocytic trafficking of eukaryotes is essential for the internalization and trafficking of macromolecules, fluid, membranes, and membrane proteins. There are two basic pathways for endocytic internalization. Some receptors and their associated ligands cluster into clathrin-coated pits. The other type of endocytosis is clathrin-independent (Nichols, 2003; Gesbert *et al.*, 2004).

Recycling pathways are essential for maintaining the proper composition of various organelles and for returning essential molecules to the appropriate membrane. Endocytic recycling is also essential for maintaining the distinction between apical and basolateral membranes in polarized cells. Some proteins that specifically regulate recycling from the endocytic recycling compartment (ERC) have been characterized, such as Rab11 and the Eps15-homology-domain protein Ehd1/RME-1 (Grant *et al.*, 2001; Lin *et al.*, 2001). Rab proteins belong to Ras superfamily of small GTPase with more than 60 members, and many of them play regulatory roles in membrane transport steps. Rab4, Rab5 and Rab11 have been reported to regulate recycling (Sonnichsen *et al.*, 2000). Rab4 and Rab5 are localized to sorting endosomes and Rab4 is also associated with the ERC. Rab11, which is localized to the ERC and trans-Golgi-network (TGN) membranes, has a role in recycling to the plasma membrane (Ullrich *et al.*, 1996; Chen *et al.*, 1998). RAB-10 was demonstrated to be crucial for basolateral endocytic recycling in the *C. elegans* intestine (Chen *et al.*, 2006). RAB-10 is physically associated with endosomes along the recycling pathway. Studies of RAB-10 in our lab suggest its function upstream of RME-1 in the basolateral transport of specific recycling cargos. Similar results were found by our collaborators in MDCK cells.

In a screen to identify interacting partners of RAB-10, we recovered full length CNT-1. CNT-1 is the *C. elegans* homolog of mammalian ACAP1/2 (Arf GAP, with Coil, ANK repeat, PH domain), Arf6 GTPase-activating proteins. Arf6 (ADP-ribosylation factor 6) belongs to Arf family of small GTPase. There are six mammalian Arfs and many more Arf-like proteins. Arf1 and Arf6 are the most well studied members of this family. Arf6 is involved in membrane trafficking and actin cytoskeleton regulation at the plasma membrane and endosomes (Donaldson, 2005; Donaldson and Honda, 2005). Interestingly, Arf6 has been shown to be closely associated with membrane lipid modifications and modulation of the actin cytoskeleton (D'Souza-Schorey and Chavrier, 2006). In tissue culture cells, Arf6 localizes with and activates PIP5KI (Honda *et al.*, 1999). PIP5KI is responsible for generating phosphatidylinositol 4,5-bisphosphate (PIP2), a major PM phosphoinositide involved in membrane traffic and actin rearrangements (Honda *et al.*, 1999; Yin and Janmey, 2003). These results provide us with an important clue to understanding Arf6 function. Arf6 also activates phospholipase D (PLD), an enzyme that hydrolyzes phosphatidylcholine to produce phosphatidic acid (PA). PA can also activate PIP5KI. Thus by activating PIP5KI directly and indirectly, Arf6 stimulates production of PIP2.

Published data suggest that Arf6 is activated and inactivated at many locations and Arf6(GTP) can recruit cytosolic coat proteins *in vitro*. *In vivo* Arf6 has been proposed to facilitate sorting and vesicle formation, and to modulate membrane associated actin assembly (Donaldson, 2005). A requirement for Arf6 in endosomal recycling was first documented in CHO cells, in which the expression of a dominant negative Arf6(T27N) mutant blocked the recycling of certain cargos (D'Souza-Schorey *et al.*, 1998). In HeLa

cells, a GTP hydrolysis defective mutant of Arf6, Q67L, induces PIP2 accumulation and actin coated endosome accumulation, sequestering clathrin independent cargos but not affecting clathrin dependent cargo (Brown *et al.*, 2001). Specifically, Arf6 activity only affects the recycling of integral plasma-membrane proteins that lack cytoplasmic AP2 and clathrin sorting sequences, including the IL2 receptor α-subunit (TAC), MHCI, and glycosylphosphatidylinositol (GPI) anchored proteins (Radhakrishna and Donaldson, 1997; Naslavsky *et al.*, 2003). Additionally, recycling through this tubular system also involves the Ehd1/RME-1 protein (Caplan *et al.*, 2002) and PLD (Jovanovic *et al.*, 2006). MHCI and Arf6 are found to be present on Ehd1/RME-1 positive tubular compartments (Caplan *et al.*, 2002)

Arf6 activation and inactivation are catalyzed by guanine nucleotide exchange factors (GEFs) that facilitate GTP binding and GTPase-activating proteins (GAPs) that catalyze GTP hydrolysis. There are two major types of Arf GAPs, ArfGAP1 and AZAP. ACAP1/2 (Centaurin beta 1/2) belong to AZAP-type, characterized by a PH, Arf GAP and C-terminal ANK repeat (Inoue and Randazzo, 2007). Biochemical studies suggest that ACAP1/2 have preference for Arf6 over Arf1 and could be activated by PI(4,5)P2 (Jackson *et al.*, 2000). Previous studies on ACAP1 in mammalian cells showed that ACAP1 is part of a clathrin complex and functions in the TfR and integrin recycling (Dai *et al.*, 2004; Li *et al.*, 2005; Li *et al.*, 2007). In addition, it has been reported that PI5-kinase, which is positively regulated by Arf6, could function together with ACAP1 to enhance endosomal tubulation (Shinozaki-Narikawa *et al.*, 2006). These observations suggest that ACAP1 could function as an adaptor in the recycling process.

Although ACAPs are identified as Arf6 GAP and thought to function in endosomal recycling of some cargo proteins in mammals, their precise roles and functional connections with other recycling regulators remain poorly defined. Here we report that *C. elegans* ACAP1/2 homolog CNT-1 binds to RAB-10 through its C-terminal ANK repeats, and appears to function as a RAB-10 effector. For the first time, our data provide evidence of a functional connection between small GTPase RAB-10 and ARF-6 via CNT-1, and show genetic evidences that ARF-6 and its GAP CNT-1 function downstream of RAB-10 in basolateral recycling pathway.

.

RESULTS

RAB-10 binds to the C-terminal ANK repeats of CNT-1

To identify proteins that could function with RAB-10 in the regulation if endocytic recycling, we employed a yeast two-hybrid screen using a constitutively active GTP-bound mutant form of RAB-10, RAB-10(Q68L), as bait. Two positive clones were identified encoding full length CNT-1 (see material and methods). CNT-1 is the *C. elegans* homolog of mammalian ACAP1 and ACAP2. ACAP1 has been previously reported to function in the recycling of the TfR and integrin from endosomes to the cell surface (Dai *et al.*, 2004; Li *et al.*, 2005). CNT-1 contains an N-terminal BAR domain, known to be associated with membrane remodeling and curvature sensing, a PtdIns(4,5)P2 binding PH (Pleckstrin Homology) domain, an ARF GAP domain, and a C-terminal ankyrin (ANK) repeats domain. In subsequent experiments we delimited the RAB-10 binding site within CNT-1. We found that the N-terminal Bar domain is not required for the interaction, however, deletion of the C-terminal ANK repeats and a short sequence thereafter (Δaa656-826) abolished the binding activity (Figure 1B-C). Further analysis indicated that this ANK repeats containing region (aa656-826) is sufficient to mediate the interaction with RAB-10 (Figure 1B-C).

To determine the specificity of the CNT-1 interaction, we assayed other Rabs with known functions in endocytic transport, including RAB-5(Q78L), RAB-7(Q68L), RAB-8(Q67L), RAB-11(Q70L), or RAB-35(Q69L). RAB-8(Q67L) and RAB-35(Q69L) were also found to interact with CNT-1 (Figure 1A). RAB-8 is the closest paralog of RAB-10 in *C. elegans* representing the branch of the metazoan Rabs closest to Sec4p (Salminen

and Novick, 1987). Our previous work showed that RAB-35 is an important regulator of the recycling of the RME-2 yolk receptor in *C. elegans* (Sato *et al.*, 2008b). No interaction of CNT-1 with RAB-5(Q78L), RAB-7(Q68L), and RAB-11(Q70L) was observed (Figure 1A). Taken together, these binding results suggest that the C-terminal ANK repeats of CNT-1 provides a binding surface that has the potential to interacting with RAB-10, RAB-8 and RAB-35.

CNT-1 colocalizes with RAB-10

Yeast two-hybrid studies suggest that CNT-1 functions with RAB-10, and possibly other Rabs, in endocytic recycling. A series of *in vivo* colocalization studies in the *C. elegans* intestinal cells were performed to compare functional mCherry-tagged CNT-1 with GFP-tagged endosomal markers described previously (Chen *et al.*, 2006; Shi *et al.*, 2007). Consistent with the binding data, we observed extensive colocalization of CNT-1-MC with GFP-RAB-10 and GFP-RAB-8 positive endosomal punctae in the intestinal cells (Figure 2A-A", Supplemental Figure 1A-A"). Rab10 was reported to label the common recycling endosome in polarized MDCK cells (Babbey *et al.*, 2006). In *C. elegans* we previously found that RAB-10 partially colocalizes with basolateral early and basolateral recycling endosomes in polarized epithelial cells of the intestine, and that RAB-10 is required for transport between these two compartments (Chen *et al.*, 2006). RAB-8 shows a similar localization (Shi *et al*, submitted. See Chapter 4). CNT-1 primarily associates with punctate structures-presumed endosomes. On puncta near the basolateral plasma membrane, CNT-1-MC showed partial colocalization with early endosome marker GFP-RAB-5 and partial colocalization with basolateral recycling endosome marker GFP-RME-1, similar to that previously shown for RAB-10 (Figure 2B-B", D-D").

Our previous studies also indicate that ALX-1 labels two independent classes of endosomes: RME-1 positive basolateral recycling endosomes and HGRS-1 labeled MVEs (Shi *et al.*, 2007). We find that CNT-1-MC also partially colocalizes with GFP-ALX-1 labeled endosomes near the basolateral plasma membrane (Figure 2E-E"). Taken together these results suggest that CNT-1 localizes to intermediate structures along the basolateral recycling pathway. We also noticed that TGN marker GFP-MANS labeled Golgi ministacks were often found partially overlapping or closely juxtaposed to CNT-1-MC-labeled endosomes (Figure 2F-F"), similar to the localization we previously described for RAB-10 (Chen *et al.*, 2006). This localization is similar to that we previously showed for RME-8 and SNX-1 (see Chapter 3), and may indicate that such endosomes exchange cargo with the Golgi, in anterograde and/or retrograde fashion. Collectively, our results indicate that CNT-1 is enriched on endosomes where it could potentially interact with both RAB-10 and RAB-8 to regulate endosome-to-plasma membrane transport of cargo derived from the PM and/or the Golgi.

CNT-1 functions with ARF-6

Given the known function of the CNT-1 homolog ACAP1 with Arf6 in mammalian cells, we also assayed for colocalization of ARF-6 and CNT-1 (Figure 2C-C"). Mammalian Arf6 labels recycling endosomal structures and remains membrane-associated even after GTP hydrolysis (Cavenagh *et al.*, 1996; Song *et al.*, 1998). We found that a functional ARF-6-GFP fusion protein labels punctate and tubular membrane structures in the intestinal cells, and overlaps with CNT-1-MC on punctate elements near the basolateral plasma membrane (Figure 2C-C"). ARF-6/Arf6 has been suggested to function in the recycling pathway. This was confirmed by assaying the localization of ARF-6-GFP in

rab-10 and *rme-1* mutants that accumulates grossly enlarged endosomes associated with accumulated recycling cargo (Chen *et al.*, 2006). We found clear localization of ARF-6-GFP to the limiting membrane of the grossly enlarged endosomes of both mutants (Figure 3F-G), providing further evidence that ARF-6 is associated with the recycling endosomes regulated by both RAB-10 and RME-1.

Loss of CNT-1 affects cargo localization

To test the specificity and the potential functional-regulation of CNT-1 in cargo recycling, we assayed the effect of depletion-of-CNT-1 on well defined recycling cargo proteins hTAC-GFP and hTfR-GFP (Chen *et al.*, 2006; Shi *et al.*, 2007). Loss of RAB-10 preferentially traps clathrin independent cargo protein hTAC-GFP in the endosomal system, but has very little effect on clathrin dependent cargo protein hTfR-GFP (Chen *et al.*, 2006). Mammalian Arf6 is known to be a key regulator of clathrin independent endocytosis (CIE) cargo recycling including MHCI and TAC (Radhakrishna and Donaldson, 1997; Naslavsky *et al.*, 2003). Consistent with this, we find dramatic intracellular accumulation (~50-fold) of hTAC-GFP in the intestinal cells of *arf-6(tm1447)* deletion mutants (Figure 2I and M). Similarly we found that *cnt-1(tm2313)* mutants also accumulate hTAC-GFP intracellularly, but to a lesser extent than *arf-6* mutants (Figure 2H and M). We found that clathrin dependent endocytosis (CDE) type cargo protein hTfR-GFP localization was not affected by *arf-6* or *cnt-1* mutants (Figure 2J-L and M).

According to studies in mammalian cells, a full GTPase cycle by Arf6 is required for efficient recycling of CIE cargo (D'Souza-Schorey and Chavrier, 2006). MHCI and TAC recycling is impaired upon expression of GDP-locked Arf6(T23N) or GTP hydrolysis

defect mutant Arf6(Q67L), although there are differences in the morphology of the compartments accumulating CIE cargo under the two conditions (Naslavsky *et al.*, 2003). As a presumed ARF-6 GAP, loss of CNT-1 would be expected to result in reduced cycling of ARF-6(GTP) to ARF-6(GDP), and the accumulation of hTAC-GFP in *cnt-1(tm2313)* mutants might result from the over-accumulation of ARF-6(GTP). Our results thus provide *in vivo* evidence of the importance of the ARF-6 GTPase cycle in the regulation of CIE cargo recycling. The connection of CNT-1 to RAB-10 suggests that RAB-10 may also play an important role in regulating this cycle.

RAB-10 is required for CNT-1 endosomal recruitment

In many cases proteins that interact with GTP-bound Rabs are effector proteins, and such effectors are often localized and/or activated by interaction with the Rab protein (Stenmark, 2009). To determine if RAB-10 and CNT-1 display such a relationship we assayed for changes in the localization of CNT-1-GFP in a *rab-10* mutant background. Consistent with CNT-1 acting as a RAB-10 effector, we found that CNT-1-GFP lost its endosomal localization in *rab-10(q373)* mutants. CNT-1-GFP appeared very diffuse in *rab-10* mutants and most CNT-1-GFP puncta were lost (Figure 3C). This finding suggests that RAB-10 recruits CNT-1 to endosomal membranes. Conversely we found that the number and intensity of CNT-1-GFP-labeled endosomes was not affected in *rme-1(b1045)* mutants that are defective in a later step in the basolateral recycling pathway (Figure 3B).

Mammalian Rab8 has been suggested to function in the secretory pathway in mammalian cells (Hattula *et al.*, 2002; Ang *et al.*, 2003), and this delivery process may use the recycling endosomes as an intermediate (Ang *et al.*, 2004). Studies in polarized MDCK

cells also implied that Rab8 and Rab10 may function redundantly in exocytic membrane trafficking, perhaps by sharing some effectors (Schuck *et al.*, 2007). This redundancy in function of Rab8 and Rab10 is supported by their interactions with EHBP-1 and apparent redundant function in the secretory pathway of the worm germ cells (Shi *et al*, submitted. See Chapter 4). We find that RAB-8 can bind to CNT-1 *in vitro*, CNT-1-MC and GFP-RAB-8 colocalize on endosomes, and that GFP-RAB-8 labeled endosomes overaccumulate in *cnt-1* mutants (Figure 1 and Supplemental Figure 1A-C). Collectively, these observations suggest that CNT-1 may function as a shared effector of RAB-8 and RAB-10, but the critical test of this hypothesis remains to be performed. We will need to determine of CNT-1-GFP endosome association is reduced upon loss of RAB-8, or if there is an increased loss of CNT-1 endosome association upon loss of both RAB-8 and RAB-10 compared to the *rab-10* single mutant. However, the strong effect of loss of *rab-10* on CNT-1-GFP endosomal recruitment suggests that, at least in the intestine, RAB-10 is the dominant Rab GTPase recruiting CNT-1 to endosomes.

Loss of CNT-1 or RAB-10 leads to increased accumulation of PI(4,5)P2

Mammalian Arf6 is well-known to regulate membrane lipid modifications by directly and indirectly activate PIP5KI, therefore increasing the level of recycling endosome and plasma membrane PIP2 (Honda *et al.*, 1999; Yin and Janmey, 2003; D'Souza-Schorey and Chavrier, 2006). To assay the subcellular distribution pattern of PIP2 *in vivo* in the *C. elegans* intestinal cells, we expressed a widely used PIP2 biosensor PH(PLCδ)-GFP, which contains the PIP2-specific binding activity of the pleckstrin homology (PH) domain of rat phospholipase C δ (reference for PH PLCd). As control, we also assayed

PI(3)P and PI(3,4,5)P3 subcellular localization using widely used *in vivo* biosensors for these phosphoinositide lipids, GFP-2xFYVE and PH(Akt)-GFP respectively.

In wild-type animals we noted that PH(PLCδ)-GFP labeled the apical and basolateral plasma membrane as well as internal puncta and tubules consistent with endosomal enrichment (Figure 4A and 5A-A'). The PH(PLCδ)-GFP-labeled intracellular puncta and tubules colocalize extensively with ARF-6-MC, identifying them as endosomes along the recycling pathway (Supplemental Figure S3). Further colocalization analysis will be required to more precisely identify the endosome type, although the pattern is highly reminiscent of the RME-1-positive basolateral recycling endosomes. The PI3P marker GFP-2XFYVE localizes diffusely in the intestinal cells (Figure 4D), although in other tissues such as the coelomocyte this marker labels early endosomes (Dang *et al.*, 2004). The PIP3 marker PH(AKT)-GFP labeled the apical and basolateral plasma membrane, although not as strongly as the PIP2 marker, and did not appear enriched on endosomes (Figure 4G).

Given the known role of Arf6(GTP) in activating PIP2 production in other organisms, and the observation above that RAB-10 is required to recruit the predicted ARF-6 GAP CNT-1 to endosomes, we might expect that loss of RAB-10 or CNT-1 lead to increased cellular ARF-6(GTP) and higher levels of PIP2. Consistent with this model, we found that in *cnt-1* mutants and *rab-10* mutants PH(PLCδ)-GFP labeling on the basolateral plasma membrane and intracellular tubular elements was dramatically increased (Figure 4B and 5C-C'). The increased labeling by PH(PLCδ)-GFP suggests that PIP2 lipid levels become abnormally high in the absence of CNT-1 or RAB-10, probably due a corresponding increase in ARF-6(GTP) levels under these conditions.

There was no similar increase in PH(PLCδ)-GFP labeling in *rme-1* mutants that affect a later step in the recycling pathway, although some of the endosomes labeled by PH(PLCδ)-GFP were grossly enlarged in *rme-1* mutants, consistent with the presence of PIP2 on basolateral recycling endosomes (Figure 5B-B'). The levels of PI(3)P (labeled by GFP-2xFYVE) and PI(3,4,5)P3 (labeled by PH(AKT)-GFP) appeared unperturbed in *cnt-1* and *rab-10* mutants, indicating the specificity of the altered phosphoinositide distribution (Figure 4E and H). Although ARF-6 colocalizes well with PH(PLCδ)-GFP (Supplemental Figure S3), *arf-6* deletion mutants did not appear altered in the steady-state distribution of PIP2, or PI(3)P and PI(3,4,5)P3 (Figure 4, C, F and I). The lack of visible effect on PIP2 level in *arf-6* mutants was somewhat unexpected, and suggests that ARF-6(GTP) is not normally the primary regulator of cellular PIP2 production, but rather probably regulates PIP2 production transiently and in restricted locations, such as during endosomal maturation or budding processes. An important experiment that remains to be done is to determine if the abnormally increased levels of PIP2, identified in the *cnt-1* and *rab-10* mutants, is ARF-6 dependent. This can be tested by depleting *cnt-1* and *rab-10* mutant animals of ARF-6, by mutation or RNAi, and determining if PIP2 levels revert to normal levels.

Endosome morphology defects in CNT-1 and ARF-6 mutants

To help establish the extent of endosomal dysfunction upon loss of CNT-1, we assayed the steady state subcellular distribution of a set of endosomal markers in *cnt-1* mutant intestines. Compared with wild type animals, GFP-RAB-10 labeling intensity on endosome increased in *cnt-1* mutants (Figure 6B). Interestingly a similar increase in GFP-RAB-10 labeling was also observed in *arf-6* mutants (Figure 6C). Taken together,

these results are consistent with both CNT-1 and ARF-6 functioning at the same step in endosomal transport, perhaps the budding of recycling vesicles leaving the endosome.

CNT-1 and ARF-6 differed, however, in their effects on recycling endosome markers. GFP-RME-1 labeled tubular and punctate endosomal labeling increased in the medial cytoplasm of *cnt-1* mutants, while GFP-RME-1 labeling was greatly decreased in *arf-6* mutants with most GFP-RME-1 becoming diffuse in the cytoplasm (Figure 6D-F). A similar result was observed with another recycling endosome regulator SDPN-1/Syndapin. GFP-SDPN-1 increased its endosome association in *cnt-1* mutants, but greatly decreased it endosome association in *arf-6* mutants (Figure 6G-I). This is a particularly interesting result, because both RME-1 and SDPN-1/Syndapin are PIP2 binding proteins (Kessels and Qualmann, 2004; Pant *et al.*, 2009). Thus their altered localizations may reflect changes in PIP2 levels in these mutant backgrounds.

To clarify the extent of endosomal defects in *cnt-1* mutants, we also assayed the steady state subcellular localization of the late endosomal markers GFP-RAB-7 and LMP-1-GFP, and the MVE/MVB marker HGRS-1 (Figure 6J-R). No overt abnormalities were observed in *cnt-1* mutants, suggesting that CNT-1 is not critical for endocytic transport to the lysosome. Taken together these results indicate that CNT-1 specifically regulates the morphology and function of recycling endosomes *in vivo*.

Next, we sought to better define the step in transport associated with ARF-6. We found that loss of ARF-6 resulted in increased numbers of CNT-1-GFP labeled endosomes (Figure 3D). GFP-RAB-10 labeled structures also accumulate in *arf-6* mutants (Figure 6C). Double labeling experiments indicate that CNT-1 and RAB-10 co-accumulate on endosomes under these conditions (Supplemental Figure 2A-A"). Taken together these

observations further suggest that CNT-1 and RAB-10 function together with ARF-6 in the recycling process.

Clathrin accumulates on CNT-1 positive endosomes in *arf-6* mutants

ACAP1 in mammalian cells has been reported to be part of a clathrin complex that somehow functions on endosomes to promote the recycling of the insulin responsive glucose transporter Glut4, and the adhesion molecule β-integrin (Li *et al.*, 2007). That work indicated that endosomal clathrin overaccumulates when ACAP1 is overexpressed, but this study never established if this effect on endosomal clathrin requires Arf6 (Li *et al.*, 2007). In our studies, we noticed that CNT-1-GFP accumulates in *arf-6* mutants (Figure 3D). We further found that a functional GFP-tagged clathrin heavy chain (GFP-CHC-1) showed a similar strong intracellular accumulation in *arf-6* mutants (Figure 7B).

Importantly we noted that CNT-1-MC colocalizes with GFP-CHC-1 in wild type animals (Figure 7C-C"), and that CNT-1-MC and GFP-CHC-1 co-accumulate of on the enlarged puncta in *arf-6* deletion mutant animals (Figure 7D-D"). Although we do not yet understand the role of this pool of endosomal clathrin, our results suggest that such a pool of clathrin could interact with CNT-1 and ARF-6 during endocytic recycling.

DISCUSSION

In this study, we investigated functional role of the mammalian ACAP homolog CNT-1 in basolateral recycling pathway in the *C. elegans* intestinal epithelium, and provided evidence that CNT-1 interacts with RAB-10 and ARF-6 in a process that is essential for recycling regulation.

We defined the RAB-10 binding motif within CNT-1, the ANK repeats, and provided genetic evidence that RAB-10 is required for the membrane recruitment of CNT-1. These results are similar to recent studies by Kanno et al. (Kanno *et al.*, 2010). In their study, a biochemical screen for Rab-binding proteins yields putative Arf6-GAP centaurin β2/ACAP2 as a Rab35-binding protein. ACAP2 is closest paralog of ACAP1 and both ACAP1 and ACAP2 are GAPs for Arf6 (Jackson *et al.*, 2000). Further, the Kano et al. studies also pointed out that the ACAP2 ANK repeats is involved in the interaction with Rab35 and ACAP2 plasma membrane localization (Kanno *et al.*, 2010). Indeed, our binding studies also demonstrated that CNT-1 can interact with RAB-35 in *C. elegans*, although we do not yet know the functional significance of this interaction (Figure 1A). Together, these observations provide compelling evidence that Arf6 GAP proteins can be recruited to the membrane through interaction with Rabs. Acting as Rab effectors, ACAPs provide a functional connection between different GTPase classes that are vital for endocytic regulation.

Like recycling regulators we previously reported, loss of CNT-1 causes significant accumulation of clathrin independent cargo hTAC (Figure 2H). Additionally, recycling endosome markers, such as RME-1 and SDPN-1, are found accumulated on the medial

endosomes of *cnt-1* mutants (Figure 3E and H). In out studies, we noticed that GFP-tagged CNT-1 mainly resides on punctate endosomes with little labeling of the typical tubular elements of recycling endosomes. This is very different from the tubular and punctate subcellular localization pattern of ARF-6. It is possible that CNT-1 functions in two functionally separate steps in recycling regulation. One is the presumed ARF-6 inactivation function in a late step of recycling pathway. Studies in mammals suggest that a complete ARF-6 GTPase cycle (activation of ARF-6 via GDP-to-GTP exchange, and ARF-6 inactivation through GTP-to-GDP hydrolysis) is probably necessary for functional transport, since expression of GDP or GTP locked forms of Arf6 impairs cargo recycling (D'Souza-Schorey *et al.*, 1998; Brown *et al.*, 2001). Unlike most Rab proteins, Arf6 is thought to be constitutively membrane associated, whether bound to GDP or GTP. This precise management of activation and deactivation is necessary for function rather than membrane recruitment of the Arf6. Loss of CNT-1 potentially blocks the hydrolysis of GTP on ARF-6, therefore, increased the level of active ARF-6-GTP, which could be harmful for the process of recycling endosome transport. In addition to increased recycling structures mislocalized to the medial cytosol, over-accumulation of PIP2 marker PH(PLCδ)-GFP in the *cnt-1* mutants also indicates abnormally high level of ARF-6-GTP (Figure 4B).

As a RAB-10 effector CNT-1 may also contribute additional functions to the recycling process. CNT-1 harbors an N-terminal BAR domain. Proteins with BAR domains such as amphiphysin, endophilins, and sorting nexins have been reported to sense membrane curvatures and are involved in membrane remodeling (Casal *et al.*, 2006). Recruited onto membrane by RAB-10, CNT-1 could function through its BAR domain to help remodel

membrane to form functional subdomains or buds on endosomes, into which specific types of recycling cargo could be sequestered for next step of delivery. Our data suggest that the exit of hTAC from early endosomes, *en route* to the recycling endosome, was substantially affected by the loss of CNT-1.

Study in mammals demonstrated a role for ACAP1 in Glut4 and integrin recycling (Dai *et al.*, 2004; Li *et al.*, 2005). Furthermore, ACAP1 was reported to be part of a clathrin coat complex on endosomes (Li *et al.*, 2007). Although clathrin coats have been suggested to participate in the recycling process (van Dam and Stoorvogel, 2002), it the role of clathrin coats in endocytic recycling remains controversial. In our studies, GFP-CHC-1 colocalizes with CNT-1-MC on endosomes (Figure 7C-C''), and they co-accumulate on the enlarged endosomes of *arf-6* mutants (Figure 7D-D''), which provides indirect evidence of clathrin and CNT-1/ACAPs interaction. However the traditional role of an Arf protein is in recruiting clathrin adaptors, and thus loss of the Arf would be expected to reduce the formation of clathrin buds (Krauss *et al.*, 2003). As discussed in Chapter 3, a flat Clathrin lattice on endosomes has been suggested to create and/or maintain degredative subdomains on endosomes associated with HRS and ESCRT proteins, regulating the sorting of cargo proteins in the endosome (Raiborg *et al.*, 2001a; Raiborg *et al.*, 2006; Shi *et al.*, 2009). Thus it will also be worthwhile to test for any functional involvement of CNT-1 in the retrograde transport and degradation pathway which is very sensitive to changes in such clathrin-coated subdomains.

MATERIALS AND METHODS

General Methods and Strains

All *C. elegans* strains were derived originally from the wild-type Bristol strain N2. Worm cultures, genetic crosses, and other *C. elegans* husbandry were performed according to standard protocols (Brenner, 1974). Strains expressing transgenes were grown at 20°C. A complete list of strains used in this study can be found in Supplementary Table 1.

Yeast Two-hybrid Analyses

Yeast two-hybrid screen for candidates of RAB-10 interacting proteins was performed according to the procedure of the DupLEX-A yeast two-hybrid system (OriGene Technologies, Rockville MD). The cDNA sequences of *C. elegans* rab-10(Q68L) in the entry vector pDONR221 were cloned into the pEG202-Gtwy bait vector by Gateway recombination cloning (Invitrogen, Carlsbad, CA) to generate N-terminal fusions with the LexA DNA binding domain. The pEG202-rab-5(Q78L), rab-7(Q68L), rab-8(Q67L), rab-11(Q70L) and rab-35(Q69L) were constructed accordingly. The preprylation motifs for membrane attachment at the C-terminal ends of RAB were also deleted to improve entry of bait fusion proteins into the yeast nucleus. The *C. elegans* cDNA library was purchased from the DupLEX-A yeast two-hybrid system (OriGene Technologies, Rockville MD).

The LexA-based DupLEX-A yeast two-hybrid system (OriGene Technologies Inc., Rockville, MD) was used for all subsequent truncation analysis. All two-hybrid plasmids were generated as PCR products with Gateway attB.1 and attB.2 sequence extensions, and were introduced into the Gateway entry vector pDONR221 by BP reaction. The bait

vector pEG202-Gtwy and target vector pJG4-5-Gtwy have been described previously (Sato *et al.*, 2008b). Origene plasmid pSH18-34 [*URA3*, 8 ops.-LacZ] was used as reporter in all the yeast two-hybrid experiments. Constructs were introduced into the yeast strain EGY48 [MATα trp1 his3 ura3 leu2::6 LexAop-*LEU2*] included in the system. Transformants were selected on plates lacking leucine, histidine, tryptophan and uracil, containing 2% galactose/1% raffinose at 30^{o}C for 3 days and assayed for the expression of the *LEU2* reporter. Blue/white β-galactosidase assays confirmed results shown for growth assays, according to manufacturer's instructions.

Plasmids and Transgenic Strains

To construct GFP or RFP/mCherry (a gift from R. Tsien, Stanford University School of Medicine) fusion transgenes for expression specifically in the worm intestine, a previously described *vha-6* promoter driven vector modified with a Gateway cassette inserted at the Asp718I site just upstream of the GFP or RFP coding region was used. The sequences of *C. elegans cnt-1(cDNA)* (a gift from H. A. Baylis, University of Cambridge) and *C. elegans arf-6(genomic DNA)* lacking stop codon were cloned into entry vector pDONR221 by PCR and BP reaction, and then transferred into intestinal expression vectors by Gateway recombination cloning LR reaction to generate C-terminal fusions (Chen *et al.*, 2006). Complete plasmid sequences are available on request. Low copy integrated transgenic lines for all of these plasmids were obtained by the microparticle bombardment method (Praitis *et al.*, 2001).

Microscopy and Image Analysis

Live worms were mounted on 2% agarose pads with 10 mM levamisol as described previously (Sato *et al.*, 2005). Multi-wavelength fluorescence images were obtained

using an Axiovert 200M (Carl Zeiss MicroImaging, Oberkochen, Germany) microscope equipped with a digital CCD camera (C4742–12ER, Hamamatsu Photonics, Hamamatsu, Japan), captured using Metamorph software ver 6.3r2 (Universal Imaging, West Chester, PA), and then deconvolved using AutoDeblur Gold software ver 9.3 (AutoQuant Imaging, Watervliet, NY). Images taken in the DAPI channel were used to identify broad-spectrum intestinal autofluorescence caused by lipofuscin-positive lysosome-like organelles (Clokey and Jacobson, 1986; Hermann *et al.*, 2005). To obtain images of GFP fluorescence without interference from autofluorescence, we used argon 488nm excitation and the spectral fingerprinting function of the Zeiss LSM510 Meta confocal microscope system (Carl Zeiss MicroImaging) as described previously (Chen *et al.*, 2006). Quantification of images was performed with Metamorph software ver 6.3r2 (Universal Imaging). Most GFP/RFP colocalization experiments were performed on L3 and L4 larvae expressing GFP and RFP-markers as previously described.

ACKNOWLEDGEMENTS

We thank Howard A Baylis and Shohei Mitani for important reagents. We thank Peter Schweinsberg and Zui Pan for their generous advice and technical assistance. R.B. was supported by Aresty Research Center grant. This work was supported by NIH Grant GM067237 to B.D.G.

Table 1. Transgenic and Mutant Strains Used in This Study

Transgenic and Mutant Strains Used in This Study
*pwIs724[*p*vha6::CNT-1::GFP]*
*pwIs728[*p*vha6::CNT-1::mCherry]*
*pwIs601[*p*vha6::ARF-6::GFP]*
*pwIs206[*p*vha6::GFP::RAB-10](Chen et al., 2006)*
*pwIs72[*p*vha6::GFP::RAB-5](Chen et al., 2006)*
*pwIs87[*p*vha6::GFP::RME-1](Chen et al., 2006)*
*pwIs524[*p*vha6::GFP::ALX-1](Shi et al., 2007)*
*pwIs481[*p*vha6::MANS::GFP](Chen et al., 2006)*
*pwIs112[*p*vha6::hTAC::GFP](Chen et al., 2006)*
*pwIs90[*p*vha6::hTfR::GFP](Chen et al., 2006)*
*pwIs722[*p*vha6::SDPN-1::GFP](Pant et al., 2009)*
*pwIs170[*p*vha6::GFP::RAB-7](Chen et al., 2006)*
*pwIs50[*p*lmp-1::LMP-1::GFP](Treusch et al., 2004)*
*pwIs518[*p*vha6::GFP::HGRS-1](Shi et al., 2007)*
*pwIs446[*p*vha6::PH::GFP]*
*pwIs140[*p*vha6::GFP::2xFYVE]*
*pwIs890[*p*vha6::Akt-PH::GFP]*
*dkIs8 [*p*vha6::GFP::CHC-1](Sato, 2008)*
*pwIs68[*p*vha6::GFP::RAB-8]*
*pwIs625[*p*vha6::ARF-6::mCherry]*
rme-1(b1045)(Grant et al., 2001)
rab-10(q373)(Chen et al., 2006)
alx-1 (gk275)(Shi et al., 2007)
cnt-1(tm2313) (Dr. Shohei Mitani, Japanese National Bioresource Project for the Experimental Animal "Nematode *C. elegans*"*)*
arf-6(tm1447) (Dr. Shohei Mitani, Japanese National Bioresource Project for the Experimental Animal "Nematode *C. elegans*"*)*

A

	CNT-1
RAB-10(Q68L)	+
RAB-8(Q67L)	+
RAB-5(Q78L)	-
RAB-7(Q68L)	-
RAB-11(Q70L)	-
RAB-35(Q69L)	+

B

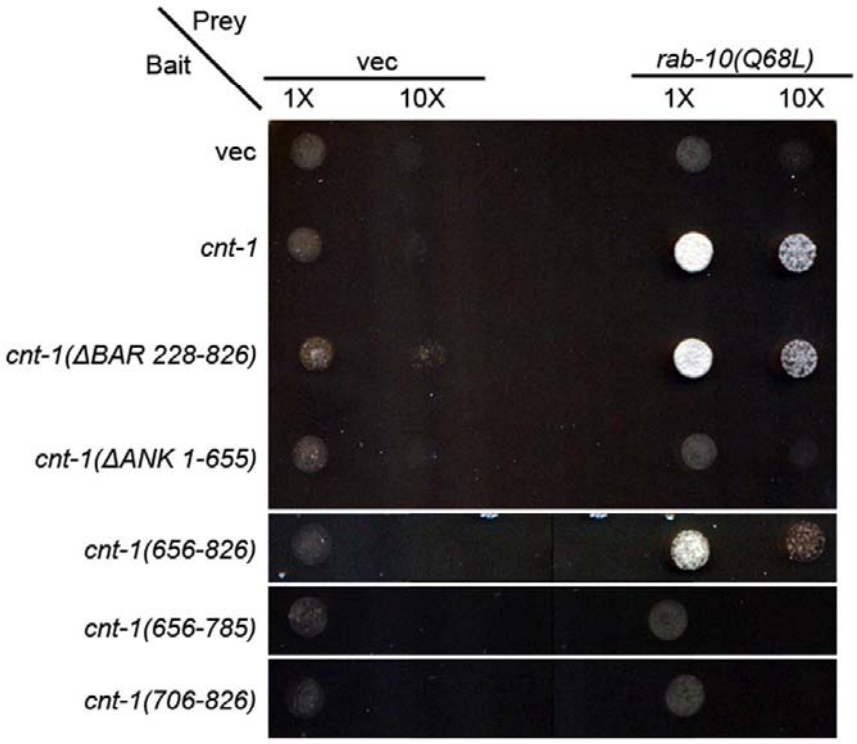

C

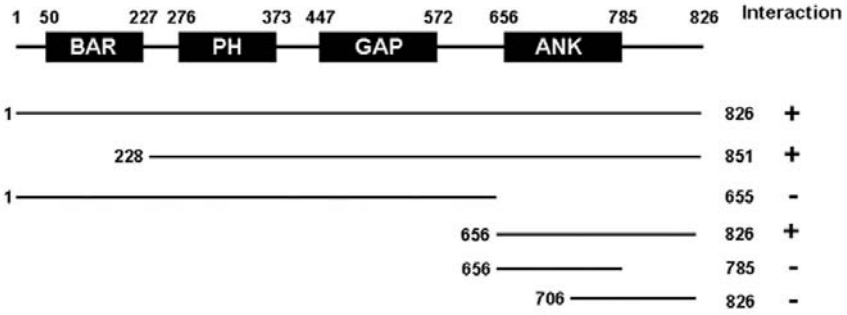

Figure 1. EHBP-1 physically interacts with RAB-10(Q68L) and RAB-8(Q67L).

(A) Binding specificity of CNT-1 with RAB-8, RAB-10 and RAB-35. Using full-length CNT-1 as bait, Rabs with reported endosomal trafficking involvement were used as prey in the yeast two-hybrid assays, including active RAB-5(Q78L), RAB-7(Q68L), RAB-8(Q67L), RAB-10(Q68L), RAB-11(Q70L), RAB-35(Q69L).

(B) The interaction between CNT-1 and RAB-10(Q68L) requires C-terminal CNT-1 ANK repeat domain. RAB-10(Q68L) was expressed in a yeast reporter strain as a fusion with the DNA-binding domain of LexA (bait). CNT-1 truncated forms were expressed in the same yeast cells as fusions with the B42 transcriptional activation domain (prey). Interaction between bait and prey was assayed by complementation of leucine auxotrophy (LEU2 growth assay). Colonies were diluted in liquid and spotted on solid growth medium directly or after further 10X dilution.

(C) Schematic representations of CNT-1 domains and the truncated fragments used in the Y2H analysis. Protein domains are displayed as dark boxes above protein sequence used in the study (shown as dark lines). Amino acid numbers are indicated.

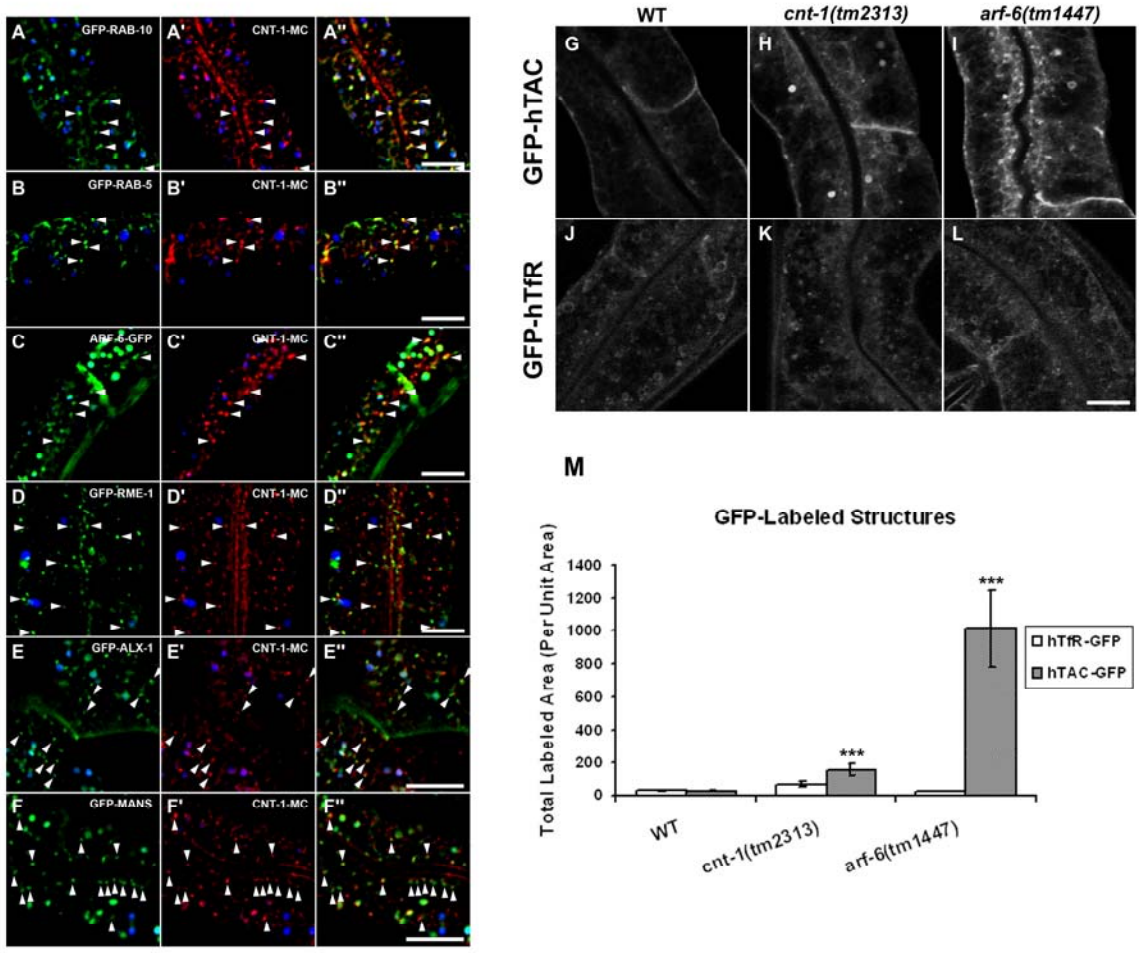

Figure 2. CNT-1 colocalizes with RAB-10 on endosomes and regulates hTAC recycling.

(A-F") Colocalization images are from deconvolved 3-D image stacks acquired in intact living animals expressing GFP and mCherry tagged proteins specifically in intestinal epithelial cells. (A-A") CNT-1-MC colocalizes with GFP-RAB-10. Arrowheads indicate endosomes labeled by both CNT-1-MC and GFP-RAB-10. (B-B") CNT-1-MC partially colocalizes with GFP-RAB-5 on endosomal structures. Arrowheads indicate endosomes labeled by both CNT-1-MC and GFP-RAB-5. (C-C") CNT-1-MC colocalizes with ARF-6-GFP on basolateral endosomal structures. Arrowheads indicate endosomes labeled by

both CNT-1-MC and ARF-6-GFP. (D-D") CNT-1-MC partially colocalizes with recycling endosome marker GFP-RME-1. Arrowheads indicate endosomes labeled by both CNT-1-MC and GFP-RME-1. (E-E") CNT-1-MC partially colocalizes with GFP-ALX-1. Arrowheads indicate CNT-1-MC positive endosomes partially overlapped with GFP-ALX-1 labeled structures. (F-F") CNT-1-MC does not colocalize with Golgi marker GFP-Mannosidase. In each image autofluorescent lysosome-like organelles can be seen in all three channels with the strongest signal in blue, whereas GFP appears only in the green channel and mCherry only in the red channel. Signals observed in the green or red channels that do not overlap with signals in the blue channel are considered bone fide GFP or RFP signals, respectively. Scale bar represents 10 μm.

(G-M) Loss of CNT-1 induces endocytic recycling defects of hTAC in the *C. elegans* intestine. Confocal images of the worm intestine expressing GFP-tagged cargo proteins that recycle via the recycling endosome, the human transferrin receptor (hTfR-GFP) and the IL-2 receptor alpha chain (hTAC-GFP) in wild type, *cnt*-1(tm2313) and *arf-6(tm1447)* mutant animals. Compared with wild type animals (G), hTAC-GFP significantly accumulates on the intestinal cytosolic endosomal structures (~6-fold increase) in *cnt*-1(tm2313) and increases in *arf-6(tm1447)* (~50-fold increase), respectively (H-I and M). hTfR-GFP was not affected in *cnt*-1(tm2313) and *arf-6(tm1447)* mutants (J-L and M). Error bars are SEM (n=18 each, 6 animals of each genotype sampled in three different regions of each intestine defined by a 100 x 100 ($pixl^2$) box positioned at random). Asterisks indicate a significant difference in the one-tailed Student's t-test ($p<0.001$). Scale bar represents 10 μm.

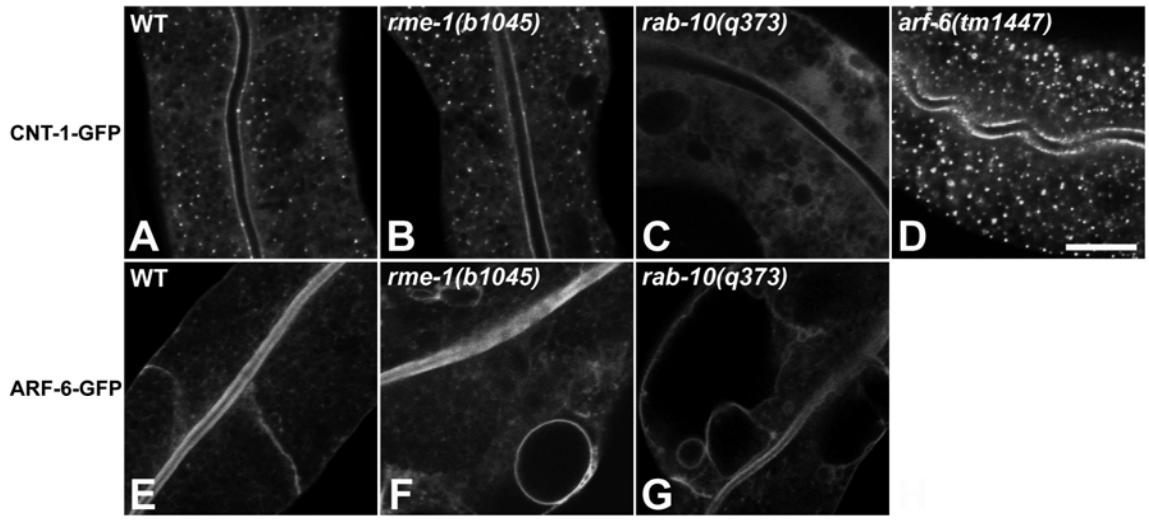

Figure 3. CNT-1 lost its endosomal association in *rab-10(q373)* mutants and ARF-6 associates with vacuoles in recycling mutants.

(A-D) Representative confocal images are shown for CNT-1-GFP in wild-type animals, *rme-1(b1045)*, *rab-10(q373)* and *arf-6(tm1447)* mutants. Loss of function RAB-10 disrupts CNT-1 endosomal association (C and I). Instead, depletion of ARF-6 induces greatly accumulated CNT-1-GFP positive puncta, approximate 10-fold average total intensity increase (D and I).

(E-G) Representative confocal images are shown for ARF-6-GFP in wild-type animals, *rme-1(b1045)* and *rab-10(q373)* mutants. ARF-6 labels limiting membrane of vacuoles in *rme-1(b1045)* and *rab-10(q373)* mutants.

Scale bar represents 10 μm.

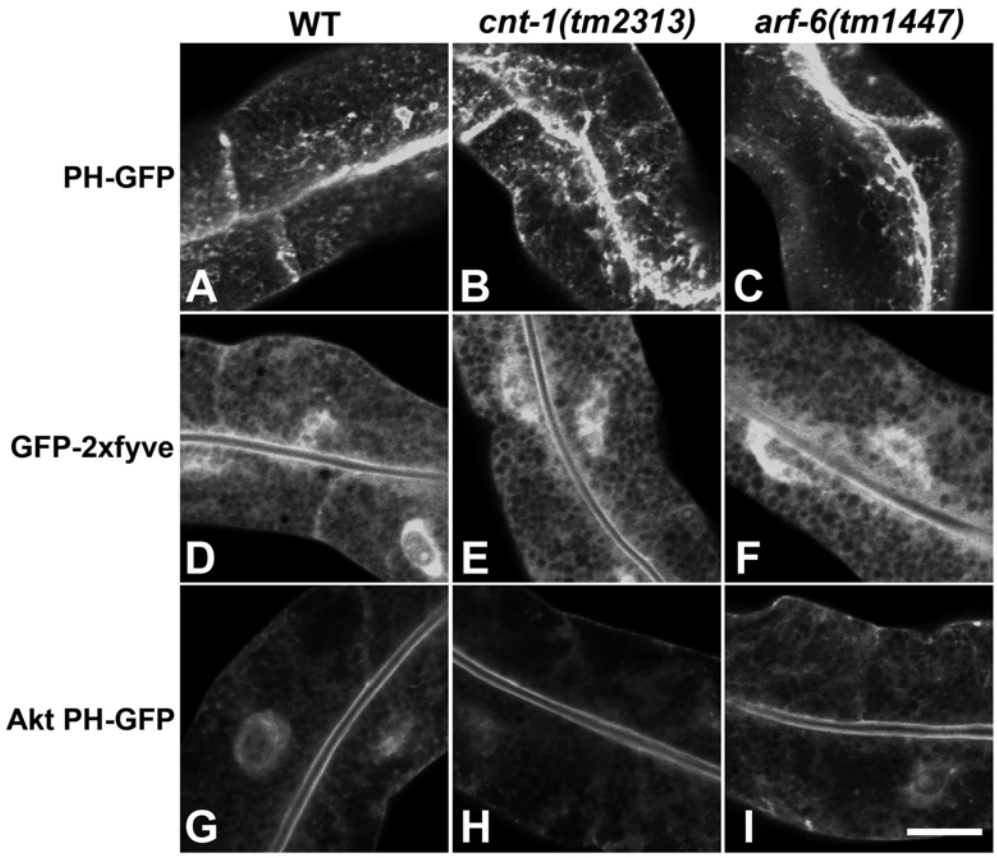

Figure 4. Up-regulation of subcellular PH-GFP (PI(4,5)P2) in *cnt-1(tm2313)* mutants.

(A-C) Representative confocal images are shown for PH-GFP in wild-type animals, *cnt-1(tm2313)* and *arf-6(tm1447)* mutants. Depletion of RAB-10 induces PH-GFP labeled structures accumulation on the basolateral membrane (B and J). No significant changes observed in animals depleted of ARF-6 (C and J).

(D-F) Confocal images are shown for GFP-2xFYVE (PI(3)P) in wild-type animals, *cnt-1(tm2313)* and *arf-6(tm1447)* mutants.

(G-I) Confocal images are shown for Akt-PH-GFP (PI(3,4,5)P3) in wild-type animals, *cnt-1(tm2313)* and *arf-6(tm1447)* mutants. Scale bar represents 10 μm.

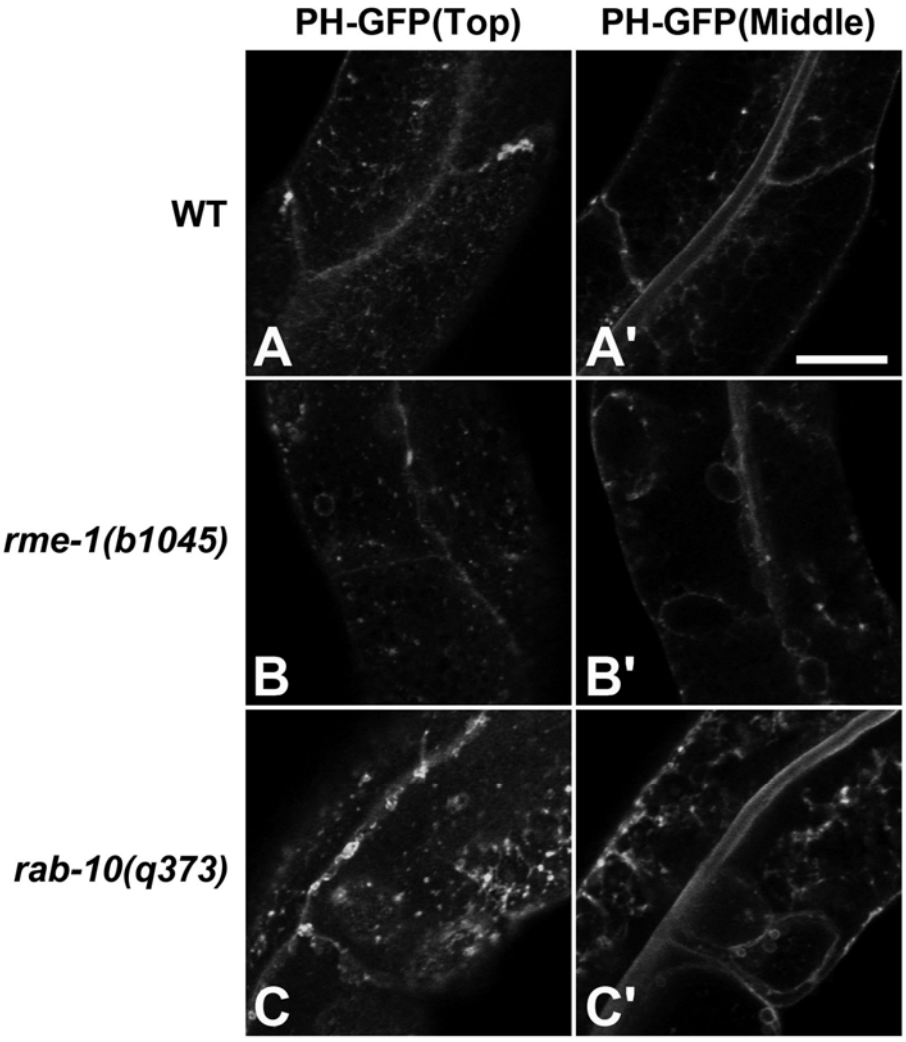

Figure 5. PH-GFP labels recycling endosomes and accumulates on enlarged endosomes in recycling defective mutants.

(A-C') Representative confocal images are shown for PH-GFP in wild-type animals, *rme-1(b1045)* and *rab-10(q373)* mutants. Depletion of RME-1 or RAB-10 induces PH-GFP labeled Phosphatidylinositol 4,5-bisphosphate (PIP2) accumulates on limiting membranes of vacuoles and enlarged endosomes at basolateral focal plane (Top) and medial focal plane (Middle) (B' and C'). Scale bar represents 10 μm.

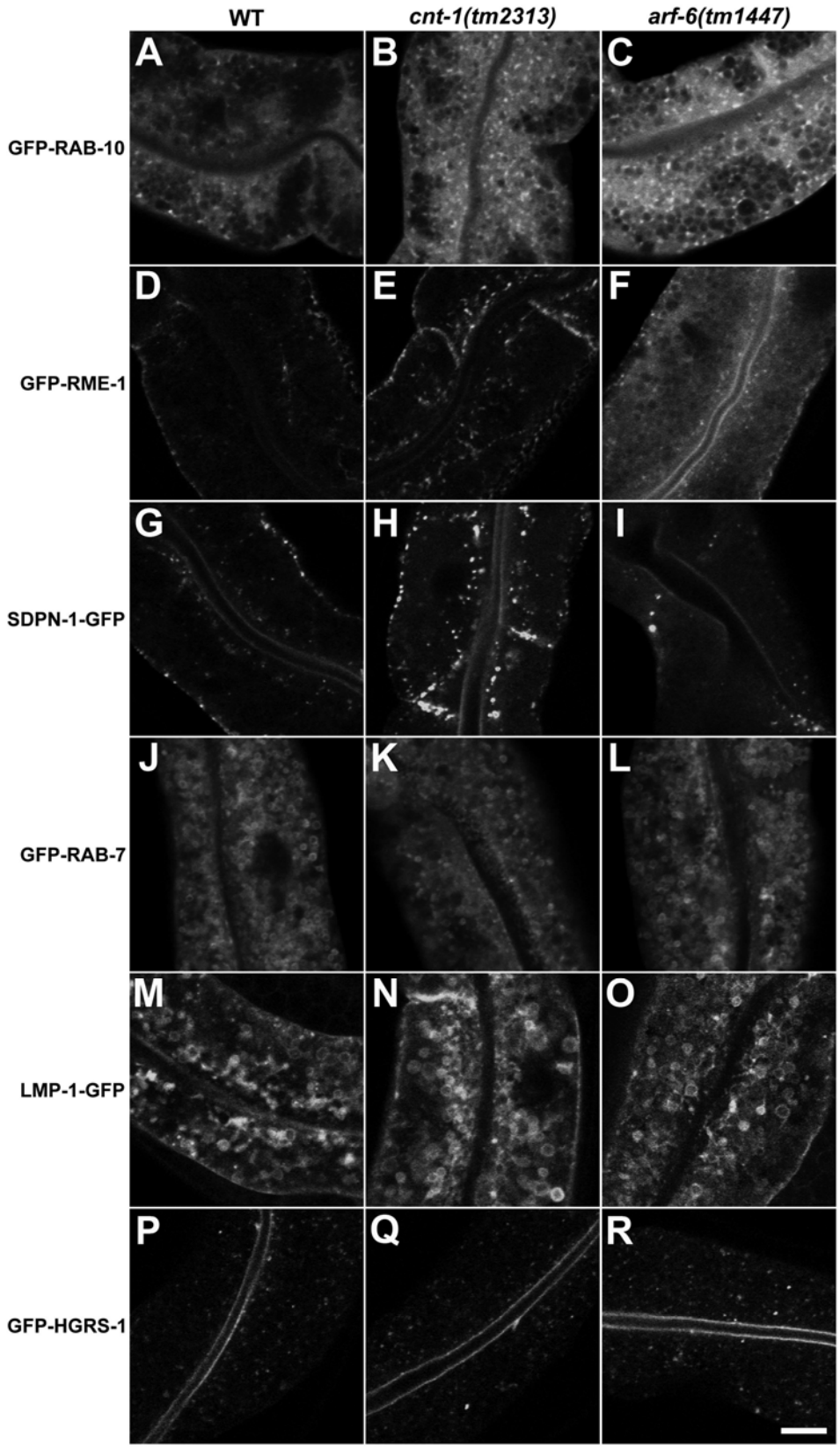
WT
cnt-1(tm2313)
arf-6(tm1447)
A
B
C
GFP-RAB-10
D
E
F
GFP-RME-1
G
H
I
SDPN-1-GFP
J
K
L
GFP-RAB-7
M
N
O
LMP-1-GFP
P
Q
R
GFP-HGRS-1

Figure 6. Loss of CNT-1 induces RAB-10-labeled endosomes accumulation and recycling membrane structures mislocalization.

Representative confocal images are shown in wild-type background for GFP-RAB-10 (A), GFP-RME-1 (D), SDPN-1-GFP (G), GFP-RAB-7 (J), LMP-1-GFP (M), and GFP-HGRS-1 (P). Confocal images in *cnt-1(tm2313*) background are shown for GFP-RAB-10 (B), GFP-RME-1 (E), SDPN-1-GFP (H), GFP-RAB-7 (K), LMP-1-GFP (N), and GFP-HGRS-1 (Q). Confocal images in *arf-6(tm1447*) background are shown for GFP-RAB-10 (C), GFP-RME-1 (F), SDPN-1-GFP (I), GFP-RAB-7 (L), LMP-1-GFP (O), and GFP-HGRS-1 (R). Scale bar represents 10 μm.

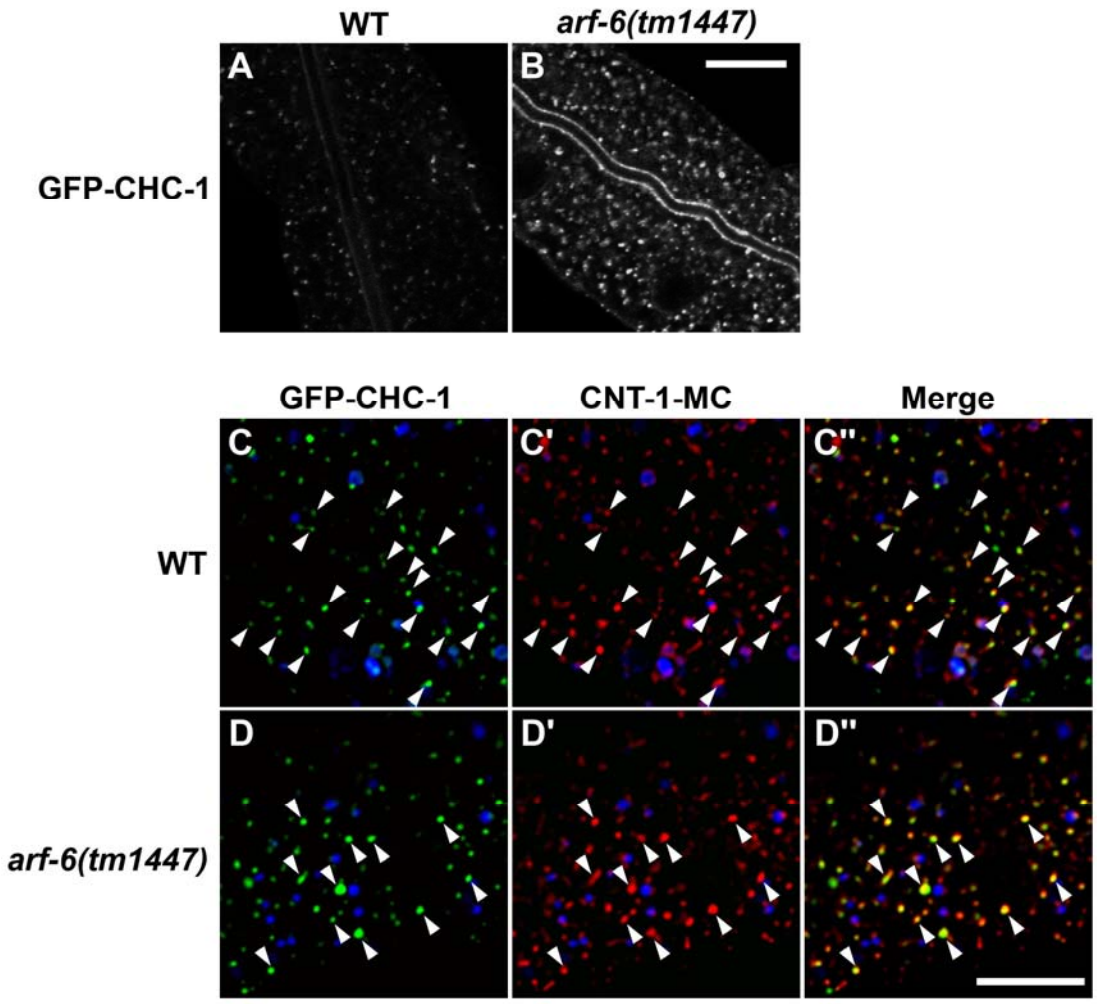

Figure 7. Clathrin accumulates and overlaps with CNT-1 on enlarged endosomes in *arf-6* mutants

(A-B) Representative confocal images are shown for GFP-tagged clathrin heavy chain (GFP-CHC-1) in wild-type animals and *arf-6(tm1447)* mutants. Scale bar represents 10 μm.

(C-D") Colocalization images of CHC-1 and CNT-1 in both WT and *arf-6* mutant background are from deconvolved 3-D image stacks acquired in intact living animals expressing GFP and mCherry tagged proteins specifically in intestinal epithelial cells. (C-

C") CNT-1-MC colocalizes with GFP-CHC-1 in wild type animals. Arrowheads indicate representative endosomes labeled by both CNT-1-MC and GFP-CHC-1. (D-D") CNT-1-MC colocalizes with GFP-CHC-1 on enlarged endosomal structures. Arrowheads indicate endosomes labeled by both CNT-1-MC and GFP-CHC-1 on large puncta. In each image autofluorescent lysosome-like organelles can be seen in all three channels with the strongest signal in blue. Scale bar represents 10 μm.

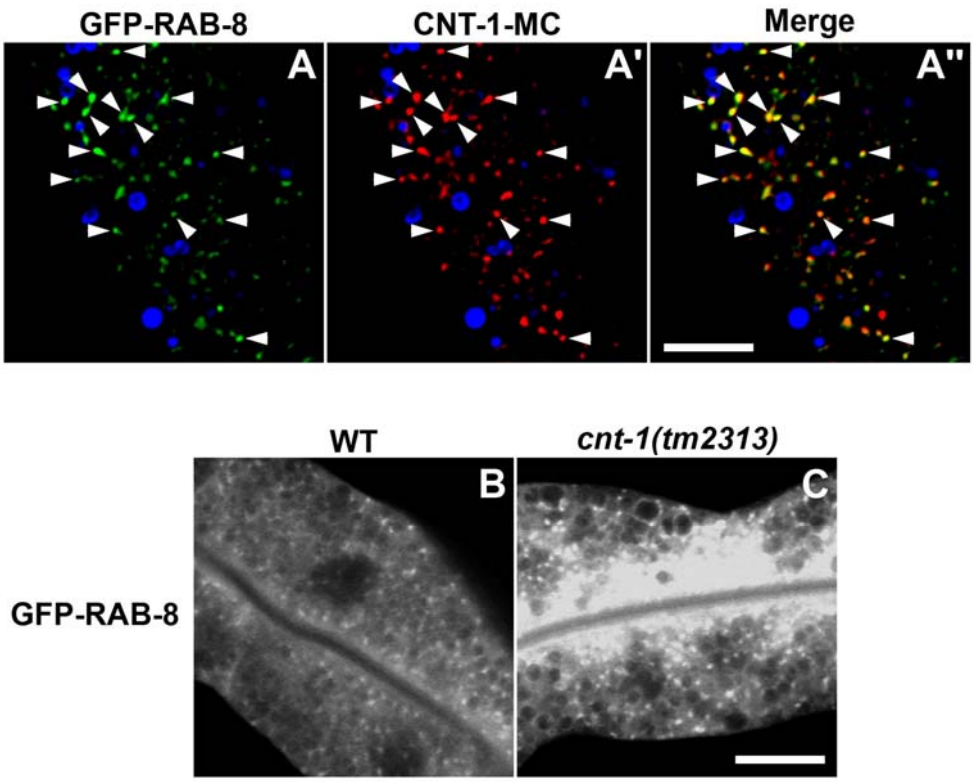

Figure S1. RAB-8 colocalizes with CNT-1 on endosomes and accumulates in *cnt-1* mutants.

(A-A") Colocalization images are from deconvolved 3-D image stacks acquired in intact living animals expressing GFP and mCherry tagged proteins specifically in intestinal epithelial cells. CNT-1-MC colocalizes with GFP-RAB-8. Arrowheads indicate endosomes labeled by both CNT-1-MC and GFP-RAB-8. Scale bar represents 10 μm.

(B-C) Loss of CNT-1 causes subcellular localization defects of GFP-RAB-8 in the *C. elegans* intestine. Representative confocal images are shown for GFP-RAB-8 in wild-type animals and *cnt-1(tm2313)* mutants. Scale bar represents 10 μm.

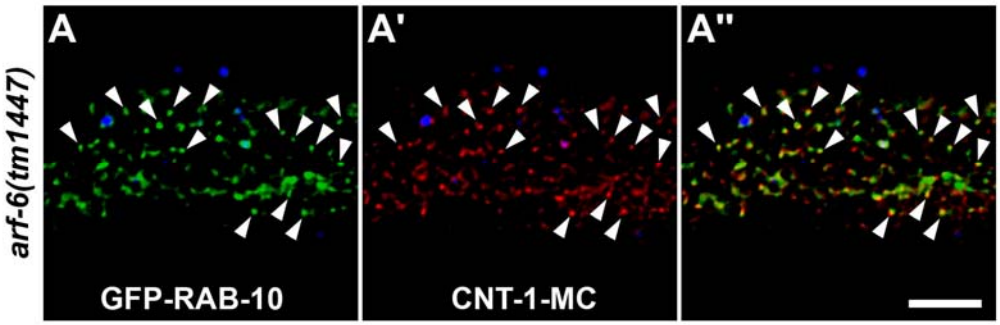

Figure S2. RAB-10 and CNT-1 co-accumulate on endosomes in *arf-6* mutants.

(A-A") Colocalization images are from deconvolved 3-D image stacks acquired in intact living animals expressing GFP and mCherry tagged proteins specifically in intestinal epithelial cells. Arrowheads indicate endosomes labeled by both CNT-1-MC and GFP-RAB-10. Scale bar represents 10 μm.

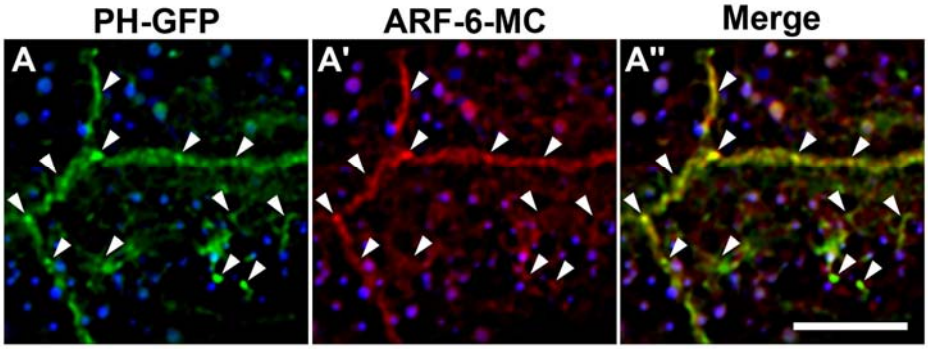

Figure S3. ARF-6 colocalizes with PH-GFP on basolateral tubular and puncta.

(A-A") Colocalization images are from deconvolved 3-D image stacks acquired in intact living animals expressing GFP and mCherry tagged proteins specifically in intestinal epithelial cells. Arrowheads indicate tubular and puncta labeled by both ARF-6-MC and PH-GFP. Scale bar represents 10 μm.

CHAPTER 6: CONCLUSIONS

Grant Lab focuses on identification and functional analysis of regulators in the endocytic traffic. Using *C. elegans* intestines as model, we take genetic, biochemical and cell biological approaches to dissect the function and contribution of these regulators in endocytic processes. Many intestinal molecular markers of subcellular organelles (such as RAB-5, -7, -8, -10, -11, LMP-1, HGRS-1, SDPN-1 and RME-1) and transmembrane cargos (such as hTfR, hTAC and MIG-14) have been well defined in our previous studies (Chen *et al.*, 2006; Shi *et al.*, 2007; Shi *et al.*, 2009), which make the *C. elegans* intestine an ideal model for membrane trafficking study.

Cells balance the endocytosed plasma membrane proteins and lipids through endosomal recycling pathways. Previous studies provided basic endocytic recycling pathways blueprint, however, many molecular components mediating these pathways remain to be identified. Furthermore, some previously defined regulators were also found to participate in different processes, these novel functional roles add additional complexity to the current functional models.

After endocytosis, cargo proteins will be sorted and delivered into different destinations such as lysosomes, plasma membrane via recycling endosomes or Golgi apparatus via retrograde pathway. Studies in our lab established that recycling regulator RME-1 and RAB-10 function at two sequential steps in recycling transport (Grant *et al.*, 2001; Chen *et al.*, 2006; Pant *et al.*, 2009). RME-1 was first identified in the genetic screen for endocytic mutants in *C. elegans* (Grant *et al.*, 2001). Structural study on RME-1 related protein EHD2 suggests that RME-1-family proteins might function similarly to dynamin, assembling around membranes and promoting fission (Daumke *et al.*, 2007). Recent studies in our lab provide the evidence of interaction between RME-1 and

Amphiphysin/AMPH-1 in regulating membrane tubulation and possibly fission at the recycling endosome (Pant *et al.*, 2009). AMPH-1 was known to regulate Dynamin mediated scission of the clathrin coated pit. AMPH-1 novel function in the recycling provides further insight into the functional mechanism of RME-1.

Our screen for RME-1 interacting proteins also identified *C. elegans* ALX-1 (ALIX or PDCD6IP in mammals and Bro1 in yeast) as a novel RME-1-binding partner. In Chapter 2, we showed that ALX-1 is associated with a subset of RME-1-positive endosomes and required for recycling of clathrin-independent cargo hTAC specifically. Alix/Bro1 is known to be associated with the ESCRT complex during MVB biogenesis in mammals and yeast. ALX-1 mutants with RME-1-binding defect still function in MVB and late endosomal processes in our studies, which clearly indicate the dual functions of ALX-1 in two difference trafficking processes. Our assays in culture cells confirmed the results in worm, showing that overexpression of truncated human ALIX in HeLa cells strongly inhibited the recycling of MHC class I molecules. Similar to ALX-1, another important MVB regulator Hrs has also been suggested to have dual functions, being implicated in the recycling process and associated with tubular endosomes *in vivo* (Yan *et al.*, 2005; Welsch *et al.*, 2006). Our studies on ALX-1 and AMPH-1 provided additional examples of novel function of previously defined regulatory components.

To better understand RAB-10 regulated basolateral endocytic recycling, similar screen strategy was used to identify RAB-10 effectors, and EHBP-1 and CNT-1 were recovered. In Chapter 4, our functional studies of EHBP-1 demonstrate an important relationship between EHBP-1 with RAB-10 during endocytic recycling. EHBP-1 specifically binds to active GTP-bound RAB-10, and animals lacking EHBP-1 fail to recycle hTAC properly.

EHBP-1 turns to be an unconventional Rab effector, regulating RAB-10 endosomal localization. EHBP-1 mammalian homolog Ehbp1 was shown to be binding partner of EHD1 and EHD2 (Guilherme *et al.*, 2004a; Guilherme *et al.*, 2004b). Although the direct association of EHBP-1 with RME-1/EHDs does not appear to be evolutionarily conserved, our data provide evidence that EHBP-1 functions upstream of RME-1 in basolateral recycling and affect RME-1 localization to tubular recycling endosome. In Chapter 5, another RAB-10 interacting protein, CNT-1, was analyzed. In term of binding specificity, CNT-1 is not just specific for RAB-8 and RAB-10, but also binds to RAB-35, which was previously shown to function in the rapid recycling pathway (Sato *et al.*, 2008b). CNT-1 is the *C. elegans* homolog of mammalian ACAP1/2, Arf6 GTPase-activating proteins. ACAP1 is known to associate with endosomal clathrin and functions in the endocytic recycling pathway. In our studies, we showed that CNT-1 binds to RAB-10 through its C-terminal ANK repeats, and colocalizes with RAB-10 on endosomes *in vivo*. Loss of CNT-1 causes accumulation of RAB-10 positive endosomes and RME-1 labeled recycling structures, furthermore, depletion of CNT-1 causes significant hTAC accumulation in the *C. elegans* intestine. For the first time, we provide evidence of cross-talk between small GTPases RAB-10 and ARF-6 through CNT-1, and show genetic evidence that ARF-6 and its GAP CNT-1 function downstream of RAB-10 in basolateral endocytic recycling. Collectively, our studies of RAB-10 interacting proteins in Chapter 4 and 5 extend the understanding of RAB-10 functions and present a broader picture of RAB-10 and its effectors regulated recycling transport. Future analysis will be needed to identify more regulators in the process and clarify the functional relationship between different components.

In Chapter 3, we focus on RME-8 function in retrograde transport, which is responsible for the Golgi proteins retrieval from endosomes. RME-8 was also identified in the genetic screen for endocytosis mutants in *C. elegans*, labeling endosomes in vivo (Zhang *et al.*, 2001). Using retrograde recycling cargo MIG-14/Wntless, we established the functional model of RME-8 in the transport. SNX-1 regulates endosomal clathrin dynamics through RME-8 and clathrin chaperone HSP-1/Hsc70, therefore, promote the sorting of recycling cargo into the retrograde pathway. In this model, J-domain protein RME-8 associates with the retromer component SNX-1. Without RME-8, clathrin over-accumulate on endosomes and MIG-14 is missorted to the lysosome. Our RME-8 functional study also provides insight into the clathrin subdomain regulation on endosome. Clathrin subdomains have been implicated in the sorting of cargo into the degradative pathway through their association with Hrs. Hrs binds to ubiquitinated cargo and endosomal clathrin. In the absence of Hrs or endosomal clathrin, the normal subdomain organization of the early endosome is disrupted (Raiborg *et al.*, 2001b; Raiborg *et al.*, 2002; Raiborg *et al.*, 2006). Conversely, retromer, through RME-8 and Hsc70, negatively regulate endosomal clathrin dynamics. Oppsite clathrin regulations by retromer and Hrs on endosomes probably function together as a sorting mechanism in cargo fate determination. Significant future works are required to better understand the relationship between RME-8/SNX-1 and Hrs, and explore the balance maintenance mechanism of endosomal clathrin subdomains.

REFERENCES

Al-Awar, O., Radhakrishna, H., Powell, N.N., and Donaldson, J.G. (2000). Separation of membrane trafficking and actin remodeling functions of ARF6 with an effector domain mutant. Molecular and cellular biology *20*, 5998-6007.

Altschuler, Y., Liu, S., Katz, L., Tang, K., Hardy, S., Brodsky, F., Apodaca, G., and Mostov, K. (1999). ADP-ribosylation factor 6 and endocytosis at the apical surface of Madin-Darby canine kidney cells. The Journal of cell biology *147*, 7-12.

Ang, A.L., Folsch, H., Koivisto, U.M., Pypaert, M., and Mellman, I. (2003). The Rab8 GTPase selectively regulates AP-1B-dependent basolateral transport in polarized Madin-Darby canine kidney cells. The Journal of cell biology *163*, 339-350.

Ang, A.L., Taguchi, T., Francis, S., Folsch, H., Murrells, L.J., Pypaert, M., Warren, G., and Mellman, I. (2004). Recycling endosomes can serve as intermediates during transport from the Golgi to the plasma membrane of MDCK cells. The Journal of cell biology *167*, 531-543.

Apodaca, G., Katz, L.A., and Mostov, K.E. (1994). Receptor-mediated transcytosis of IgA in MDCK cells is via apical recycling endosomes. The Journal of cell biology *125*, 67-86.

Arighi, C.N., Hartnell, L.M., Aguilar, R.C., Haft, C.R., and Bonifacino, J.S. (2004). Role of the mammalian retromer in sorting of the cation-independent mannose 6-phosphate receptor. The Journal of cell biology *165*, 123-133.

Audhya, A., Desai, A., and Oegema, K. (2007a). A role for Rab5 in structuring the endoplasmic reticulum. The Journal of cell biology *178*, 43-56.

Audhya, A., McLeod, I.X., Yates, J.R., and Oegema, K. (2007b). MVB-12, a fourth subunit of metazoan ESCRT-I, functions in receptor downregulation. PloS one *2*, e956.

Babbey, C.M., Ahktar, N., Wang, E., Chen, C.C., Grant, B.D., and Dunn, K.W. (2006). Rab10 regulates membrane transport through early endosomes of polarized Madin-Darby canine kidney cells. Molecular biology of the cell *17*, 3156-3175.

Balklava, Z., Pant, S., Fares, H., and Grant, B.D. (2007). Genome-wide analysis identifies a general requirement for polarity proteins in endocytic traffic. Nature cell biology *9*, 1066-1073.

Bateman, A., Birney, E., Cerruti, L., Durbin, R., Etwiller, L., Eddy, S.R., Griffiths-Jones, S., Howe, K.L., Marshall, M., and Sonnhammer, E.L. (2002). The Pfam protein families database. Nucleic acids research *30*, 276-280.

Belenkaya, T.Y., Wu, Y., Tang, X., Zhou, B., Cheng, L., Sharma, Y.V., Yan, D., Selva, E.M., and Lin, X. (2008). The retromer complex influences Wnt secretion by recycling wntless from endosomes to the trans-Golgi network. Developmental cell *14*, 120-131.

Bembenek, J.N., Richie, C.T., Squirrell, J.M., Campbell, J.M., Eliceiri, K.W., Poteryaev, D., Spang, A., Golden, A., and White, J.G. (2007). Cortical granule exocytosis in C. elegans is regulated by cell cycle components including separase. Development (Cambridge, England) *134*, 3837-3848.

Bonifacino, J.S., and Hurley, J.H. (2008). Retromer. Current opinion in cell biology *20*, 427-436.

Borrego-Diaz, E., Kerff, F., Lee, S.H., Ferron, F., Li, Y., and Dominguez, R. (2006). Crystal structure of the actin-binding domain of alpha-actinin 1: evaluating two competing actin-binding models. Journal of structural biology *155*, 230-238.

Bowers, K., Lottridge, J., Helliwell, S.B., Goldthwaite, L.M., Luzio, J.P., and Stevens, T.H. (2004). Protein-protein interactions of ESCRT complexes in the yeast Saccharomyces cerevisiae. Traffic (Copenhagen, Denmark) *5*, 194-210.
Braun, A., Pinyol, R., Dahlhaus, R., Koch, D., Fonarev, P., Grant, B.D., Kessels, M.M., and Qualmann, B. (2005). EHD proteins associate with syndapin I and II and such interactions play a crucial role in endosomal recycling. Molecular biology of the cell *16*, 3642-3658.
Brenner, S. (1973). The genetics of behaviour. British medical bulletin *29*, 269-271.
Brenner, S. (1974). The genetics of Caenorhabditis elegans. Genetics *77*, 71-94.
Brown, F.D., Rozelle, A.L., Yin, H.L., Balla, T., and Donaldson, J.G. (2001). Phosphatidylinositol 4,5-bisphosphate and Arf6-regulated membrane traffic. The Journal of cell biology *154*, 1007-1017.
Burack, M.A., Silverman, M.A., and Banker, G. (2000). The role of selective transport in neuronal protein sorting. Neuron *26*, 465-472.
Burbea, M., Dreier, L., Dittman, J.S., Grunwald, M.E., and Kaplan, J.M. (2002). Ubiquitin and AP180 regulate the abundance of GLR-1 glutamate receptors at postsynaptic elements in C. elegans. Neuron *35*, 107-120.
Cabezas, A., Bache, K.G., Brech, A., and Stenmark, H. (2005). Alix regulates cortical actin and the spatial distribution of endosomes. Journal of cell science *118*, 2625-2635.
Caplan, S., Naslavsky, N., Hartnell, L.M., Lodge, R., Polishchuk, R.S., Donaldson, J.G., and Bonifacino, J.S. (2002). A tubular EHD1-containing compartment involved in the recycling of major histocompatibility complex class I molecules to the plasma membrane. The EMBO journal *21*, 2557-2567.
Carlton, J., Bujny, M., Peter, B.J., Oorschot, V.M., Rutherford, A., Mellor, H., Klumperman, J., McMahon, H.T., and Cullen, P.J. (2004). Sorting nexin-1 mediates tubular endosome-to-TGN transport through coincidence sensing of high- curvature membranes and 3-phosphoinositides. Curr Biol *14*, 1791-1800.
Casal, E., Federici, L., Zhang, W., Fernandez-Recio, J., Priego, E.M., Miguel, R.N., DuHadaway, J.B., Prendergast, G.C., Luisi, B.F., and Laue, E.D. (2006). The crystal structure of the BAR domain from human Bin1/amphiphysin II and its implications for molecular recognition. Biochemistry *45*, 12917-12928.
Cavenagh, M.M., Whitney, J.A., Carroll, K., Zhang, C., Boman, A.L., Rosenwald, A.G., Mellman, I., and Kahn, R.A. (1996). Intracellular distribution of Arf proteins in mammalian cells. Arf6 is uniquely localized to the plasma membrane. The Journal of biological chemistry *271*, 21767-21774.
Chang, H.C., Hull, M., and Mellman, I. (2004). The J-domain protein Rme-8 interacts with Hsc70 to control clathrin-dependent endocytosis in Drosophila. The Journal of cell biology *164*, 1055-1064.
Chang, H.C., Newmyer, S.L., Hull, M.J., Ebersold, M., Schmid, S.L., and Mellman, I. (2002). Hsc70 is required for endocytosis and clathrin function in Drosophila. The Journal of cell biology *159*, 477-487.
Chatellard-Causse, C., Blot, B., Cristina, N., Torch, S., Missotten, M., and Sadoul, R. (2002). Alix (ALG-2-interacting protein X), a protein involved in apoptosis, binds to endophilins and induces cytoplasmic vacuolization. The Journal of biological chemistry *277*, 29108-29115.

Cheeseman, I.M., Niessen, S., Anderson, S., Hyndman, F., Yates, J.R., 3rd, Oegema, K., and Desai, A. (2004). A conserved protein network controls assembly of the outer kinetochore and its ability to sustain tension. Genes & development *18*, 2255-2268.
Chen, C.C., Schweinsberg, P.J., Vashist, S., Mareiniss, D.P., Lambie, E.J., and Grant, B.D. (2006). RAB-10 is required for endocytic recycling in the Caenorhabditis elegans intestine. Molecular biology of the cell *17*, 1286-1297.
Chen, W., Feng, Y., Chen, D., and Wandinger-Ness, A. (1998). Rab11 is required for trans-golgi network-to-plasma membrane transport and a preferential target for GDP dissociation inhibitor. Molecular biology of the cell *9*, 3241-3257.
Choi, J.Y., Stukey, J., Hwang, S.Y., and Martin, C.E. (1996). Regulatory elements that control transcription activation and unsaturated fatty acid-mediated repression of the Saccharomyces cerevisiae OLE1 gene. The Journal of biological chemistry *271*, 3581-3589.
Chun, D.K., McEwen, J.M., Burbea, M., and Kaplan, J.M. (2008). UNC-108/Rab2 regulates postendocytic trafficking in Caenorhabditis elegans. Mol Biol Cell *19*, 2682-2695.
Clokey, G.V., and Jacobson, L.A. (1986). The autofluorescent "lipofuscin granules" in the intestinal cells of Caenorhabditis elegans are secondary lysosomes. Mechanisms of ageing and development *35*, 79-94.
Collins, B.M. (2008). The structure and function of the retromer protein complex. Traffic (Copenhagen, Denmark) *9*, 1811-1822.
D'Souza-Schorey, C., and Chavrier, P. (2006). ARF proteins: roles in membrane traffic and beyond. Nature reviews *7*, 347-358.
D'Souza-Schorey, C., van Donselaar, E., Hsu, V.W., Yang, C., Stahl, P.D., and Peters, P.J. (1998). ARF6 targets recycling vesicles to the plasma membrane: insights from an ultrastructural investigation. The Journal of cell biology *140*, 603-616.
Dai, J., Li, J., Bos, E., Porcionatto, M., Premont, R.T., Bourgoin, S., Peters, P.J., and Hsu, V.W. (2004). ACAP1 promotes endocytic recycling by recognizing recycling sorting signals. Developmental cell *7*, 771-776.
Dang, H., Li, Z., Skolnik, E.Y., and Fares, H. (2004). Disease-related myotubularins function in endocytic traffic in Caenorhabditis elegans. Molecular biology of the cell *15*, 189-196.
Daumke, O., Lundmark, R., Vallis, Y., Martens, S., Butler, P.J., and McMahon, H.T. (2007). Architectural and mechanistic insights into an EHD ATPase involved in membrane remodelling. Nature *449*, 923-927.
de Beer, T., Hoofnagle, A.N., Enmon, J.L., Bowers, R.C., Yamabhai, M., Kay, B.K., and Overduin, M. (2000). Molecular mechanism of NPF recognition by EH domains. Nature structural biology *7*, 1018-1022.
Donaldson, J.G. (2005). Arfs, phosphoinositides and membrane traffic. Biochemical Society transactions *33*, 1276-1278.
Donaldson, J.G., and Honda, A. (2005). Localization and function of Arf family GTPases. Biochemical Society transactions *33*, 639-642.
Eisenberg, E., and Greene, L.E. (2007). Multiple roles of auxilin and hsc70 in clathrin-mediated endocytosis. Traffic (Copenhagen, Denmark) *8*, 640-646.
Fares, H., and Grant, B. (2002). Deciphering endocytosis in Caenorhabditis elegans. Traffic (Copenhagen, Denmark) *3*, 11-19.

Fares, H., and Greenwald, I. (2001). Genetic analysis of endocytosis in Caenorhabditis elegans: coelomocyte uptake defective mutants. Genetics *159*, 133-145.
Fisher, R.D., Chung, H.Y., Zhai, Q., Robinson, H., Sundquist, W.I., and Hill, C.P. (2007). Structural and Biochemical Studies of ALIX/AIP1 and Its Role in Retrovirus Budding. Cell *128*, 841-852.
Forgac, M. (1992). Structure and properties of the coated vesicle proton pump. Annals of the New York Academy of Sciences *671*, 273-283.
Franch-Marro, X., Wendler, F., Guidato, S., Griffith, J., Baena-Lopez, A., Itasaki, N., Maurice, M.M., and Vincent, J.P. (2008). Wingless secretion requires endosome-to-Golgi retrieval of Wntless/Evi/Sprinter by the retromer complex. Nature cell biology *10*, 170-177.
Franco, M., Peters, P.J., Boretto, J., van Donselaar, E., Neri, A., D'Souza-Schorey, C., and Chavrier, P. (1999). EFA6, a sec7 domain-containing exchange factor for ARF6, coordinates membrane recycling and actin cytoskeleton organization. The EMBO journal *18*, 1480-1491.
Fujibayashi, A., Taguchi, T., Misaki, R., Ohtani, M., Dohmae, N., Takio, K., Yamada, M., Gu, J., Yamakami, M., Fukuda, M., Waguri, S., Uchiyama, Y., Yoshimori, T., and Sekiguchi, K. (2008). Human RME-8 is involved in membrane trafficking through early endosomes. Cell structure and function *33*, 35-50.
Gavin, A.C., Bosche, M., Krause, R., Grandi, P., Marzioch, M., Bauer, A., Schultz, J., Rick, J.M., Michon, A.M., Cruciat, C.M., Remor, M., Hofert, C., Schelder, M., Brajenovic, M., Ruffner, H., Merino, A., Klein, K., Hudak, M., Dickson, D., Rudi, T., Gnau, V., Bauch, A., Bastuck, S., Huhse, B., Leutwein, C., Heurtier, M.A., Copley, R.R., Edelmann, A., Querfurth, E., Rybin, V., Drewes, G., Raida, M., Bouwmeester, T., Bork, P., Seraphin, B., Kuster, B., Neubauer, G., and Superti-Furga, G. (2002). Functional organization of the yeast proteome by systematic analysis of protein complexes. Nature *415*, 141-147.
Gesbert, F., Sauvonnet, N., and Dautry-Varsat, A. (2004). Clathrin-lndependent endocytosis and signalling of interleukin 2 receptors IL-2R endocytosis and signalling. Current topics in microbiology and immunology *286*, 119-148.
Gimona, M., Djinovic-Carugo, K., Kranewitter, W.J., and Winder, S.J. (2002). Functional plasticity of CH domains. FEBS letters *513*, 98-106.
Girard, M., and McPherson, P.S. (2008). RME-8 regulates trafficking of the epidermal growth factor receptor. FEBS letters *582*, 961-966.
Girard, M., Poupon, V., Blondeau, F., and McPherson, P.S. (2005). The DnaJ-domain protein RME-8 functions in endosomal trafficking. The Journal of biological chemistry *280*, 40135-40143.
Glodowski, D.R., Chen, C.C., Schaefer, H., Grant, B.D., and Rongo, C. (2007). RAB-10 regulates glutamate receptor recycling in a cholesterol-dependent endocytosis pathway. Mol Biol Cell *18*, 4387-4396.
Grant, B., and Hirsh, D. (1999). Receptor-mediated endocytosis in the Caenorhabditis elegans oocyte. Molecular biology of the cell *10*, 4311-4326.
Grant, B., Zhang, Y., Paupard, M.C., Lin, S.X., Hall, D.H., and Hirsh, D. (2001). Evidence that RME-1, a conserved C. elegans EH-domain protein, functions in endocytic recycling. Nature cell biology *3*, 573-579.

Grant, B.D., and Caplan, S. (2008). Mechanisms of EHD/RME-1 protein function in endocytic transport. Traffic (Copenhagen, Denmark) *9*, 2043-2052.
Grant, B.D., and Donaldson, J.G. (2009). Pathways and mechanisms of endocytic recycling. Nature reviews *10*, 597-608.
Greener, T., Grant, B., Zhang, Y., Wu, X., Greene, L.E., Hirsh, D., and Eisenberg, E. (2001). Caenorhabditis elegans auxilin: a J-domain protein essential for clathrin-mediated endocytosis in vivo. Nature cell biology *3*, 215-219.
Grosshans, B.L., Ortiz, D., and Novick, P. (2006). Rabs and their effectors: achieving specificity in membrane traffic. Proceedings of the National Academy of Sciences of the United States of America *103*, 11821-11827.
Gruenberg, J., and Stenmark, H. (2004). The biogenesis of multivesicular endosomes. Nature reviews *5*, 317-323.
Guilherme, A., Soriano, N.A., Bose, S., Holik, J., Bose, A., Pomerleau, D.P., Furcinitti, P., Leszyk, J., Corvera, S., and Czech, M.P. (2004a). EHD2 and the novel EH domain binding protein EHBP1 couple endocytosis to the actin cytoskeleton. The Journal of biological chemistry *279*, 10593-10605.
Guilherme, A., Soriano, N.A., Furcinitti, P.S., and Czech, M.P. (2004b). Role of EHD1 and EHBP1 in perinuclear sorting and insulin-regulated GLUT4 recycling in 3T3-L1 adipocytes. The Journal of biological chemistry *279*, 40062-40075.
Hao, M., and Maxfield, F.R. (2000). Characterization of rapid membrane internalization and recycling. The Journal of biological chemistry *275*, 15279-15286.
Harris, T.W., Schuske, K., and Jorgensen, E.M. (2001). Studies of synaptic vesicle endocytosis in the nematode C. elegans. Traffic (Copenhagen, Denmark) *2*, 597-605.
Hart, A.C., Sims, S., and Kaplan, J.M. (1995). Synaptic code for sensory modalities revealed by *C. elegans* GLR-1 glutamate receptor. Nature *378*, 82-84.
Hattula, K., Furuhjelm, J., Arffman, A., and Peranen, J. (2002). A Rab8-specific GDP/GTP exchange factor is involved in actin remodeling and polarized membrane transport. Molecular biology of the cell *13*, 3268-3280.
Hermann, G.J., Schroeder, L.K., Hieb, C.A., Kershner, A.M., Rabbitts, B.M., Fonarev, P., Grant, B.D., and Priess, J.R. (2005). Genetic analysis of lysosomal trafficking in Caenorhabditis elegans. Molecular biology of the cell *16*, 3273-3288.
Hicke, L. (2001). A new ticket for entry into budding vesicles-ubiquitin. Cell *106*, 527-530.
Hoekstra, D., Tyteca, D., and van, I.S.C. (2004). The subapical compartment: a traffic center in membrane polarity development. Journal of cell science *117*, 2183-2192.
Honda, A., Nogami, M., Yokozeki, T., Yamazaki, M., Nakamura, H., Watanabe, H., Kawamoto, K., Nakayama, K., Morris, A.J., Frohman, M.A., and Kanaho, Y. (1999). Phosphatidylinositol 4-phosphate 5-kinase alpha is a downstream effector of the small G protein ARF6 in membrane ruffle formation. Cell *99*, 521-532.
Hopkins, C.R. (1983). Intracellular routing of transferrin and transferrin receptors in epidermoid carcinoma A431 cells. Cell *35*, 321-330.
Inoue, H., and Randazzo, P.A. (2007). Arf GAPs and their interacting proteins. Traffic (Copenhagen, Denmark) *8*, 1465-1475.
Jackson, C.L., and Casanova, J.E. (2000). Turning on ARF: the Sec7 family of guanine-nucleotide-exchange factors. Trends in cell biology *10*, 60-67.

Jackson, T.R., Brown, F.D., Nie, Z., Miura, K., Foroni, L., Sun, J., Hsu, V.W., Donaldson, J.G., and Randazzo, P.A. (2000). ACAPs are arf6 GTPase-activating proteins that function in the cell periphery. The Journal of cell biology *151*, 627-638.
Jovanovic, O.A., Brown, F.D., and Donaldson, J.G. (2006). An effector domain mutant of Arf6 implicates phospholipase D in endosomal membrane recycling. Molecular biology of the cell *17*, 327-335.
Kachur, T.M., Audhya, A., and Pilgrim, D.B. (2008). UNC-45 is required for NMY-2 contractile function in early embryonic polarity establishment and germline cellularization in C. elegans. Developmental biology *314*, 287-299.
Kamath, R.S., and Ahringer, J. (2003). Genome-wide RNAi screening in Caenorhabditis elegans. Methods (San Diego, Calif *30*, 313-321.
Kanno, E., Ishibashi, K., Kobayashi, H., Matsui, T., Ohbayashi, N., and Fukuda, M. (2010). Comprehensive screening for novel Rab-binding proteins by GST pull-down assay using 60 different mammalian Rabs. Traffic (Copenhagen, Denmark).
Katoh, K., Shibata, H., Hatta, K., and Maki, M. (2004). CHMP4b is a major binding partner of the ALG-2-interacting protein Alix among the three CHMP4 isoforms. Archives of biochemistry and biophysics *421*, 159-165.
Katoh, K., Shibata, H., Suzuki, H., Nara, A., Ishidoh, K., Kominami, E., Yoshimori, T., and Maki, M. (2003). The ALG-2-interacting protein Alix associates with CHMP4b, a human homologue of yeast Snf7 that is involved in multivesicular body sorting. The Journal of biological chemistry *278*, 39104-39113.
Katzmann, D.J., Babst, M., and Emr, S.D. (2001). Ubiquitin-dependent sorting into the multivesicular body pathway requires the function of a conserved endosomal protein sorting complex, ESCRT-I. Cell *106*, 145-155.
Katzmann, D.J., Odorizzi, G., and Emr, S.D. (2002). Receptor downregulation and multivesicular-body sorting. Nature reviews *3*, 893-905.
Kessels, M.M., and Qualmann, B. (2004). The syndapin protein family: linking membrane trafficking with the cytoskeleton. Journal of cell science *117*, 3077-3086.
Kim, J., Sitaraman, S., Hierro, A., Beach, B.M., Odorizzi, G., and Hurley, J.H. (2005). Structural basis for endosomal targeting by the Bro1 domain. Developmental cell *8*, 937-947.
Kouranti, I., Sachse, M., Arouche, N., Goud, B., and Echard, A. (2006). Rab35 regulates an endocytic recycling pathway essential for the terminal steps of cytokinesis. Curr Biol *16*, 1719-1725.
Krauss, M., Kinuta, M., Wenk, M.R., De Camilli, P., Takei, K., and Haucke, V. (2003). ARF6 stimulates clathrin/AP-2 recruitment to synaptic membranes by activating phosphatidylinositol phosphate kinase type Igamma. The Journal of cell biology *162*, 113-124.
Lauvrak, S.U., Torgersen, M.L., and Sandvig, K. (2004). Efficient endosome-to-Golgi transport of Shiga toxin is dependent on dynamin and clathrin. Journal of cell science *117*, 2321-2331.
Lawe, D.C., Chawla, A., Merithew, E., Dumas, J., Carrington, W., Fogarty, K., Lifshitz, L., Tuft, R., Lambright, D., and Corvera, S. (2002). Sequential roles for phosphatidylinositol 3-phosphate and Rab5 in tethering and fusion of early endosomes via their interaction with EEA1. The Journal of biological chemistry *277*, 8611-8617.

Lee, D.W., Zhao, X., Zhang, F., Eisenberg, E., and Greene, L.E. (2005). Depletion of GAK/auxilin 2 inhibits receptor-mediated endocytosis and recruitment of both clathrin and clathrin adaptors. Journal of cell science *118*, 4311-4321.
Li, J., Ballif, B.A., Powelka, A.M., Dai, J., Gygi, S.P., and Hsu, V.W. (2005). Phosphorylation of ACAP1 by Akt regulates the stimulation-dependent recycling of integrin beta1 to control cell migration. Developmental cell *9*, 663-673.
Li, J., Peters, P.J., Bai, M., Dai, J., Bos, E., Kirchhausen, T., Kandror, K.V., and Hsu, V.W. (2007). An ACAP1-containing clathrin coat complex for endocytic recycling. The Journal of cell biology *178*, 453-464.
Lin, S.X., Grant, B., Hirsh, D., and Maxfield, F.R. (2001). Rme-1 regulates the distribution and function of the endocytic recycling compartment in mammalian cells. Nature cell biology *3*, 567-572.
Lin, S.X., Gundersen, G.G., and Maxfield, F.R. (2002). Export from pericentriolar endocytic recycling compartment to cell surface depends on stable, detyrosinated (glu) microtubules and kinesin. Molecular biology of the cell *13*, 96-109.
Lin, S.X., Mallet, W.G., Huang, A.Y., and Maxfield, F.R. (2004). Endocytosed cation-independent mannose 6-phosphate receptor traffics via the endocytic recycling compartment en route to the trans-Golgi network and a subpopulation of late endosomes. Molecular biology of the cell *15*, 721-733.
Lombardi, D., Soldati, T., Riederer, M.A., Goda, Y., Zerial, M., and Pfeffer, S.R. (1993). Rab9 functions in transport between late endosomes and the trans Golgi network. The EMBO journal *12*, 677-682.
Luhtala, N., and Odorizzi, G. (2004). Bro1 coordinates deubiquitination in the multivesicular body pathway by recruiting Doa4 to endosomes. The Journal of cell biology *166*, 717-729.
Marcusson, E.G., Horazdovsky, B.F., Cereghino, J.L., Gharakhanian, E., and Emr, S.D. (1994). The sorting receptor for yeast vacuolar carboxypeptidase Y is encoded by the VPS10 gene. Cell *77*, 579-586.
Maricq, A.V., Peckol, E., Driscoll, M., and Bargmann, C.I. (1995). Mechanosensory signalling in *C. elegans* mediated by the GLR-1 glutamate receptor. Nature *378*, 78-81.
Martin-Serrano, J., Yarovoy, A., Perez-Caballero, D., and Bieniasz, P.D. (2003). Divergent retroviral late-budding domains recruit vacuolar protein sorting factors by using alternative adaptor proteins. Proceedings of the National Academy of Sciences of the United States of America *100*, 12414-12419.
Mateer, S.C., Morris, L.E., Cromer, D.A., Bensenor, L.B., and Bloom, G.S. (2004). Actin filament binding by a monomeric IQGAP1 fragment with a single calponin homology domain. Cell motility and the cytoskeleton *58*, 231-241.
Matsuo, H., Chevallier, J., Mayran, N., Le Blanc, I., Ferguson, C., Faure, J., Blanc, N.S., Matile, S., Dubochet, J., Sadoul, R., Parton, R.G., Vilbois, F., and Gruenberg, J. (2004). Role of LBPA and Alix in multivesicular liposome formation and endosome organization. Science *303*, 531-534.
Matyash, V., Geier, C., Henske, A., Mukherjee, S., Hirsh, D., Thiele, C., Grant, B., Maxfield, F.R., and Kurzchalia, T.V. (2001). Distribution and transport of cholesterol in Caenorhabditis elegans. Molecular biology of the cell *12*, 1725-1736.
Maxfield, F.R., and McGraw, T.E. (2004). Endocytic recycling. Nature reviews *5*, 121-132.

Mellem, J.E., Brockie, P.J., Zheng, Y., Madsen, D.M., and Maricq, A.V. (2002). Decoding of polymodal sensory stimuli by postsynaptic glutamate receptors in *C. elegans*. Neuron *36*, 933-944.
Mellman, I. (1996). Endocytosis and molecular sorting. Annual review of cell and developmental biology *12*, 575-625.
Meyer, C., Zizioli, D., Lausmann, S., Eskelinen, E.L., Hamann, J., Saftig, P., von Figura, K., and Schu, P. (2000). mu1A-adaptin-deficient mice: lethality, loss of AP-1 binding and rerouting of mannose 6-phosphate receptors. The EMBO journal *19*, 2193-2203.
Missotten, M., Nichols, A., Rieger, K., and Sadoul, R. (1999). Alix, a novel mouse protein undergoing calcium-dependent interaction with the apoptosis-linked-gene 2 (ALG-2) protein. Cell death and differentiation *6*, 124-129.
Mukherjee, S., Ghosh, R.N., and Maxfield, F.R. (1997). Endocytosis. Physiological reviews *77*, 759-803.
Murray, J.T., Panaretou, C., Stenmark, H., Miaczynska, M., and Backer, J.M. (2002). Role of Rab5 in the recruitment of hVps34/p150 to the early endosome. Traffic (Copenhagen, Denmark) *3*, 416-427.
Naslavsky, N., Boehm, M., Backlund, P.S., Jr., and Caplan, S. (2004a). Rabenosyn-5 and EHD1 interact and sequentially regulate protein recycling to the plasma membrane. Molecular biology of the cell *15*, 2410-2422.
Naslavsky, N., and Caplan, S. (2005). C-terminal EH-domain-containing proteins: consensus for a role in endocytic trafficking, EH? Journal of cell science *118*, 4093-4101.
Naslavsky, N., Rahajeng, J., Sharma, M., Jovic, M., and Caplan, S. (2006). Interactions between EHD proteins and Rab11-FIP2: a role for EHD3 in early endosomal transport. Molecular biology of the cell *17*, 163-177.
Naslavsky, N., Weigert, R., and Donaldson, J.G. (2003). Convergence of non-clathrin- and clathrin-derived endosomes involves Arf6 inactivation and changes in phosphoinositides. Molecular biology of the cell *14*, 417-431.
Naslavsky, N., Weigert, R., and Donaldson, J.G. (2004b). Characterization of a nonclathrin endocytic pathway: membrane cargo and lipid requirements. Molecular biology of the cell *15*, 3542-3552.
Newmyer, S.L., and Schmid, S.L. (2001). Dominant-interfering Hsc70 mutants disrupt multiple stages of the clathrin-coated vesicle cycle in vivo. The Journal of cell biology *152*, 607-620.
Nichols, B. (2003). Caveosomes and endocytosis of lipid rafts. Journal of cell science *116*, 4707-4714.
Nonet, M.L., Saifee, O., Zhao, H., Rand, J.B., and Wei, L. (1998). Synaptic transmission deficits in Caenorhabditis elegans synaptobrevin mutants. J Neurosci *18*, 70-80.
Odorizzi, G. (2006). The multiple personalities of Alix. Journal of cell science *119*, 3025-3032.
Odorizzi, G., Katzmann, D.J., Babst, M., Audhya, A., and Emr, S.D. (2003). Bro1 is an endosome-associated protein that functions in the MVB pathway in Saccharomyces cerevisiae. Journal of cell science *116*, 1893-1903.
Oegema, K., Desai, A., Rybina, S., Kirkham, M., and Hyman, A.A. (2001). Functional analysis of kinetochore assembly in Caenorhabditis elegans. The Journal of cell biology *153*, 1209-1226.

Ortiz, D., Medkova, M., Walch-Solimena, C., and Novick, P. (2002). Ypt32 recruits the Sec4p guanine nucleotide exchange factor, Sec2p, to secretory vesicles; evidence for a Rab cascade in yeast. The Journal of cell biology *157*, 1005-1015.
Page, L.J., Sowerby, P.J., Lui, W.W., and Robinson, M.S. (1999). Gamma-synergin: an EH domain-containing protein that interacts with gamma-adaptin. The Journal of cell biology *146*, 993-1004.
Paleotti, O., Macia, E., Luton, F., Klein, S., Partisani, M., Chardin, P., Kirchhausen, T., and Franco, M. (2005). The small G-protein Arf6GTP recruits the AP-2 adaptor complex to membranes. The Journal of biological chemistry *280*, 21661-21666.
Pan, C.L., Baum, P.D., Gu, M., Jorgensen, E.M., Clark, S.G., and Garriga, G. (2008). C. elegans AP-2 and retromer control Wnt signaling by regulating mig-14/Wntless. Developmental cell *14*, 132-139.
Pan, S., Wang, R., Zhou, X., He, G., Koomen, J., Kobayashi, R., Sun, L., Corvera, J., Gallick, G.E., and Kuang, J. (2006). Involvement of the conserved adaptor protein Alix in actin cytoskeleton assembly. The Journal of biological chemistry *281*, 34640-34650.
Pant, S., Sharma, M., Patel, K., Caplan, S., Carr, C.M., and Grant, B.D. (2009). AMPH-1/Amphiphysin/Bin1 functions with RME-1/Ehd1 in endocytic recycling. Nature cell biology *11*, 1399-1410.
Park, E.C., Glodowski, D.R., and Rongo, C. (2009). The ubiquitin ligase RPM-1 and the p38 MAPK PMK-3 regulate AMPA receptor trafficking. PLoS ONE *4*, e4284.
Patton, A., Knuth, S., Schaheen, B., Dang, H., Greenwald, I., and Fares, H. (2005). Endocytosis function of a ligand-gated ion channel homolog in Caenorhabditis elegans. Curr Biol *15*, 1045-1050.
Peters, P.J., Hsu, V.W., Ooi, C.E., Finazzi, D., Teal, S.B., Oorschot, V., Donaldson, J.G., and Klausner, R.D. (1995). Overexpression of wild-type and mutant ARF1 and ARF6: distinct perturbations of nonoverlapping membrane compartments. The Journal of cell biology *128*, 1003-1017.
Popoff, V., Mardones, G.A., Tenza, D., Rojas, R., Lamaze, C., Bonifacino, J.S., Raposo, G., and Johannes, L. (2007). The retromer complex and clathrin define an early endosomal retrograde exit site. Journal of cell science *120*, 2022-2031.
Port, F., Kuster, M., Herr, P., Furger, E., Banziger, C., Hausmann, G., and Basler, K. (2008). Wingless secretion promotes and requires retromer-dependent cycling of Wntless. Nature cell biology *10*, 178-185.
Powelka, A.M., Sun, J., Li, J., Gao, M., Shaw, L.M., Sonnenberg, A., and Hsu, V.W. (2004). Stimulation-dependent recycling of integrin beta1 regulated by ARF6 and Rab11. Traffic (Copenhagen, Denmark) *5*, 20-36.
Praitis, V., Casey, E., Collar, D., and Austin, J. (2001). Creation of low-copy integrated transgenic lines in Caenorhabditis elegans. Genetics *157*, 1217-1226.
Prasad, B.C., and Clark, S.G. (2006). Wnt signaling establishes anteroposterior neuronal polarity and requires retromer in C. elegans. Development (Cambridge, England) *133*, 1757-1766.
Puffer, B.A., Parent, L.J., Wills, J.W., and Montelaro, R.C. (1997). Equine infectious anemia virus utilizes a YXXL motif within the late assembly domain of the Gag p9 protein. Journal of virology *71*, 6541-6546.
Qualmann, B., and Kelly, R.B. (2000). Syndapin isoforms participate in receptor-mediated endocytosis and actin organization. The Journal of cell biology *148*, 1047-1062.

Radhakrishna, H., and Donaldson, J.G. (1997). ADP-ribosylation factor 6 regulates a novel plasma membrane recycling pathway. The Journal of cell biology *139*, 49-61.
Raiborg, C., Bache, K.G., Gillooly, D.J., Madshus, I.H., Stang, E., and Stenmark, H. (2002). Hrs sorts ubiquitinated proteins into clathrin-coated microdomains of early endosomes. Nature cell biology *4*, 394-398.
Raiborg, C., Bache, K.G., Mehlum, A., Stang, E., and Stenmark, H. (2001a). Hrs recruits clathrin to early endosomes. The EMBO journal *20*, 5008-5021.
Raiborg, C., Bremnes, B., Mehlum, A., Gillooly, D.J., D'Arrigo, A., Stang, E., and Stenmark, H. (2001b). FYVE and coiled-coil domains determine the specific localisation of Hrs to early endosomes. Journal of cell science *114*, 2255-2263.
Raiborg, C., Wesche, J., Malerod, L., and Stenmark, H. (2006). Flat clathrin coats on endosomes mediate degradative protein sorting by scaffolding Hrs in dynamic microdomains. Journal of cell science *119*, 2414-2424.
Randhawa, V.K., Ishikura, S., Talior-Volodarsky, I., Cheng, A.W., Patel, N., Hartwig, J.H., and Klip, A. (2008). GLUT4 vesicle recruitment and fusion are differentially regulated by Rac, AS160, and Rab8A in muscle cells. The Journal of biological chemistry *283*, 27208-27219.
Ren, M., Xu, G., Zeng, J., De Lemos-Chiarandini, C., Adesnik, M., and Sabatini, D.D. (1998). Hydrolysis of GTP on rab11 is required for the direct delivery of transferrin from the pericentriolar recycling compartment to the cell surface but not from sorting endosomes. Proceedings of the National Academy of Sciences of the United States of America *95*, 6187-6192.
Rink, J., Ghigo, E., Kalaidzidis, Y., and Zerial, M. (2005). Rab conversion as a mechanism of progression from early to late endosomes. Cell *122*, 735-749.
Rojas, R., Kametaka, S., Haft, C.R., and Bonifacino, J.S. (2007). Interchangeable but essential functions of SNX1 and SNX2 in the association of retromer with endosomes and the trafficking of mannose 6-phosphate receptors. Molecular and cellular biology *27*, 1112-1124.
Roland, J.T., Kenworthy, A.K., Peranen, J., Caplan, S., and Goldenring, J.R. (2007). Myosin Vb interacts with Rab8a on a tubular network containing EHD1 and EHD3. Molecular biology of the cell *18*, 2828-2837.
Rongo, C., Whitfield, C.W., Rodal, A., Kim, S.K., and Kaplan, J.M. (1998). LIN-10 is a shared component of the polarized protein localization pathways in neurons and epithelia. Cell *94*, 751-759.
Roudier, N., Lefebvre, C., and Legouis, R. (2005). CeVPS-27 is an endosomal protein required for the molting and the endocytic trafficking of the low-density lipoprotein receptor-related protein 1 in Caenorhabditis elegans. Traffic (Copenhagen, Denmark) *6*, 695-705.
Sadoul, R. (2006). Do Alix and ALG-2 really control endosomes for better or for worse? Biology of the cell / under the auspices of the European Cell Biology Organization *98*, 69-77.
Saint-Pol, A., Yelamos, B., Amessou, M., Mills, I.G., Dugast, M., Tenza, D., Schu, P., Antony, C., McMahon, H.T., Lamaze, C., and Johannes, L. (2004). Clathrin adaptor epsinR is required for retrograde sorting on early endosomal membranes. Developmental cell *6*, 525-538.

Sakisaka, T., Itoh, T., Miura, K., and Takenawa, T. (1997). Phosphatidylinositol 4,5-bisphosphate phosphatase regulates the rearrangement of actin filaments. Molecular and cellular biology *17*, 3841-3849.
Salminen, A., and Novick, P.J. (1987). A ras-like protein is required for a post-Golgi event in yeast secretion. Cell *49*, 527-538.
Sano, H., Eguez, L., Teruel, M.N., Fukuda, M., Chuang, T.D., Chavez, J.A., Lienhard, G.E., and McGraw, T.E. (2007). Rab10, a target of the AS160 Rab GAP, is required for insulin-stimulated translocation of GLUT4 to the adipocyte plasma membrane. Cell metabolism *5*, 293-303.
Santolini, E., Salcini, A.E., Kay, B.K., Yamabhai, M., and Di Fiore, P.P. (1999). The EH network. Experimental cell research *253*, 186-209.
Sato, K., Sato, M., Audhya, A., Oegema, K., Schweinsberg, P., and Grant, B.D. (2006). Dynamic regulation of caveolin-1 trafficking in the germ line and embryo of Caenorhabditis elegans. Molecular biology of the cell *17*, 3085-3094.
Sato, K.*e.a.* (2008). Differential requirements for clathrin in receptor-mediated endocytosis and maintenance of synaptic vesicle pools. Proceedings of the National Academy of Sciences, USA.
Sato, M., and Grant, B.D. Intracellular trafficking. In: WormBook, ed. T.C.e.R. Community: WormBook.
Sato, M., Grant, B.D., Harada, A., and Sato, K. (2008a). Rab11 is required for synchronous secretion of chondroitin proteoglycans after fertilization in Caenorhabditis elegans. Journal of cell science *121*, 3177-3186.
Sato, M., Sato, K., Fonarev, P., Huang, C.J., Liou, W., and Grant, B.D. (2005). Caenorhabditis elegans RME-6 is a novel regulator of RAB-5 at the clathrin-coated pit. Nature cell biology *7*, 559-569.
Sato, M., Sato, K., Liou, W., Pant, S., Harada, A., and Grant, B.D. (2008b). Regulation of endocytic recycling by C. elegans Rab35 and its regulator RME-4, a coated-pit protein. The EMBO journal *27*, 1183-1196.
Schmidt, M.H., Chen, B., Randazzo, L.M., and Bogler, O. (2003). SETA/CIN85/Ruk and its binding partner AIP1 associate with diverse cytoskeletal elements, including FAKs, and modulate cell adhesion. Journal of cell science *116*, 2845-2855.
Schmidt, M.H., Hoeller, D., Yu, J., Furnari, F.B., Cavenee, W.K., Dikic, I., and Bogler, O. (2004). Alix/AIP1 antagonizes epidermal growth factor receptor downregulation by the Cbl-SETA/CIN85 complex. Molecular and cellular biology *24*, 8981-8993.
Schuck, S., Gerl, M.J., Ang, A., Manninen, A., Keller, P., Mellman, I., and Simons, K. (2007). Rab10 is involved in basolateral transport in polarized Madin-Darby canine kidney cells. Traffic (Copenhagen, Denmark) *8*, 47-60.
Seaman, M.N. (2004). Cargo-selective endosomal sorting for retrieval to the Golgi requires retromer. The Journal of cell biology *165*, 111-122.
Sharma, M., Giridharan, S.S., Rahajeng, J., Naslavsky, N., and Caplan, S. (2009). MICAL-L1 links EHD1 to tubular recycling endosomes and regulates receptor recycling. Molecular biology of the cell *20*, 5181-5194.
Sharrock, W.J. (1983). Yolk proteins of Caenorhabditis elegans. Developmental biology *96*, 182-188.

Shaye, D.D., and Greenwald, I. (2005). LIN-12/Notch trafficking and regulation of DSL ligand activity during vulval induction in Caenorhabditis elegans. Development (Cambridge, England) *132*, 5081-5092.
Sheff, D.R., Daro, E.A., Hull, M., and Mellman, I. (1999). The receptor recycling pathway contains two distinct populations of early endosomes with different sorting functions. The Journal of cell biology *145*, 123-139.
Shi, A., Pant, S., Balklava, Z., Chen, C.C., Figueroa, V., and Grant, B.D. (2007). A novel requirement for C. elegans Alix/ALX-1 in RME-1-mediated membrane transport. Curr Biol *17*, 1913-1924.
Shi, A., Sun, L., Banerjee, R., Tobin, M., Zhang, Y., and Grant, B.D. (2009). Regulation of endosomal clathrin and retromer-mediated endosome to Golgi retrograde transport by the J-domain protein RME-8. The EMBO journal *28*, 3290-3302.
Shinozaki-Narikawa, N., Kodama, T., and Shibasaki, Y. (2006). Cooperation of phosphoinositides and BAR domain proteins in endosomal tubulation. Traffic (Copenhagen, Denmark) *7*, 1539-1550.
Silady, R.A., Ehrhardt, D.W., Jackson, K., Faulkner, C., Oparka, K., and Somerville, C.R. (2008). The GRV2/RME-8 protein of Arabidopsis functions in the late endocytic pathway and is required for vacuolar membrane flow. Plant J *53*, 29-41.
Silady, R.A., Kato, T., Lukowitz, W., Sieber, P., Tasaka, M., and Somerville, C.R. (2004). The gravitropism defective 2 mutants of Arabidopsis are deficient in a protein implicated in endocytosis in Caenorhabditis elegans. Plant physiology *136*, 3095-3103; discussion 3002.
Sjoblom, B., Ylanne, J., and Djinovic-Carugo, K. (2008). Novel structural insights into F-actin-binding and novel functions of calponin homology domains. Current opinion in structural biology *18*, 702-708.
Skanland, S.S., Walchli, S., Brech, A., and Sandvig, K. (2009). SNX4 in complex with clathrin and dynein: implications for endosome movement. PloS one *4*, e5935.
Slep, K.C., and Vale, R.D. (2007). Structural basis of microtubule plus end tracking by XMAP215, CLIP-170, and EB1. Molecular cell *27*, 976-991.
Someya, A., Sata, M., Takeda, K., Pacheco-Rodriguez, G., Ferrans, V.J., Moss, J., and Vaughan, M. (2001). ARF-GEP(100), a guanine nucleotide-exchange protein for ADP-ribosylation factor 6. Proceedings of the National Academy of Sciences of the United States of America *98*, 2413-2418.
Song, J., Khachikian, Z., Radhakrishna, H., and Donaldson, J.G. (1998). Localization of endogenous ARF6 to sites of cortical actin rearrangement and involvement of ARF6 in cell spreading. Journal of cell science *111 (Pt 15)*, 2257-2267.
Sonnichsen, B., De Renzis, S., Nielsen, E., Rietdorf, J., and Zerial, M. (2000). Distinct membrane domains on endosomes in the recycling pathway visualized by multicolor imaging of Rab4, Rab5, and Rab11. The Journal of cell biology *149*, 901-914.
Stenmark, H. (2009). Rab GTPases as coordinators of vesicle traffic. Nature reviews *10*, 513-525.
Strack, B., Calistri, A., Craig, S., Popova, E., and Gottlinger, H.G. (2003). AIP1/ALIX is a binding partner for HIV-1 p6 and EIAV p9 functioning in virus budding. Cell *114*, 689-699.
Timmons, L., and Fire, A. (1998). Specific interference by ingested dsRNA. Nature *395*, 854.

Treusch, S., Knuth, S., Slaugenhaupt, S.A., Goldin, E., Grant, B.D., and Fares, H. (2004). Caenorhabditis elegans functional orthologue of human protein h-mucolipin-1 is required for lysosome biogenesis. Proceedings of the National Academy of Sciences of the United States of America *101*, 4483-4488.
Ullrich, O., Reinsch, S., Urbe, S., Zerial, M., and Parton, R.G. (1996). Rab11 regulates recycling through the pericentriolar recycling endosome. The Journal of cell biology *135*, 913-924.
Ungewickell, E., Ungewickell, H., Holstein, S.E., Lindner, R., Prasad, K., Barouch, W., Martin, B., Greene, L.E., and Eisenberg, E. (1995). Role of auxilin in uncoating clathrin-coated vesicles. Nature *378*, 632-635.
van Dam, E.M., and Stoorvogel, W. (2002). Dynamin-dependent transferrin receptor recycling by endosome-derived clathrin-coated vesicles. Molecular biology of the cell *13*, 169-182.
van der Sluijs, P., Hull, M., Webster, P., Male, P., Goud, B., and Mellman, I. (1992). The small GTP-binding protein rab4 controls an early sorting event on the endocytic pathway. Cell *70*, 729-740.
van Weert, A.W., Geuze, H.J., Groothuis, B., and Stoorvogel, W. (2000). Primaquine interferes with membrane recycling from endosomes to the plasma membrane through a direct interaction with endosomes which does not involve neutralisation of endosomal pH nor osmotic swelling of endosomes. European journal of cell biology *79*, 394-399.
Vincent, O., Rainbow, L., Tilburn, J., Arst, H.N., Jr., and Penalva, M.A. (2003). YPXL/I is a protein interaction motif recognized by aspergillus PalA and its human homologue, AIP1/Alix. Molecular and cellular biology *23*, 1647-1655.
Vito, P., Pellegrini, L., Guiet, C., and D'Adamio, L. (1999). Cloning of AIP1, a novel protein that associates with the apoptosis-linked gene ALG-2 in a Ca2+-dependent reaction. The Journal of biological chemistry *274*, 1533-1540.
von Schwedler, U.K., Stuchell, M., Muller, B., Ward, D.M., Chung, H.Y., Morita, E., Wang, H.E., Davis, T., He, G.P., Cimbora, D.M., Scott, A., Krausslich, H.G., Kaplan, J., Morham, S.G., and Sundquist, W.I. (2003). The protein network of HIV budding. Cell *114*, 701-713.
Walhout, A.J., Sordella, R., Lu, X., Hartley, J.L., Temple, G.F., Brasch, M.A., Thierry-Mieg, N., and Vidal, M. (2000). Protein interaction mapping in C. elegans using proteins involved in vulval development. Science (New York, N.Y *287*, 116-122.
Walhout, A.J., and Vidal, M. (2001). High-throughput yeast two-hybrid assays for large-scale protein interaction mapping. Methods (San Diego, Calif *24*, 297-306.
Walseng, E., Bakke, O., and Roche, P.A. (2008). Major histocompatibility complex class II-peptide complexes internalize using a clathrin- and dynamin-independent endocytosis pathway. The Journal of biological chemistry *283*, 14717-14727.
Walsh, P., Bursac, D., Law, Y.C., Cyr, D., and Lithgow, T. (2004). The J-protein family: modulating protein assembly, disassembly and translocation. EMBO reports *5*, 567-571.
Weide, T., Teuber, J., Bayer, M., and Barnekow, A. (2003). MICAL-1 isoforms, novel rab1 interacting proteins. Biochemical and biophysical research communications *306*, 79-86.
Weigert, R., and Donaldson, J.G. (2005). Fluorescent microscopy-based assays to study the role of Rab22a in clathrin-independent endocytosis. Methods in enzymology *403*, 243-253.

Weigert, R., Yeung, A.C., Li, J., and Donaldson, J.G. (2004). Rab22a regulates the recycling of membrane proteins internalized independently of clathrin. Molecular biology of the cell *15*, 3758-3770.
Welsch, S., Habermann, A., Jager, S., Muller, B., Krijnse-Locker, J., and Krausslich, H.G. (2006). Ultrastructural Analysis of ESCRT Proteins Suggests a Role for Endosome-Associated Tubular-Vesicular Membranes in ESCRT Function. Traffic (Copenhagen, Denmark) *7*, 1551-1566.
Wilkinson, H.A., Fitzgerald, K., and Greenwald, I. (1994). Reciprocal changes in expression of the receptor lin-12 and its ligand lag-2 prior to commitment in a C. elegans cell fate decision. Cell *79*, 1187-1198.
Wu, X., Zhao, X., Baylor, L., Kaushal, S., Eisenberg, E., and Greene, L.E. (2001). Clathrin exchange during clathrin-mediated endocytosis. The Journal of cell biology *155*, 291-300.
Yamamura, R., Nishimura, N., Nakatsuji, H., Arase, S., and Sasaki, T. (2008). The interaction of JRAB/MICAL-L2 with Rab8 and Rab13 coordinates the assembly of tight junctions and adherens junctions. Molecular biology of the cell *19*, 971-983.
Yamashiro, D.J., and Maxfield, F.R. (1984). Acidification of endocytic compartments and the intracellular pathways of ligands and receptors. Journal of cellular biochemistry *26*, 231-246.
Yan, Q., Sun, W., Kujala, P., Lotfi, Y., Vida, T.A., and Bean, A.J. (2005). CART: an Hrs/actinin-4/BERP/myosin V protein complex required for efficient receptor recycling. Molecular biology of the cell *16*, 2470-2482.
Yang, P.T., Lorenowicz, M.J., Silhankova, M., Coudreuse, D.Y., Betist, M.C., and Korswagen, H.C. (2008). Wnt signaling requires retromer-dependent recycling of MIG-14/Wntless in Wnt-producing cells. Developmental cell *14*, 140-147.
Yin, H.L., and Janmey, P.A. (2003). Phosphoinositide regulation of the actin cytoskeleton. Annual review of physiology *65*, 761-789.
Yu, X., Odera, S., Chuang, C.H., Lu, N., and Zhou, Z. (2006). C. elegans Dynamin mediates the signaling of phagocytic receptor CED-1 for the engulfment and degradation of apoptotic cells. Developmental cell *10*, 743-757.
Zhang, Y., Grant, B., and Hirsh, D. (2001). RME-8, a conserved J-domain protein, is required for endocytosis in Caenorhabditis elegans. Mol Biol Cell *12*, 2011-2021.
Zheng, Y., Brockie, P.J., Mellem, J.E., Madsen, D.M., and Maricq, A.V. (1999). Neuronal control of locomotion in C. elegans is modified by a dominant mutation in the GLR-1 ionotropic glutamate receptor. Neuron *24*, 347-361.

CURRICULUM VITA

ANBING SHI

Educational History

Sept, 2005 – May 2010 Doctor of Philosophy, Program of Microbiology and Molecular Genetics, Rutgers University, Piscataway N.J.
Thesis Advisor: Dr. Barth D. Grant.
Thesis title "Regulation of Endocytic Recycling in *Caenorhabditis elegans*".

Sept, 1999 - May, 2003 Master of Science, Program of Microbiology and Molecular Genetics, Rutgers University, Piscataway N.J.
Thesis Advisor: Dr. Linda Brzustowicz.
Thesis title "Molecular Assessment of 22q11.2 Deletion in Adults with Schizophrenia or Tetralogy of Fallot".

Sept, 1996 - June, 1999 Master of Science, Molecular Genetics Program, Nankai University, Tianjin, China.
Thesis title "An investigation of the role of amyloid precursor protein during cell transformation".
.
Sept, 1992 - June, 1996 Bachelor of Science, Microbiology Program, Nankai University, Tianjin, China.

Working Experience

Senior Research Assistant
Sept, 2004 - July, 2005 Kimmel Cancer Institute/Kimmel Cancer Center, Microarray Core Facility, Thomas Jefferson University, PA. Supervisor: Dr. Carlo Croce

Research Associate
Dec, 2002 – Aug, 2004 Center for Applied Genomics, Public Health Research Institute, NJ. Supervisor: Dr. Peter Tolias

Publications

Anbing Shi, Riju Banerjee, Carlos Chih-Hsiung Chen and Barth D. Grant. ARF-6 GTPase-activating protein CNT-1 interacts with RAB-10 and regulates endocytic recycling of clathrin-independent cargo. *In preparation*.

Anbing Shi, Carlos Chih-Hsiung Chen, Riju Banerjee, Doreen Glodowski, Anjon Audya, Christopher Rongo and Barth D. Grant. EHBP-1 functions with RAB-10 during Endocytic Recycling in *C. elegans*. *In revision*.

Vincent Popoff, Gonzalo A. Mardones, Siau-Kun Bai, Valérie Chambon, Danièle Tenza, Patricia V. Burgos, **Anbing Shi**, Philippe Benaroch, Sylvie Urbé, Christophe Lamaze, Barth

D. Grant, Graça Raposo and Ludger Johannes. Analysis of Articulation Between Clathrin and Retromer in Retrograde Sorting on Early Endosomes (2009) **Traffic** 2009; 10: 1868–1880.

Anbing Shi, Lin Sun, Riju Banerjee, Michael Tobin, Yinhua Zhang and Barth D. Grant. Regulation of Endosomal Clathrin and Retromer mediated Endosome to Golgi Retrograde Transport by the J-Domain Protein RME-8. **The EMBO Journal** Sep 17 (2009) 28, 3290 - 3302 (evaluated by Faculty of 1000 Biology)

Anbing Shi, Saumya Pant, Zita Balklava, Carlos Chih-Hsiung Chen, Vanesa Figueroa and Barth D. Grant. A novel requirement for C. elegans Alix/ALX-1 in RME-1 mediated membrane transport. **Current Biology** 2007 Nov 20;17(22):1913-24.

Anbing Shi, Jianyu Zheng. Interaction between presenilins and amyloid precursor protein and production of the A beta. **Chinese Bulletin of Life Sciences.**11(5):235-237. 1999